JAERI-M
88-125

EVALUATION REPORT ON SCTF CORE-III TEST S3-SHI
(EFFECT OF HOT LEG INJECTION ON CORE THERMAL-HYDRAULICS FOR PWR'S WITH A COMBINED INJECTION TYPE ECCS)

July 1988

Takamichi IWAMURA, Tadashi IGUCHI, Hajime AKIMOTO
Tsutomu OKUBO, Akira OHNUKI, Isao SAKAKI
Hiromichi ADACHI and Yoshio MURAO

日 本 原 子 力 研 究 所
Japan Atomic Energy Research Institute

JAERI-Mレポートは，日本原子力研究所が不定期に公刊している研究報告書です。
入手の問合わせは，日本原子力研究所技術情報部情報資料課（〒319－11茨城県那珂郡東海村）あて，お申しこしください。なお，このほかに財団法人原子力弘済会資料センター（〒319-11茨城県那珂郡東海村日本原子力研究所内）で複写による実費頒布をおこなっております。

JAERI-M reports are issued irregularly.
Inquiries about availability of the reports should be addressed to Information Division, Department of Technical Information, Japan Atomic Energy Research Institute, Tokai-mura, Naka-gun, Ibaraki-ken 319-11, Japan.

編集兼発行　日本原子力研究所
印　　刷　日立高速印刷株式会社

JAERI-M 88-125

Evaluation Report on SCTF Core-III Test S3-SH1
(Effect of Hot Leg Injection on Core Thermal-Hydraulics for PWR's with a Combined Injection Type ECCS)

Takamichi IWAMURA, Tadashi IGUCHI, Hajime AKIMOTO
Tsutomu OKUBO, Akira OHNUKI, Isao SAKAKI
Hiromichi ADACHI and Yoshio MURAO

Department of Reactor Safety Research
Tokai Research Establishment
Japan Atomic Energy Research Institute
Tokai-mura, Naka-gun, Ibaraki-ken

(Received June 11, 1988)

In order to investigate the thermal-hydraulic characteristics in the core for PWR's with a combined injection type ECCS, a core cooling base case test (S3-SH1) was performed using the Slab Core Test Facility (SCTF) Core-III. Subcooled ECC water was injected into the upper plenum simulating a hot leg injection under evaluation model (EM) condition.

Thermal-hydraulic behavior in the core was separated into two regions; a water down-flow region and an up-flow region, corresponding to the non-uniform ECC injection. A significant circulating flow was observed in the core and resultantly the effective flooding velocity was increased in the up-flow region. Before the initiation of bottom reflood, the water down-flow region was significantly cooled while the up-flow region was slightly cooled. After that time, the heat transfer coefficient in the up-flow region was approximately two times higher than a predicted value with a Bromley-type film boiling heat transfer correlation which was successfully applied to a cold leg injection mode. On the other hand, the heat transfer coefficient was predicted well with dispersed flow heat transfer correlations.

The work was performed under contract with Atomic Energy Bureau of Science and Technology Agency of Japan.

Keywords: LOCA, ECCS, Combined Injection, Two-Phase Flow, Fall Back, Two-dimensional Flow, Heat Transfer, Reflood

JAERI-M 88-125

ＳＣＴＦ第３次炉心試験Ｓ３－ＳＨ１評価報告書
（複合注水型ＥＣＣＳ付ＰＷＲの炉心熱水挙動に及ぼすホットレグ注水の効果）

日本原子力研究所東海研究所原子炉安全工学部
岩村　公道・井口　　正・秋本　　肇・大久保　努
大貫　　晃・榊　　勲・安達　公道・村尾　良夫

（１９８８年６月１１日受理）

複合注水型ＥＣＣＳ付ＰＷＲの炉心熱水力挙動を調べるため，平板炉心試験装置（ＳＣＴＦ）第３次炉心を用いて，炉心冷却基準試験（Ｓ３－ＳＨ１）を実施した。本試験では，安全評価解析条件（ＥＭ条件）下でのホットレグ注入を模擬して，サブクールを有する緊急冷却水を，上部プレナムに注入した。

緊急冷却水注入の不均一性に応じて，炉心流動状況は落水域と上昇域の２領域に分割された。炉心内には顕著な循環流が形成され，その結果，上昇域での実効冠水速度が増加した。下部からの再冠水開始以前には，落水域においては炉心冷却効果が大きかったが，上昇域においては冷却効果は小さかった。下部からの再冠水開始後には，上昇域での熱伝達率は，コールドレグ注入時に適用できたBromley型の膜沸騰熱伝達相関式による予測値の約２倍となった。一方，液滴分散流モデルを用いれば，熱伝達率の予測性能は向上した。

本報告書は，電源開発促進対策特別会計法に基づき，科学技術庁からの受託によって行った研究の成果である。

東海研究所：〒319-11　茨城県那珂郡東海村白方字白根２－４

Contents

目　　次

[NOMENCLATURE]

C_p	:	Specific heat	(J/kg•K)
D_h	:	Hydraulic diameter	(m)
g	:	Acceleration due to gravity	(m/s^2)
H_{fg}	:	Latent heat of evaporation	(J/kg)
h	:	Heat transfer coefficient	(W/m^2•K)
K_r	:	Constant in eq. (10)	
k	:	Thermal conductivity	(W/m•K)
L_q	:	Distance from quench front	(m)
Pr	:	Prandtle number	
q	:	Heat flux	
Q	:	Heat transfer rate	(W)
Re	:	Reynolds number	
T	:	Temperature	(K)
ΔT_{sat}	:	$T_w - T_{sat}$, wall superheat	(K)
u	:	velocity	(m/s)
W	:	Mass flow rate	(kg/s)
Z	:	Vertical coordinate	(m)
α	:	Void fraction	
δ	:	Droplet diameter	(m)
ε	:	Emissivity	
μ	:	Dynamic viscosity	(Pa•S)
ρ	:	Density	(kg/m^3)
σ_{SB}	:	Stefan Boltzman constant	($W/m^2•K^4$)

[Subscripts]

BF : Core baffle

C : Calculated

core : Core

cond : Condensation

d : Droplet

D : Drag body

down : Downward flow

f : Fall back

fc : Forced convection

fℓ : Flooding

g : Gas phase

HL : Hot leg

inj : Injection into upper plenum

ℓ : Liquid phase

m : Measured

n : Net

r : Radiation

sat : Saturation

sd : Steam to droplet

w : Wall

wd : Wall to droplet

Up : Upper plenum

[Superscript]

i : Bundle number

in : Inlet of core

M : Mass balance

D : Drag body

List of Tables

List of Figures

1. INTRODUCTION

The Slab Core Test Facility (SCTF) test program is a part of the large scale reflood test program performed under contract with Atomic Energy Bureau of Science and Technology Agency of Japan together with the Cylindrical Core Test Facility (CCTF) test program. The SCTF test program is one of the research activities based on the trilateral agreement among Japan Atomic Energy Research Institute (JAERI), the United States Nuclear Regulatory Commission (USNRC) and the Federal Minister for Research and Technology (BMFT) of the Federal Republic of Germany (FRG).

The SCTF Core-I and Core-II test series have been performed mainly to investigate the two-dimensional thermal-hydraulic behavior in the core during the refood phase of a loss-of-coolant accident (LOCA) of a Westinghous-type (US/J-type) pressurized water reactor (PWR). On the other hand, one of the major objectives of the SCTF Core-III test series is to investigate the effectiveness of the combined-injection-type emergency core cooling system (ECCS) for a German-type PWR (GPWR). In addition, simulation tests for a US/J-type PWR are also planned with the SCTF Core-III.

Under the combined injection mode, ECC water is simultaneously injected into the hot leg and the cold leg. Therefore, the core is expected to be cooled before the beginning of the bottom-up reflood due to the fall back water from the upper plenum into the core. In a full size core, the water fall back is considered to occur non-uniformly because of the non-uniform distributions of water level and tempetature in the upper plenum. Resultantly, a two-dimensional core cooling behavior may be induced.

In order to investigate the thermal-hydraulic characteristics in the core for PWR's with a combined-injection type ECC, a core cooling base case test S3-SH1 was performed. In Test S3-SH1, subcooled ECC water was non-uniformly injected into the upper plenum so as to simulate a hot leg injection under evaluation model (EM) condition. The present report describes the major results of this test.

Presented in Appendix A is a brief description of the SCTF Core-III. Some selected data obtained in Test S3-SH1 are presented in Appendix B.

2. TEST DESCRIPTION

2.1 Test Facility

A schematic diagram of SCTF is shown in Fig. 2.1 The primary coolant loops consist of a hot leg equivalent to four actual hot legs, a steam/water separator corresponding to four actual steam generators, an intact cold leg equivalent to three intact cold legs, a broken cold leg on the pressure vessel side, and a broken cold leg on the steam/water separator side. These two broken cold legs are connected to two containment tanks one by one which are connected to each other by a pressure equalizing pipe.

The flow area scaling ratio is 1/21 of a 1,100 MWe class Westinghouse-type PWR, whereas the heights of each component are preserved.

The ECC water injection ports for SCTF-III core cooling test series are selected from the four top injection nozzles and the eight side injection nozzles located just above the upper core support plate (UCSP). The top and the side injection nozzles are used to simulate the hot leg injection of a GPWR combined injection mode.

Figure 2.2 shows a vertical cross section of the pressure vessel. The pressure vessel includes a simulated core, an upper plenum with internals, a lower plenum, a core baffle and a downcomer. The configurations of the upper plenum structure and the end box simulate those of a 1,300 MWe class GPWR as practically as possible.

The simulated core consists of 8 bundles arranged in a row with full radial width. Bundle 1 corresponds to the center bundle and Bundle 8 to the peripheral bundle of a PWR. Each bundle consists of 236 heated rods and 20 non-heated rods arranged in a 16 x 16 array. The outer diameter and the heated length of the heated rod are 10.7 mm and 3,613 mm, respectively. The arrangement pitch of the rods is 14.3 mm.

The core and the upper plenumn are enveloped by honeycomb thermal insulators with wall plates to minimize the wall thermal effects.

The description of SCTF Core-III is presented in detail in Appendix A.

2.2 Test Conditions

The test referred to in this report is Test S3-SH1 which is the first shakedown test in the SCTF Core-III series. Major test conditions for this test are listed in Table 2.1.

The test conditions for Test S3-SH1 were determined based on the CCTF combined-injection test results (C2-19) and the TRAC-PF1/MOD1 calculation results for GPWR evaluation model (EM) condition. The ECC injection ports used in Test S3-SH1 were the four upper head injection nozzles and the two side flow injection nozzles above Bundles 7 & 8, simulating the water flow from the hot leg into the upper plenum. Since the main purpose of the present test is to investigate the core cooling characteristics before and after the beginning of the bottom-up reflood, no ECC water was injected into the cold leg and the initial water inventory in the lower plenum was set to be zero. The top injection flow rate was 2.5 kg/s and the water temperature was 308 K for each of the four top injection nozzles. The total side injection flow rate was 30 kg/s and the water temperature was 343 K. Total ECC flow rate of 40 kg/s was determined from the TRAC GPWR EM calculation results. The water temperature of the side injection was based on the fluid temperature just above the UCSP at the hot leg side for CCTF Test C2-19. The radial power distribution was set to be flat so as to avoid the effect of radial power distribution on the two-dimensional core cooling behavior.

The effects of the ECC water temperature, the initial liquid level in the lower plenum, the side injection location and the radial power distribution on the two-dimensional core cooling behavior were also investigated in the SCTF-III core cooling test series and will be reported separately.

2.3 Test Procedure

Figure 2.3 shows the test sequence of Test S3-SH1.

The core heating was initiated at time "zero" under the flat radial power distribution with the total power of 7.5 MW. When four cladding temperatures exceeded 943 K (670°C), ECC injection into the upper plenum was initiated. At the same time, the core power decay started, simulating the reactor time from 25 s after shutdown. The

decay curve was based on the (1.03 × ANS standard + Actinides). The top injection through the four top injection nozzles and the side injection above Bundles 7 & 8 were terminated at 360 s and 420 s, respectively, after the initiation of injection. After the quench of the whole core, the injection location was switched from Bundles 7 & 8 to Bundles 1 & 2 so as to investigate the effect of the side injection location on the two-dimensional hydraulic behavior in the core. This is called Test S3-SH1-Phase2. The results of Test S3-SH1-Phase2 are not discussed in this report but will be reported separately.

3. TEST RESULTS

3.1 Measured Boundary Conditions

Figures 3.1 and 3.2 show top and side injection flow rates into the upper plenum through the top injection nozzles and the side injection nozzles, respectively. The side injection started at 112 s and the top injection at 114 s. The injection rates were 2.5 kg/s per each of four top injection nozzles and 30 kg/s for the side injection nozzles as specified.

Figures 3.3 and 3.4 show temperatures of the top and side injection water, respectively. The top injection water temperatures were between 308 and 320 K until 100 s after the initiation of the ECC injection and after that time the temperatures were between 308 and 312 K. The side injection water temperature was oscillating between 340 and 348 K.

Figure 3.5 shows the histories of heating power for each bundle. The radial power distribution was completely flat as shown in this figures.

Figure 3.6 shows the pressures at the core center and the top of containment tank-II. The decrease of pressure from 122 s indicates the condensation of steam by the subcooled water. After 160 s the pressures increased because of the larger steam generation rate in the core due to the beginnging of bottom-up flooding.

The chronology of major events for Test S3-SH1 is listed in Table 3.1.

3.2 Fluid Behavior except Core

3.2.1 Fluid Behavior in Upper Plenum and around UCSP

The distribution of collapsed liquid levels in the upper plenum is shown in Fig. 3.7. The collapsed liquid levels above Bundles 1,3,5,7 and 8 are less than 0.05 m before the BOCREC (bottom of core recovery) (157 s) and then increases rapidly. After the BOCREC, the collapsed liquid level is higher at the hot leg side. The low liquid level before the BOCREC indicates that most of the injected water into the upper plenum falled back to the core during this period. All of the collapsed

liquid levels exceed the bottom of hot leg nozzle (1.05 m) at 290 s.

The fluid temperatures in the upper plenum are shown in Figs. 3.8, 3.9 and 3.10 at elevations of 0.1, 0.25 and 0.6 m from the UCSP, respectively. At the elevations of 0.1 and 0.25 m, subcooled water is observed except above Bundle 1. The fluid temperature is the lowest above Bundle 7 except at 0.25 m elevation before the BOCREC. The significant spikes of the fluid temperature above Bundle 7 indicate the intermittent steam flow in the subcooled water. At the elevation of 0.6 m, subcooled water is not observed.

Figure 3.11 shows the fluid temperatures in the UCSP holes. Just after the initiation of ECC water injection, the fluid temperatures become subcooled above Bundles 7 and 8. The fluid temperatures above Bundles 1 through 5 are approximately saturated during the test. Subcooled water is observed above Bundle 6 for short time before the BOCREC and after 280 s.

Figure 3.12 shows the steam velocities measured with turbine flow meters at the UCSP holes above Bundles 2,4,6 and 8. These velocities are quantitatively reliable only for steam single-phase up-flow. Before the BOCREC, steam up-flow was not measured for all locations, suggesting that almost all amount of steam generated in the core was condensed due to a large amount of subcooled water in Bundles 7 and 8 before the BOCREC. The steam up-flow rate begins to increase rapidly just after the BOCREC above Bundles 2,4, and 6. The steam velocity is higher at the Bundle 2 side. On the other hand, steam up-flow is not observed above Bundle 8 even after the BOCREC.

3.2.2 Fluid Behavior around End Box Tie Plate

Figure 3.13 shows the differential pressures across the end box tie plate. Before the BOCREC, the differential pressure is slightly positive in Bundles 1 and 3, approximately zero in Bundles 4,5 and 6, and negative in Bundles 7 and 8. The negative differential pressure indicates the water down-flow. Since the vertical differential pressure includes the effects of gravitatioinal pressure drop, the small amount of positive differential pressure before the BOCREC in Bundles 1 and 3 does no always imply the upward flow. After the BOCREC, the flow direction at the end box tie plate in Bundles 1 through 6 is considered to be upward because the differential pressure is larger than the static

water head of 0.69×10^{-3} MPa in the measurement span. On the other hand, the large negative differential pressures in Bundles 7 and 8 indicate the strong downward flow in these bundles. The gradual decrease of differential pressure after about 200 s is resulted from the decrease of steam generation rate in the core due to the decay of heating power.

Figure 3.14 shows the steam and water mass flow rates measured with drag bodies at the end box tie plate in Bundles 4 and 8. The maximum steam mass flow rate is 1.0 kg/s in Bundle 4, while the steam mass flow rate is approximately zero in Bundle 8. The measured downward water flow rate in Bundle 8 is about 12 kg/s before the BOCREC and the maximum flow rate is about 25 kg/s during the period from 200 to 260 s.

Figure 3.15 shows the fluid temperatures just below the end box tie plate. Subcooled water is observed in Bundles 7 and 8 during the ECC water injection period. In Bundles 5 and 6 subcooled water is also observed before the BOCREC and the fluid temperatures are saturated after the BOCREC. On the other hand, the fluid temperatures are always saturated in Bundles 1 through 4 after the initiation of ECC water injection.

3.2.3 Fluid Behavior in Pressure Vessel and Primary Coolant Loop

Figure 3.16 shows the water accumulation behaviors in the pressure vessel, the containment tanks I and II, the pump simulater and the steam/water separator. Just after the initiation of ECC water injection at 112 s, the water accumulation is initiated in the lower plenum. The water accumulation rate in the lower plenum including the bottom of downcomer is estimated to be approximately 34 kg/s at 130 s. Therefore, about 85 % of the injected water penetrated the core into the lower plenum at this time.

The differential pressure across the core full height is relatively small before the BOCREC. After the BOCREC, the differential pressure increases rapidly and reaches 3.7 m water head at 320 s. That is, the core is filled with almost single-phase water after 320 s.

At 250 s the downcomer water head is saturated and the liquid level in the containment tank-I begins to increase, indicating the water overflow from the downcomer to the containment tank-I through the broken cold leg. The water overflow is also measured with a spool piece located

in the broken cold leg pressure vessel side as shown in Fig. 3.17.

The increase in the liquid level in the steam/water separator at 315 s is caused by a water back flow from the intact cold leg because the differential pressure in the pump simulator increases rapidly at the same time.

Figures 3.18 and 3.19 show the void fractions and mass flow rates measured with a spool piece in 4 regions of the hot leg. The total mass flow rate is shown in Fig. 3.20. The flow area ratios of each region are 31 %, 27 %, 26 %, and 16 % from the top to the bottom of the pipe cross-sectional area. Before the BOCREC, the mass flow rates are negliegibly small. That is, the out-flow rate from the upper plenum was almost zero during the period because most of the water injected into the upper plenum fell down into the core and almost all amount of steam generated in the core was condensed in the pressure vessel. The void fraction begins to decrease at 170 s in the bottom region and at 195 s in the top region. The reversal flow toward the upper plenum is observed before 315 s except at the top region. The total flow rate is changed from positive to negative at 240 s as shown in Fig. 3.20. After about 315 s, the mass flow rate through the hot leg is approximately zero. This is due to the water back-flow into the steam/water separator from the intact cold leg as mentioned before.

Figures 3.21 and 3.22 show the mass flow rates in the intact cold leg and the broken cold leg steam/water separator side. As shown in these figures and Figs. 3.17 and 3.20, the mass flow rates in the primary loops are relatively small before the BOCREC due to the condensation of steam in the pressure vessel and no liquid carryover into the hot leg. The mass flow rates increase after the BOCREC due to the initiation of steam out-flow from the pressure vessel to the hot leg.

3.3 Two-Dimensional Hydraulic Behavior in Core

3.3.1 Void Fraction Distribution

The vertical differential pressures measured in Bundles 2,4 and 8 at six elevations were converted directly to void fractions by neglecting the effects of frictional and accelerational pressure drops. The results are shown in Fig. 3.23. Just after the initiation of the ECC water injection, a water accumulation is observed in Bundle 8 especially

at the upper elevations. After the BOCREC, the void fractions decrease rapidly for all bundles especially at the lower elevations. The void fractions in Bundle 8 are the lowest among these bundles for most of the test period, while the void fractions in Bundles 2 and 4 are approximately the same.

However, it should be noted that the vertical differential pressure does not indicate a real void fraction in the water down-flow region (Bundles 7 and 8) because the falling water column at the center of a subchannel has little effect on the momentum balance between the water and the steam. The γ-densitometer, on the other hand, is expected to measure the real fluid density at the gap between bundles. Figure 3.24 shows the fluid densities measured with the γ-densitometers at the gap between Bundles 1 & 2, 5 & 6, and 7 & 8 at elevation of 3.235 m. Between Bundles 7 and 8, a considerable amount of water is observed before the BOCREC and then the fluid density increases rapidly at 175 s. The gap between Bundles 7 and 8 is almost filled with single-phase water at 240 s, while the fluid densities are relatively small at the gaps between Bundles 1 and 2 and between Bundles 5 and 6 at that time.

The γ-densitometer data are converted to void fraction and compared with the void fractions obtained from the differential pressure data in Fig. 3.25. In the two-phase up-flow region (Bundles 1 and 2), the void fraction obtained from the γ-densitometer is much higher than the void fraction obtained from the D/P data. One of the reasons of this discrepancy is attributed to the fact that the effects of frictional and accelerational pressure drops were neglected in the calculation of void fraction from the differential pressure data. In the water down-flow region (Bundles 7 and 8), on the other hand, the void fraction obtained from the γ-densitometer is much lower than the void fraction obtained from the D/P data. For example, at 200 s, the γ-densitometer gives the void fraction of about 0.28, while the D/P cell give the void fraction of about 0.6 at the corresponding elevation. Since the γ-densitometer is not affected by the momentum balance problem, the void fraction obtained from the γ-densitometer data is considered to be more reliable than the void fraction obtained from the D/P cell in the water down-flow region. That is, the real void fraction is considered to be very small in the region.

3.3.2 Horizontal Differential Pressures

Figure 3.26 shows the horizontal differential pressures at six elevations in the core. The positive value means that the pressure at the Bundle 1 side is higher than the pressure at the Bundle 8 side. The magnitudes of these horizontal differential pressures and the direction of cross flow in the core at 140, 160, 200, 250, 300 and 350 s are shown in Fig. 3.27. The quenched region is also shown in this figure.

The cross flow from Bundle 4 to Bundle 8 is observed at the upper elevations in the core before the quench of the whole core. This was caused by the depressurization in Bundles 7 and 8 due to the condensation of steam by the subcooled fall back water. As the bottom-up quench front proceeds upward, the direction of cross flow below and just above the quench front is reversed, indicating that the fall back water in Bundles 7 and 8 flows into the other bundles around the quench front. Above the top grid spacer (elevation 3.821 m), the cross flow direction is always from the Bundle 8 side to the Bundle 1 side.

After the quench of the whole core, the pressure at the Bundle 8 side is higher than the pressure at the Bundle 1 side in the whole core.

3.3.3 Fluid Temperature Distribution

Figure 3.28 shows the fluid temperature distribution in the core at 120, 140, 160, 200, 250 and 300 s. As illustrated in Fig. 3.29, the fluid temperature range is divided into four regions; highly subcooled region ($T \leq 370$ K), slightly subcooled region ($370\ K \leq T \leq 400$ K), approximately saturated region ($400\ K \leq T \leq 420$ K), and superheated region ($420\ K \leq T$). As shown in these figures, subcooled water is observed at the upper part of Bundles 7 and 8 at 120 s (8 s after the initiation of ECC water injection). The subcooled region expands downwards with time. The fluid temperatures at the central elevations in Bundles 1 through 5 indicate superheated steam temperature before 160 s. After this time, the superheated region rapidly diminishes due to the initiation of bottom-up reflooding.

3.4 Two-Dimensional Heat Transfer Behavior in Core

3.4.1 Heater Rod Temperatures

Figure 3.30 shows the temperature histories of the center rods for all bundles at elevations of 3.19, 1.905 and 1.38 m from the bottom of heated part. The heater rods in Bundles 7 and 8 are significantly cooled just after the initiation of the ECC injection especially at the upper elevations. On the other hand, the heater rod temperatures in Bundles 1 and 3 continue to rise almost adiabatically until the BOCREC. The heater rods in Bundles 2,4,5 and 6 are slightly cooled before the BOCREC at all elevations.

3.4.2 Quench Front Propagation

The top-down and bottom-up quench fronts at 140, 160, 200, and 250 s are shown in Fig. 3.27. The heater rods at the top and bottom parts of Bundles 7 and 8 are quenched prior to the BOCREC due to the subcooled water falling back from the upper plenum. The bottom-up quench front propagation is approximately uniform over Bundles 1 through 6 in accordance with the flat radial power distribution. It is therefore suggested that the core cooling behavior is approximately one-dimensional in the two-phase up-flow region during the bottom reflooding phase even under the condition of non-uniform ECC water injection into the upper plenum.

3.4.3 Heat Transfer Coefficients

The heat transfer coefficients for all bundles at elevations of 3.19, 1.905 and 1.38 m are shown in Fig. 3.31. These heat transfer coefficients were calculated from the heater rod temperature histories using the heat transfer calculation code "HEATT"[1].

As shown in Fig. 3.31(b), the heat transfer coefficients at 1.905 m in Bundles 6, 7 and 8 are more than 100 W/m^2K before the BOCREC, indicating the significant core cooling effect by the subcooled fall back water. On the other hand, the heat transfer coefficients in Bundles 1 and 3 are approximately zero and those in Bundles 2, 4 and 5 are relatively small before the BOCREC. The heat transfer behavior before the BOCREC indicates that the subcooled fall back water in the

water down-flow region has little effect on the core cooling behavior in the two-phase up-flow region.

After the BOCREC, the heat transfer coefficients in the two-phase up-flow region (Bundles 1 through 6) well agree with each other at the same elevation. Therefore, the heat transfer behavior is one-dimensional in this region after the BCOREC, though the significant non-uniformity is observed before the BOCREC. This is consistent with the uniform distribution of the bottom-up quench front in Fig. 3.27.

4. DISCUSSIONS

4.1 Mass and Energy Balance calculation

4.1.1 Estimation of Fall Back Flow Rate

The fall back water flow rate through the UCSP was given by the following mass balance equation;

$$W_f^M = W_{inj} - W_{HL} - W_{UP} \qquad (1)$$

where, W_f^M = Fall back water flow rate obtained by mass balance method.

W_{inj} = Total upper plenum injection rate.

W_{HL} = Carryover mass flow rate into hot leg.

W_{UP} = Water accumulation rate in upper plenum.

However, it should be noted that the effects of condensation and circulation flow in the upper plenum were not considered in this equation.

The fall back water flow rate is also obtained from the water flow rate measured with the drag body at the end box in Bundle 8 by assuming that the fall back water flow rate is equally divided into Bundles 7 and 8. That is;

$$W_f^D = -2.0 \times \langle W_{D-8} \rangle \qquad (2)$$

where, W_f^D = Fall back water flow rate obtained by measured down-flow rate.

$\langle W_{D-8} \rangle$ = Water mass flow rate measured with drag body in Bundle 8.

Figure 4.1 shows the comparison of fall back water flow rates calculated by eq. (1) and eq. (2). The total upper plenum injection rate is also shown in this figure. During the period from 30 s to 160 s after the BOCREC, the fall back water flow rate measured with the drag body is higher than that calculated by the mass balance method.

The difference between the W_f^D and W_f^M is considered to be the water effluent rate in the up-flow region, because the W_f^M is the net water flow rate at the top of the core and smaller than the real fall back water flow rate.

4.1.2 Estimation of Flooding Rate in Two-Phase Up-Flow Region

The net mass flow rate at the core inlet, W_{net}^{in}, is given by the following mass balance equation;

$$W_{net}^{in} = -(W_f^M - W_{core} - W_{BF}) \tag{3}$$

where, W_f^M = given by eq. (1).
W_{core} = Mass accumulation rate in the core.
W_{BF} = Mass accumulation rate in the core baffle.

The W_{core} and W_{BF} are obtained from differential pressure measurements.

The total water down-flow rate in Bundles 7 and 8, W_{down}, is given by;

$$W_{down} = W_f^D + W_{cond} \tag{4}$$

where, W_f^D = given by eq. (2).
W_{cond} = Steam condensation rate in Bundles 7 and 8.

The steam condensation rate in Bundles 7 and 8 is estimated as follows.

The enthalpy of the subcooled fall back water is increased by the heat flux from the heater rods and the condensation of steam. The increase of temperature due to the heat flux from the heater rods is calculated from the following equation;

$$C_{P\ell} \frac{W_f^M}{2} \frac{d\, T_c^i(z)}{d\, z} = q^i(z) \qquad i = 7, 8 \text{ (Bundle No.)} \tag{5}$$

where, $C_{P\ell}$ = Specific heat of saturated liquid.
W_f^M = given by eq. (1).
$T_c^i(z)$ = Calculated water temperature at elevation z.
$q^i(z)$ = Heat flux at elevation z.

The water temperature is also increased by the condensation of steam in addition to the heat flux from the heater rods. Therefore, the total steam condensation rate is estimated from the difference between the measured water temperature and the calculated water temperature at the bottom of core, as follows;

$$W_{cond} = W_f^M C_{P\ell} \cdot \frac{(T_m^8 - T_c^8) + (T_m^7 - T_c^7)}{2} \cdot \frac{1}{H_{fg}} \qquad (6)$$

where, W_{cond} = Total steam condensation rate in Bundles7 and 8

W_f^M = given by eq. (1).

$C_{P\ell}$ = Specific heat of saturated liquid.

H_{fg} = Latent heat of evaporation.

T_m^7, T_m^8 = Measured water temperature at the bottom of core in Bundles 7 and 8, respectively.

T_c^7, T_c^8 = Calculated water temperature at the bottom of core in Bundles 7 and 8, respectively.

After the beginning of bottom reflood, a part of the total water down-flow (given by eq. (4)) goes into the up-flow region and the rest flows into the downcomer through the lower plenum. Since the net mass flow rate at the inlet of core (given by eq. (3)) is a negative value, the effective flooding rate in the up-flow region (Bundles 1 through 6), W_{fl}, is given by:

$$W_{f\ell} = W_{down} + W_{net}^{in} \qquad (7)$$

where, W_{down} = given by eq. (4)

W_{net}^{in} = given by eq. (3)

Figure 4.2 shows the calculated results of W_{net}^{in}, W_{down}, W_{cond} and W_{fl}. As shown in this figure, the condensation rate is negliegibly small in comparison to the total water down flow rate.

The effective flooding rate is converted to the flooding velocity in the up-flow region. Figure 4.3 shows the comparison of flooding velocities in Test S3-SH1 and Test S2-SH2 which is a cold leg injection test [8]. The flooding velocity in Test S3-SH1 is much

higher than that in Test S2-SH2 except after 138 s.

4.1.3 Estimation of Steam Generation Rate

Figure 4.4 shows the steam generation rate in the two-phase up-flow region (Bundles 1 through 6). The steam generation rate was calculated from a heat balance method[8]. The major assumptions are as follows;

(1) The heat flux from the heater rods is totally absorbed in the fluid,
(2) The core inlet flow rate is equally divided into each of 8 bundles, and
(3) The steam and water mixture is always saturated.

Since a major part of the released energy in the water down-flow region was used to heat-up the subcooled water, the net steam generation rate in this region is not able to be evaluated by the above-mentioned heat balance method. The hypothetical maximum steam generation rate is obtained by dividing the total core heat release rate by the latent heat of evaporation. The effect of subcooling is not taken into account in this calculation. The result is compared with the total steam generation rate in Bundles 1 through 6 in Fig. 4.5. The actual steam generation rate is considered to be between these two curves.

4.2 Comparison of Heat Transfer Characteristics with Cold Leg Injection Test

In order to compare the heat transfer characteristics between the GPWR combined injection mode and a typical US/J-type cold leg injction mode, the heat transfer coefficients obtained in Test S3-SH1 and Test S2-SH2 are compared in Fig. 4.6 with respect to the distance from the bottom-up quench front. Test S2-SH2 is a cold leg injection test under flat radial power distribution in SCTF Core-II[8]. As shown in this figure, the heat transfer coefficient is much higher for Test S3-SH1 than for Test S2-SH2 at the same distance from the bottom-up quench front.

Liquid fraction and flooding velocity are considered to be the major factors for the difference in the heat transfer coefficients

between these two tests.

For the first approximation, the liquid fraction is calculated from the measured vertical differential pressure by neglecting the effects of frictional and accelerational pressure drops. However, those effects should be taken into accounts especially at the upper part of the core under high flooding velocity condition. Here, the frictional pressure drop is estimated by the Lockhart-Martinelli model(9) using the Chisholm's equation of the two-phase multiplier(10). The accelerational pressure drop is evaluated by using the steam and water velocities obtained by an one-dimensional mass balance method. Figure 4.7 shows the non-corrected and corrected liquid fractions for Test S3-SH1 and S2-SH2 at 1.905 m. The effects of frictional and accelerational pressure drops in Test S3-SH1 are much larger than those in Test S2-SH2 because of the higher flooding velocity in Test S3-SH1. As shown in Fig. 4.7, even the corrected liquid fraction is much larger for Test S3-SH1 than for Test S2-SH2.

The flooding velocity, which is estimated from the mass balance method, is also higher for Test S3-SH1 than for Test S2-SH2 as shown in Fig. 4.3. Therefore, it is suggested that the higher flooding velocity and the higher liquid fraction are the major reasons for the higher heat transfer coefficient in Test S3-SH1 in comparison to Test S2-SH2.

4.3 Prediction of Heat Transfer Coefficient with Heat Transfer Correlations

The heat transfer coefficients after the BOCREC in the up-flow region were compared with Murao-Sugimoto film boiling correlation(2) and dispersed flow heat transfer correlations(3).

The Murao-Sugimoto correlation is based on the Bromley-type film boiling model and used in the REFLA code developed by Murao et al.(4). This epuation is given by;

$$h = 0.94 \left[\frac{k_g^3 \rho_g \rho_\ell H_{fg} g}{L_q \mu_g \Delta T_{sat}} \right]^{\frac{1}{4}} (1 - \alpha)^{\frac{1}{4}}$$

$$+ \varepsilon \sigma_{SB} (1 - \alpha)^{\frac{1}{2}} (T_w^4 - T_{sat}^4) / \Delta T_{sat} \qquad (8)$$

On the other hand, based on the dispersed flow model, the heat transfer coefficient is given by the following three terms;

$$h = h_r + h_{wd} + h_{fc} \tag{9}$$

where, h_r, h_{wd} and h_{fc} are the heat transfer coefficients due to wall-droplets radiation, droplet impingement on the wall and forced convection of steam, respectively. Here, the heat transfer coefficients are defined at the temperature difference between the rod surface and the saturated temperature. These three terms are expressed as;

$$h_r = \left[1 - \exp\left\{-K_r \frac{3\,D_h}{2\delta}(1-\alpha)\right\}\right] \varepsilon\, \sigma_{SB}\,(T_w^4 - T_{sat}^4)/\Delta T_{sat} \tag{10}$$

where, ε and K_r were assumed to be 0.7 and 0.5, respectively.

$$h_{wd}^{(5)} = 0.2\,\frac{\pi}{4}\left(\frac{6}{\pi}\right)^{\frac{2}{3}}(1-\alpha)^{\frac{2}{3}}\left[\frac{k_g^3\, H_{fg}^*\, g\, \rho_g\, \rho_\ell}{\Delta T_{sat}\, \mu_g \left(\frac{\pi}{6}\right)^{\frac{1}{3}} \delta}\right]^{\frac{1}{4}} \tag{11}$$

where $$H_{fg}^* = H_{fg}\left[1 + \frac{7}{20}\,\frac{C_{pg}\,\Delta T_{sat}}{H_{fg}}\right]^{-3}$$

$$h_{fc} = 0.023\, Re_g^{0.8}\, Pr_g^{0.4}\,\frac{k_g\,(T_w - T_g)}{D_h\,\Delta T_{sat}} \tag{12}$$

In these calculations, the liquid fraction, $1-\alpha$, was obtained from the measured vertical differential pressures by correcting for the effects of frictional and accelerational pressure drops. The droplet diameter, δ, was assumed to be 1.73 mm. This is the Sauter mean diameter of droplets observed in the small scale reflood experiment by Sugimoto and Murao(6). The superheated steam temperatuer, T_g, was determined from the difference between the heat transfer from the wall to the steam and the interfacial heat transfer from the steam to the droplets. The interfacial heat transfer coefficient is given by;

$$h_{sd}^{(7)} = \gamma(B)(2.0 + 0.55\ Re_d^{0.5}\ Pr_g^{1/3})\ \frac{k_g}{\delta} \tag{13}$$

where

$$Re_d = \frac{\delta\ \rho_g |u_g - u_d|}{\mu_m}$$

$$\mu_m = \mu_g\ \alpha^{-2.5}\ \frac{(\mu_\ell + 0.4\mu_g)}{(\mu_\ell + \mu_g)}$$

$$\gamma(B) = \frac{\ln(1 + B)}{B}$$

$$B = \frac{C_{pg}(T_g - T_{sat})}{H_{fg}^1}$$

$$H_{fg}^1 = H_{fg}\left(\frac{Q_{sd} + Q_r + Q_{wd}}{Q_{sd}}\right)$$

The heat transfer coefficients calculated with the Murao-Sugimoto correlation (eq. (8)) and the dispersed flow correlation (eq. (9)) are compared with the experinental data in Fig. 4.8. The heat transfer coefficients in Test S3-SH1 are well predicted with eq. (9). However, the heat transfer coefficients are approximately two times higher than the predicted value with eq. (8).

As shown in Fig. 4.3, the effective flooding velocity in Test S3-SH1 is much larger than that in the cold leg injection test S3-SH2 and far beyond the applicable range of the original Murao-Sugimoto correlation. This is considered to be the major reason of the descrepancy between the measured heat transfer coefficient and calculated one with eq. (8). In order to improve the predictability of the Murao-Sugimoto correlation, the effect of flooding velocity should be taken into account.

5. CONCLUSION

A core cooling base case test (S3-SH1) was performed under an upper plenum injection simulating a hot leg injection for PWR's with a combined injection type ECCS. The overall thermal-hydraulic behavior in the pressure vessel in Test S3-SH1 is illustrated in Fig. 5.1. Followings are the major conclusions obtained in this test.

(1) Thermal-hydraulic behavior in the core was separated into two regions; a water down-flow retion (Bundles 7 and 8) and an up-flow region (Bundles 1 through 6).

(2) Steam cross flow from Bundle 4 toward Bundle 8 was observed at the upper elevations. On the other hand, water cross flow from Bundle 8 toward Bundle 4 was observed below and just above the quench front. Resultantly, the effective flooding velocity was increased in the up-flow region.

(3) In the water down-flow region, the core was significantly cooled before the beginning of bottom-up reflood especially at the upper elevations. The void fraction in this region was much lower than the void fraction in the up-flow region.

(4) In the up-flow region, the core was slightly cooled before the initiation of bottom-up reflood. After that time, the heat transfer coefficient was approximately two times higher than a predicted value with a Bromley-type film boiling correlation because the flooding velocity was far beyond the applicable range of the correlation. On the other hand, the heat transfer coefficient was predicted well with a dispersed flow model.

ACKNOWLEDGMENT

The authors would like to express their appreciation to Mr. W. Pointner, a regident engineer from Federal Republic of Germany, for his useful discussions.

5. CONCLUSION

A core cooling base case test (S3-SH1) was performed under an upper plenum injection simulating a hot leg injection for PWR's with a combined injection type ECCS. The overall thermal-hydraulic behavior in the pressure vessel in Test S3-SH1 is illustrated in Fig. 5.1. Followings are the major conclusions obtained in this test.

(1) Thermal-hydraulic behavior in the core was separated into two regions; a water down-flow retion (Bundles 7 and 8) and an up-flow region (Bundles 1 through 6).

(2) Steam cross flow from Bundle 4 toward Bundle 8 was observed at the upper elevations. On the other hand, water cross flow from Bundle 8 toward Bundle 4 was observed below and just above the quench front. Resultantly, the effective flooding velocity was increased in the up-flow region.

(3) In the water down-flow region, the core was significantly cooled before the beginning of bottom-up reflood especially at the upper elevations. The void fraction in this region was much lower than the void fraction in the up-flow region.

(4) In the up-flow region, the core was slightly cooled before the initiation of bottom-up reflood. After that time, the heat transfer coefficient was approximately two times higher than a predicted value with a Bromley-type film boiling correlation because the flooding velocity was far beyond the applicable range of the correlation. On the other hand, the heat transfer coefficient was predicted well with a dispersed flow model.

ACKNOWLEDGMENT

The authors would like to express their appreciation to Mr. W. Pointner, a regident engineer from Federal Republic of Germany, for his useful discussions.

REFERENCES

(1) M. Osakabe and Y. Sudo., Heat Transfer Calculation of Simulated Heater Rods throughout Reflood Phase in Postulated PWR-LOCA Experiments, J. Nucl. Sci. Tech. vol. 20, No.7, pp,559-570 (1983).

(2) Y. Murao and J. Sugimoto, Correlation of Heat Transfer Coefficient for Saturated Film Boiling during Reflood Phase Prior to Quenching, J. Nucl. Sci. Tech. vol. 18, No.4, pp.275-284 (1981).

(3) T. Iwamura et al., Radial Distribution of Heat Transfer Coefficient in a Full Size Core during Reflood Phase of a PWR-LOCA, 1987 ASME-JSME Thermal Engineering Joint Conference, March 22 ~ 27, Honolulu, Hawaii (1987).

(4) Y. Murao, et al., REFLA-1D/MODE3-A Computer Program for Reflood Thermo-Hydrodynamic Analysis during PWR-LOCA, User's Manual, JAERI-M 84-243 (1985).

(5) R.P. Forslund and W.M. Rohsenow, Dispersed Flow Film Boiling, J. Heat Transfer, Nov. pp.399-407 (1968).

(6) J. Sugimoto and Y. Murao, Report on Reflood Experiment of Grid Spacer Effect, JAERI-M 84-131 (1984).

(7) T.W. Hoffman and L.L. Ross, A Theoretical Investigation of the Effect of Mass Transfer on Heat Transfer to an Evaporating Droplet, Int. J. Heat and Mass Transfer, vo. 15, pp.599-617 (1972).

(8) T. Iwamura et al., Two-dimensional Thermal-Hydraulic Behavior in Core in SCTF Core-II Cold Leg Injection Tests (Radial Power Profile Test Results), JAERI-M 85-106 (1985)

(9) R.W. Lockhart and R.C. Martinelli, Chem. Eng. Prog. 45-1, 39 (1949).

(10) D. Chisholm and A.D.K. Laird, ASME 80-2, 276 (1958).

Table 2.1 Test conditions for Test S3-SH1

System pressure	0.3 MPa
Initial total power	7.5 MW
Decay curve	1.03 × ANS + Actinides from 25 s after shutdown
Radial power distribution	flat
Initial peak caldding temperature	943 K
ECC water injection mode	Upper plenum injection simulating the hot leg injection of GPWR
Total injection rate	40 kg/s (constant)
Upper head injection	
Flow rate	2.5 kg/s × 4 nozzles
Water temperature	308 K
Injection period	360 s
UCSP injection	
Flow rate	30 kg/s
Injection location	above Bundles 7 & 8
Water temperature	343 K
Injection period	420 s

Table 3.1 Chronology of major events for Test S3-SH1

	Time after core power "ON"	Time after ECC injection initiation
Core power "ON"	0 s	-112
Core power decay initiation	111	-1
Side injection initiation	112	0
Top injection initiation	114	2
BOCREC	157	45
Maximum pressure at the top of containment tank-II (0.321 MPa)	177	65
Maximum pressure at the center of core (0.338 MPa)	182	70
Maximum core temperature (1115 K)	207.5	95.5
Whole core quenched	335.5	223.5
End of top injection	470	358
End of side injection (7 & 8 Bundles)	530	418

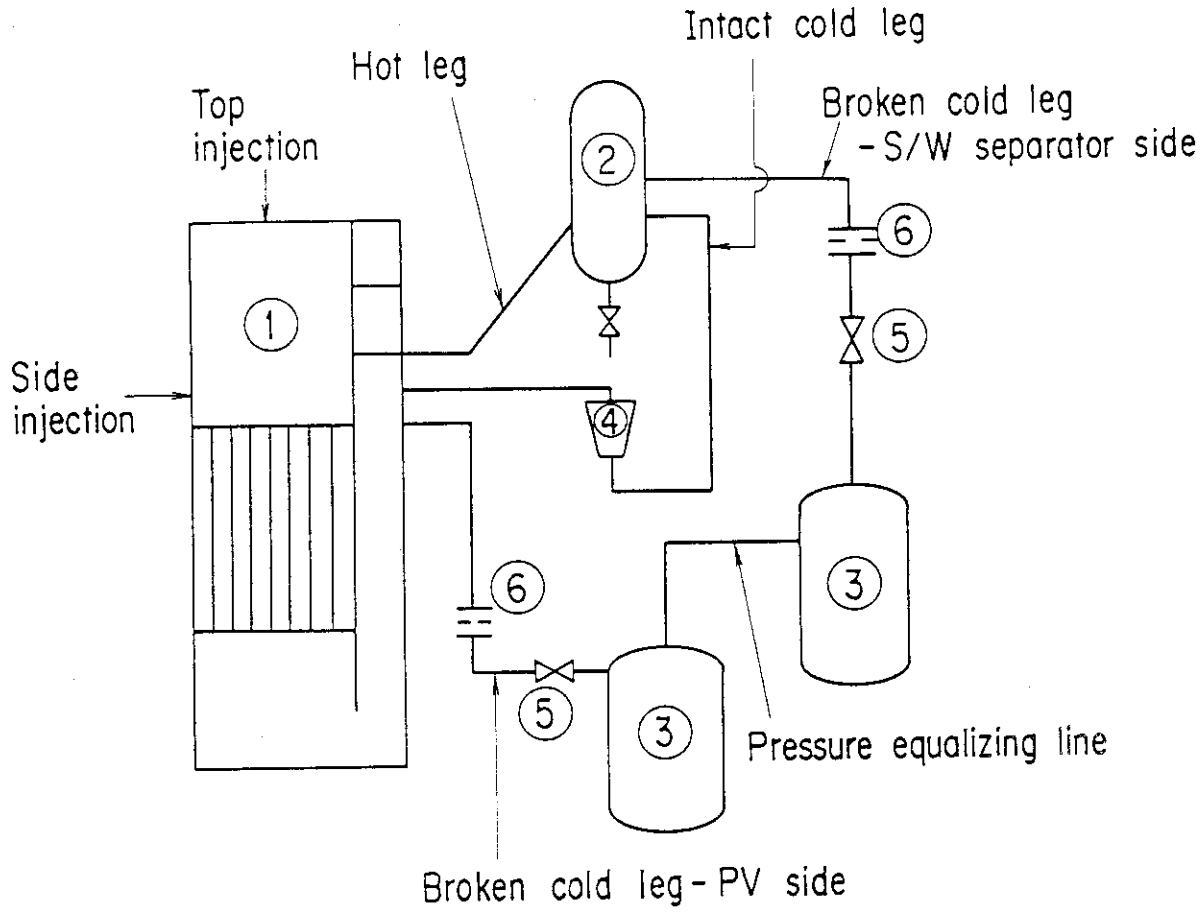

① Pressure vesel
② Steam / water separator
③ Containment tanks
④ Pump simulator
⑤ Break valves
⑥ Flow resistance simulators

Fig. 2-1 Schematic diagram of SCTF

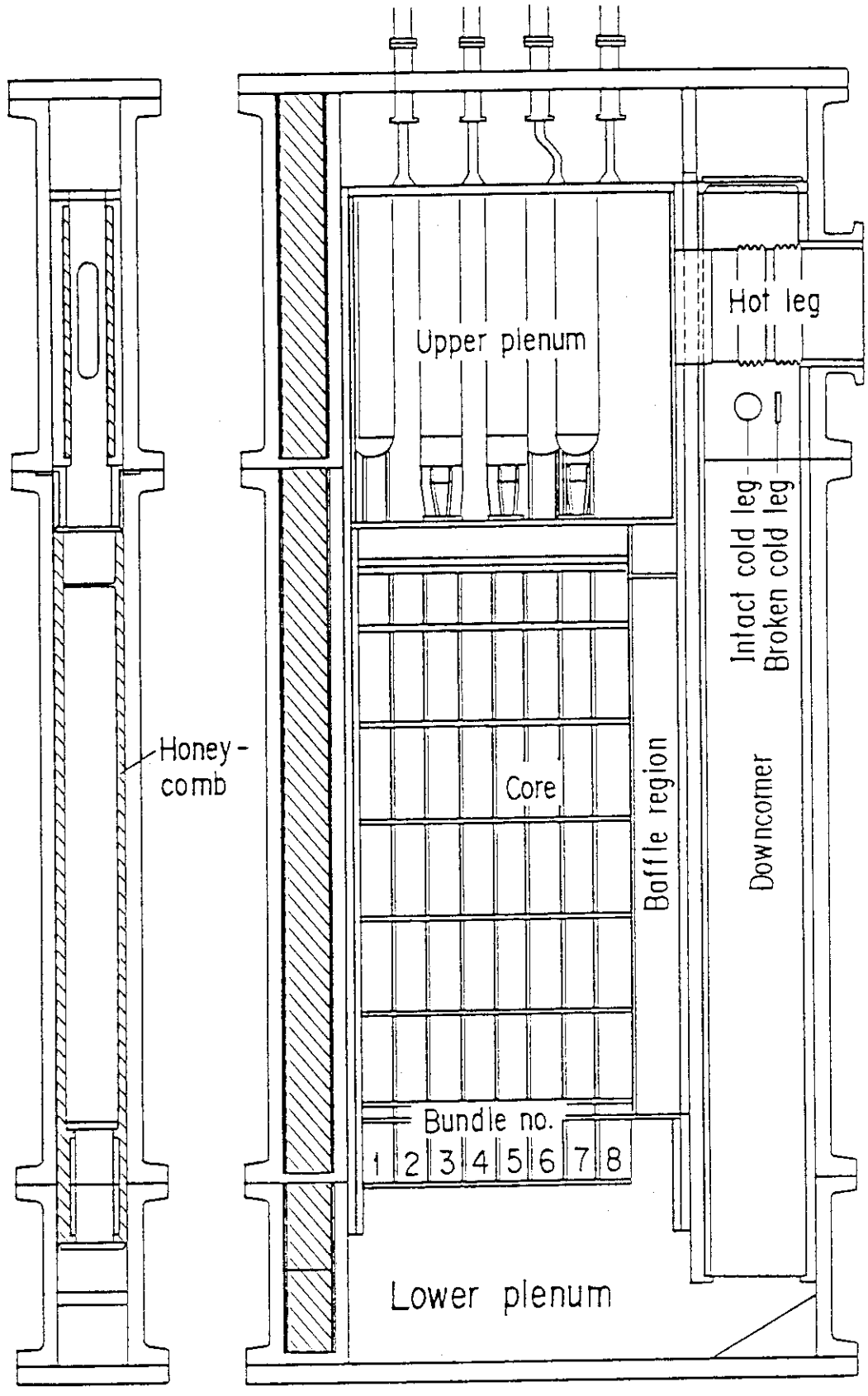

Fig. 2.2 Pressure vessel of SCTF Core-III

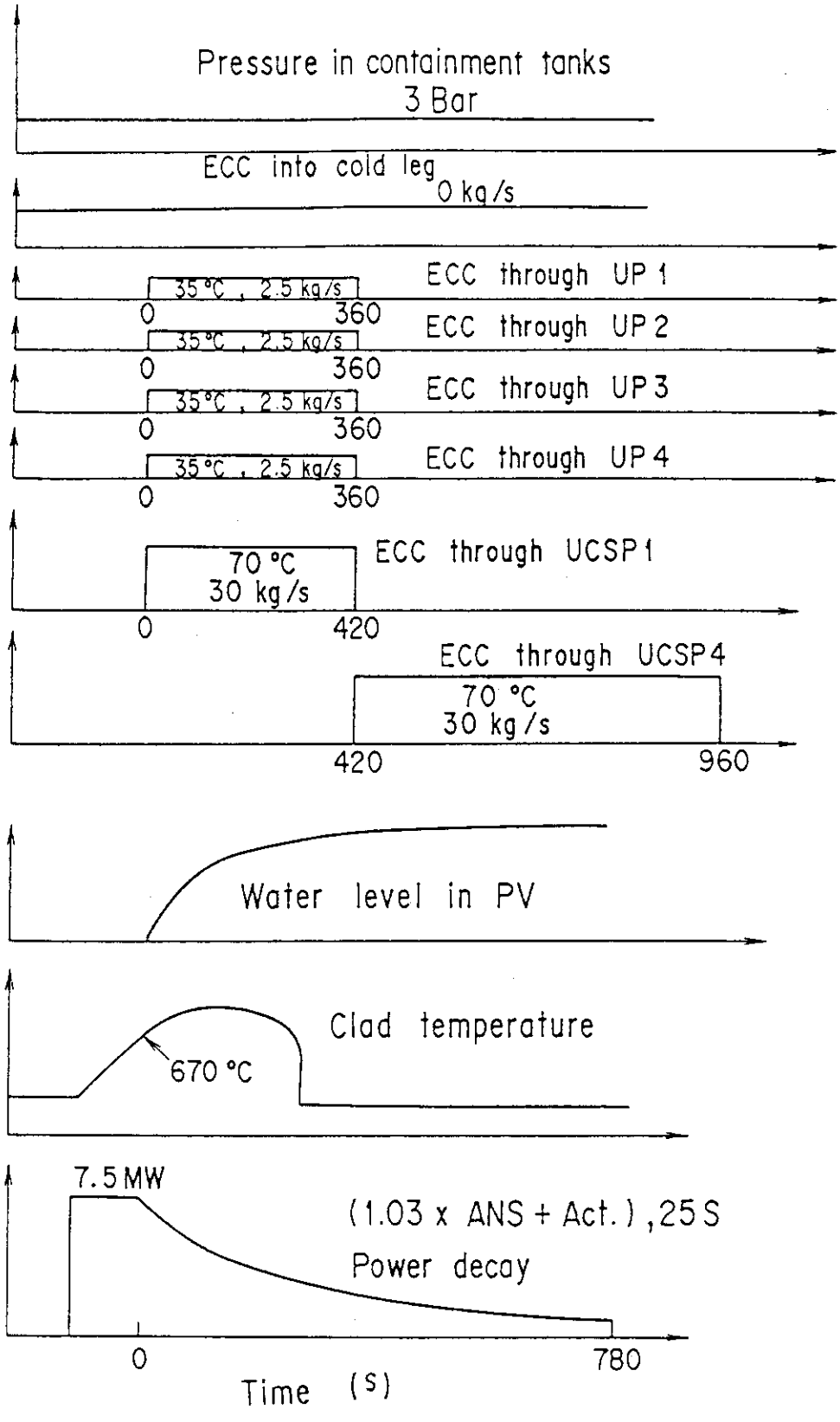

Fig. 2.3 Test Sequence of Test S3-SH1

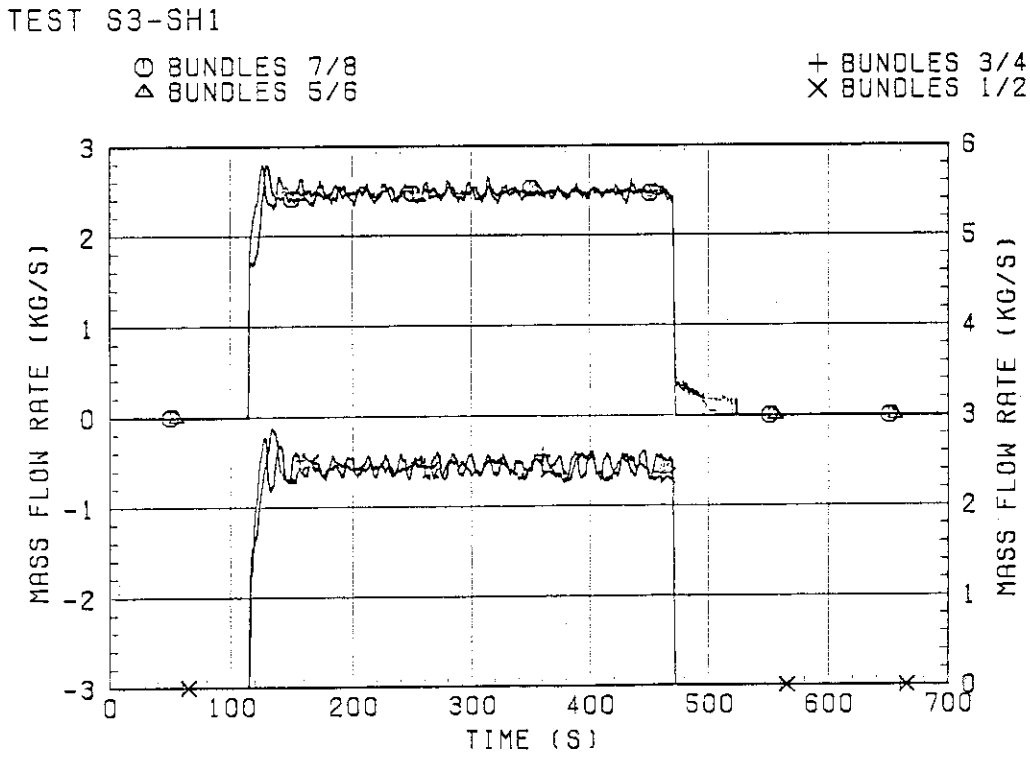

Fig. 3.1 ECC injection rates into upper plenum through top injection nozzles

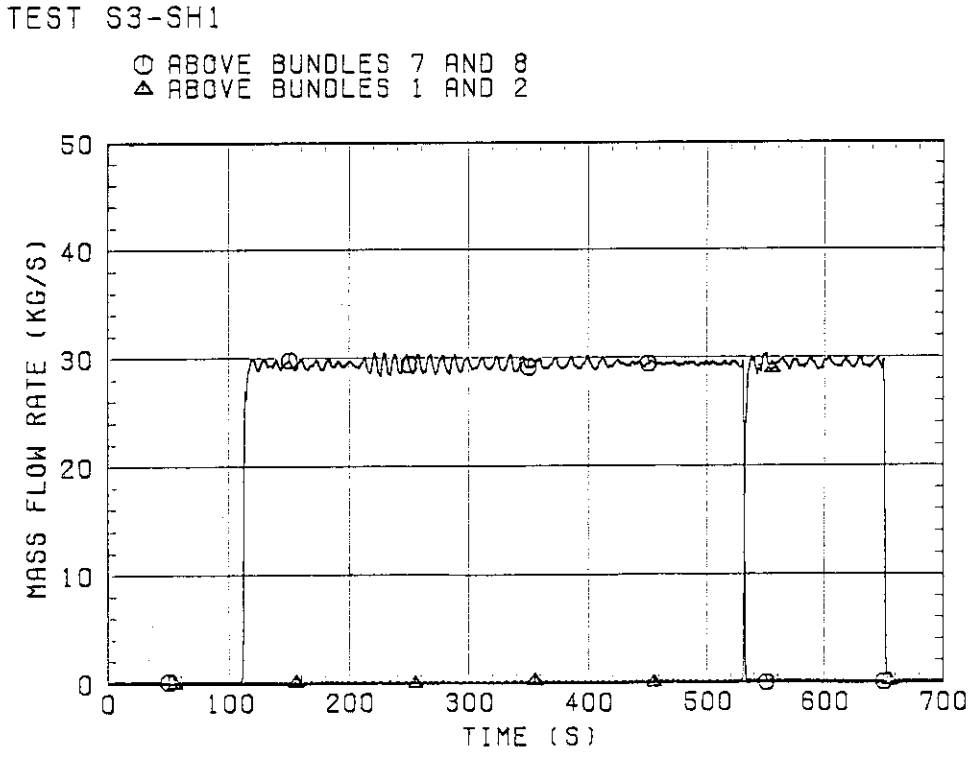

Fig. 3.2 ECC injection rates into upper plenum through side injection nozzles

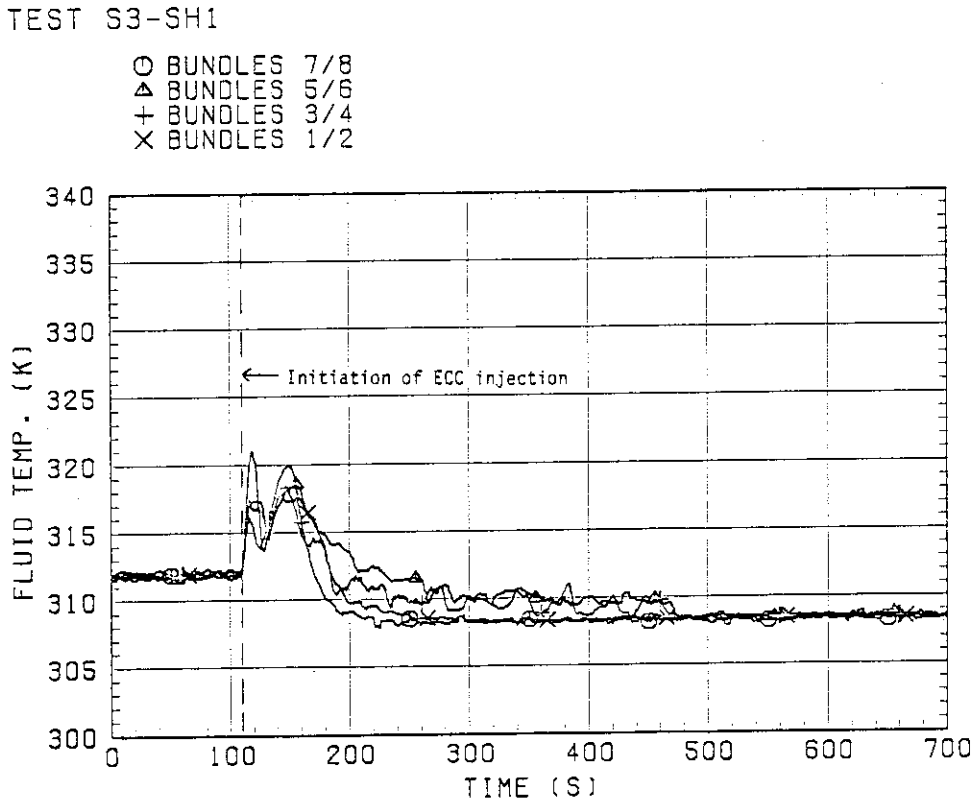

Fig. 3.3 Water temperatures for top injection

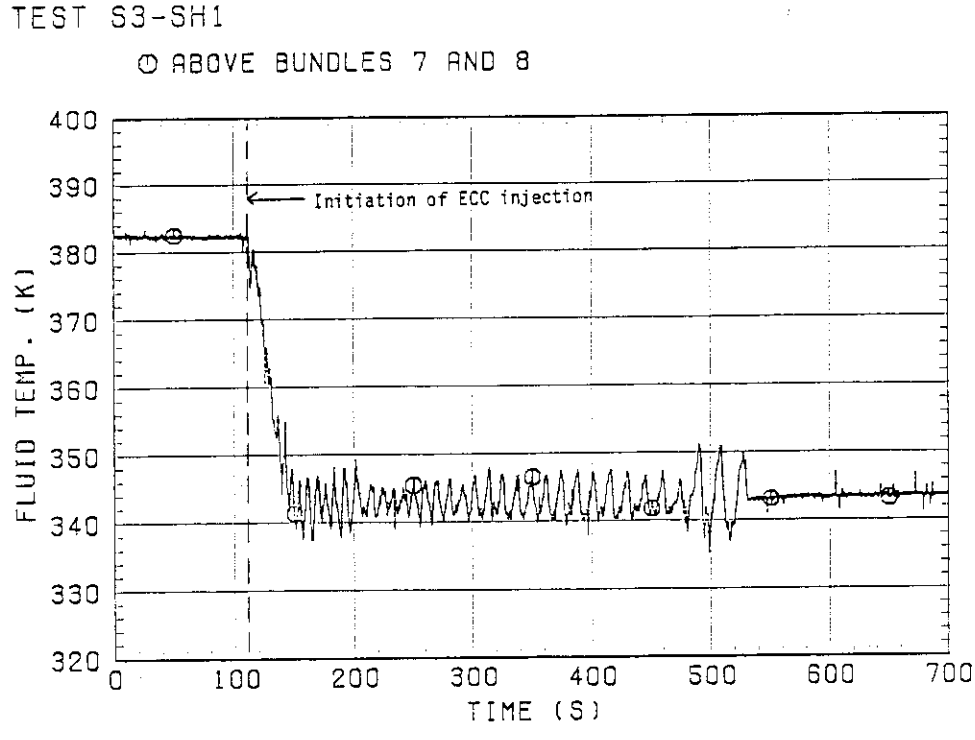

Fig. 3.4 Water temperatures for side injection

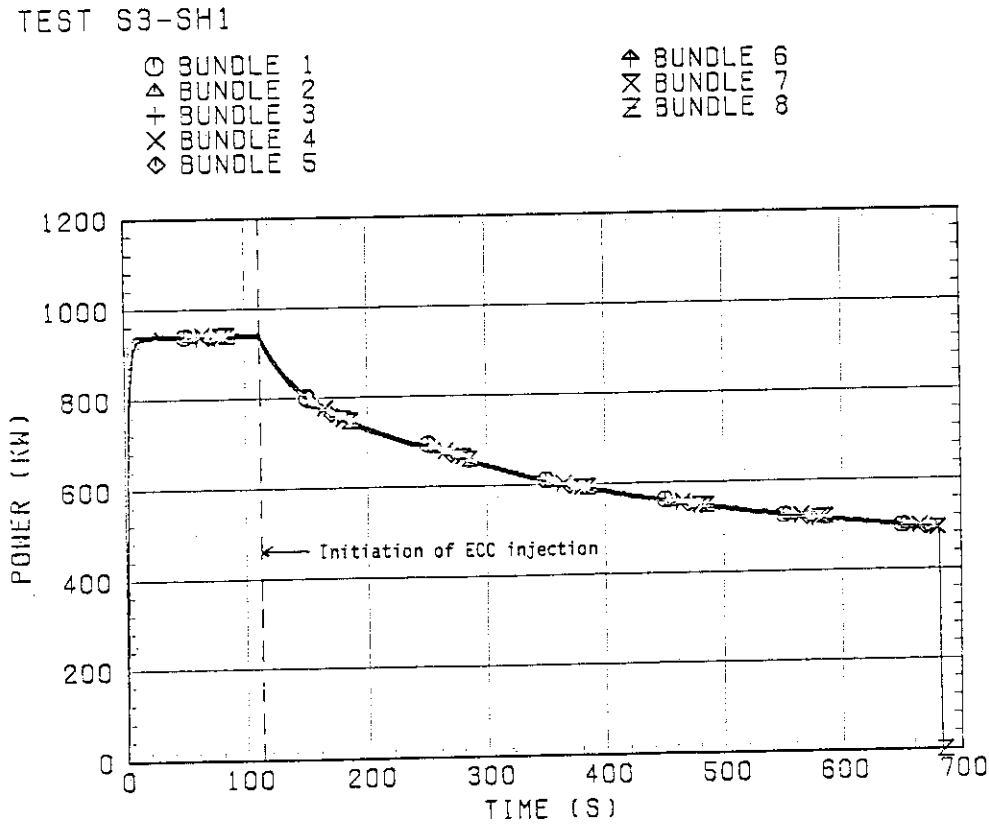

Fig. 3.5 Core heating power

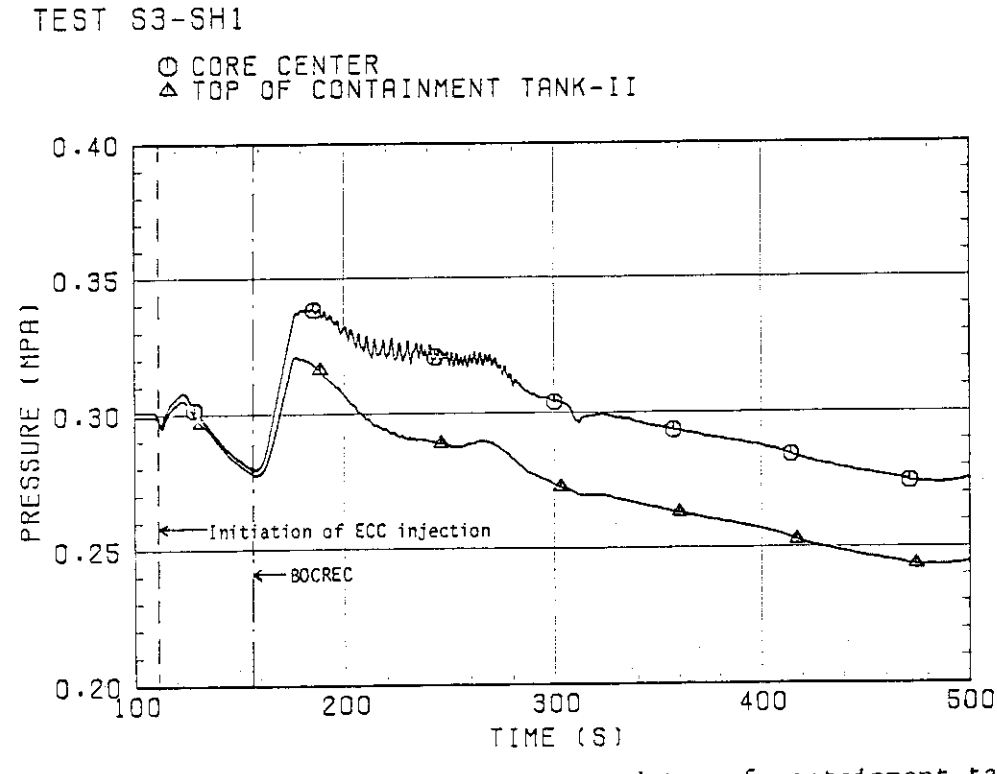

Fig. 3.6 Pressures at core center and top of containment tank-II

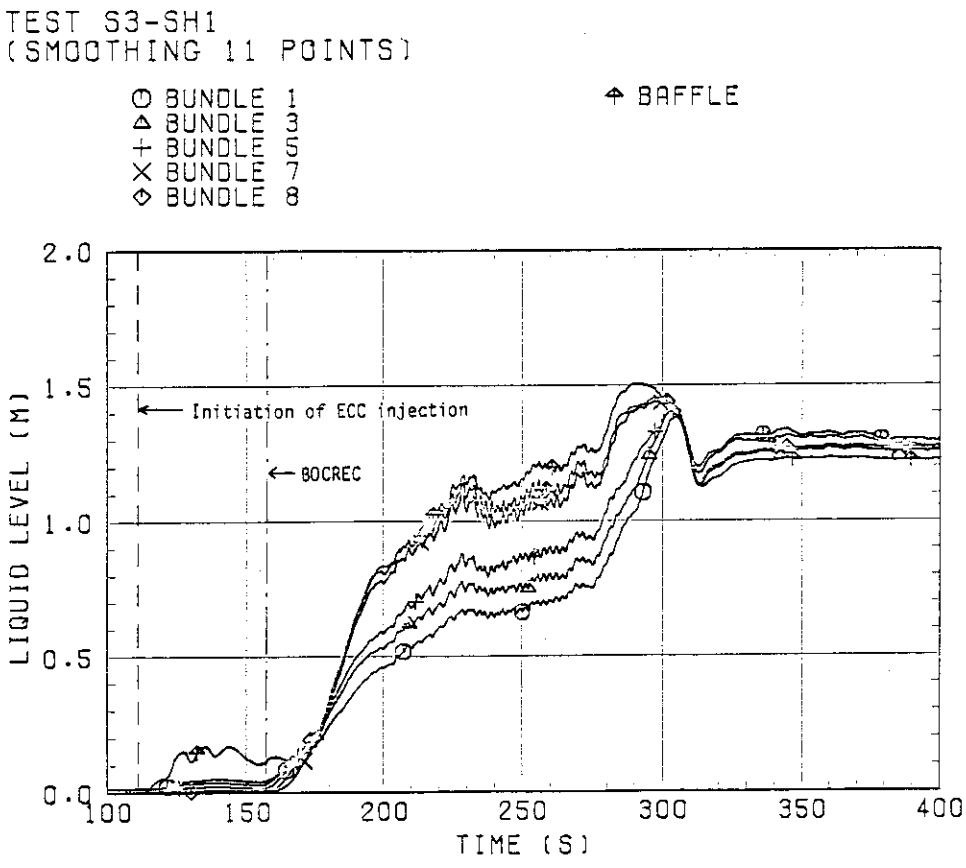

Fig. 3.7 Collapsed liquid level in upper plenum

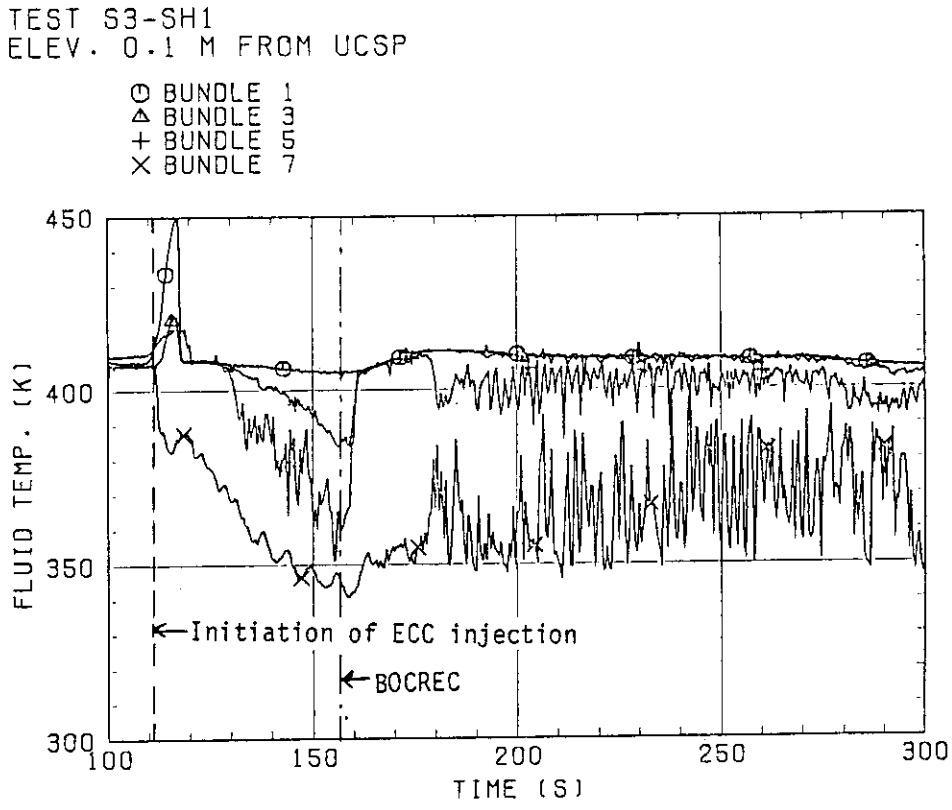

Fig. 3.8 Fluid temperatures in upper plenum at 0.1 m from UCSP

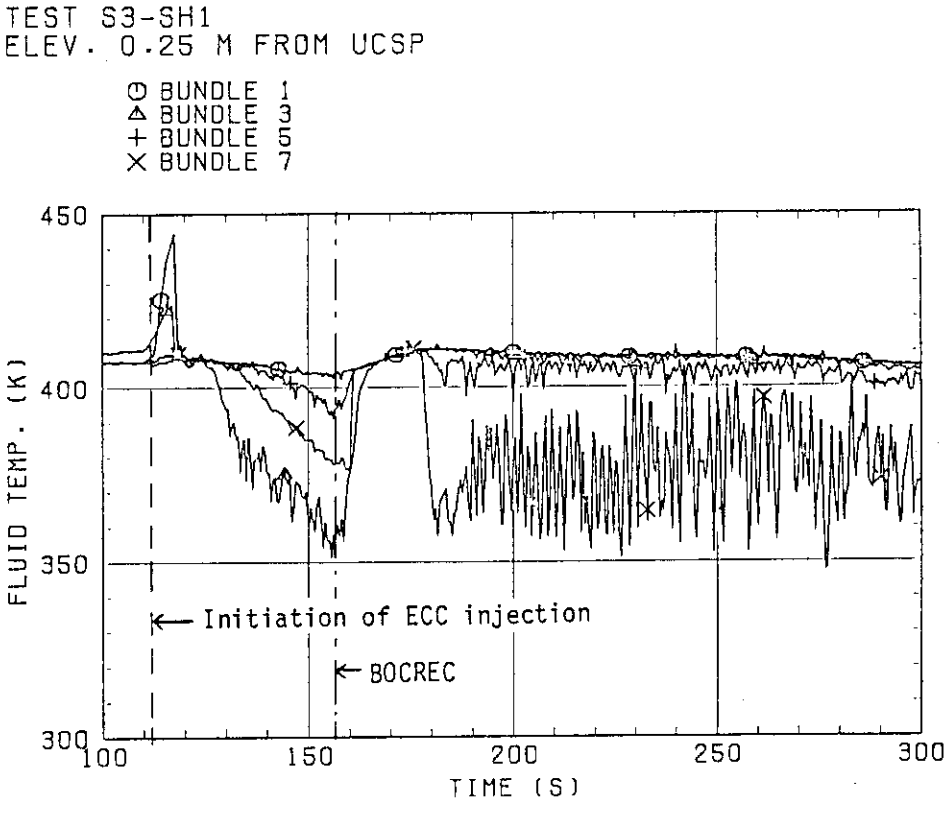

FIg. 3.9 Fluid temperatures in upper plenum at 0.25 m from UCSP

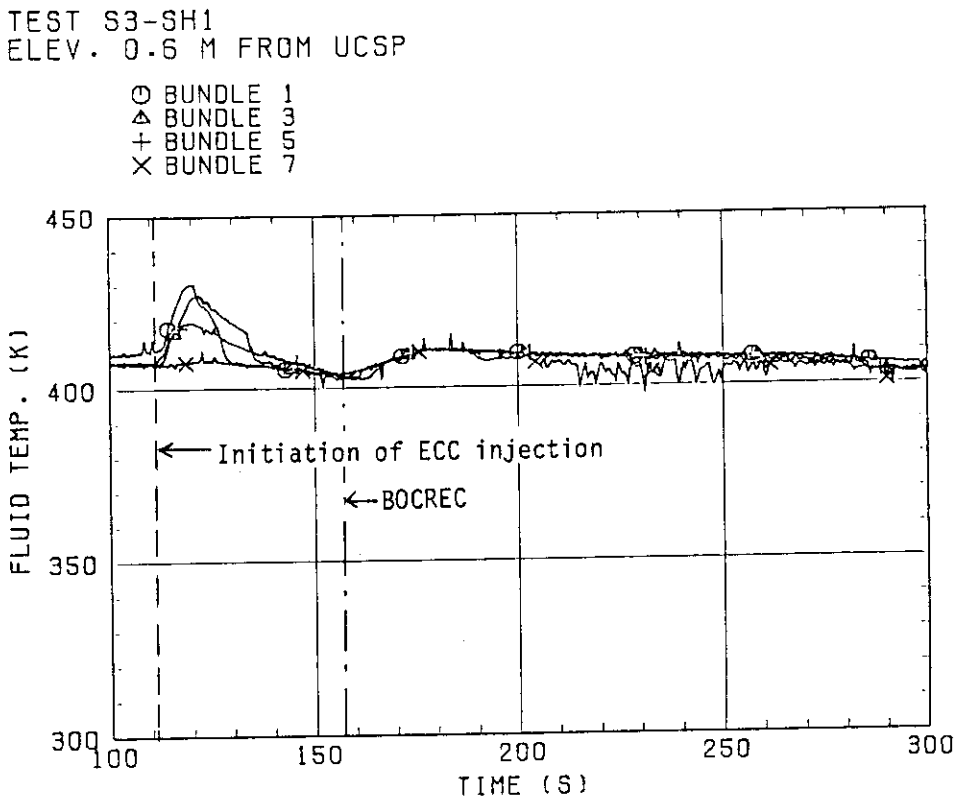

Fig. 3.10 Fluid temperatures in upper plenum at 0.6 m from UCSP

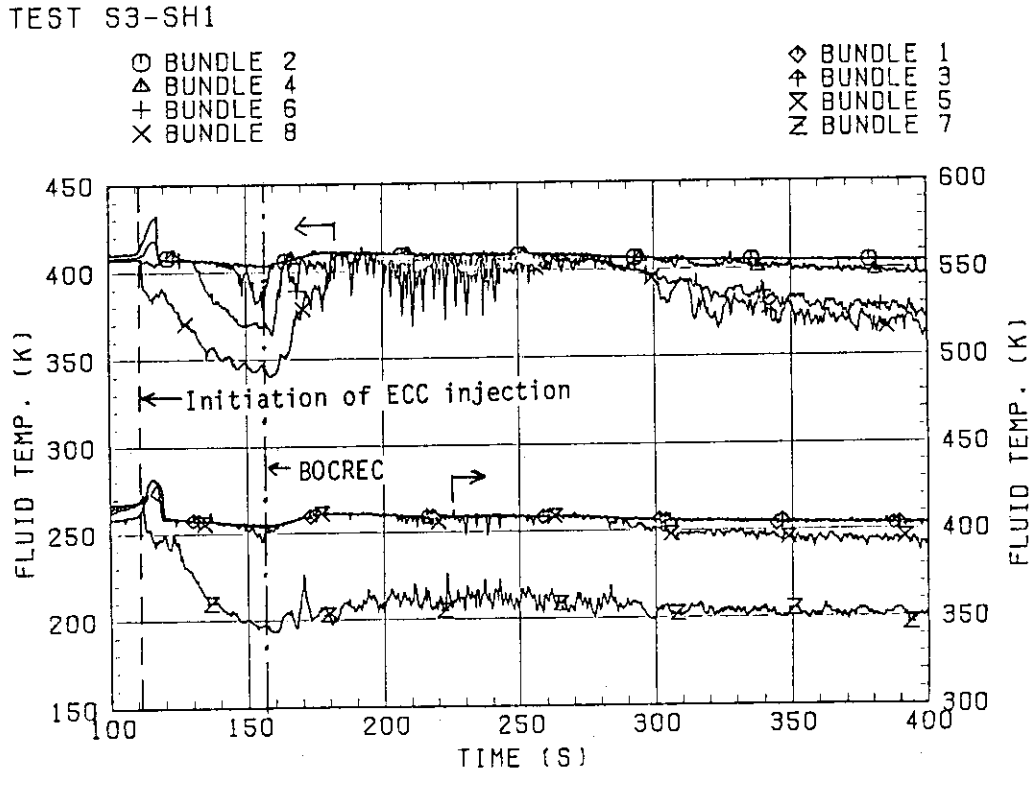

Fig. 3.11 Fluid temperatures at UCSP holes

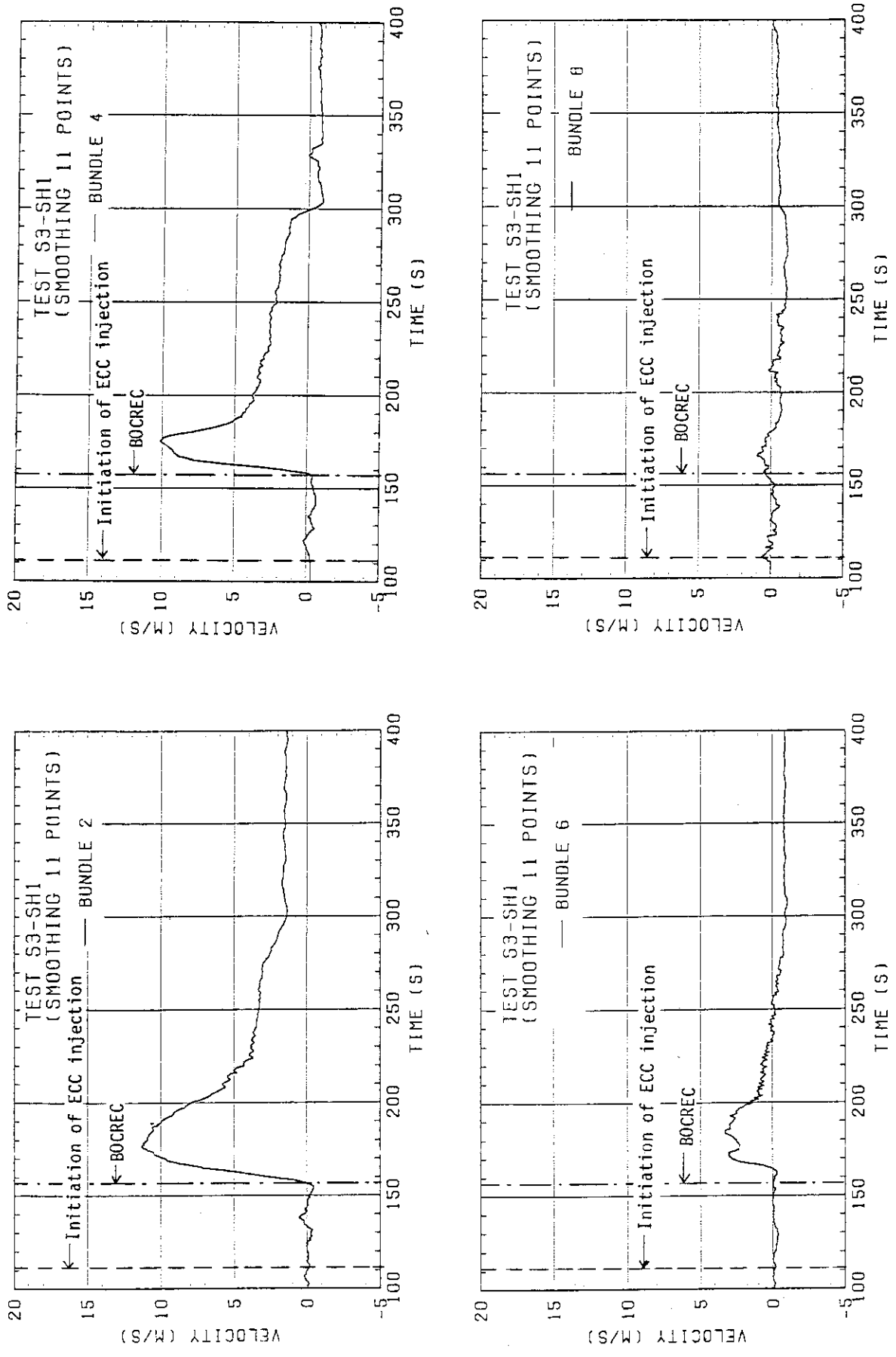

Fig. 3.12 Steam velocities at UCSP holes

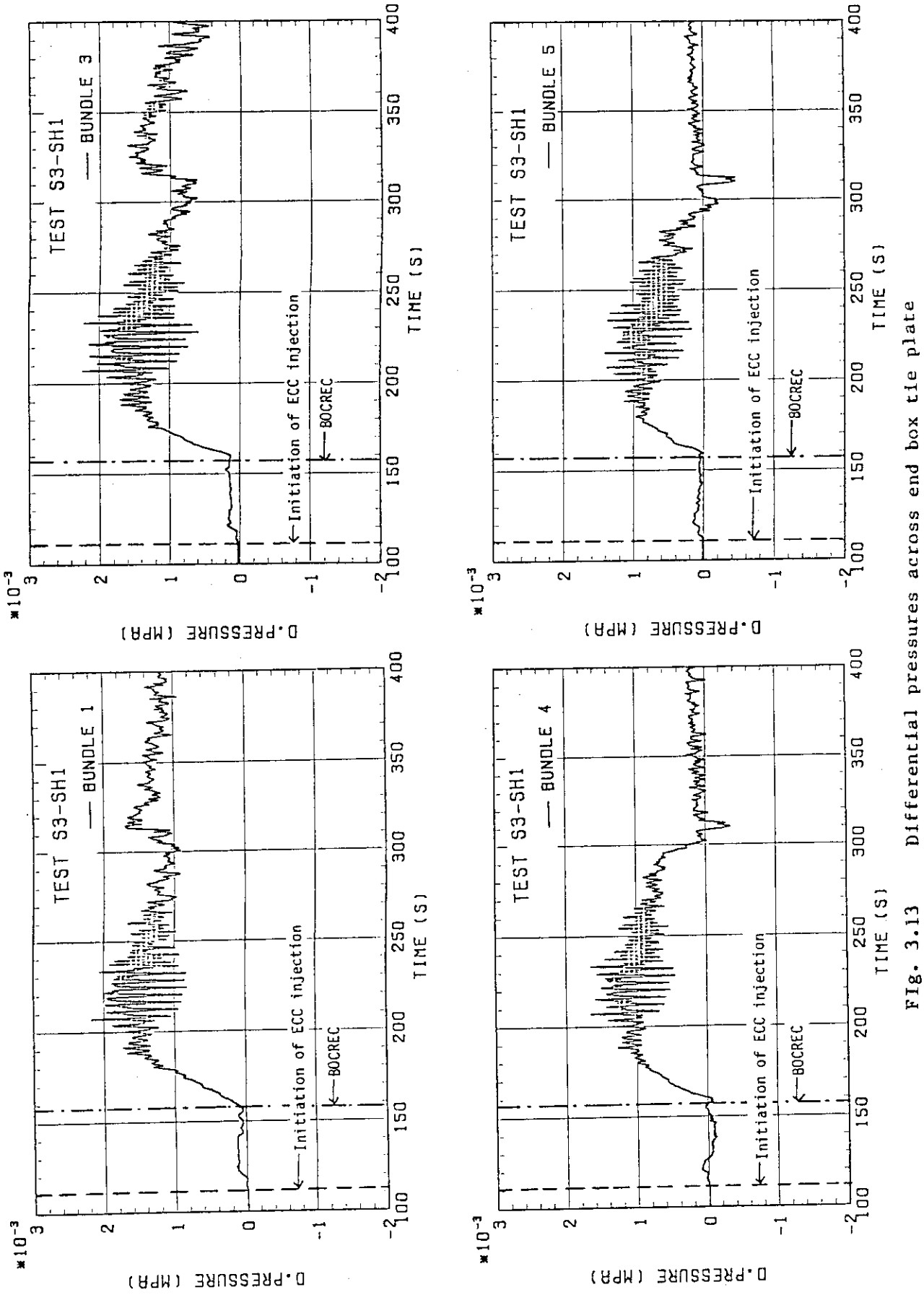

FIg. 3.13 Differential pressures across end box tie plate

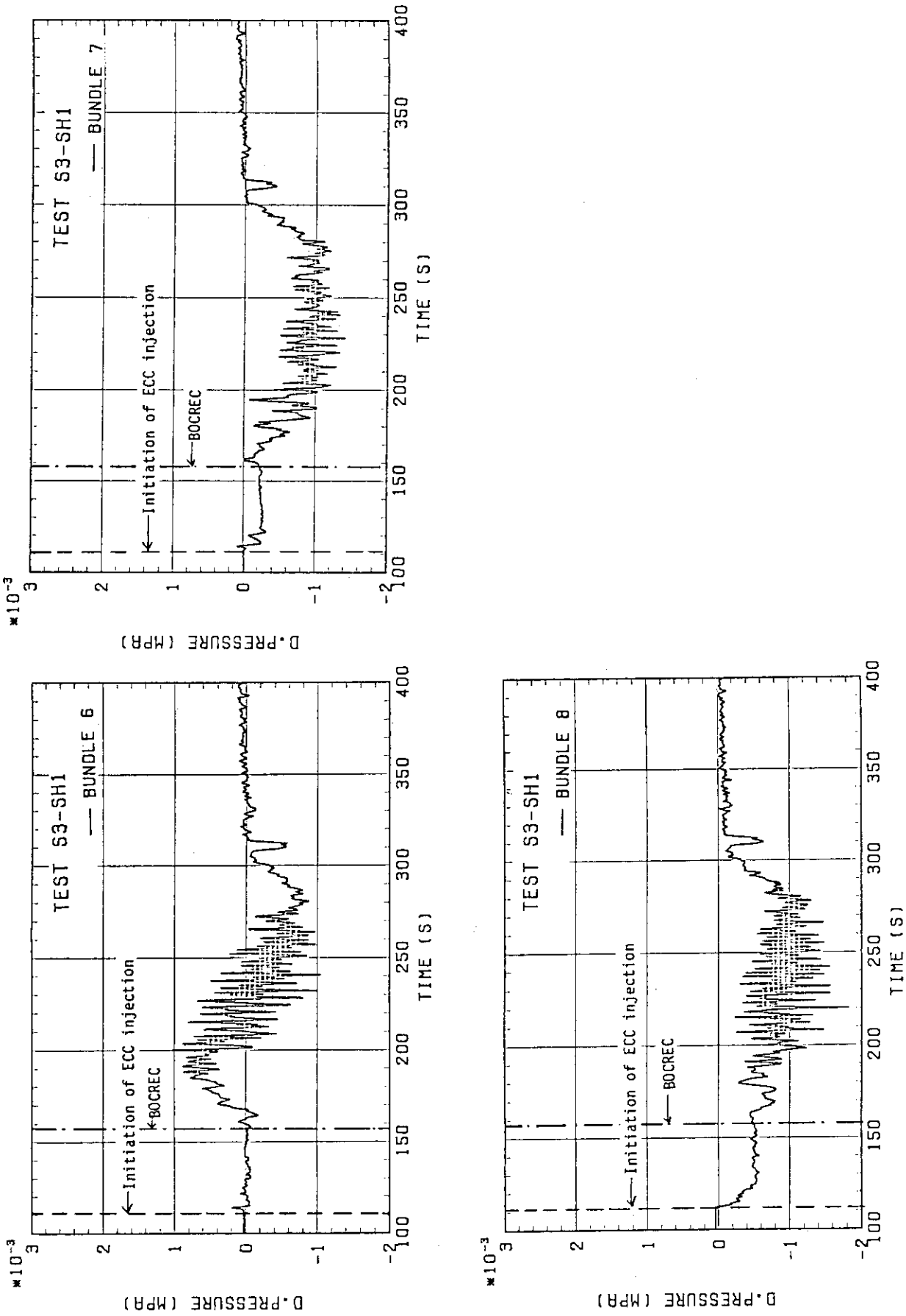

Fig. 3.13(continue)

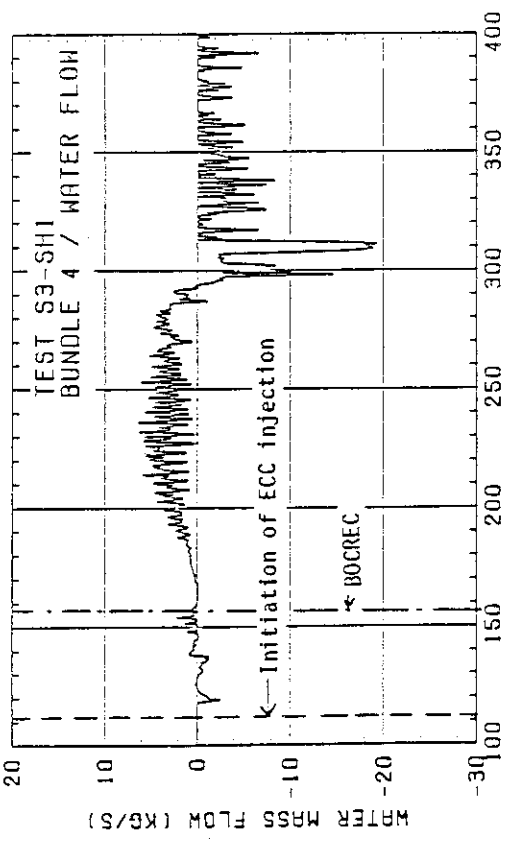

Fig. 3.14(b) Water mass flow rate at end box tie plate in Bundle 4

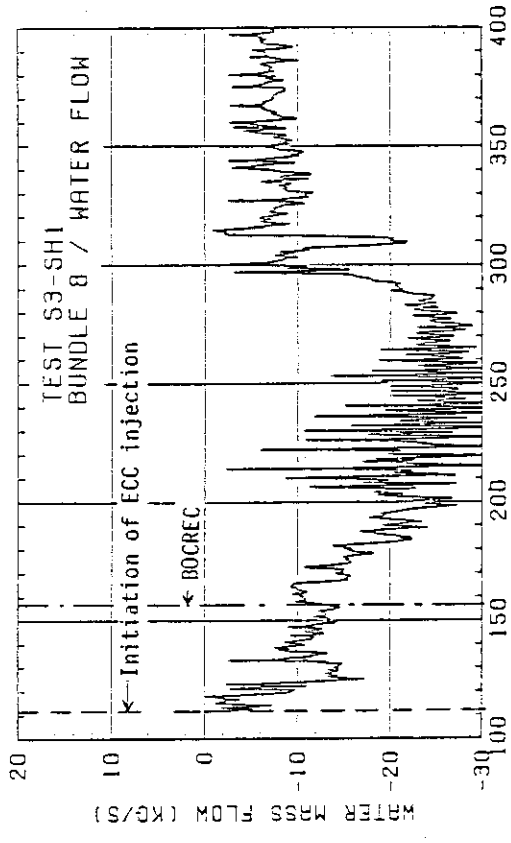

Fig. 3.14(d) Water mass flow rate at end box tie plate in Bundle 8

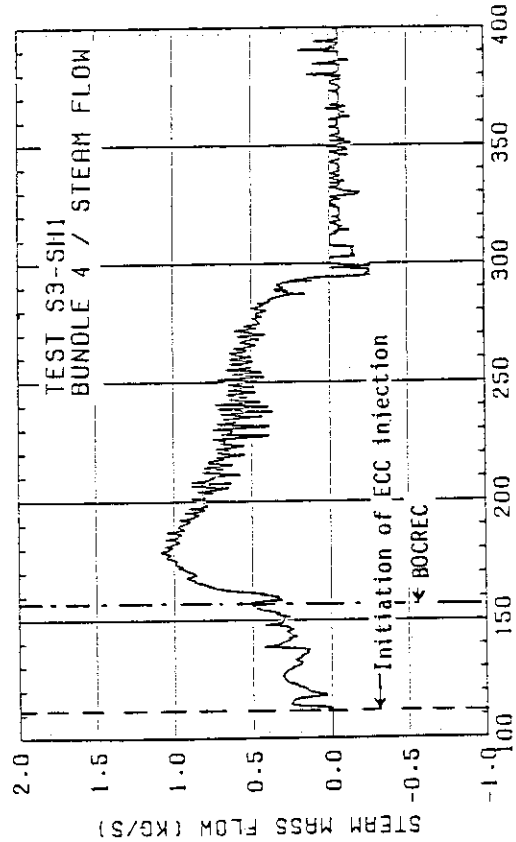

Fig. 3.14(a) Steam mass flow rate at end box tie plate in Bundle 4

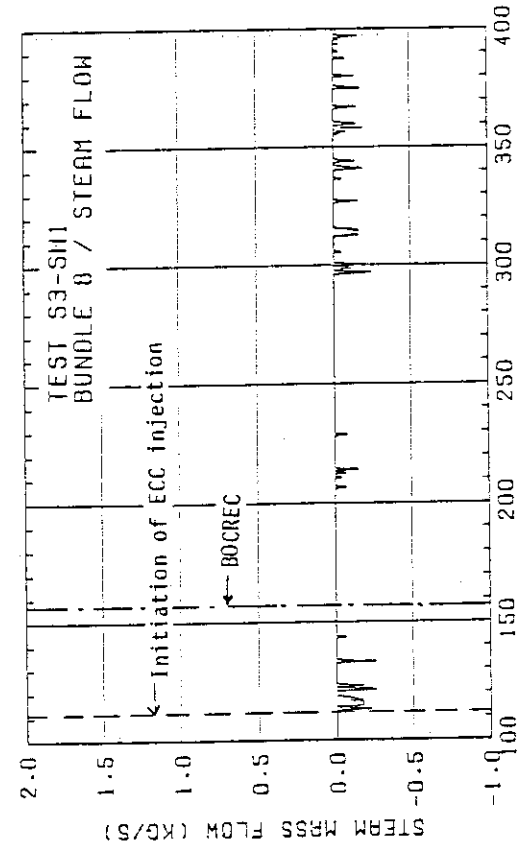

Fig. 3.14(c) Steam mass flow rate at end box tie plate in Bundle 8

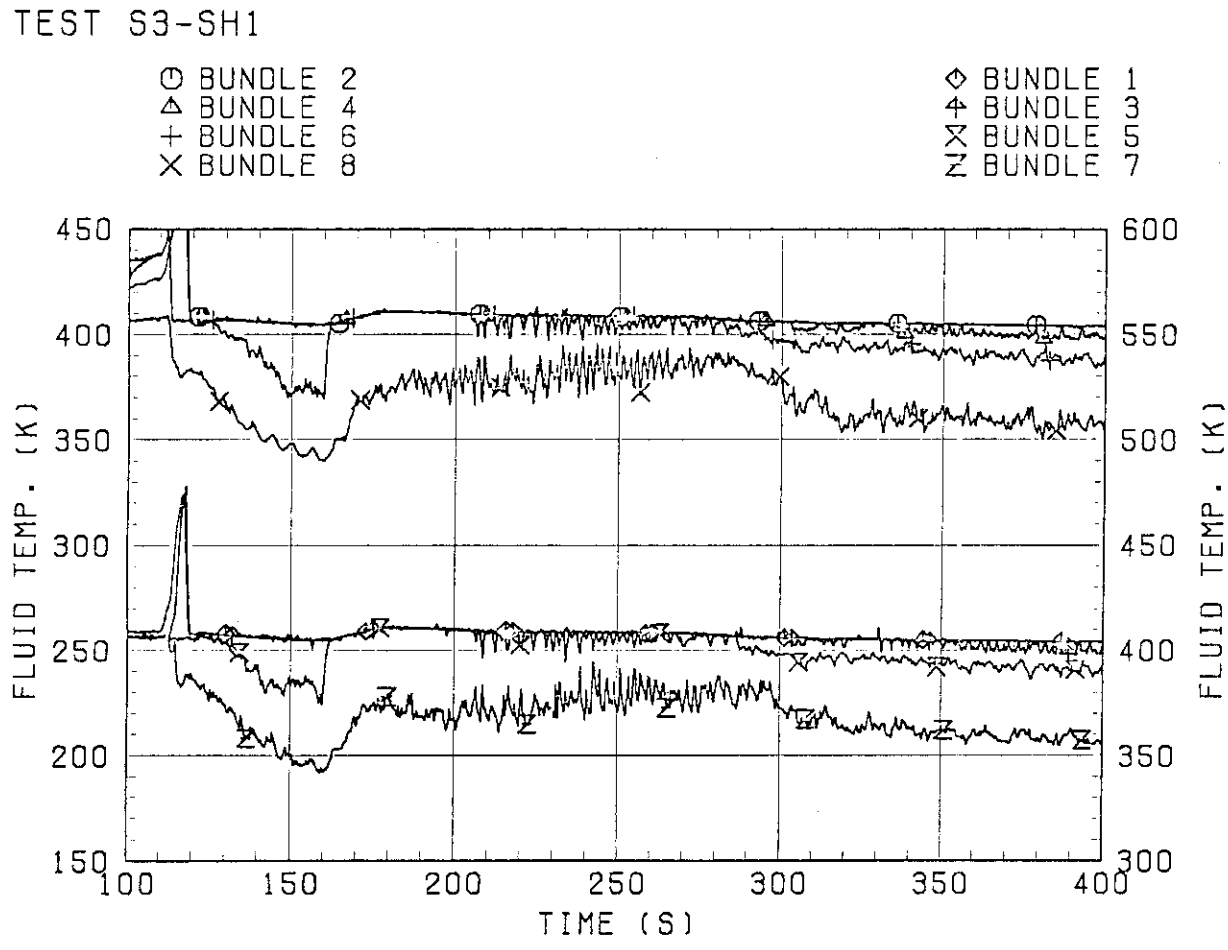

Fig. 3.15 Fluid temperatures just below end box tie plate

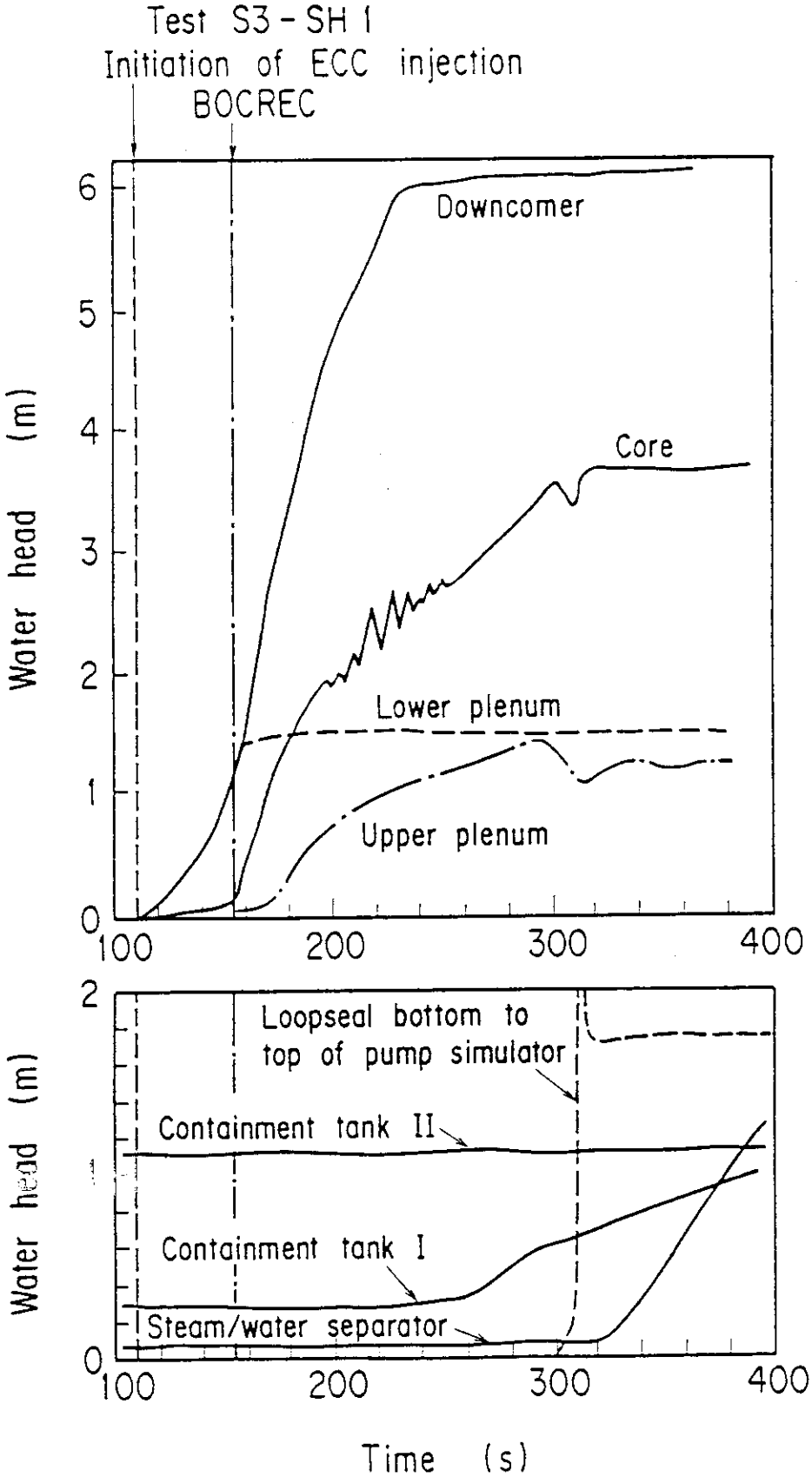

Fig. 3.16 Water accumulation in pressure vessel, containment tanks I and II, pump simulator and steam/water separator.

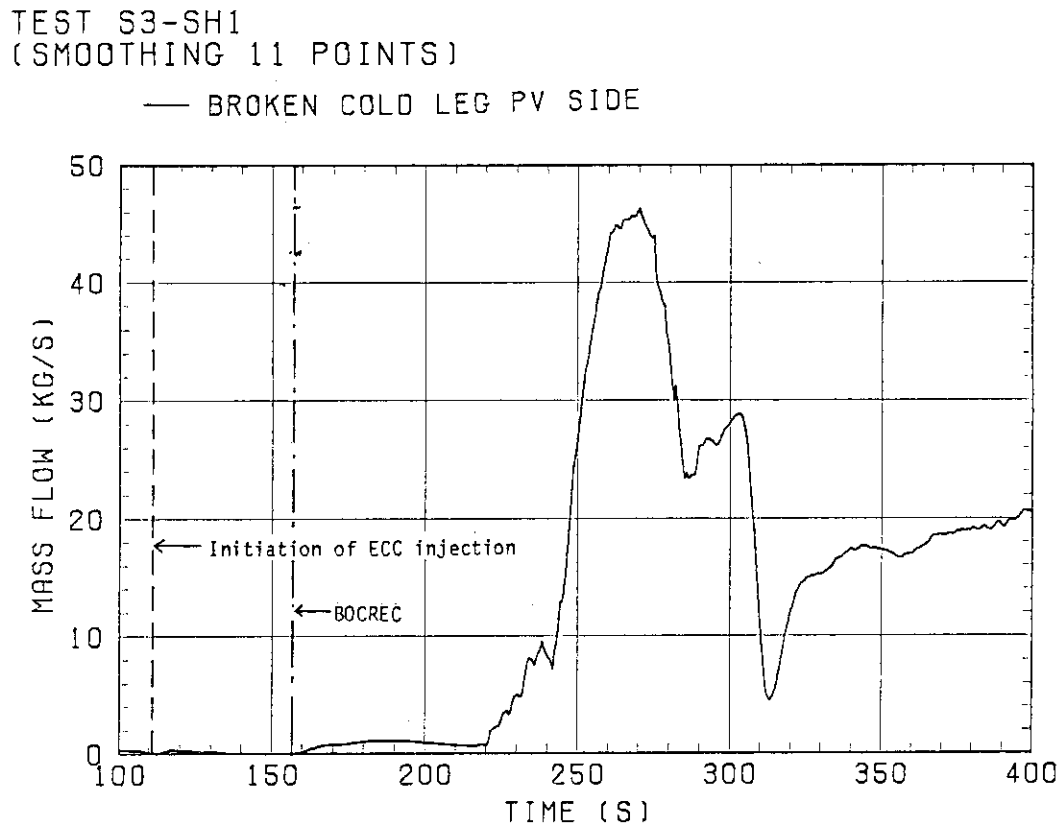

Fig. 3.17 Mass flow rate in broken cold leg pressure vessel side

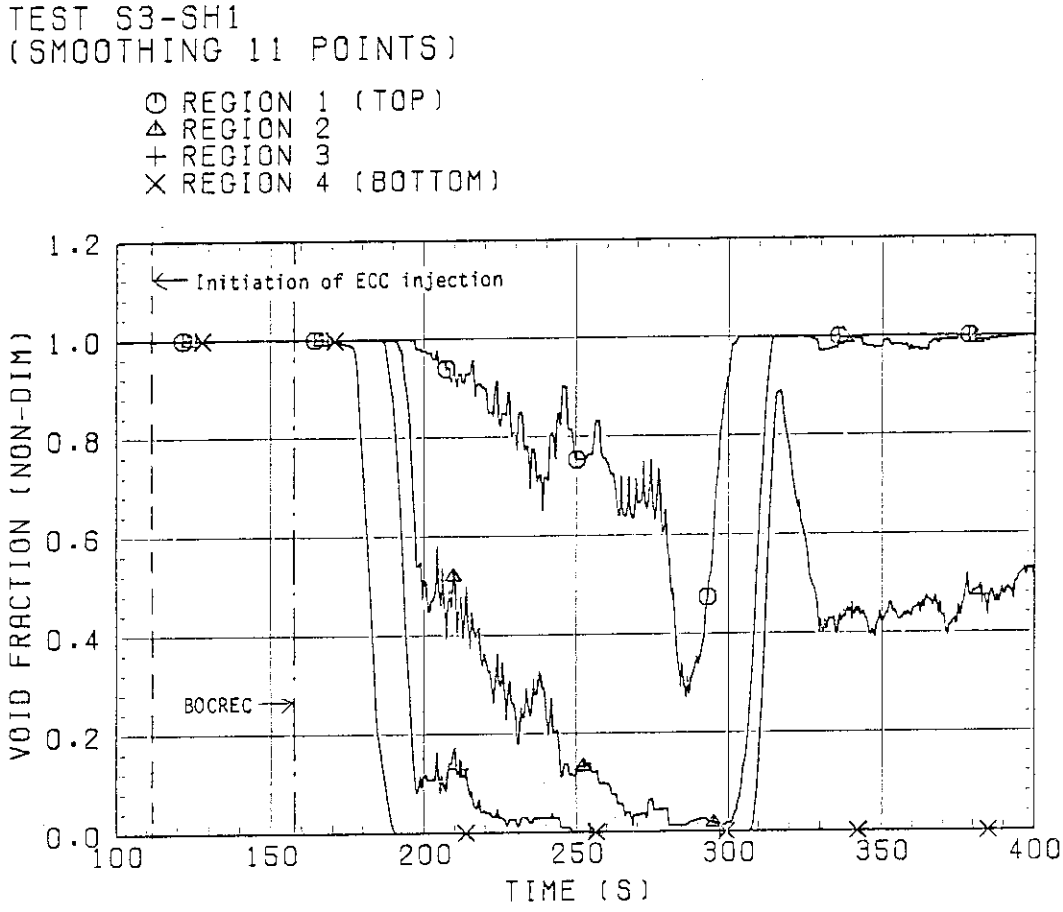

Fig. 3.18 Void fractions in 4 regions of hot leg

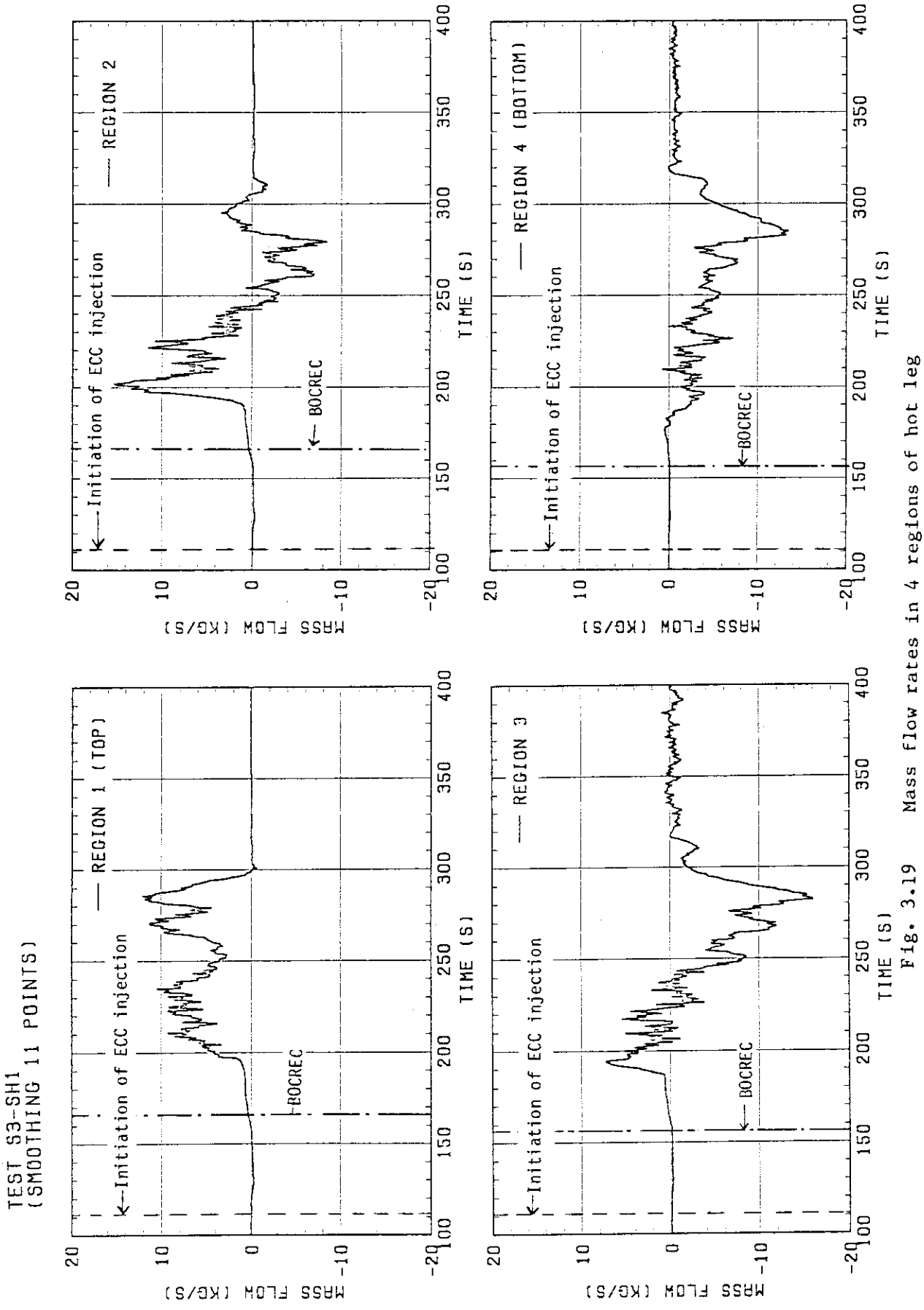

Fig. 3.19 Mass flow rates in 4 regions of hot leg

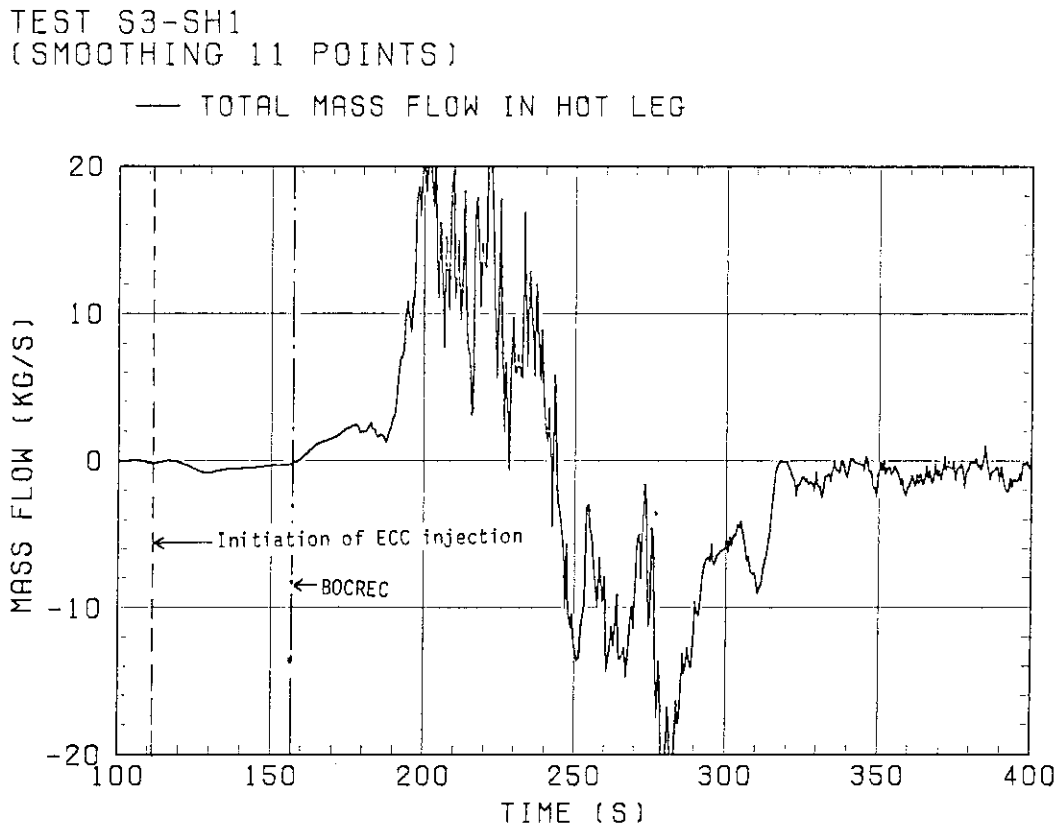

Fig. 3.20 Total mass flow rate in hot leg

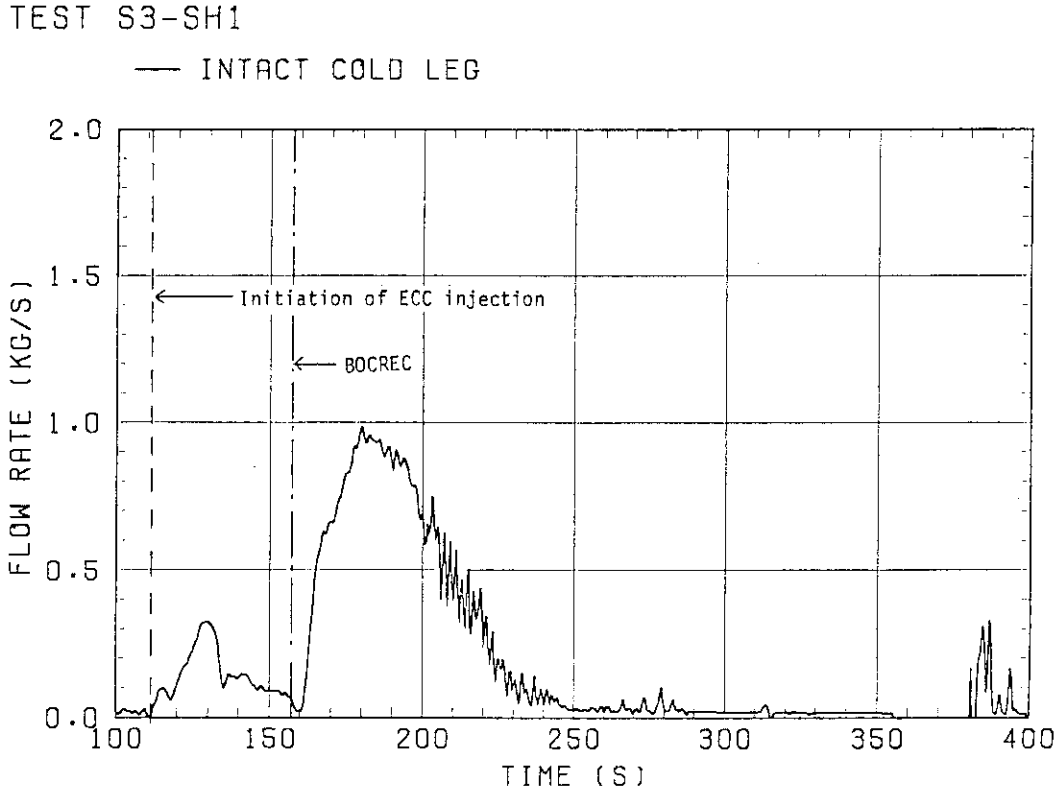

Fig. 3.21 Mass flow rate in intact cold leg

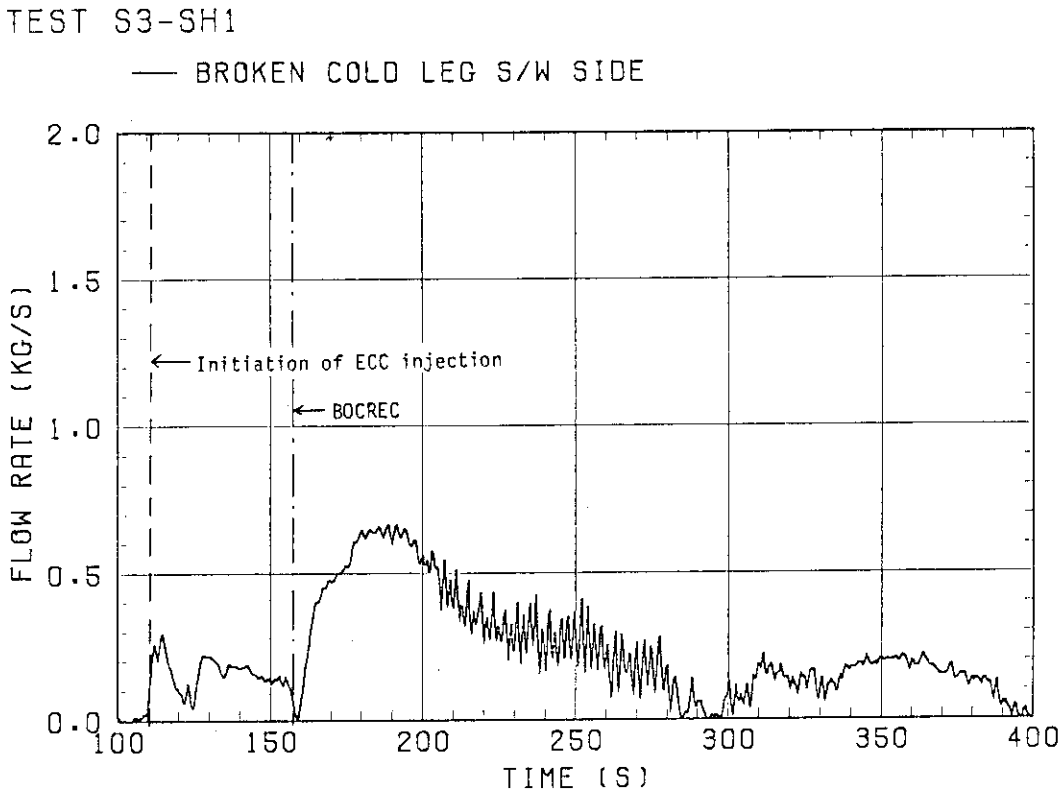

Fig. 3.22 Mass flow rate in broken cold leg steam/water separator side

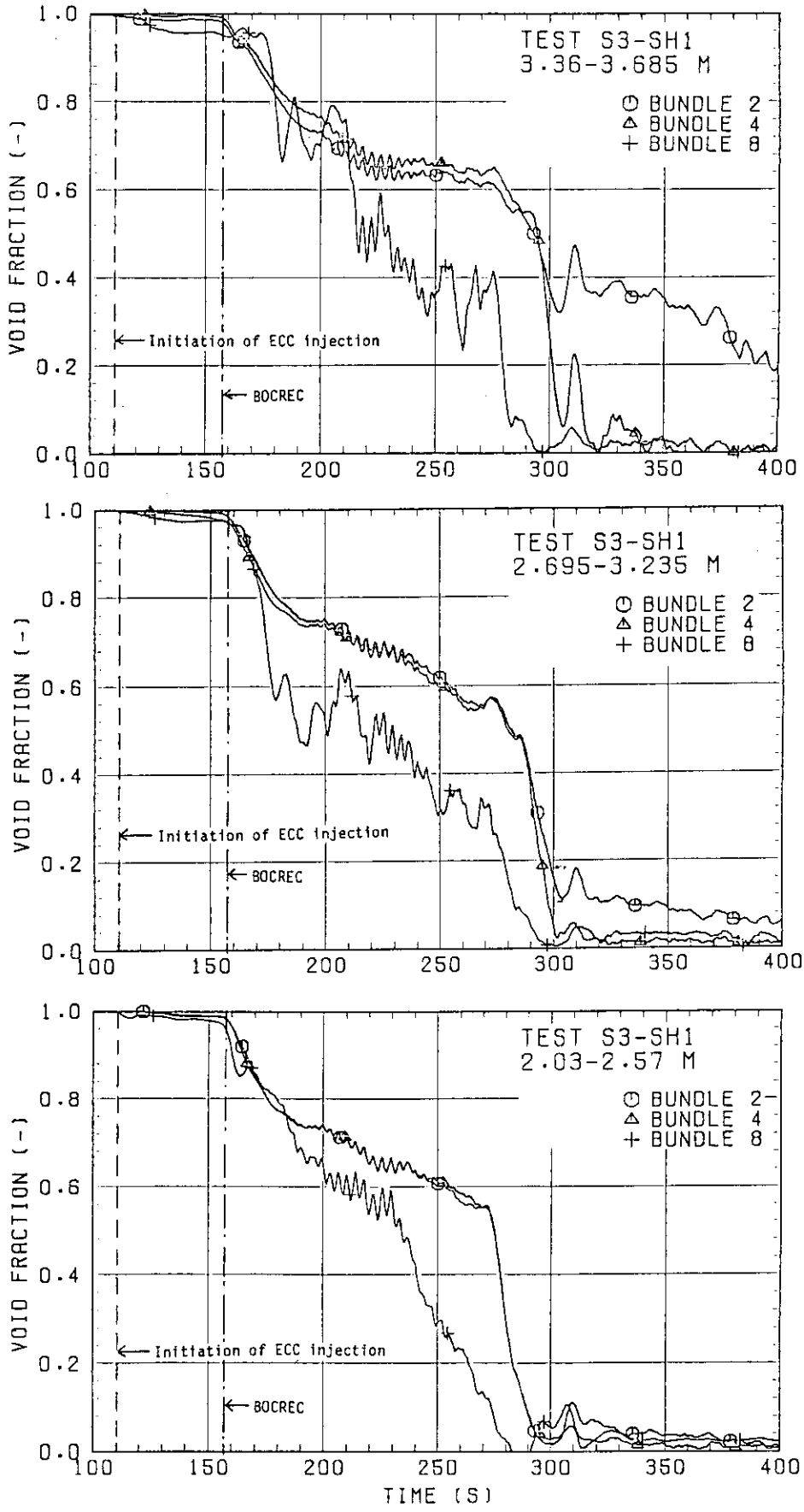

Fig. 3.23 Void fractions in core measured with D/P cells

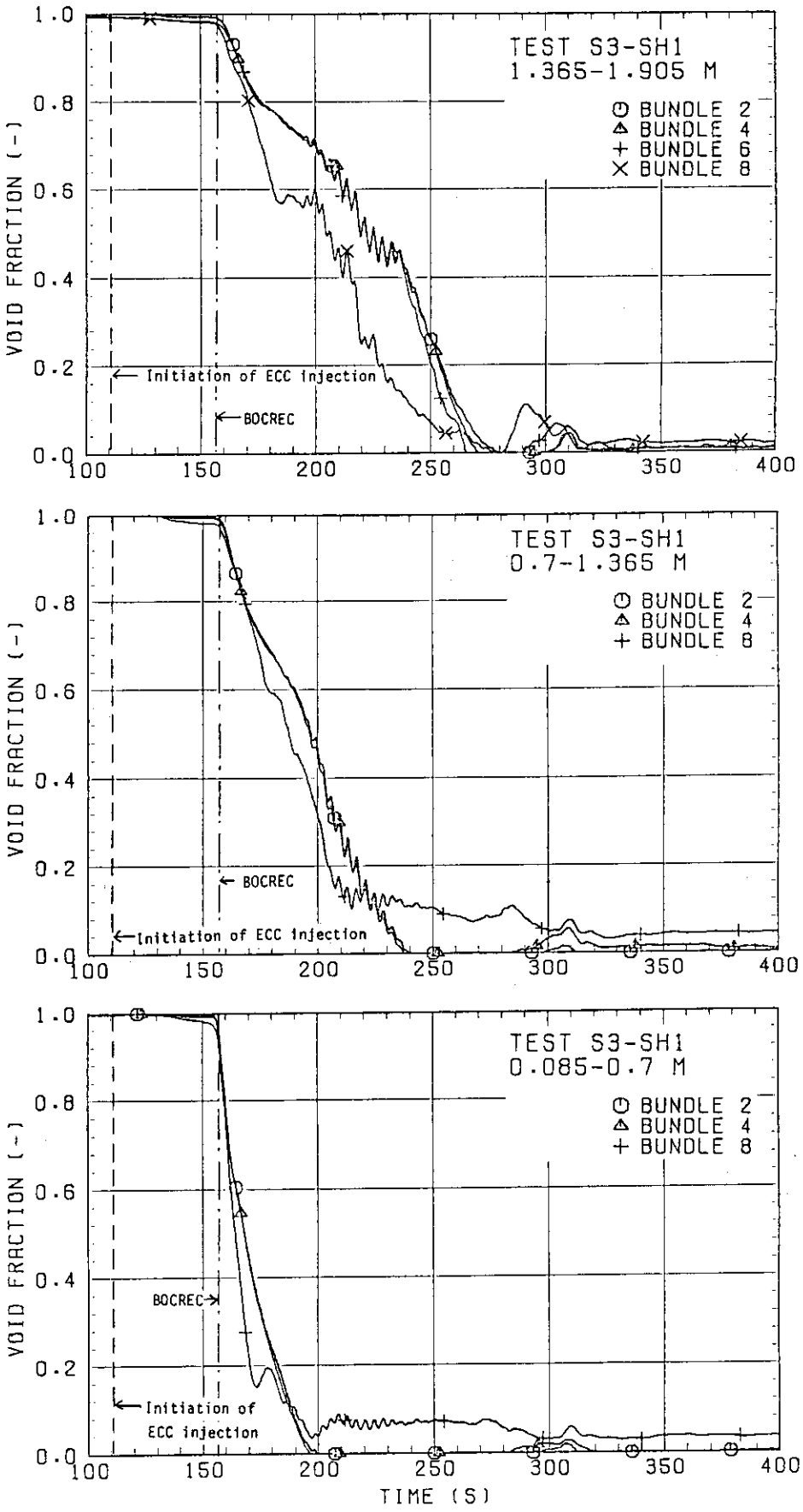

Fig. 3.23 (continue)

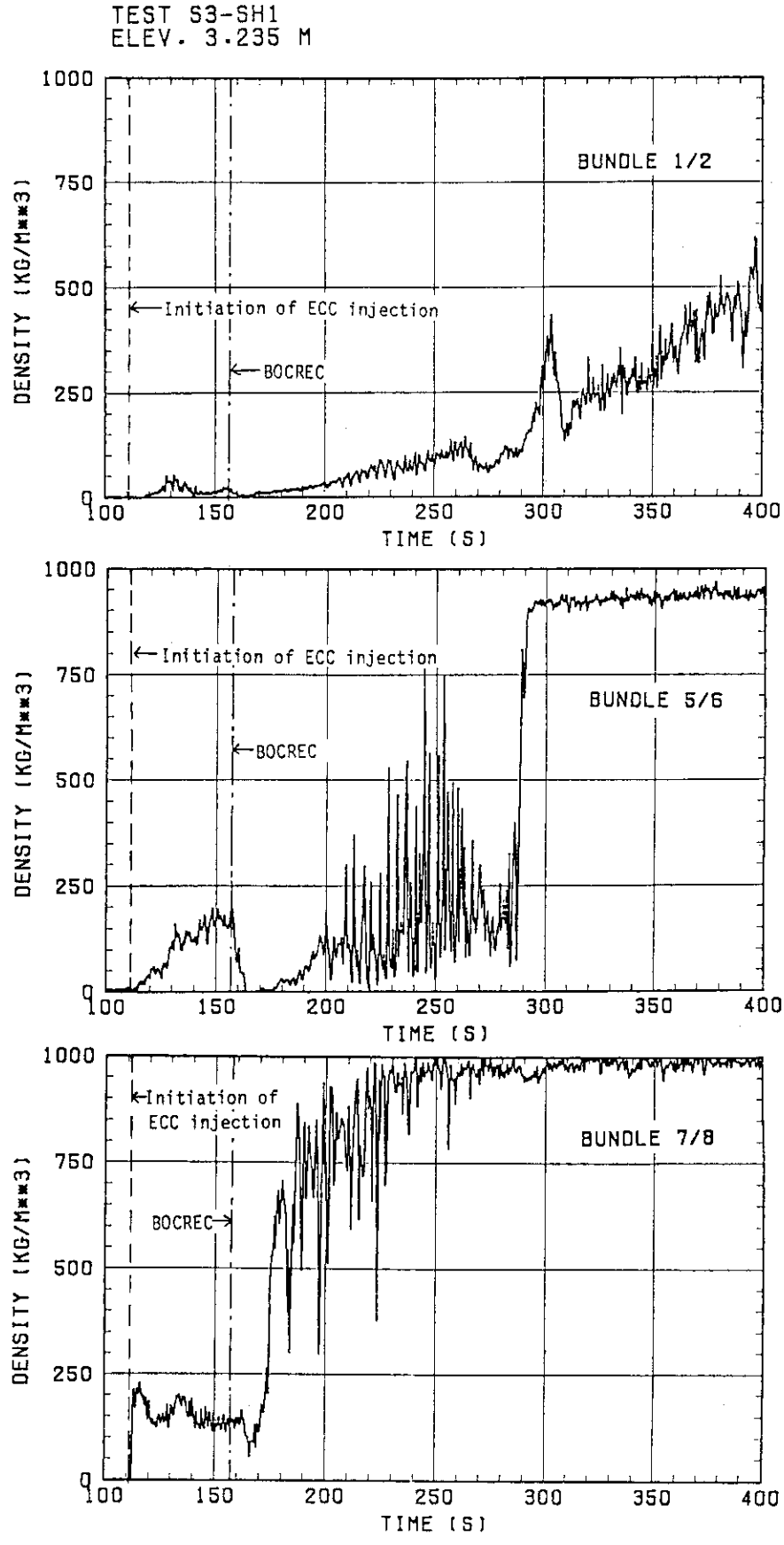

Fig. 3.24 Fluid densities in core measurd with γ-densitometers

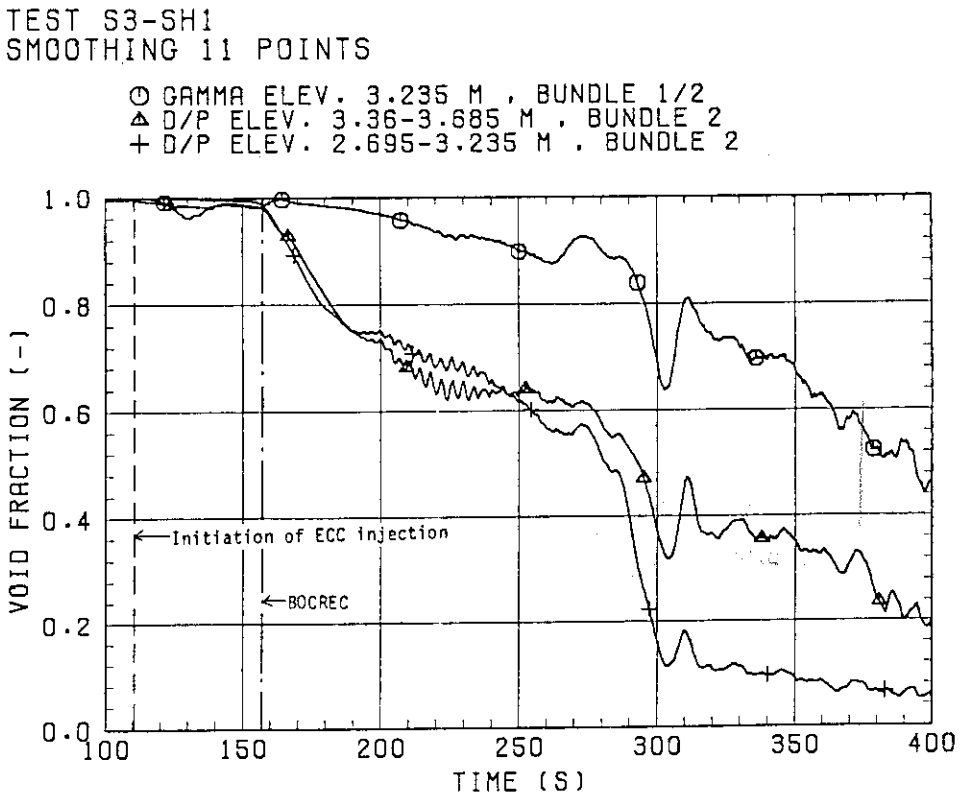

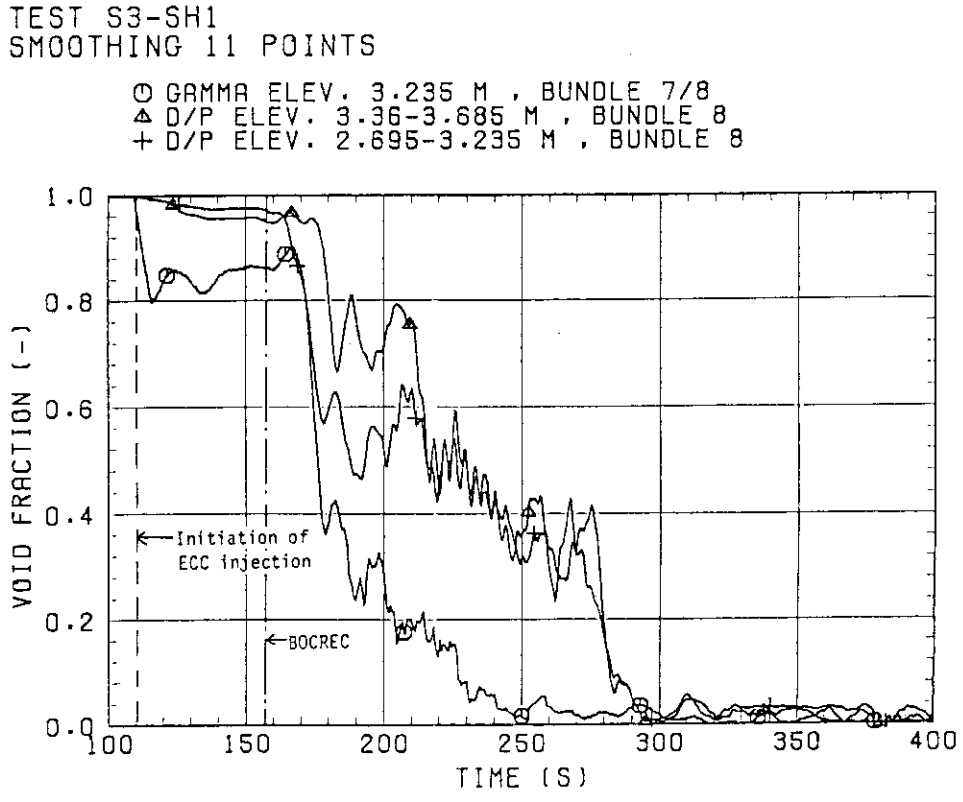

Fig. 3.25 Comparison of void fractions measurd with D/P cells and γ-densitometers

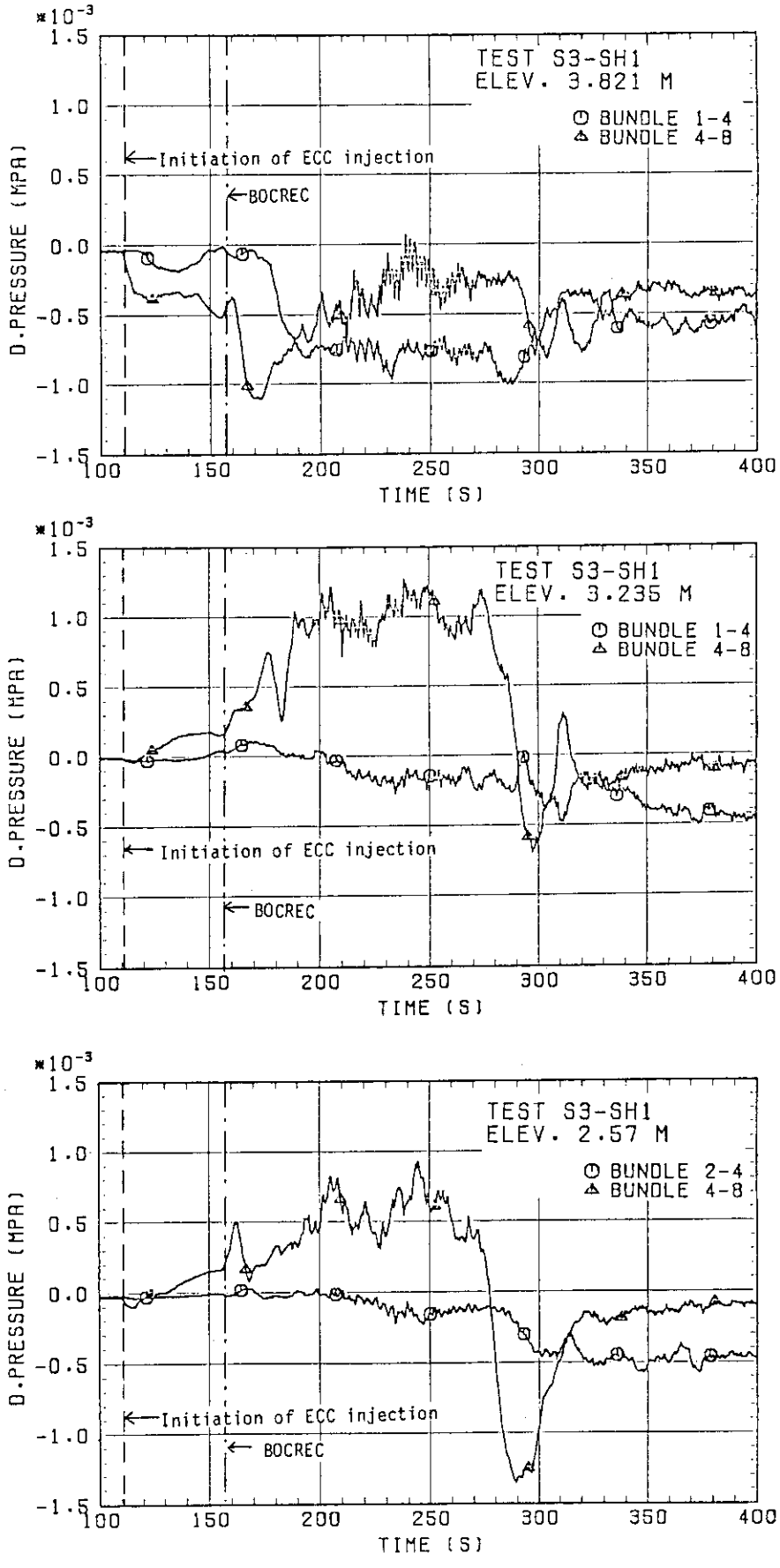

Fig. 3.26 Horizontal differential pressures in core

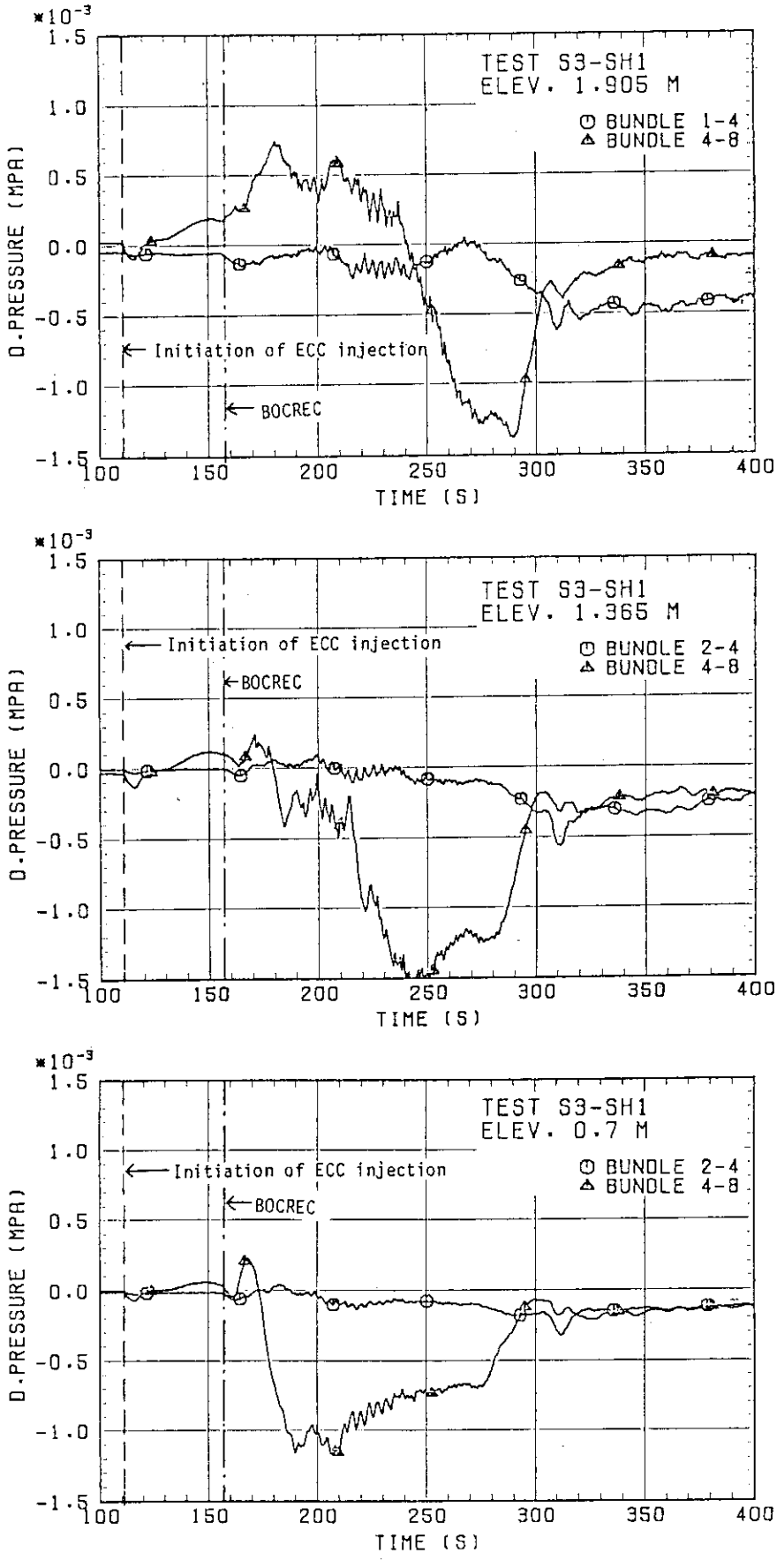

Fig. 3.26 (continue)

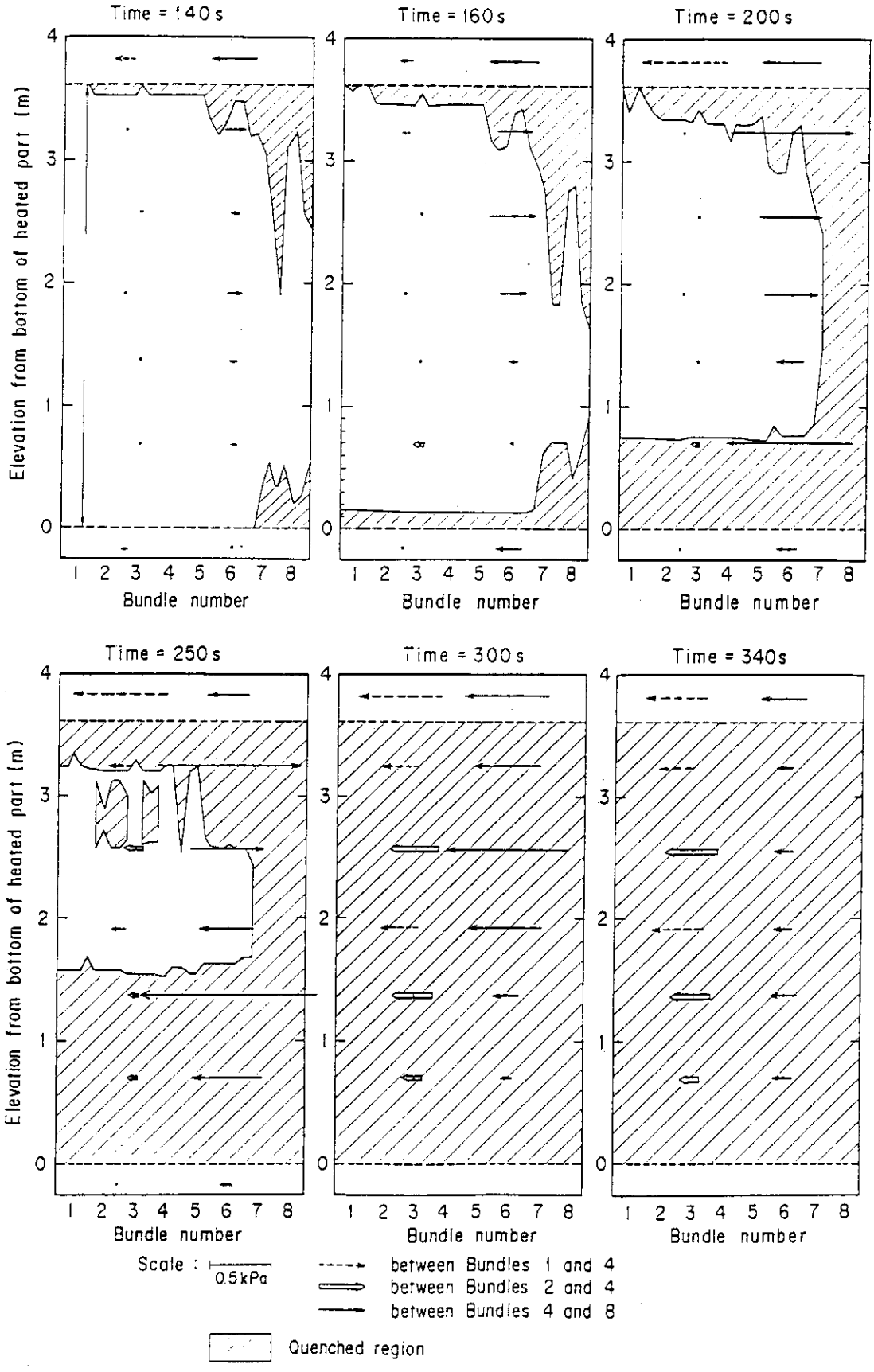

Fig. 3.27 Direction and magnitude of horizontal differntial pressures and quench front distribution

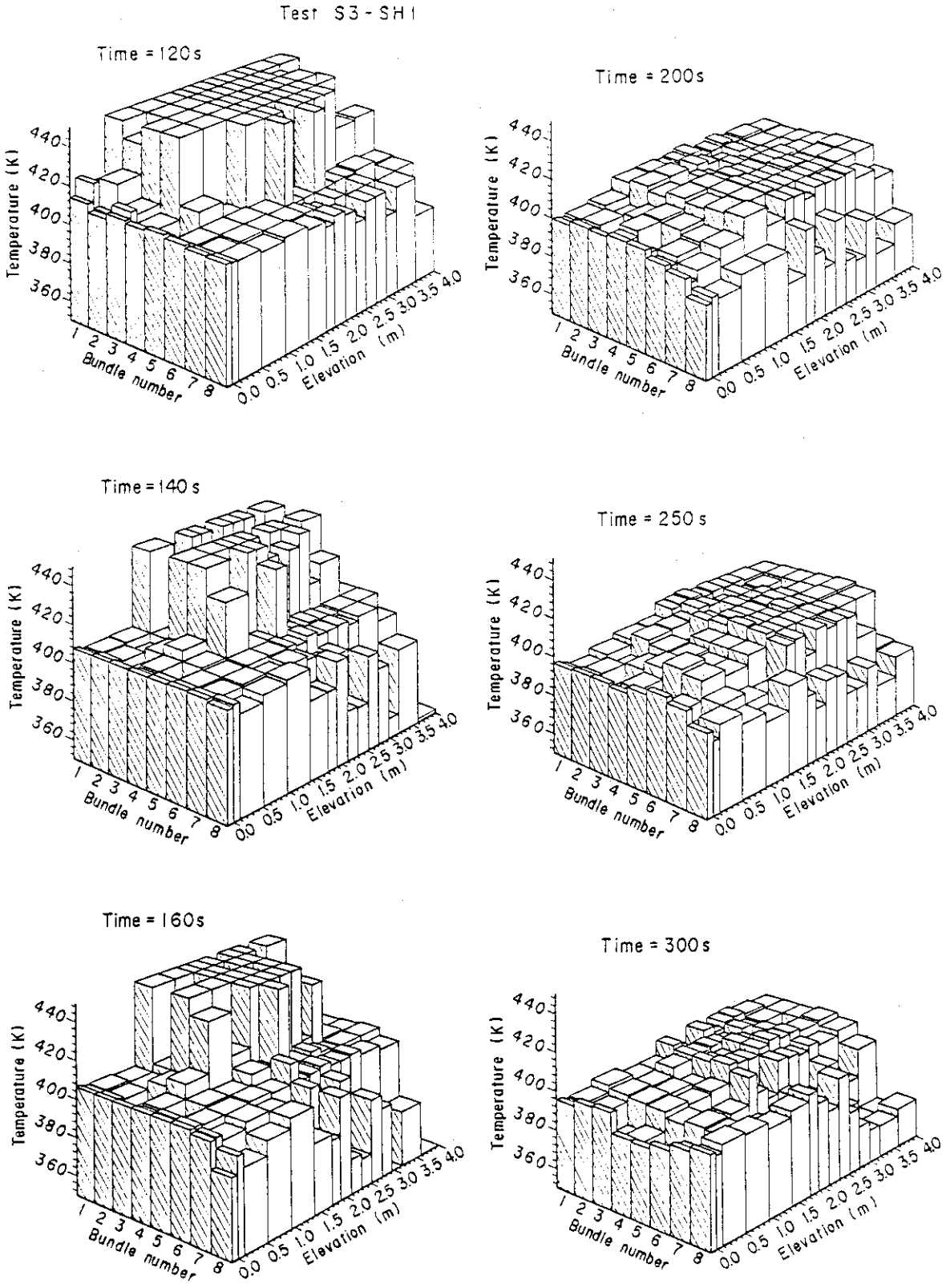

Fig. 3.28 Distribution of fluid temperatures in core at 120, 140, 160, 200, 250 and 300 s

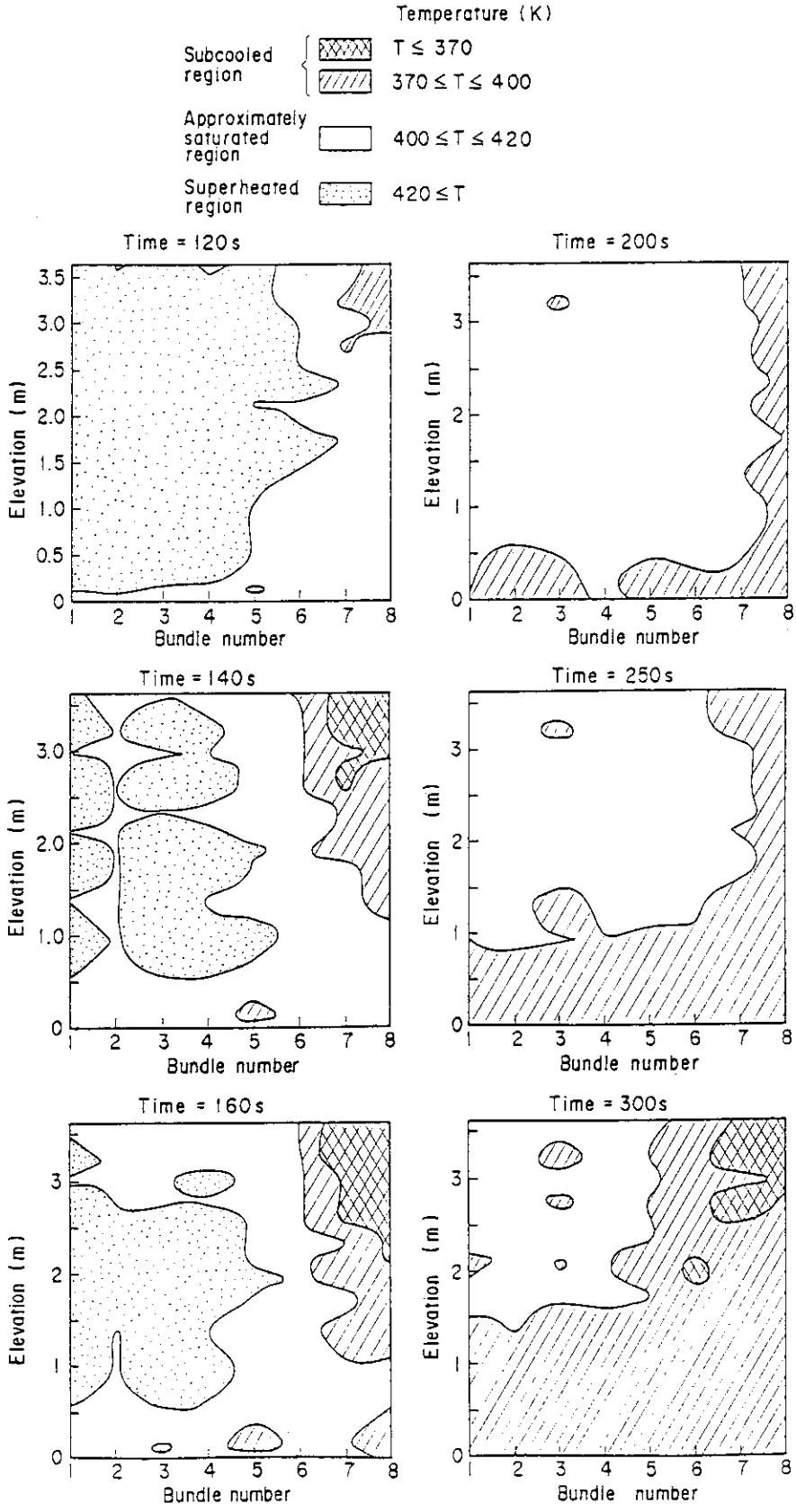

Fig. 3.29 Distribution of subcooled, saturated and superheated fluid temperature regions at 120, 140, 160, 200, 250 and 300 s

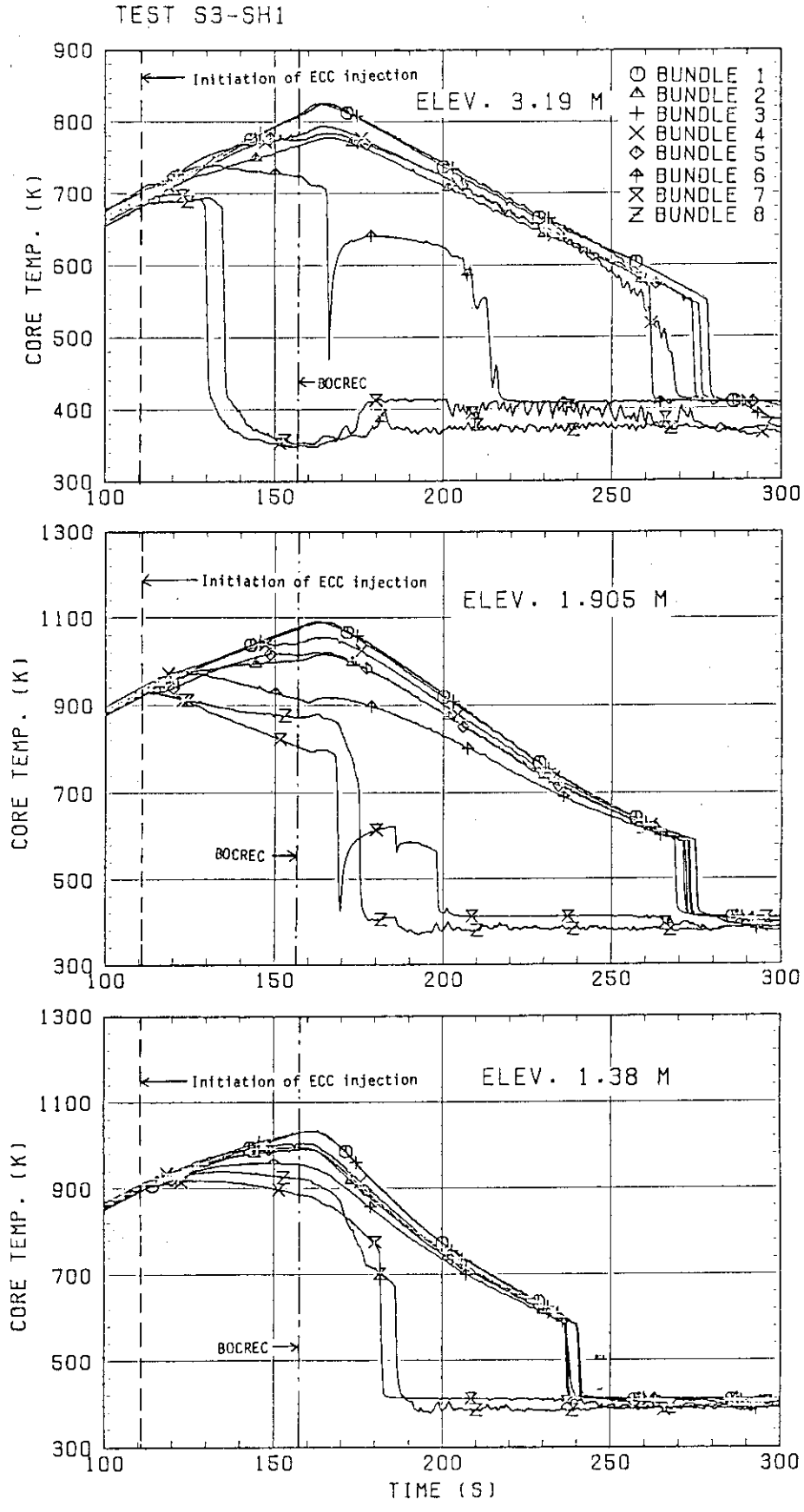

Fig. 3.30 Heater rod temperatures at 3.19, 1.905 and 1.38m

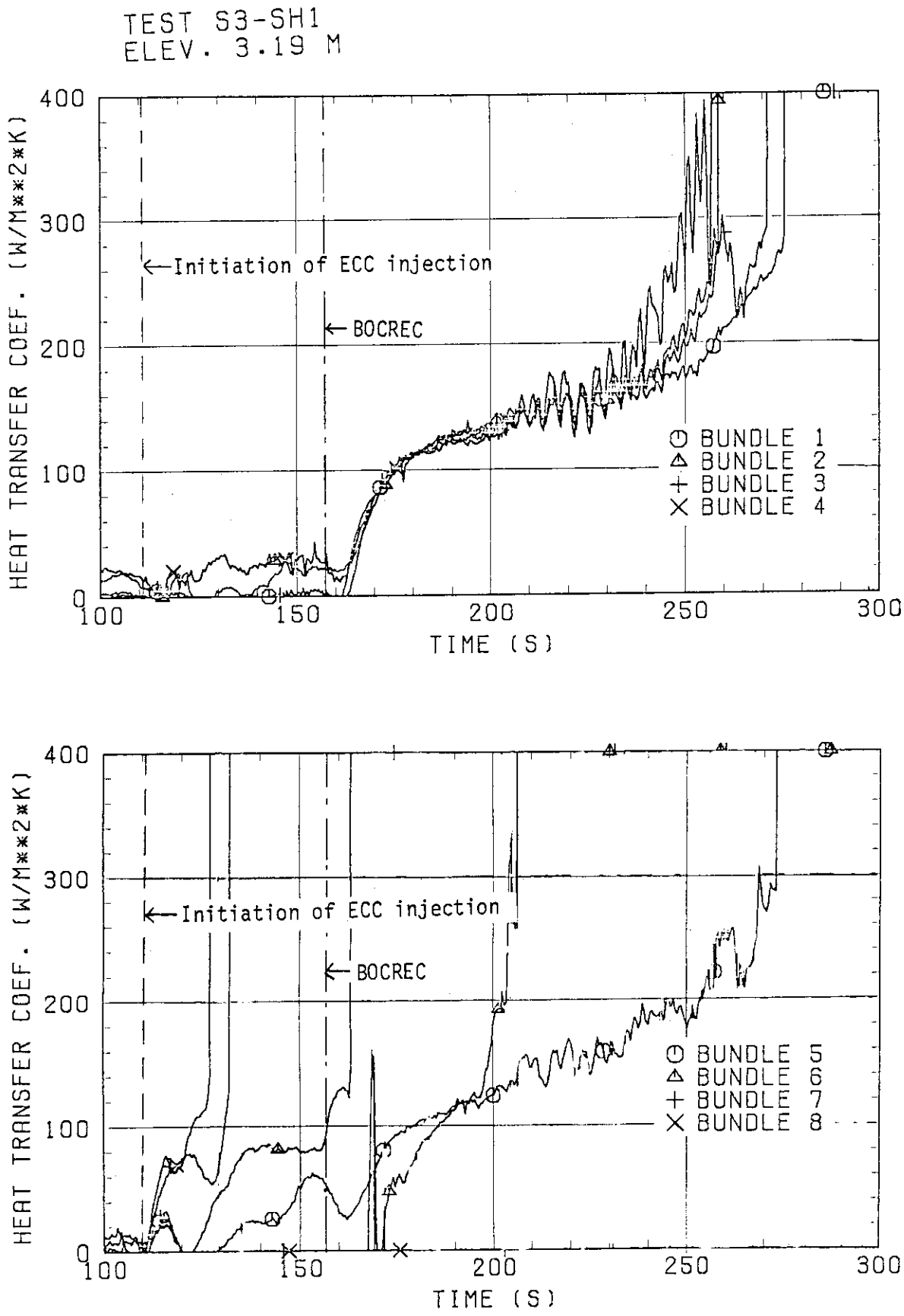

Fig. 3.31(a) Heat transfer coefficients for all bundles at 3.19m

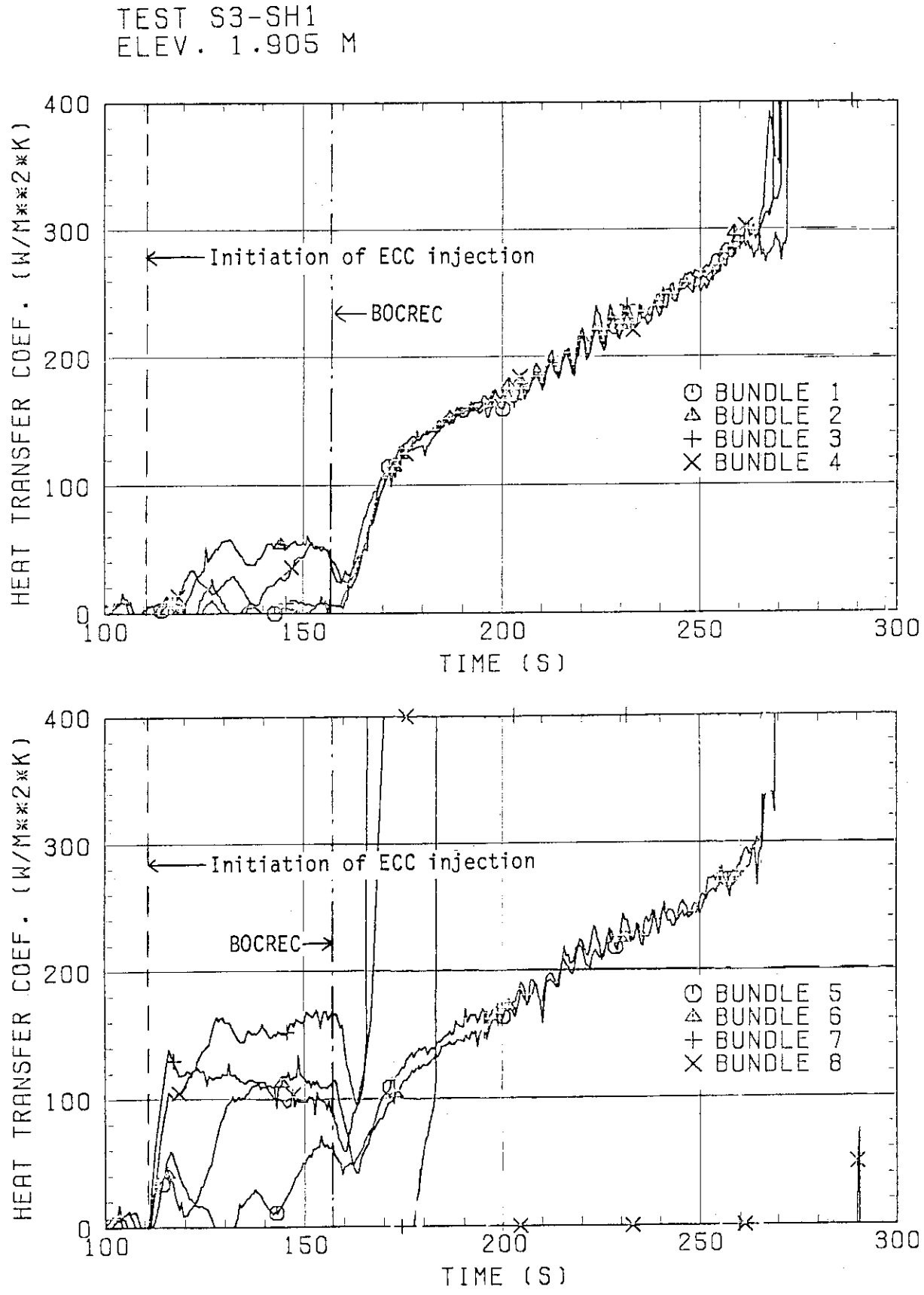

Fig. 3.31(b) Heat transfer coefficients for all bundles at 1.905m

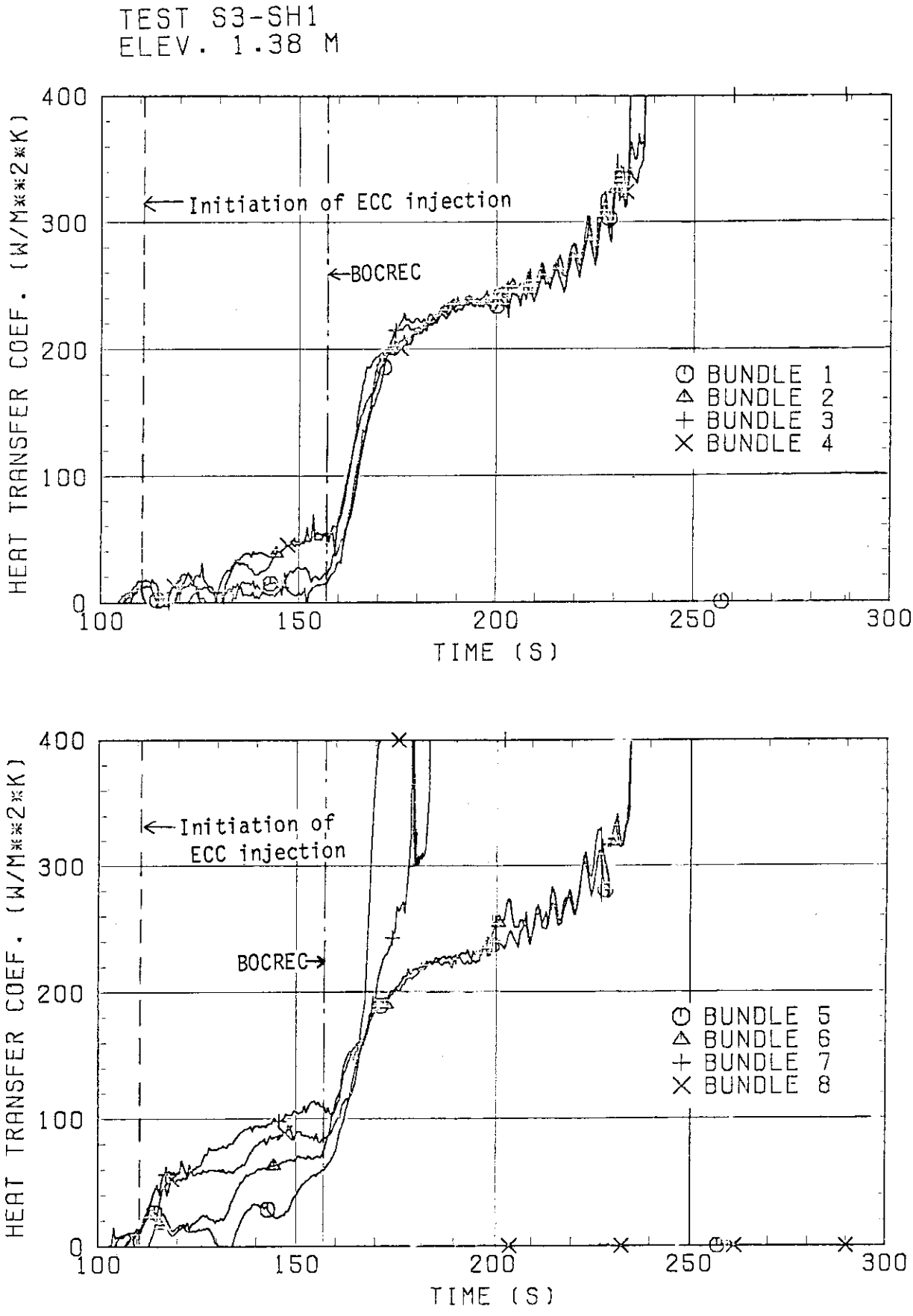

Fig. 3.31(c) Heat transfer coefficients for all bundles at 1.38m

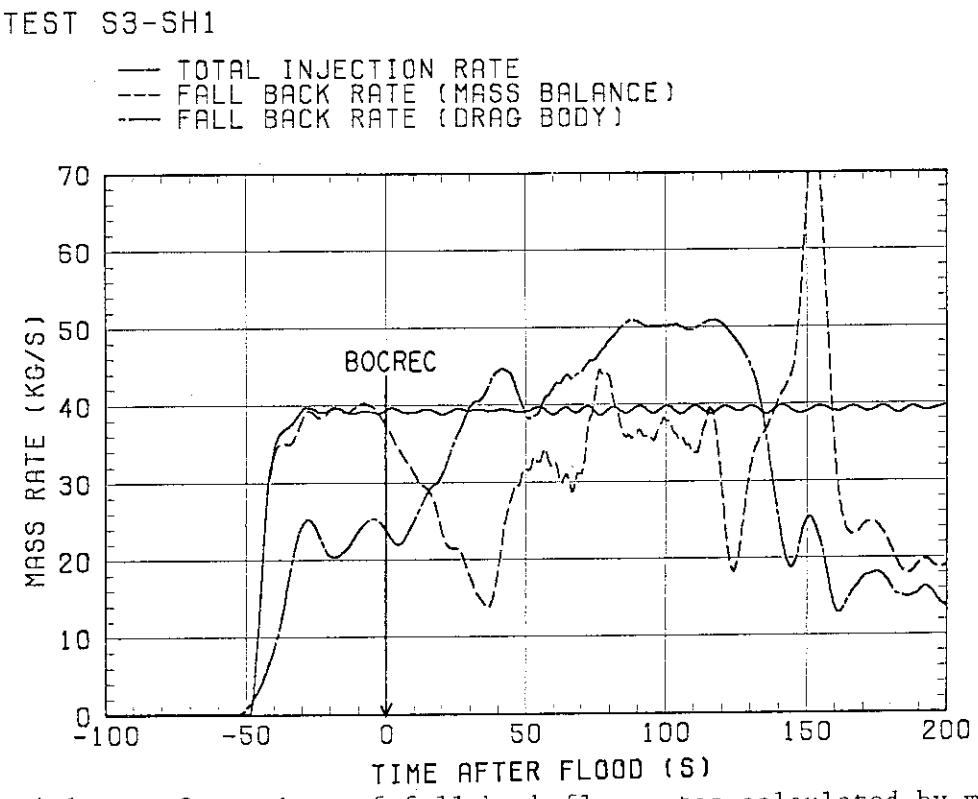

Fig. 4.1 Comparison of fall back flow rates calculated by mass balance method and measured with drag body

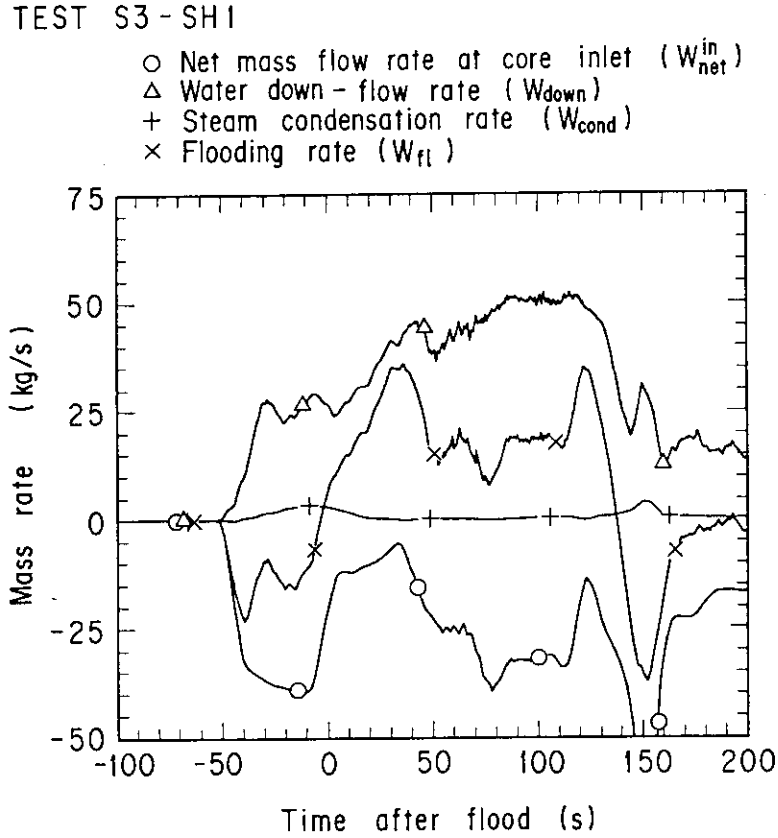

Fig. 4.2 Net mass flow rate at core inlet, total water down-flow rate, steam condensation rate and effective flooding rate

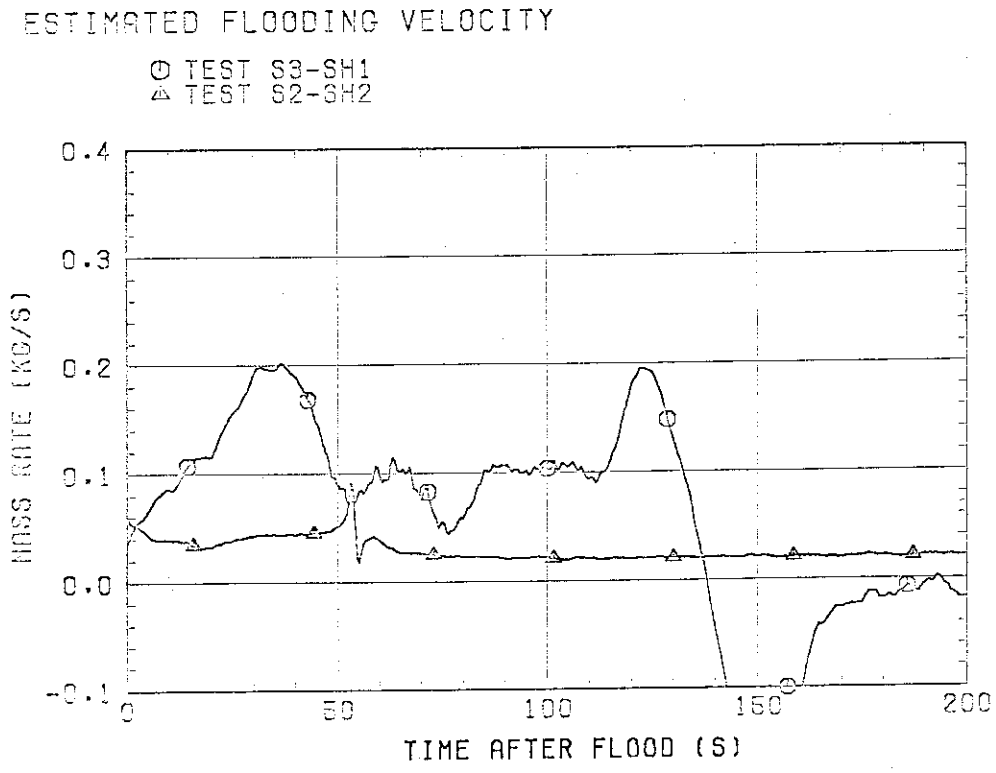

Fig. 4.3 Comparison of flooding velocities for Test S3-SH1 and cold leg injection test S2-SH2

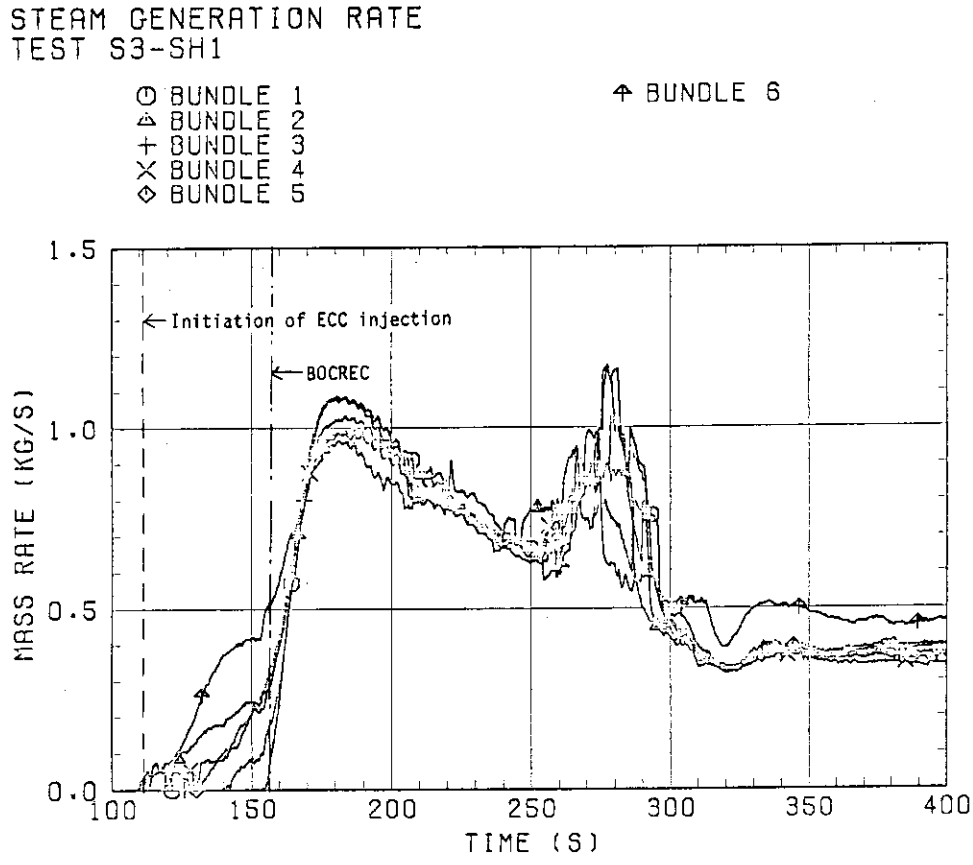

Fig. 4.4 Steam generation rates in Bundles 1 through 6

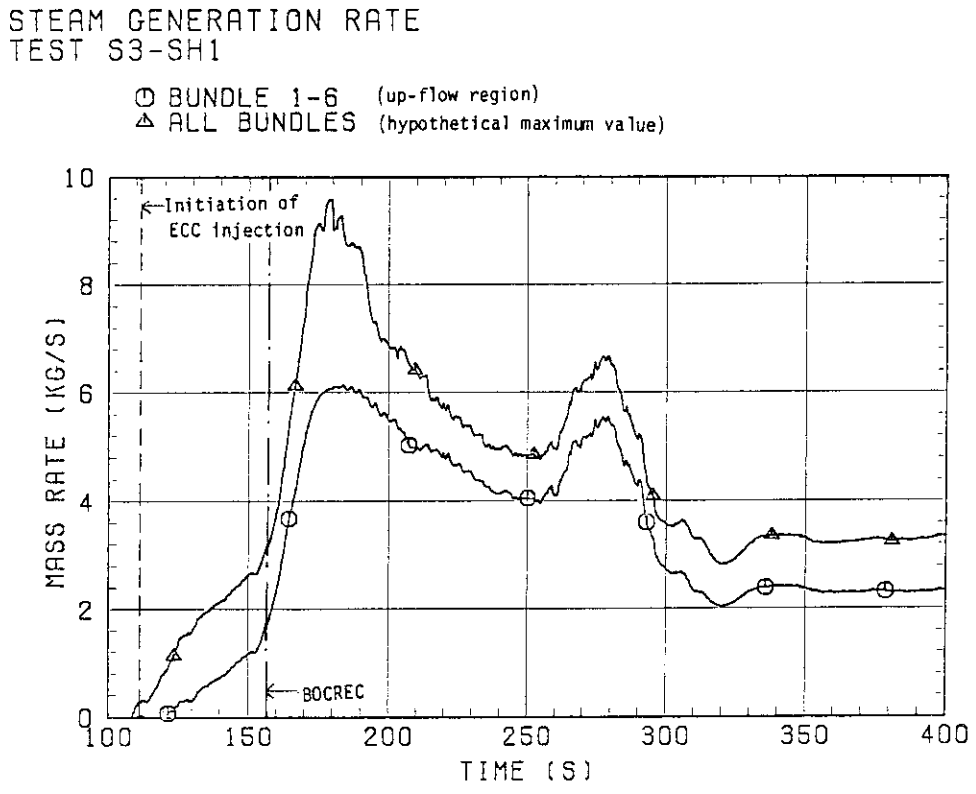

Fig. 4.5 Comparison of total steam generation rate in Bundles 1 through 6 with hypothetical maximum steam generation rate

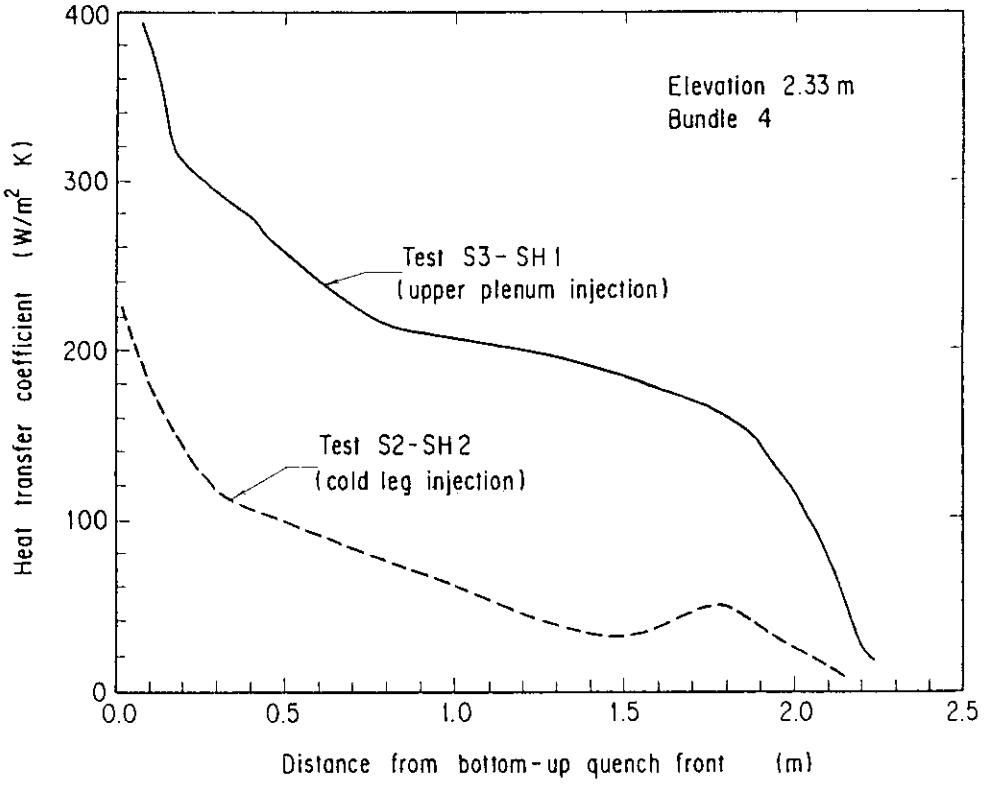

Fig. 4.6 comparison of heat transfer coefficients for Test S3-SH1 and S2-SH2

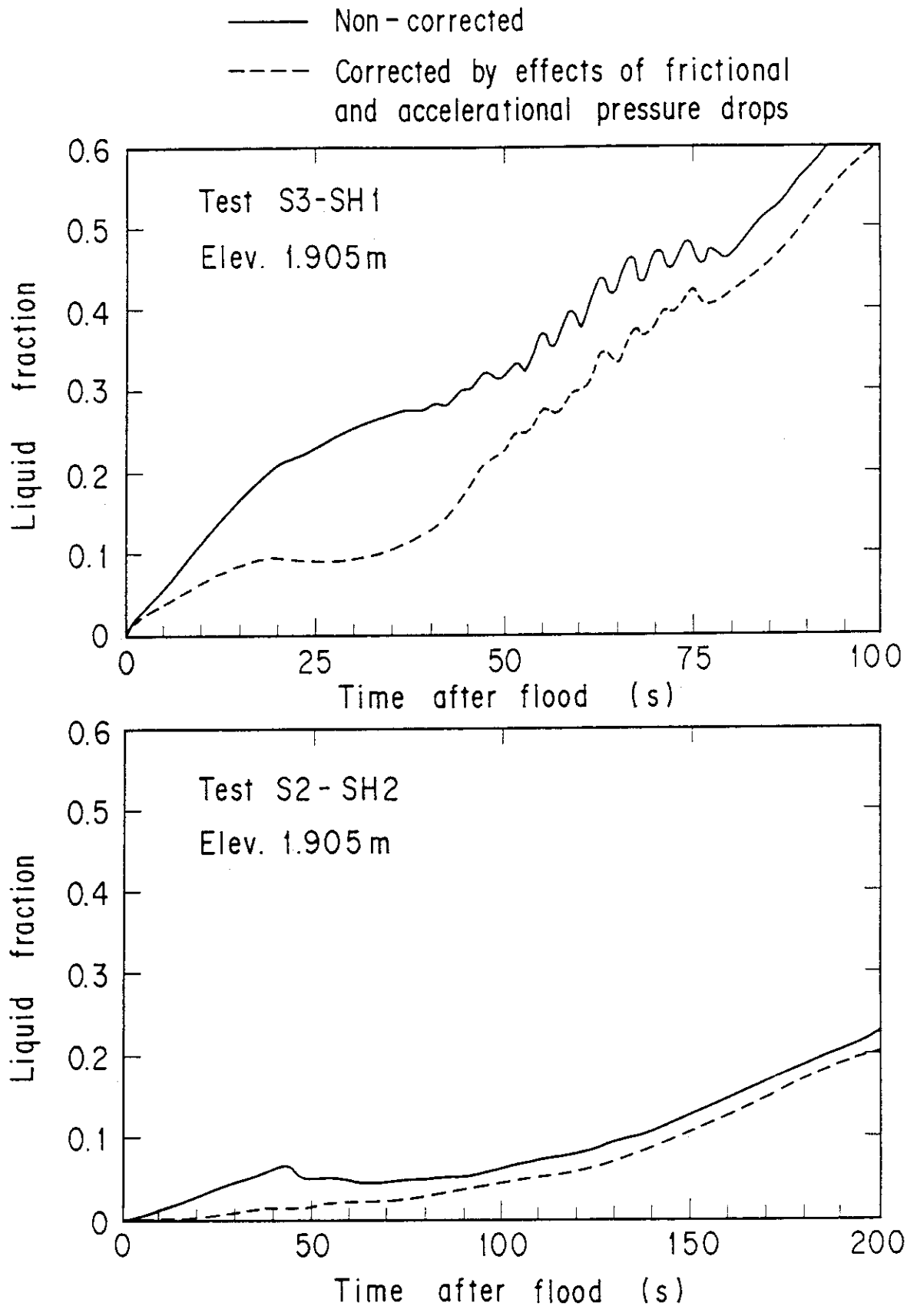

Fig. 4.7 Comparison of corrected and non-corrected liquid fraction for Tests S3-SHI and S2-SH2

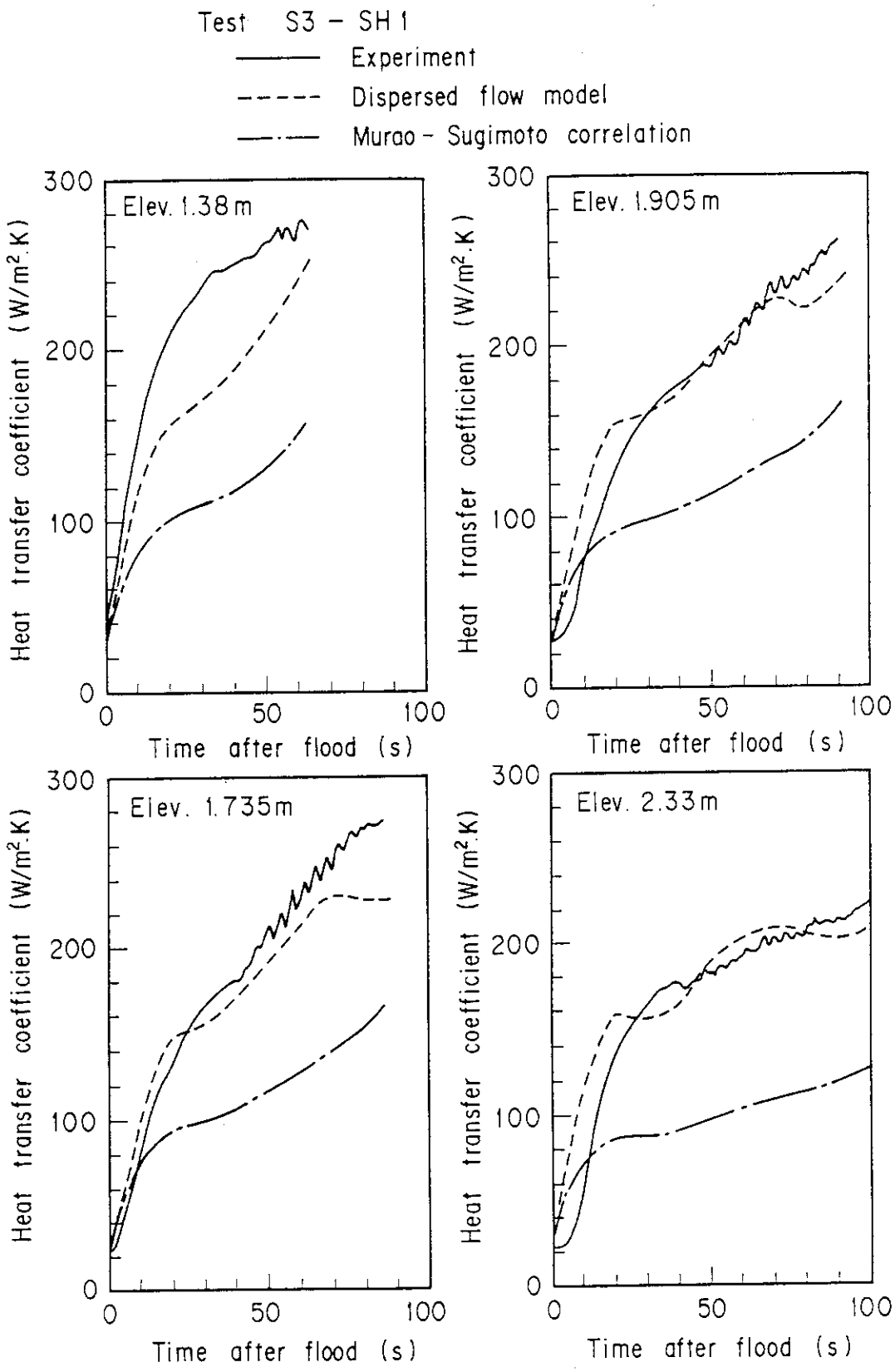

Fig. 4.8 Comparison of heat transfer coefficients with dispersed flow heat transfer correlation and Murao-Sugimoto film boiling correlation

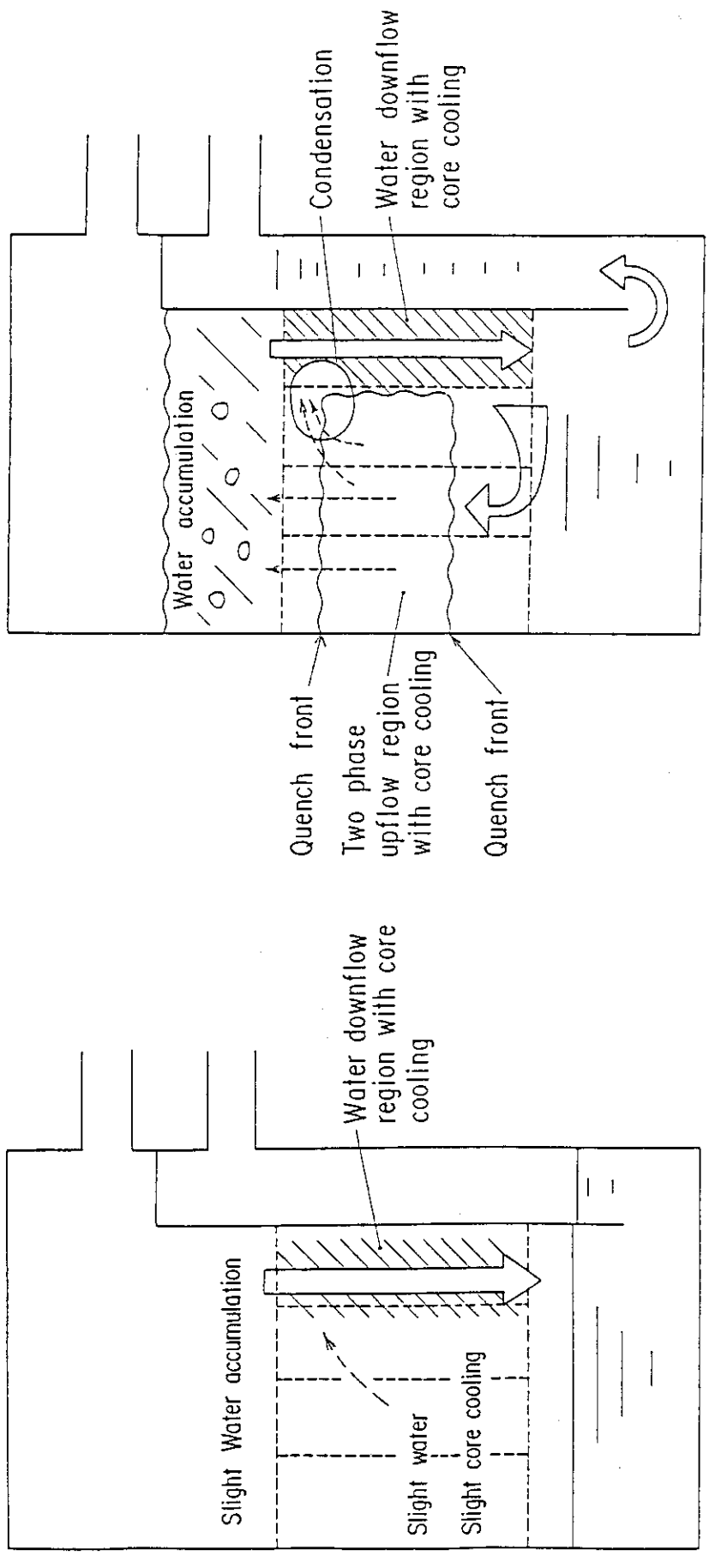

Fig. 5.1 Overall thermal-hydraulic behavior in pressure vessel

Appendix A Slab Core Test Facility (SCTF) Core-III

A.1 Test Facility

The overall schematic diagram of SCTF is shown in Fig. A-1. The principal dimensions of the facility is shown in Table A-1, and the comparison of dimensions between SCTF and the reference PWR is shown in Fig. A-2.

A.1.1 Pressure Vessel

The pressure vessel is of slab geometry as shown in Fig. A-3. The height of the components in the pressure vessel is almost the same as the reference reactor's, and the flow area and the fluid volume of each component are scaled down based on the nominal core flow area scaling, 1/21.

The core consists of 8 bundles arranged in a row and each bundle includes heater rods and non-heated rods with 16×16 array. The core is enveloped by the honeycomb thermal insulator which is attached on the back surface of core wall plate.

The downcomer is located at one end of the pressure vessel which corresponds to the periphery of the actual reactor pressure vessel. The core baffle region located between the core and the downcomer is isolated for Core-III to minimize uncertainty in actual core flow. The cross sections of the pressure vessel at the upper head, upper plenum, core and lower plenum are shown in Fig. A-4.

A.1.2 Interface between Core and Upper Plenum

The interface between the core and the upper plenum consists of upper core support plate (UCSP), end box and various structures in the end box such as control rod spider which is paired with the control rod guid assembly (CRGA) and its support column bottom and special baffle plate spider which is paired with the hold-down bridge. These structures are exactly the same as those for a German PWR except some minor modifications.

Figure A-5 shows arrangement of the UCSP, the end box and the top grid spacer. The configuration of the end box is shown in Fig. A-6.

Detail of the end boxes with drag transducer device and other internals is shown in Fig. A-7. The UCSP shown in Fig. A-8 has two kinds of holes, i.e., the square holes correspond to the end boxes with control rod spider and the circular holes correspond to the end boxes with special baffle plate spider.

A.1.3 Upper Plenum and Upper Head

The vertical and horizontal cross sections of the upper plenum are shown in Figs. A-9 and A-4, respectively. In the SCTF Core-III, the slab cut of the upper plenum of a German (KWU) PWR is simulated. The splitted and staggered arrangement of the CRGA support columns was chosen to make good simulation of horizontal flow in the upper plenum.

As shown in Fig. A-10, there are three kinds of CRGA support column. Support column-1 is installed above Bundles 3 and 5 and connected to the CRGA support column bottom with the transition cone. Cross section of the CRGA support calumn changes from a circle to a half circle in this transition cone. Support column 2 is installed above Bundles 6 and 7 and the bottom is closed with the half conical bottom seal plate with many flow holes. Support column 3 is essentially the same as support column 2 but the edge of one side is cut off in order to install above Bundle 1. Each CRGA support column has ten or eleven baffle plates with flow holes. Top flow paths to the upper head bottom and to the upper plenum top are also provided.

Figure A-11 shows vertical cross section of the bottom part of the upper plenum and the interface between the core and the upper plenum. There are eight side flow injection nozzles and eight side flow extraction nozzles just at the opposite side of the upper plenum bottom, corresponding to each bundle.

The upper plenum is separated from the upper head by an upper support plate. Four top injection nozzles penetrate the upper head and open the top of upper plenum as shown in Fig. A-12. Outlet part of the top injection nozzle has a rectangular cross section and double mesh screen with 45 degree cross angle is attached at the mouth.

A.1.4 Simulated Core

The simulated core for the SCTF Core-III consists of 8 heater rod bundles arranged in a row. Each bundle has 236 electrically heated rods and 20 non-heated rods. The arrangement of rods in a bundle is shown in Fig. A-13. The dimensions of the heater rods are based on 15×15 fuel rods bundle for a PWR and the heated length and the outer diameter of each heater rod are 3.613 m and 10.7 mm, respectively. A heater rod consists of a nichrome heater element, boron nitride (BN) or magnesium oxide (MgO) depending on elevation in the heated zone and Nichrofer 7216 (equivalent to Inconel 600) sheath. The sheath thickness is about 1.0 mm and is thicker than the actual fuel cladding because of the requirements for thermocouple installation. The heater element is a helical coil and has a 17 step chopped cosine axial power profile as shown in Fig. A-14. The peaking factor is 1.4.

Non-heated rods are either pipes or solid rods of stainless steel with 13.8 mm O.D. The heater rods and non-heated rods are fixed at the top of the core allowing downward expansion. In Fig. A-15, relative elevation of rods and spacers is shown.

For better simulation of flow resistance in the lower plenum, the simulated fuel rods end in the lower plenum and do not penetrate through the bottom plate of the lower plenum as shown in Fig. A-15.

A.1.5 Primary Loops

Primary loops consist of a hot leg equivalent to four hot legs in area, a steam/water separator for simulating single steam phase flow downstream of the steam generator and for measuring flow rate of carry over water, an intact cold leg equivalent to three intact loops, a broken cold leg on the pressure vessel side and a broken cold leg on the steam/water separator side. These two broken cold legs are connected to two containment tanks through break valves, respectively. The arrangement of the primary loops is shown in Fig. A-16. The flow area of each loop is scaled down based on the core flow area scaling, 1/21. It should be emphasized that the cross section of the hot leg is an elongated circle with an actual height to realize proper flow pattern in the hot leg. The steam/water separator has a steam generator inlet plenum simulator to correctly simulate the flow

characteristics of carryover water into the U-tubes. The cross section of the hot leg and the configuration of the steam genrator inlet plenum simulator are shown in Fig. A-17.

A pump simulator and a loop seal part are provided for the intact cold leg. The arangement of the intact cold leg is shown in Fig. A-18. The pump simulator consists of the casing and duct simulators and an orifice plate as shown in Fig. A-19. The loop resistance is adjusted with the orifice plates attached to the intact cold leg, the steam/water separator side and pressure vessel side broken cold legs and the pump simulator.

A.1.6 ECC Water Injection System

Three kinds of ECCSs are provided, i.e., the accumulator injection system (Acc), low pressure coolant injection system (LPCI) and combined injection system. Available injection locations for the former two are the intact and broken cold legs, the hot leg, the lower plenum and the downcomer. On the other hand, those for the last one are the top and bottom-side of the upper plenum and the intact and broken cold legs.

A.1.7 Containment Tanks and Auxiliary System

Two containment tanks are provided to SCTF. The containment tank-I is connected with the downcomer through the pressure vessel side broken cold leg and the containment tank-II is connected with the steam/water separator through the steam/water separator side broken cold leg. Especially in the containment tank-I, carryover water from the downcomer is measured by the differentiation of the liquid level. These containment tanks and auxiliary system such as a pressurizer for injecting water from the Acc tanks, etc. are shared with CCTF.

A.2 Instrumentation

The instrumentation in SCTF has been provided both by JAERI and USNRC. The JAERI-provided instrumentation includes the measurement of temperatures, pressures, differential pressures, liquid levels, flow velocities, and heating powers. USNRC has provided film probes, impedance probes, string probes, liquid level detectors (LLDs), fluid distribution grids (FDGs), turbine meters, drag disks, densitometers, spool pieces, drag bodies, break through detectors and video optical probes. Locations of the JAERI-provided instruments are shown in Figs. A-20 through A-43.

Table A-1 Principal Dimensions of the SCTF

1. Core Dimension		
(1) Quantity of Bundle	8 Bundles	
(2) Bundle Array	1 × 8	
(3) Bundle Pitch	230 mm	
(4) Rod Array in a Bundle	16 × 16	
(5) Rod Pitch in a Bundle	14.3 mm	
(6) Quantity of Heater Rod in a Bundle	236 rods	
(7) Quantity of Non-Heated Rod in a Bundle	20 rods	
(8) Total Quantity of Heater Rods	236×8=1,888	rods
(9) Total Quantity of Non-Heated Rods	20×8=160	rods
(10) Effective Heated Length of Heater Rod	3613 mm	
(11) Diameter of Heater Rod	10.7 mm	
(12) Diameter of Non-Heated Rod	13.8 mm	
2. Flow Area & Fluid Volume		
(1) Core Flow Area	0.25	m^2
(2) Core Fluid Volume	0.903	m^3
(3) Baffle Region Flow Area (isolated)	(0.096)	m^2
(4) Baffle Region Fluid Volume (nominal)	0.355	m^3
(5) Cross-Sectional Area of Core Additional Fluid Volumes Including Gap between Core Barrel and Pressure Vessel Wall and Various Penetration Holes	0.07 ~ 0.10	m^2
(6) Downcomer Flow Area	0.158	m^2
(7) Upper Annulus Flow Area	0.158	m^2
(8) Upper Plenum Horizontal Flow Area (max.)	0.541	m^2
(9) Upper Plenum Vertical Flow Area	0.525	m^2
(10) Upper Plenum Fluid Volume	1.156	m^3
(11) Upper Head Fluid Volume	0.86	m^3
(12) Lower Plenum Fluid Volume (excluding below downcomer)	1.305	m^3
(13) Steam Generator Inlet Plenum Simulator Flow Area	0.626	m^2
(14) Steam Generator Inlet Plenum Simulator Fluid Volume	0.931	m^3
(15) Steam Water Separator Fluid Volume	5.3	m^3
(16) Flow Area at the Top Plate of Steam Generator Inlet Plenum Simulator	0.195	m^2
(17) Hot Leg Flow Area	0.0826	m^2

Table A-1 (continue)

(18)	Intact Cold Leg Flow Area (Diameter = 297.9 mm) Inverted U-Tube with 0.0314 m^2 Cross-Sectional Area (Diameter = 200 mm) and 10 m Height from the Top of Steam Generator Inlet Plenum Simulator Can Be Added As an Option.	0.0697 m^2
(19)	Broken Cold Leg Flow Area (Diameter = 151.0 mm)	0.0197 m^2
(20)	Containment Tank-I Fluid Volume	30 m^3
(21)	Containment Tank-II Fluid Volume	50 m^3
(22)	Flow Area of Exhausted Steam Line from Containment Tank-II to the Atmosphere	see Fig. 3-63

3. Elevation & Height

(1)	Top Surface of Upper Core Support Plate (UCSP)	0 mm
(2)	Bottom Surface of UCSP	- 40 mm
(3)	Top of the Effective Heated Length of Heater Rod	- 444 mm
(4)	Bottom of the Effective Heated Length of Heater Rod	-4,057 mm
(5)	Bottom of the Skirt in the Lower Plenum	-5,270 mm
(6)	Bottom of Intact Cold Leg	+ 724 mm
(7)	Bottom of Hot Leg	+1,050 mm
(8)	Top of Upper Plenum	+2,200 mm
(9)	Bottom of Steam Generator Inlet Plenum Simulator	+1,933 mm
(10)	Centerline of Loop Seal Bottom	-2,281 mm
(11)	Bottom Surface of End Box	- 263 mm
(12)	Top of Upper Annulus of Downcomer	+2,234 mm
(13)	Height of Steam Generator Inlet Plenum Simulator	1,595 mm
(14)	Height of Loop Seal	3,140 mm
(15)	Inner Height of Hot Leg Pipe	737 mm
(16)	Bottom of Lower Plenum	-5,772 mm
(17)	Top of Upper Head	+2,887 mm

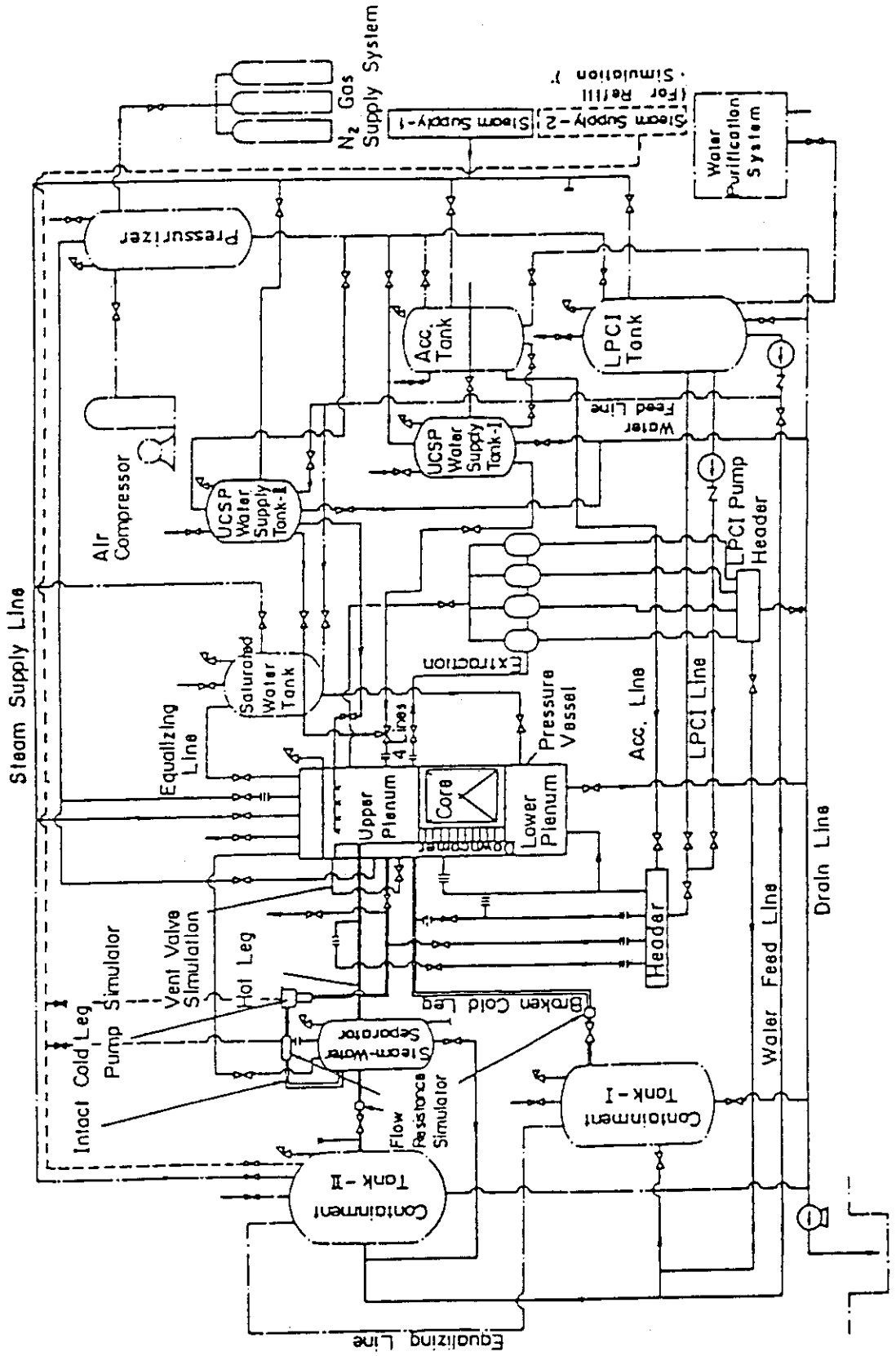

Fig. A-1 Schematic Diagram of Slab Core Test Facility

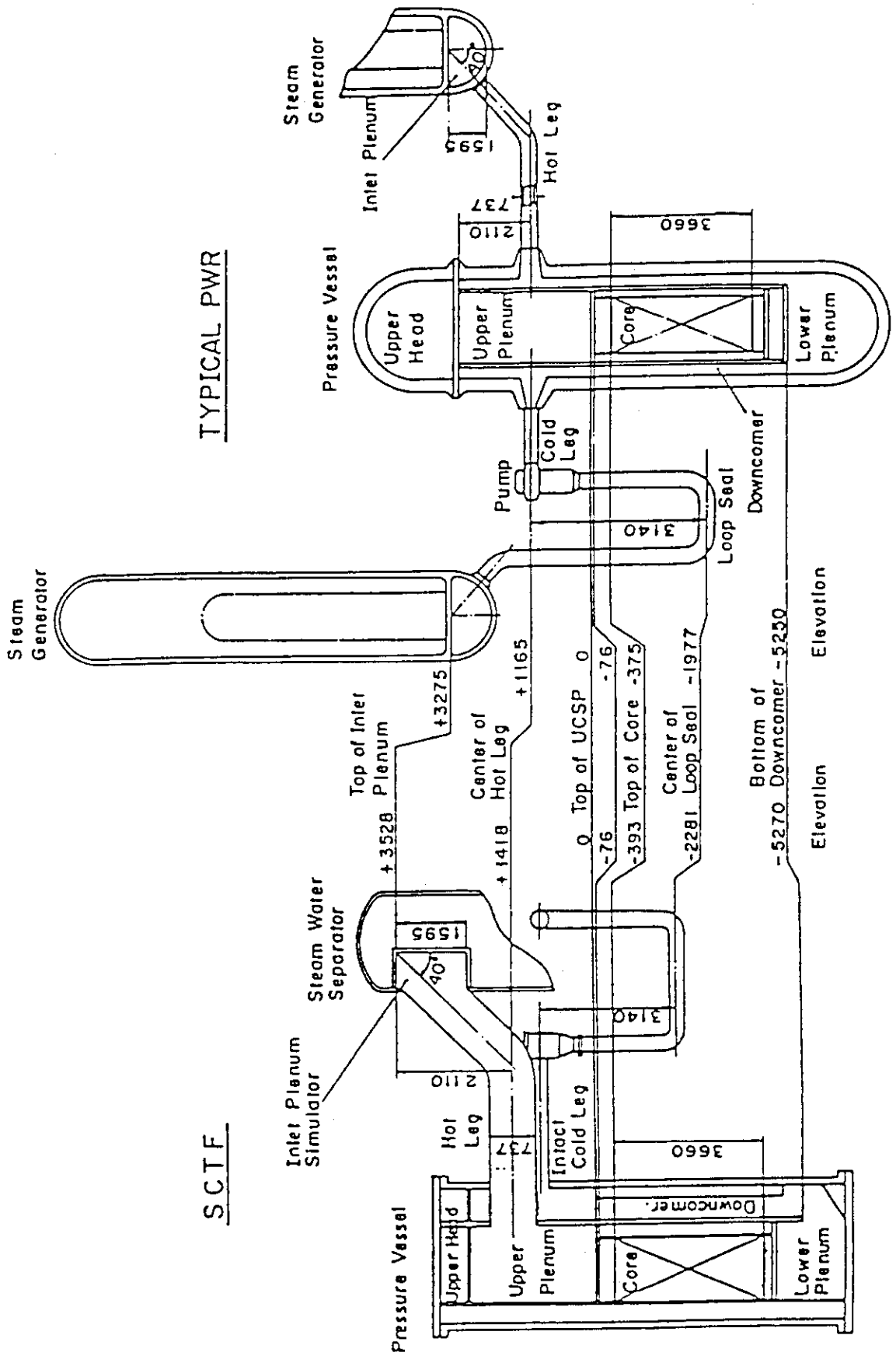

Fig. A-2 Comparison of Dimensions between SCTF and a Reference PWR

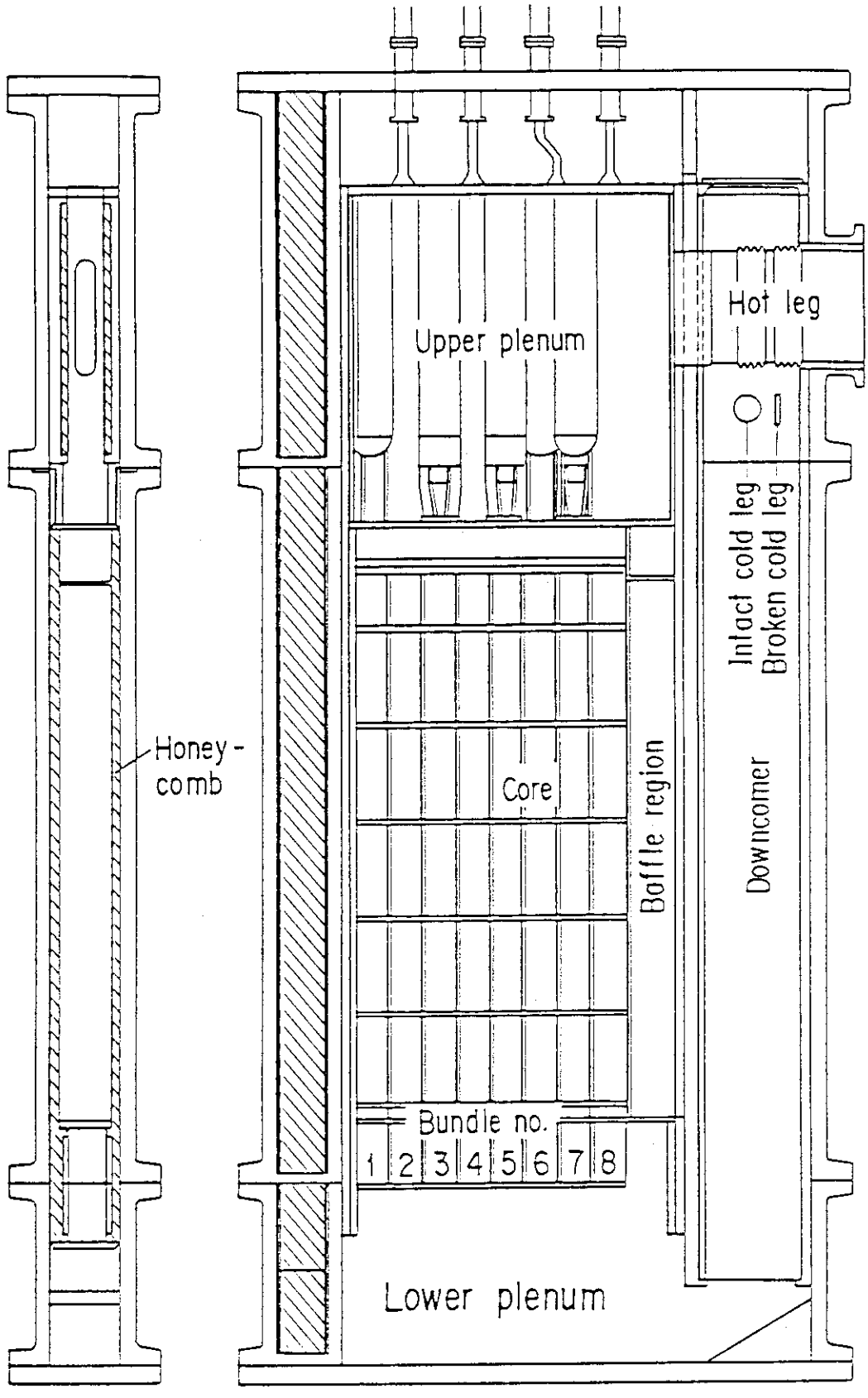

Fig. A-3 Vertical Cross Sections of Pressure Vessel

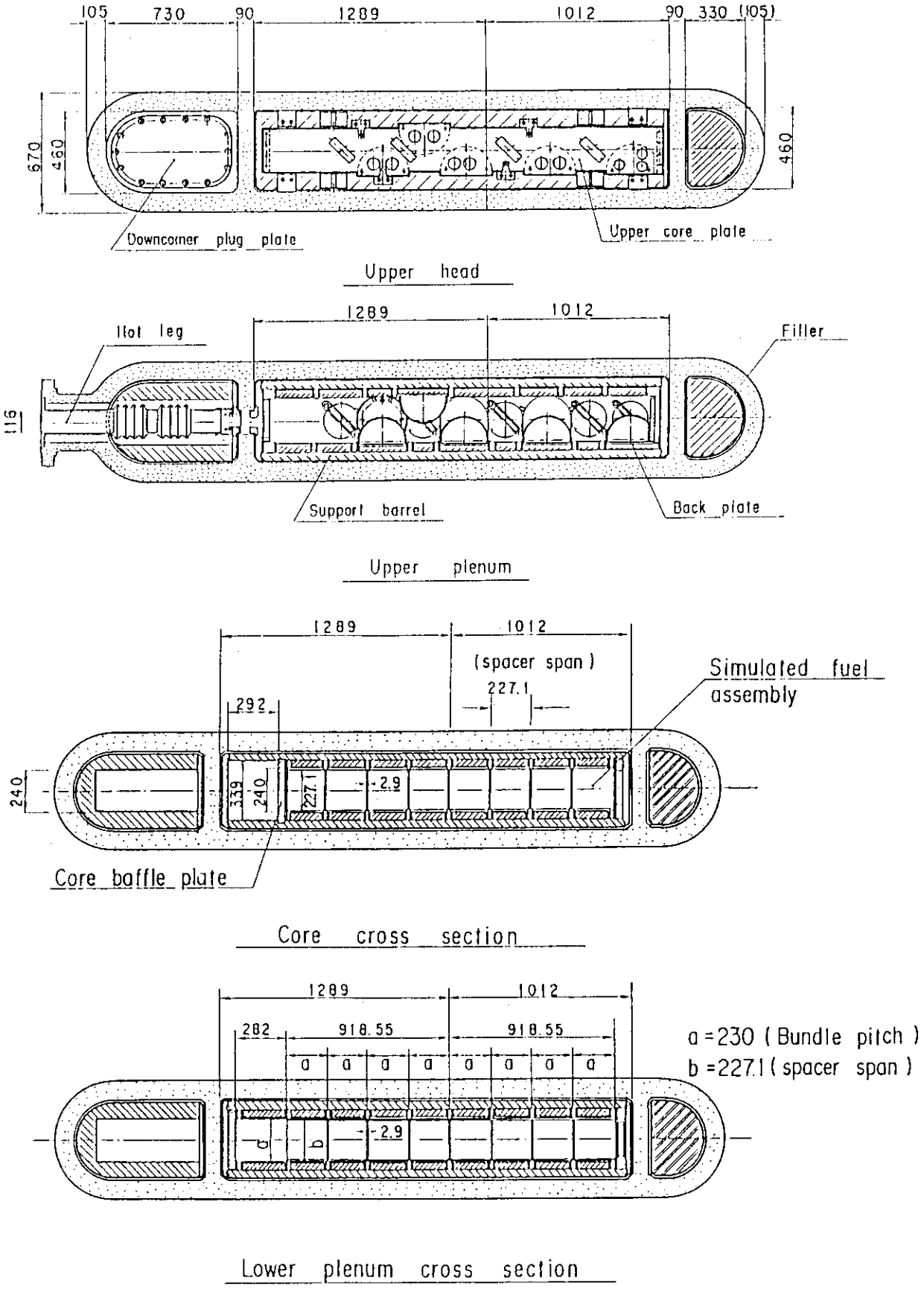

Fig. A-4 Horizontal Cross Sections of Pressure Vessel

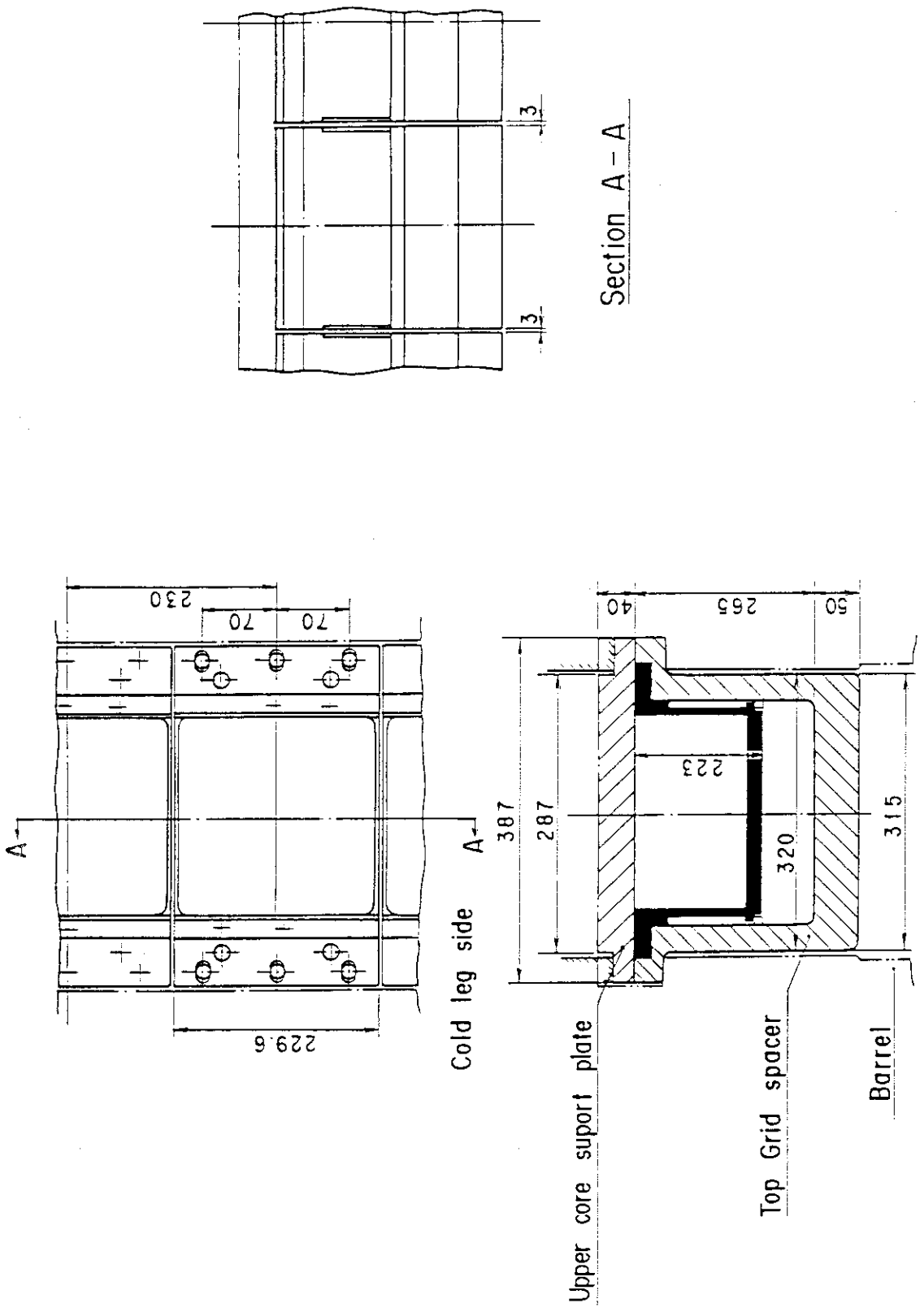

Fig. A-5 Arrangement and Principal Dimension of End Boxes and Top Grid Spacers

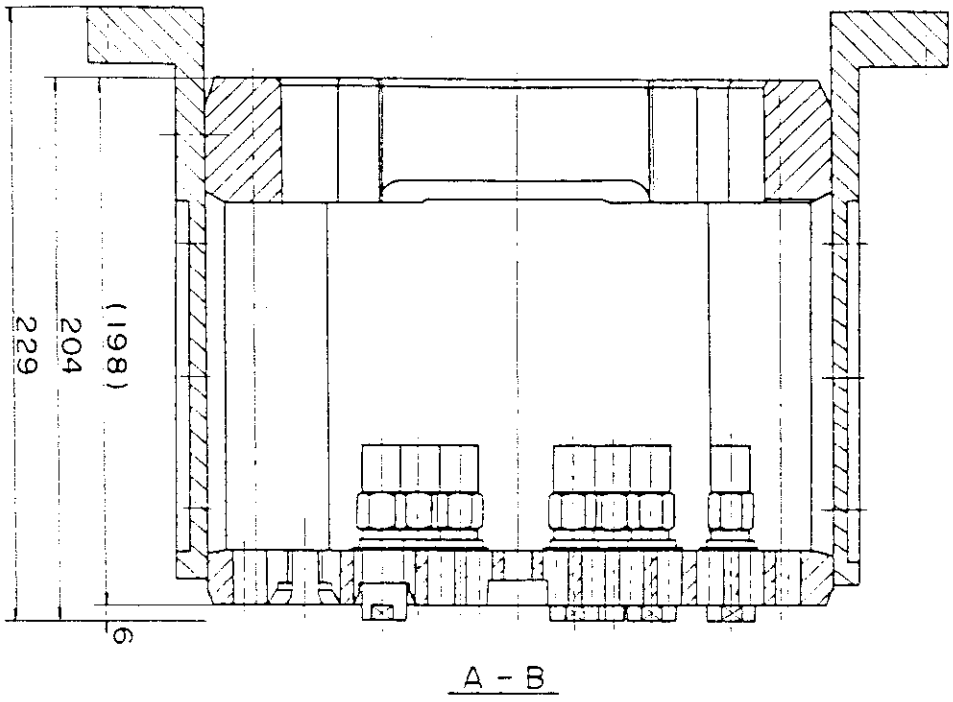

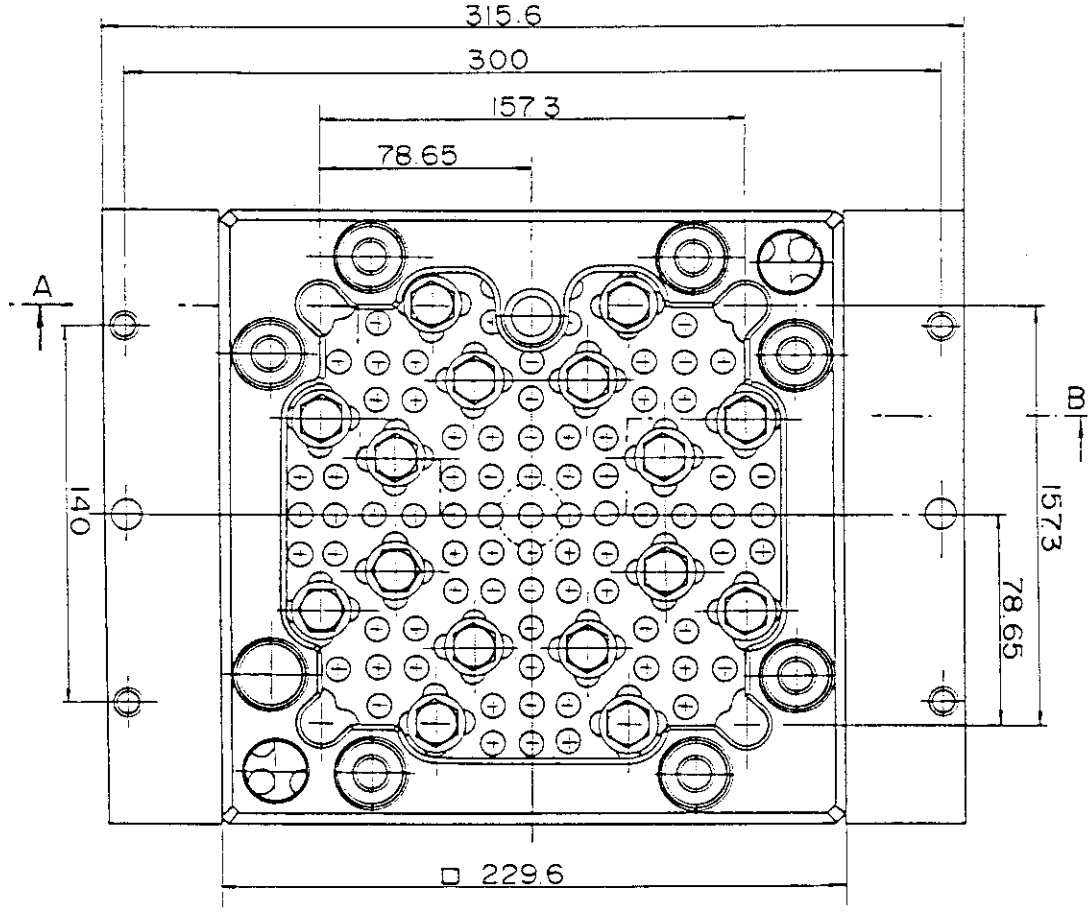

Fig. A-6 Configuration and Dimension of End Boxes

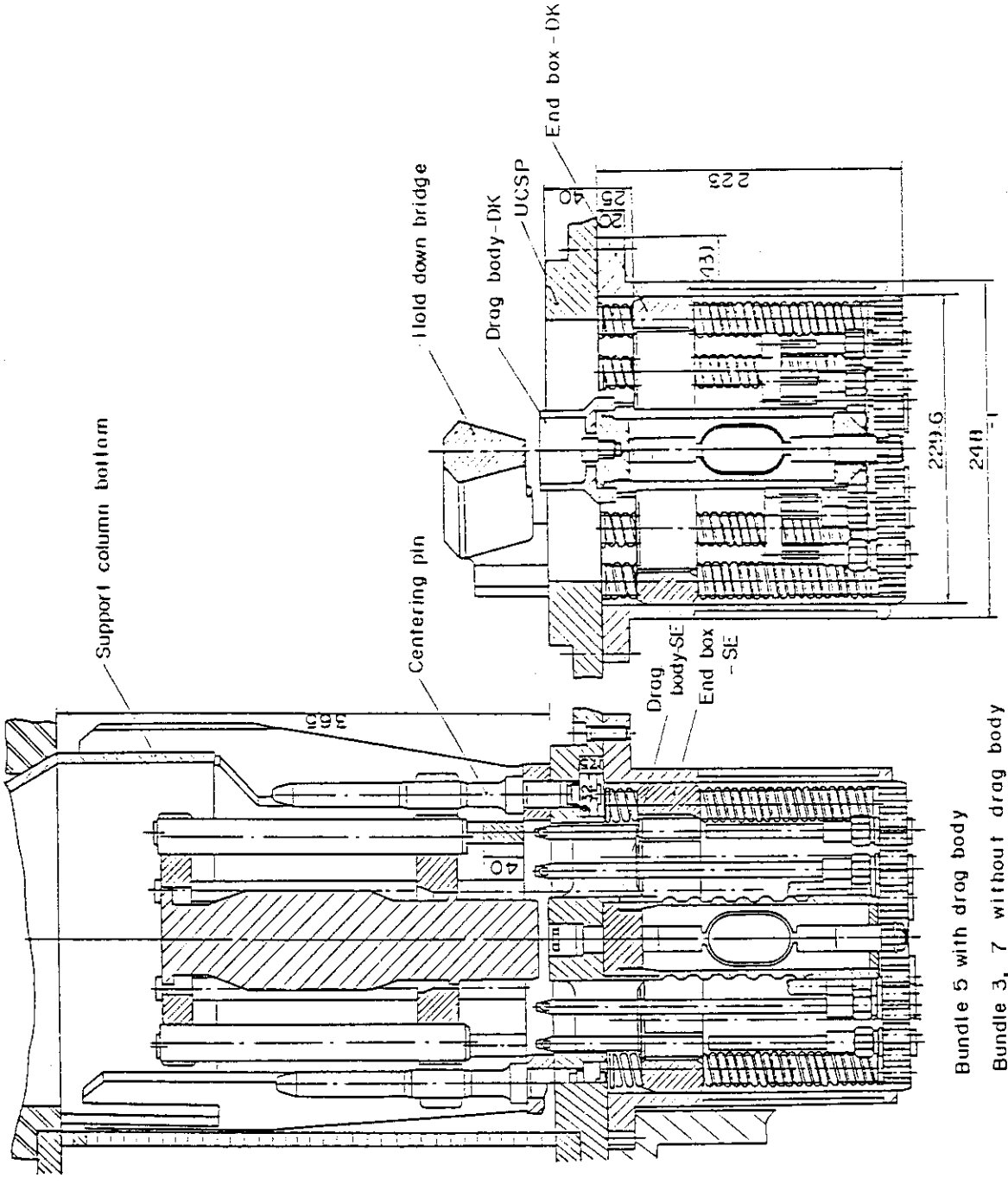

Fig. A-7 Detail of End Boxes with Drag Bodies

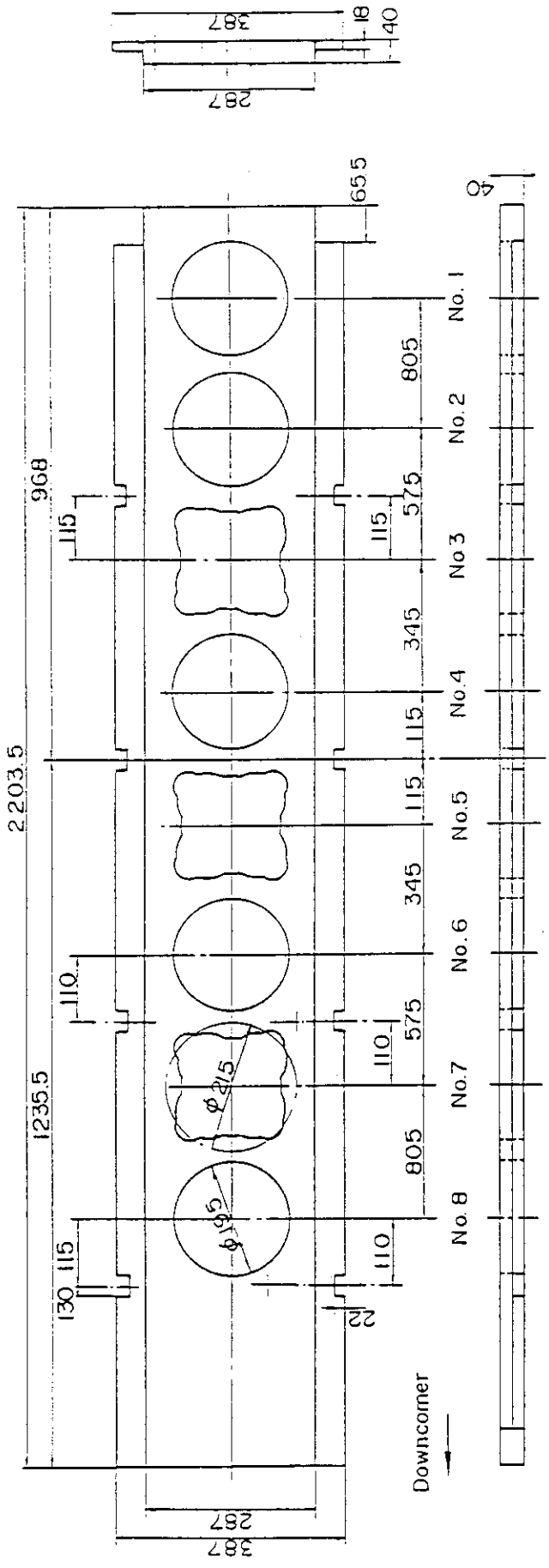

Fig. A-8 Dimension of Upper Core Support Plate

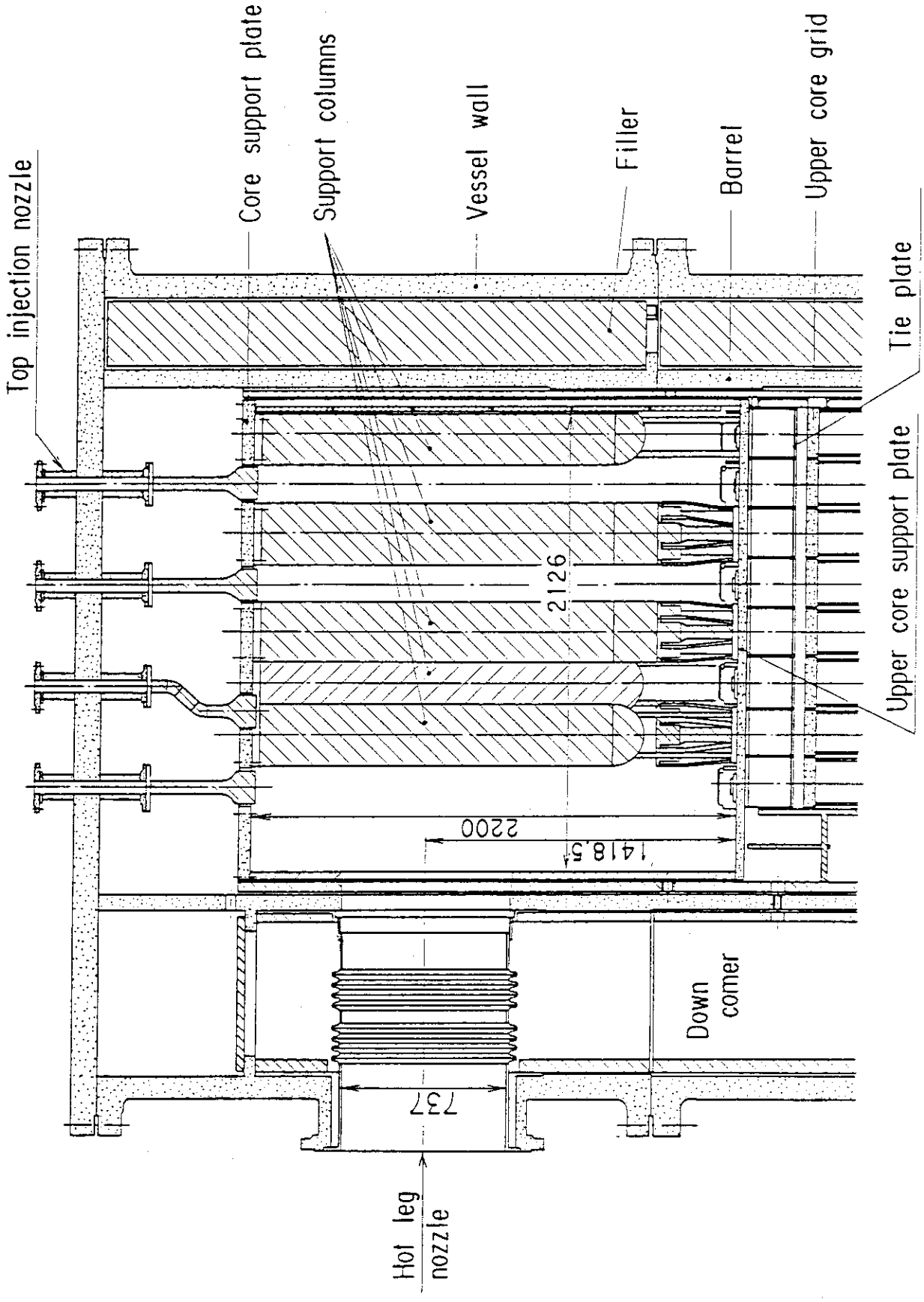

Fig. A-9 Vertical Cross Section of Upper Plenum Internals

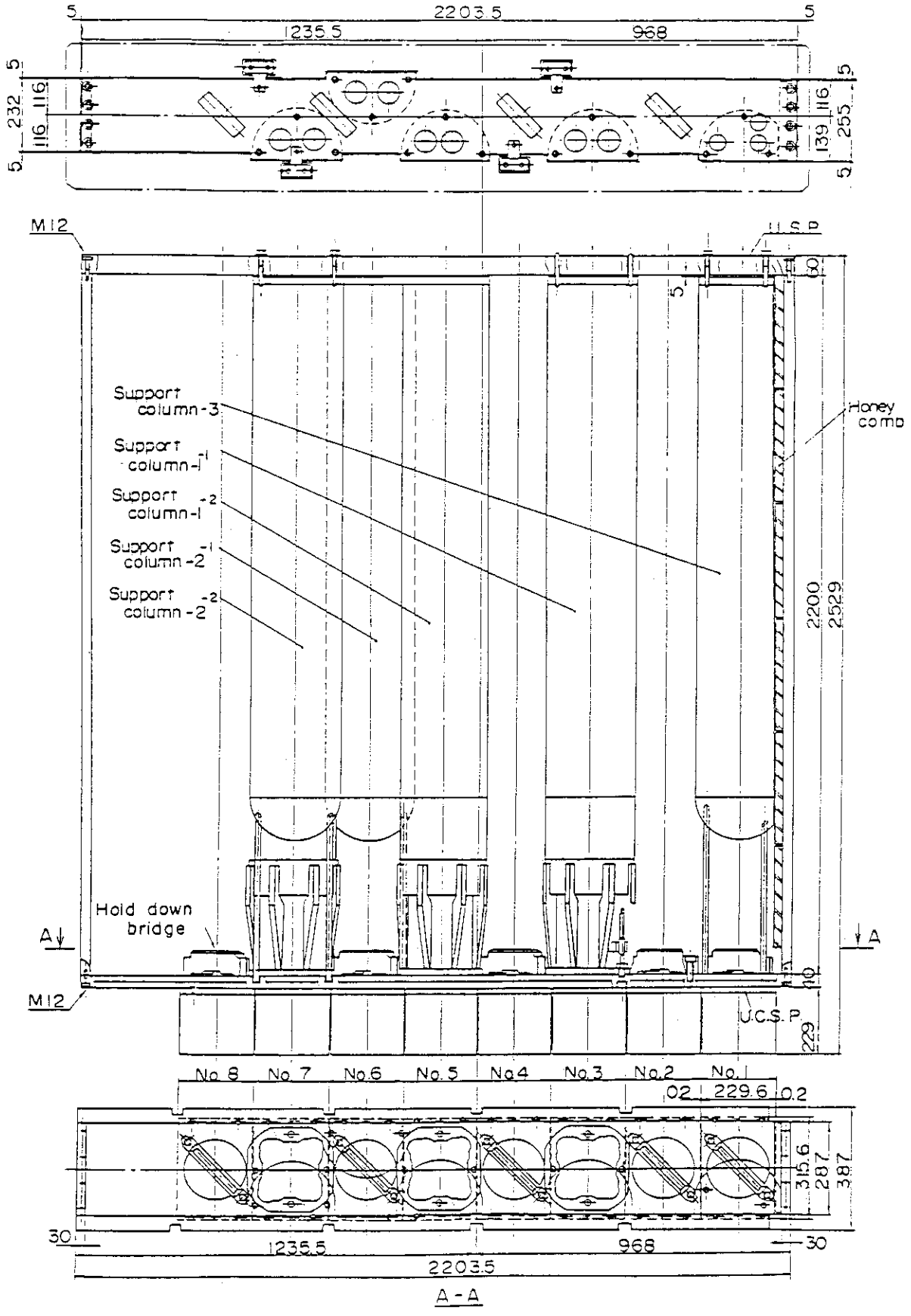

Fig. A-10 Three Kinds of CRGA Support Column

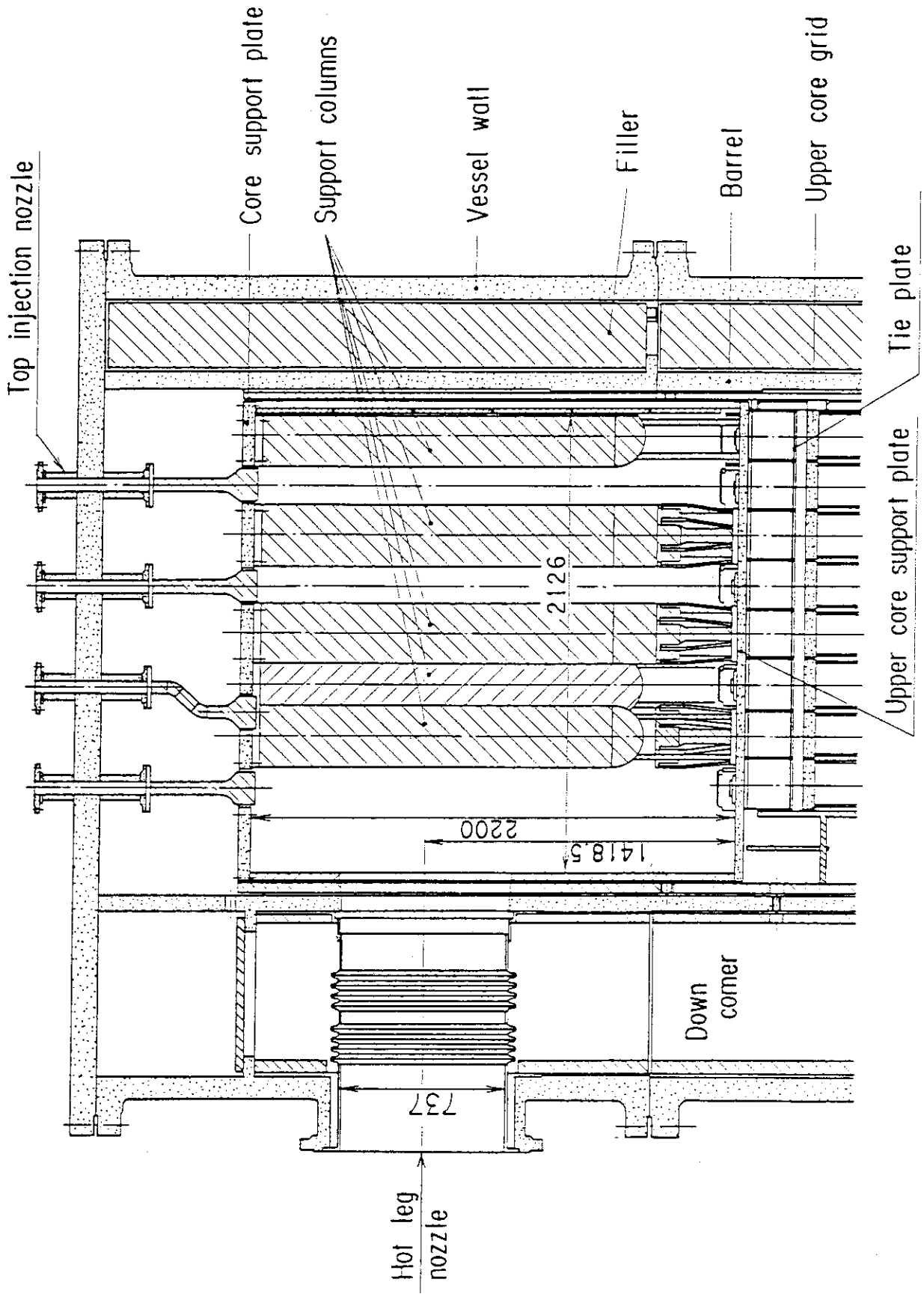

Fig. A-9 Vertical Cross Section of Upper Plenum Internals

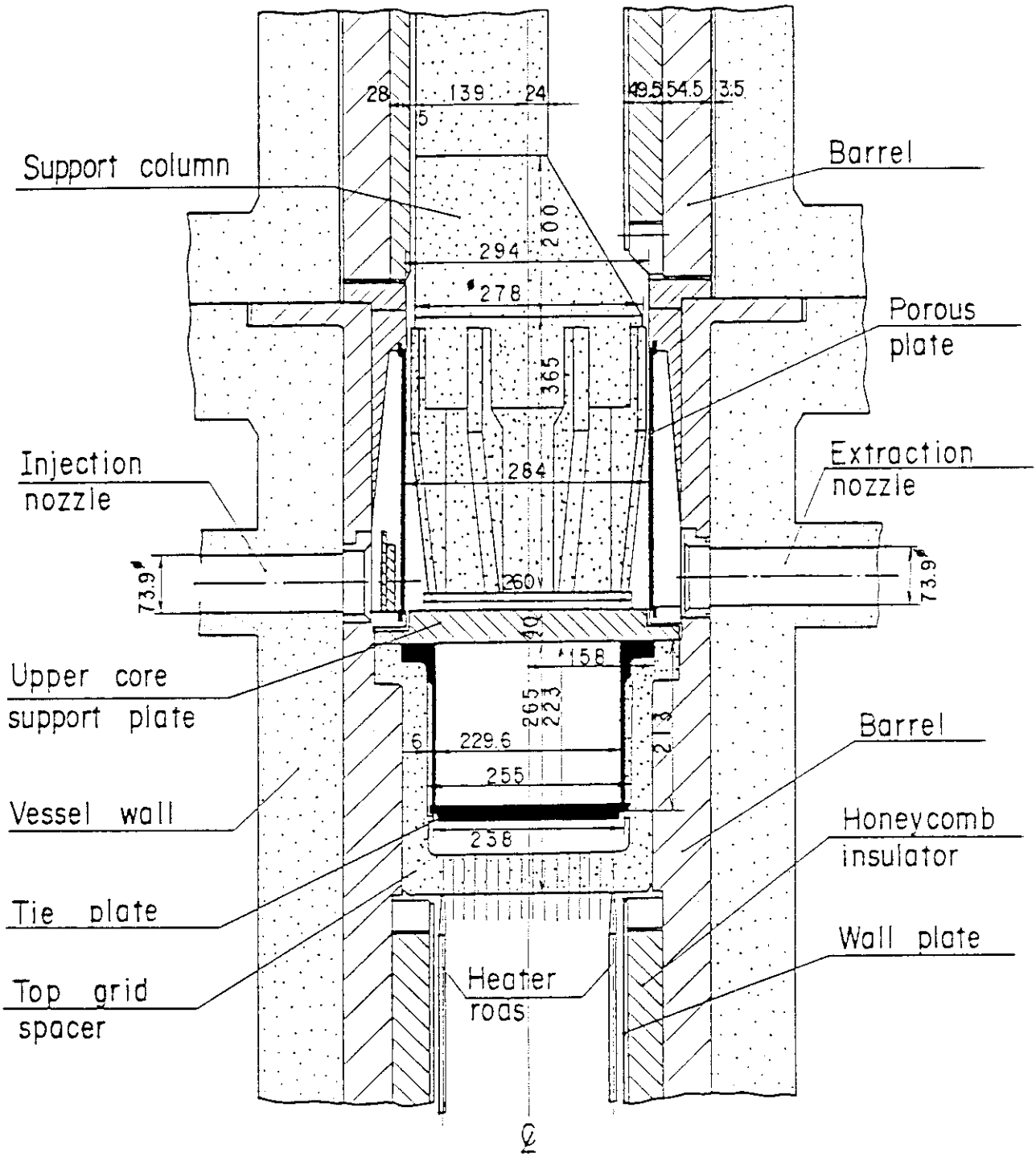

Fig. A-11 Vertical Cross Section of Interface between Core and Upper Plenum

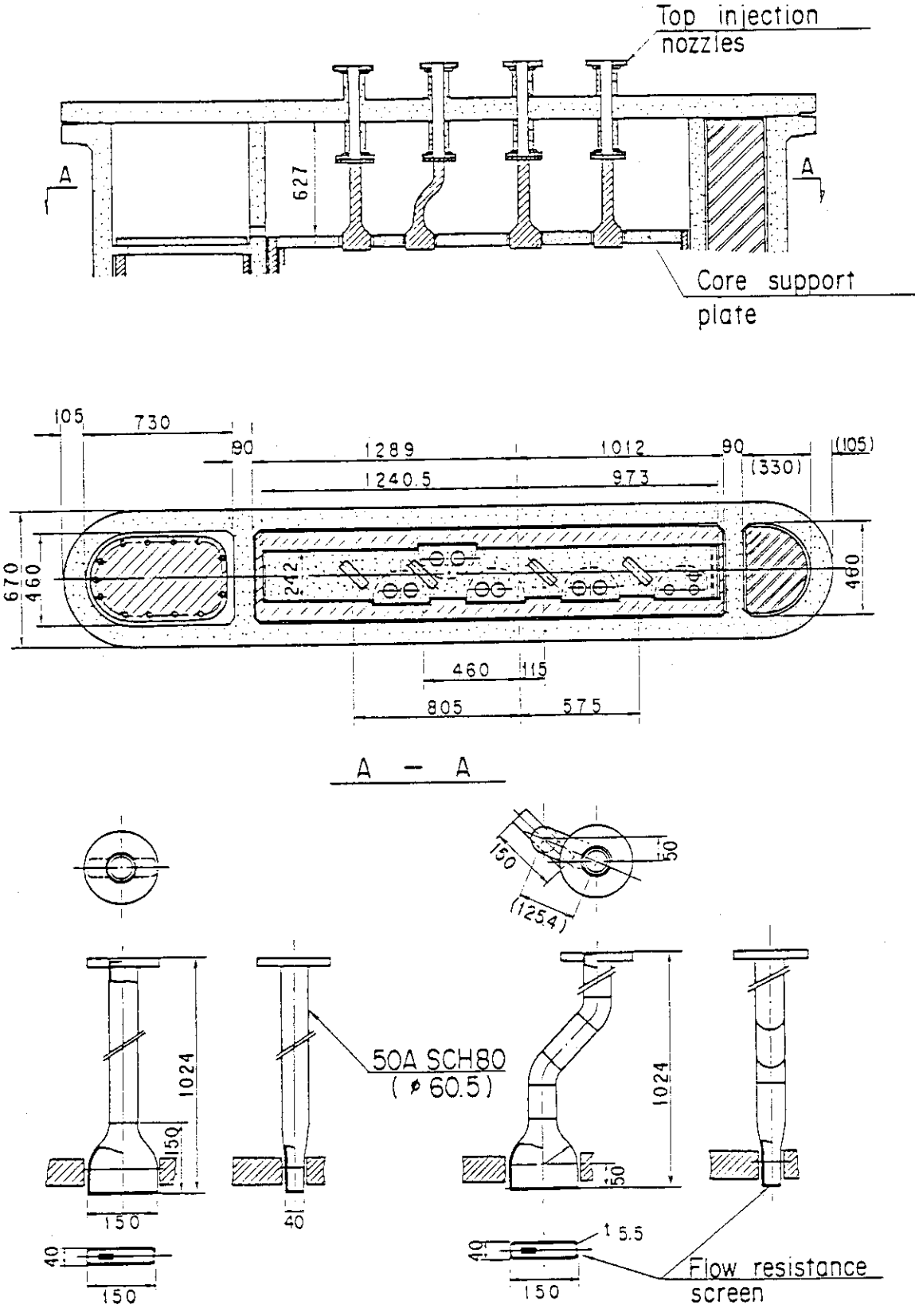

Fig. A-12 Schematic of Upper Head

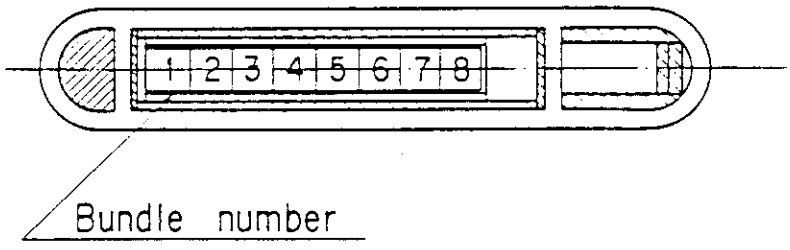

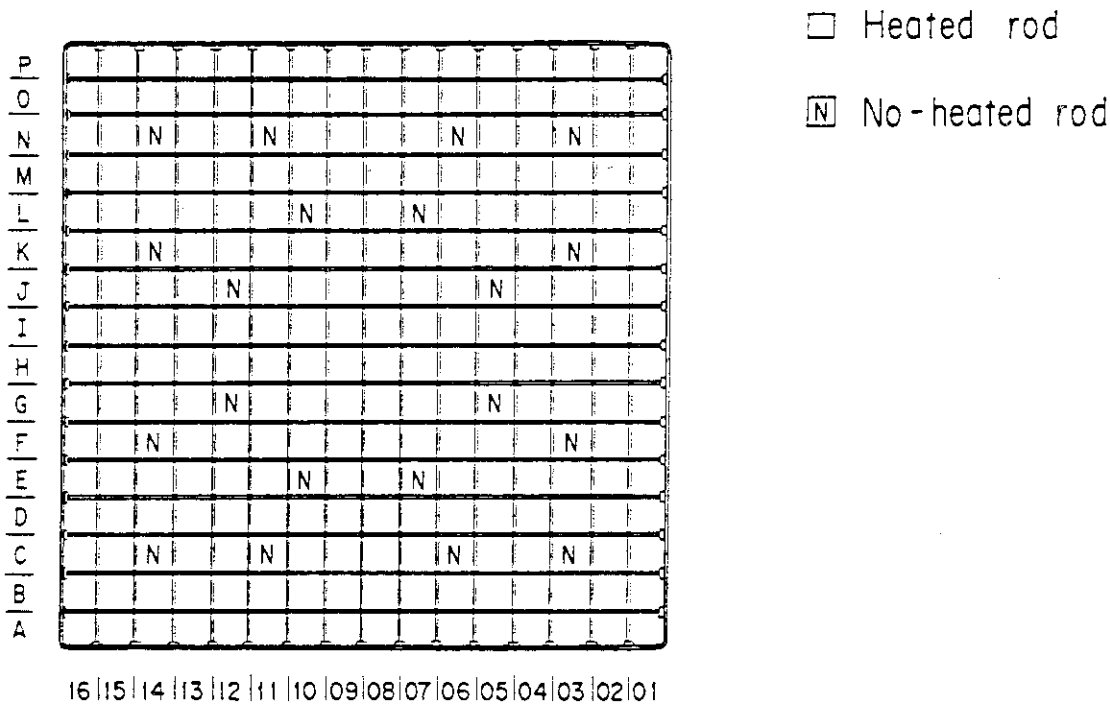

Fig. A-13 Arrangement of Heater Rod Bundles

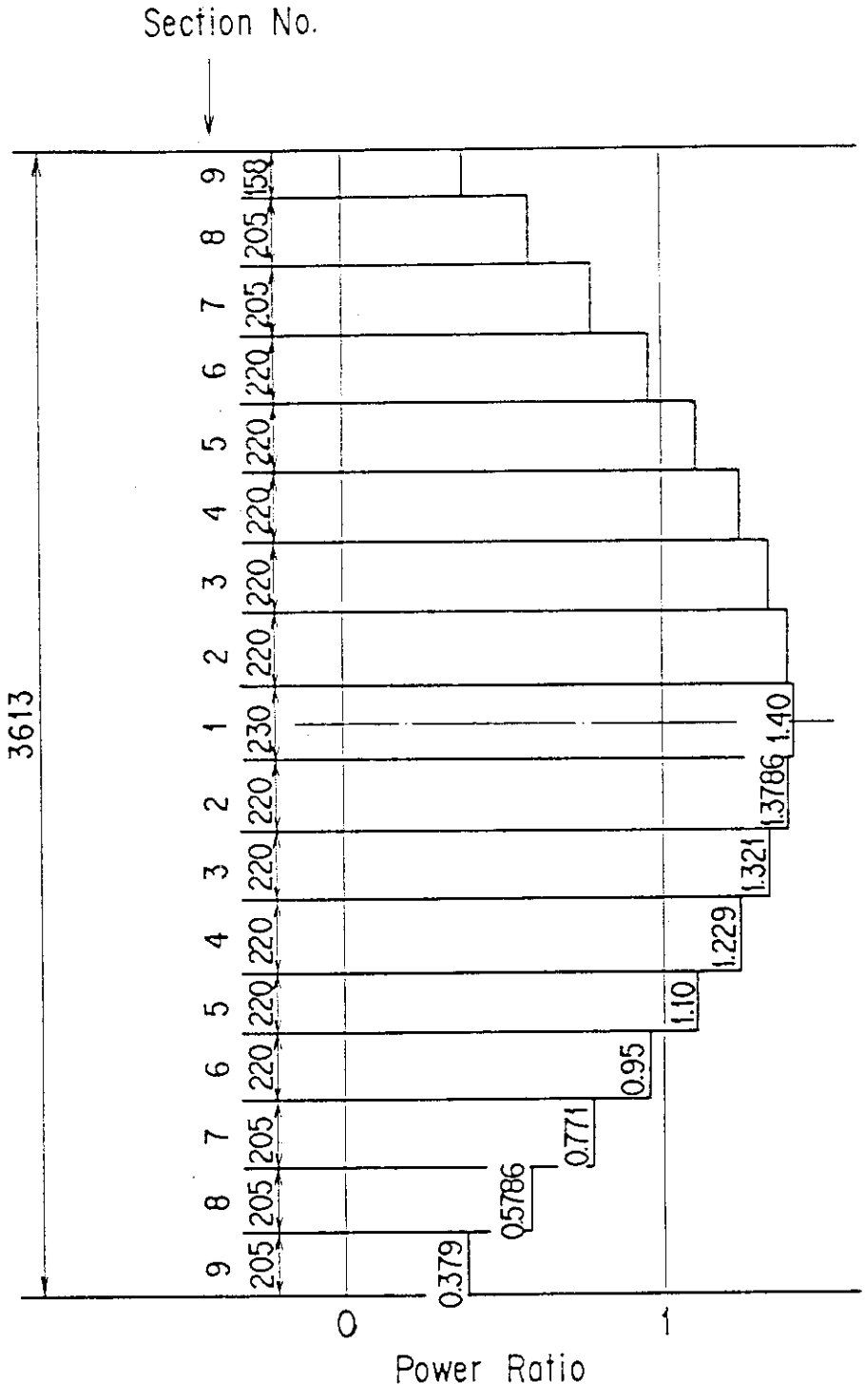

Fig. A-14 Axial Power Distribution of Heater Rods

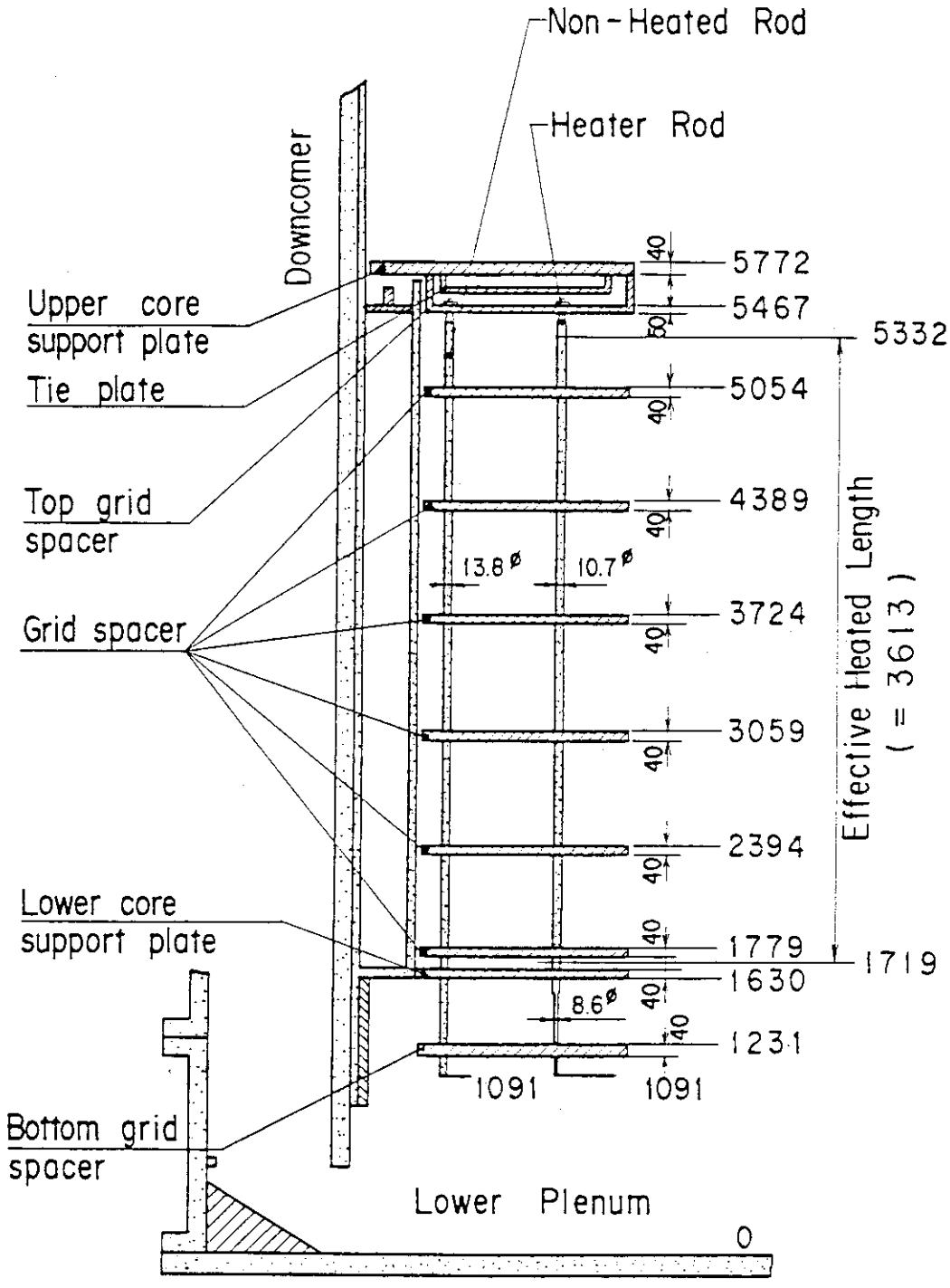

Fig. A-15 Relative Elevation and Dimension of Core

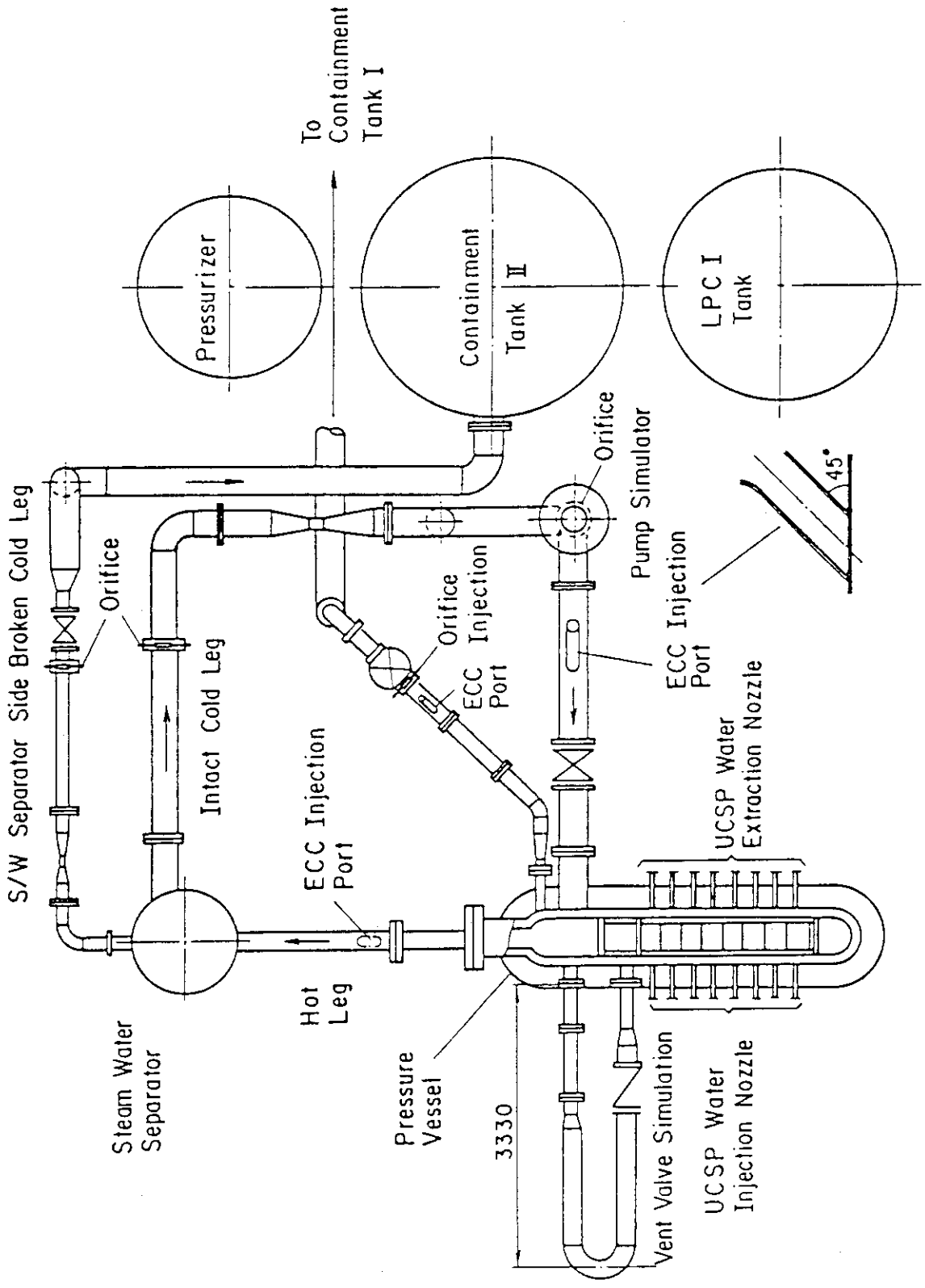

Fig. A-16 Overview of the Arrangements of SCTF

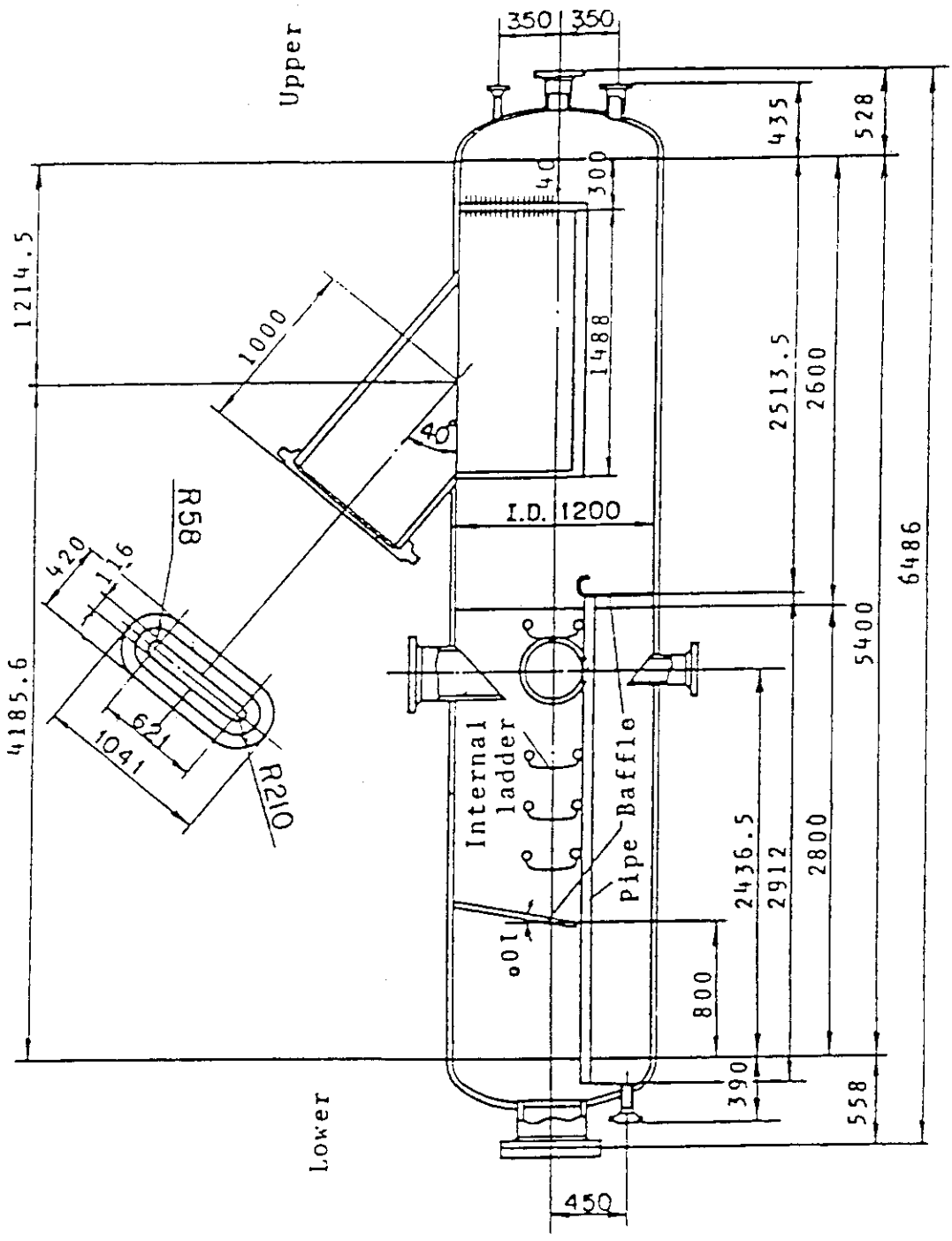

Fig. A-17 Steam/Water Separator

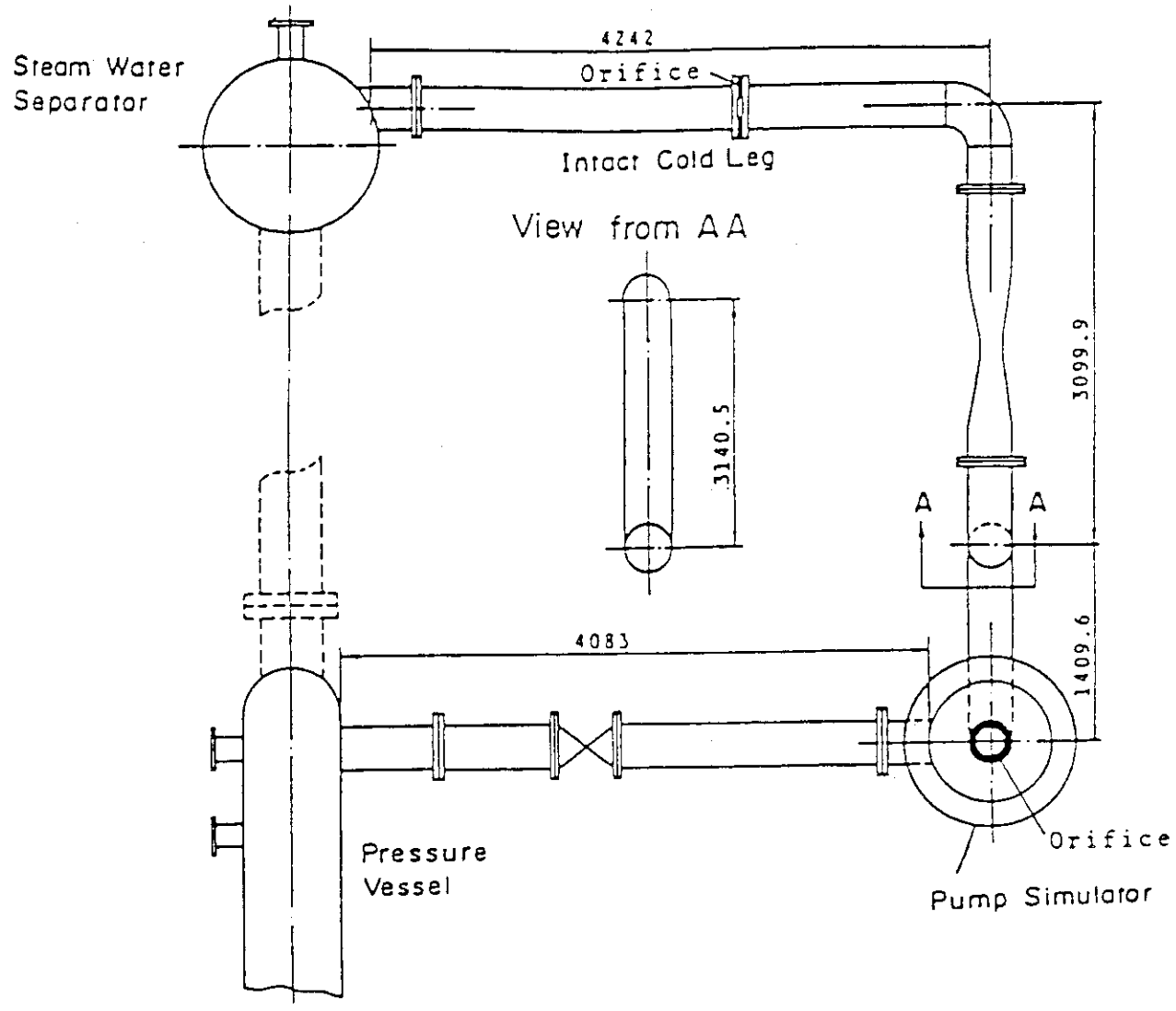

Fig. A-18 Arrangement of Intact Cold Leg

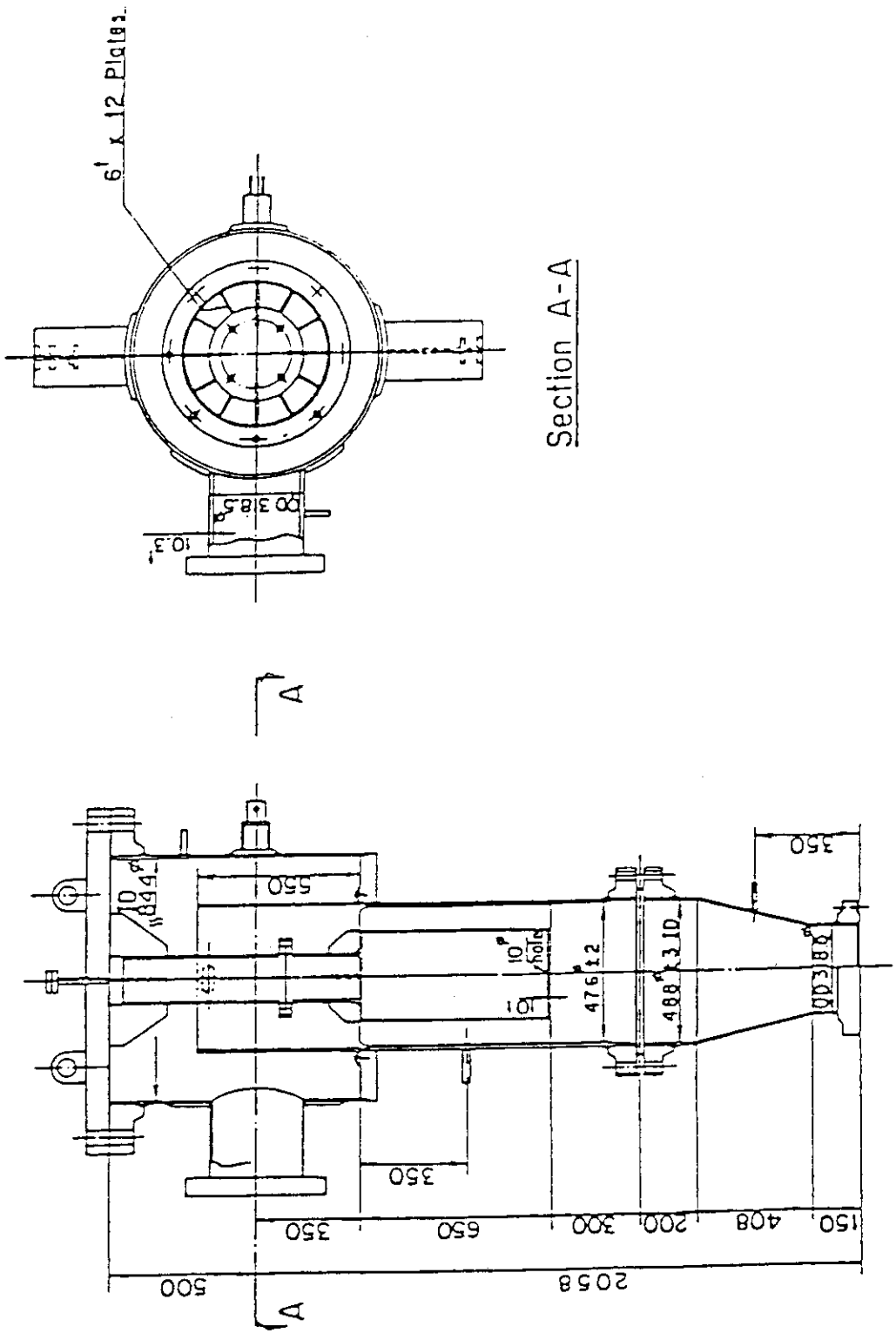

Fig. A-19 Configuration and Dimension of Pump Simulator

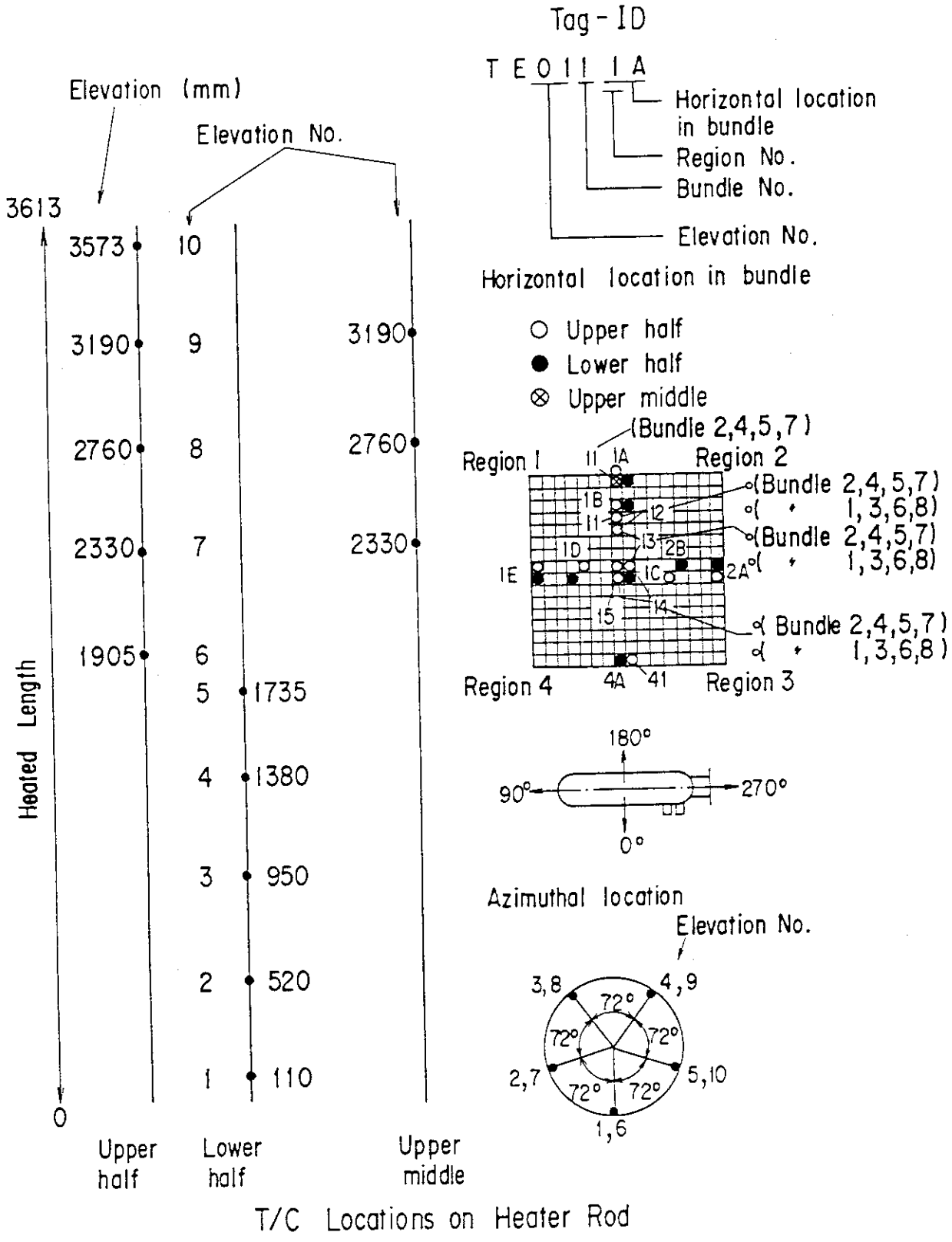

Fig. A-20 Thermocouple Locations of Heater Rod Surface Temperature Measurements

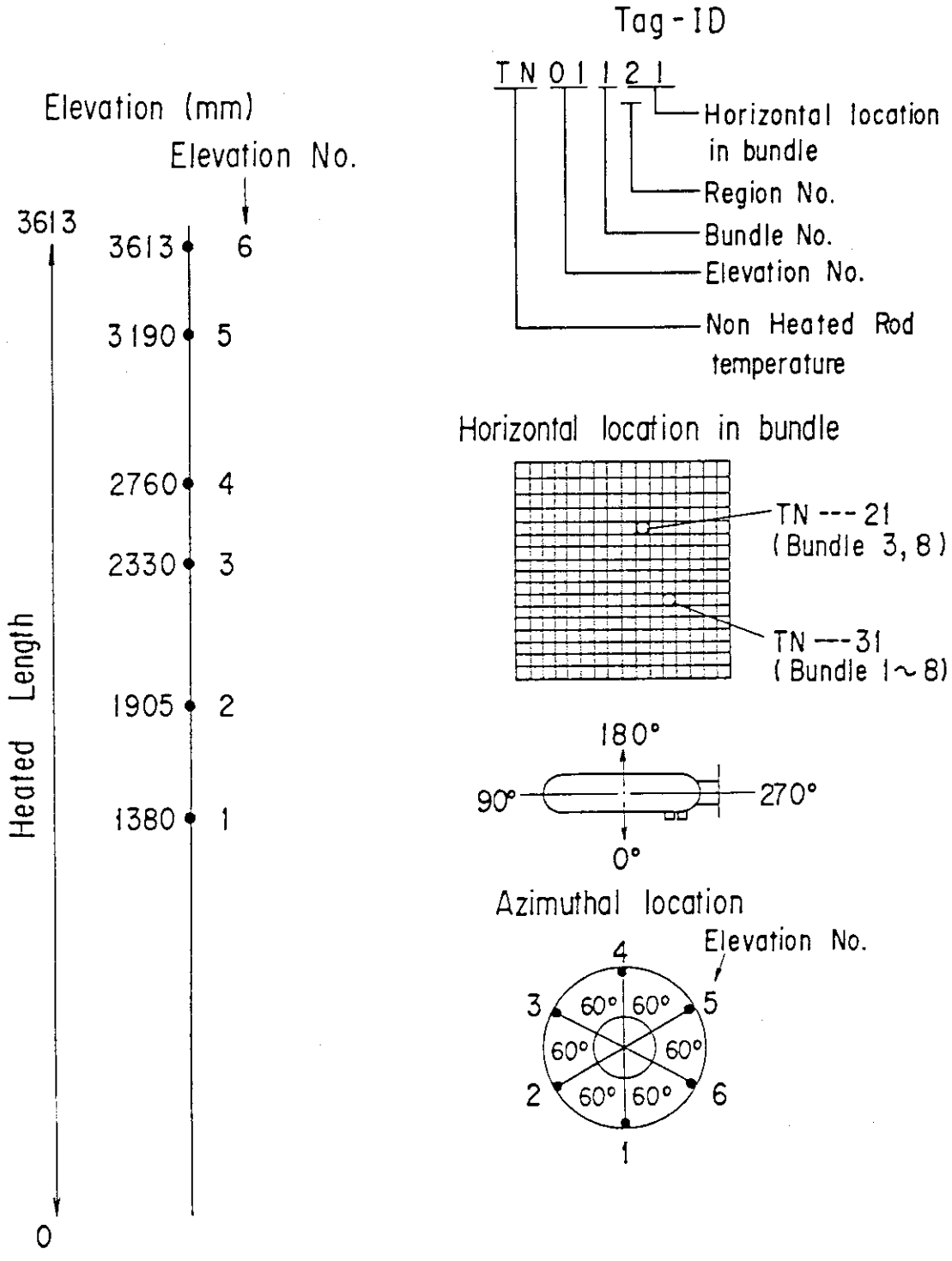

Fig. A-21 Thermocouple Locations of Non-Heated Rod Surface temperature Measurements

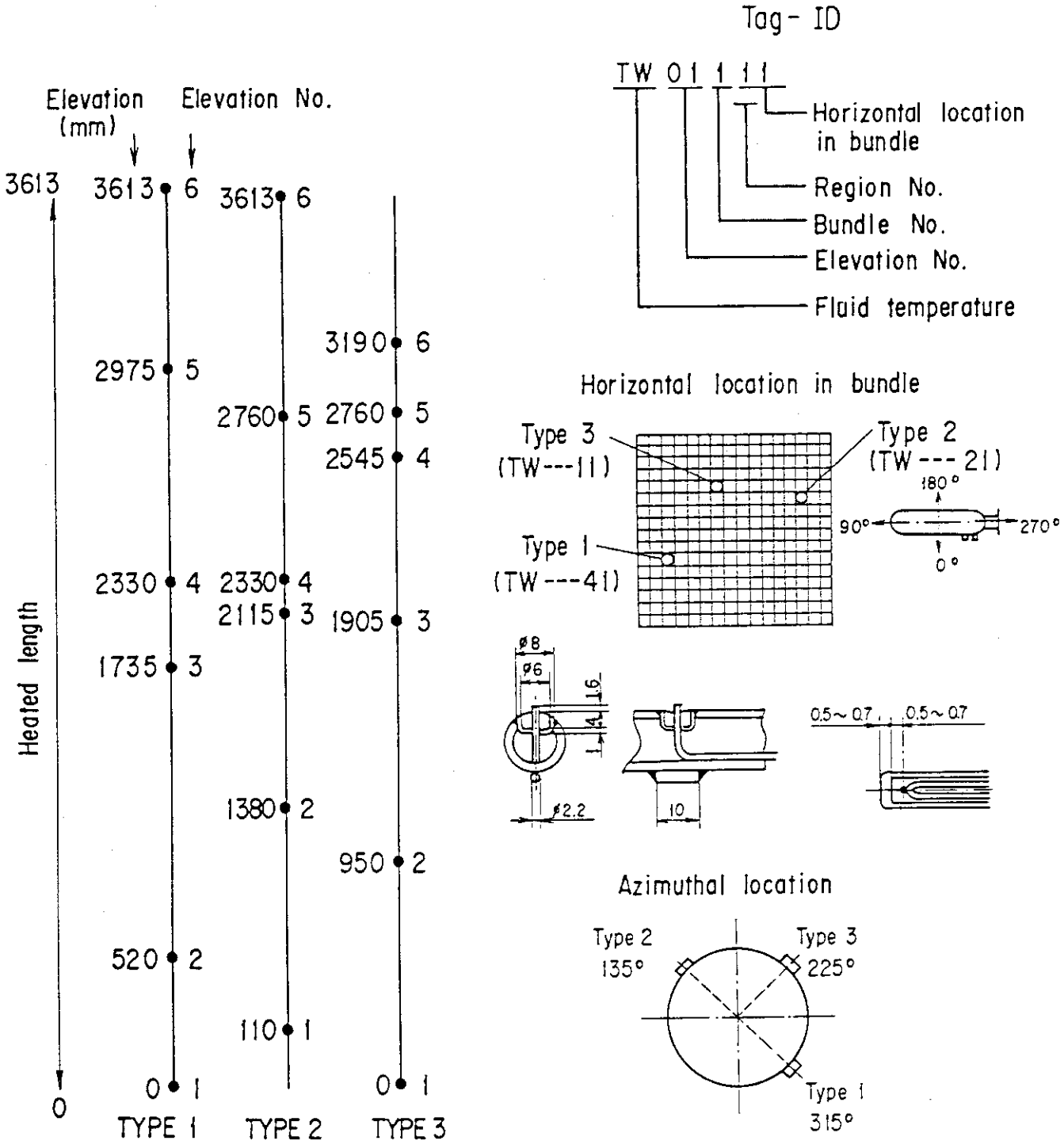

Fig. A-22 Thermocouple Locations of Fluid Temperature Measurements in Core

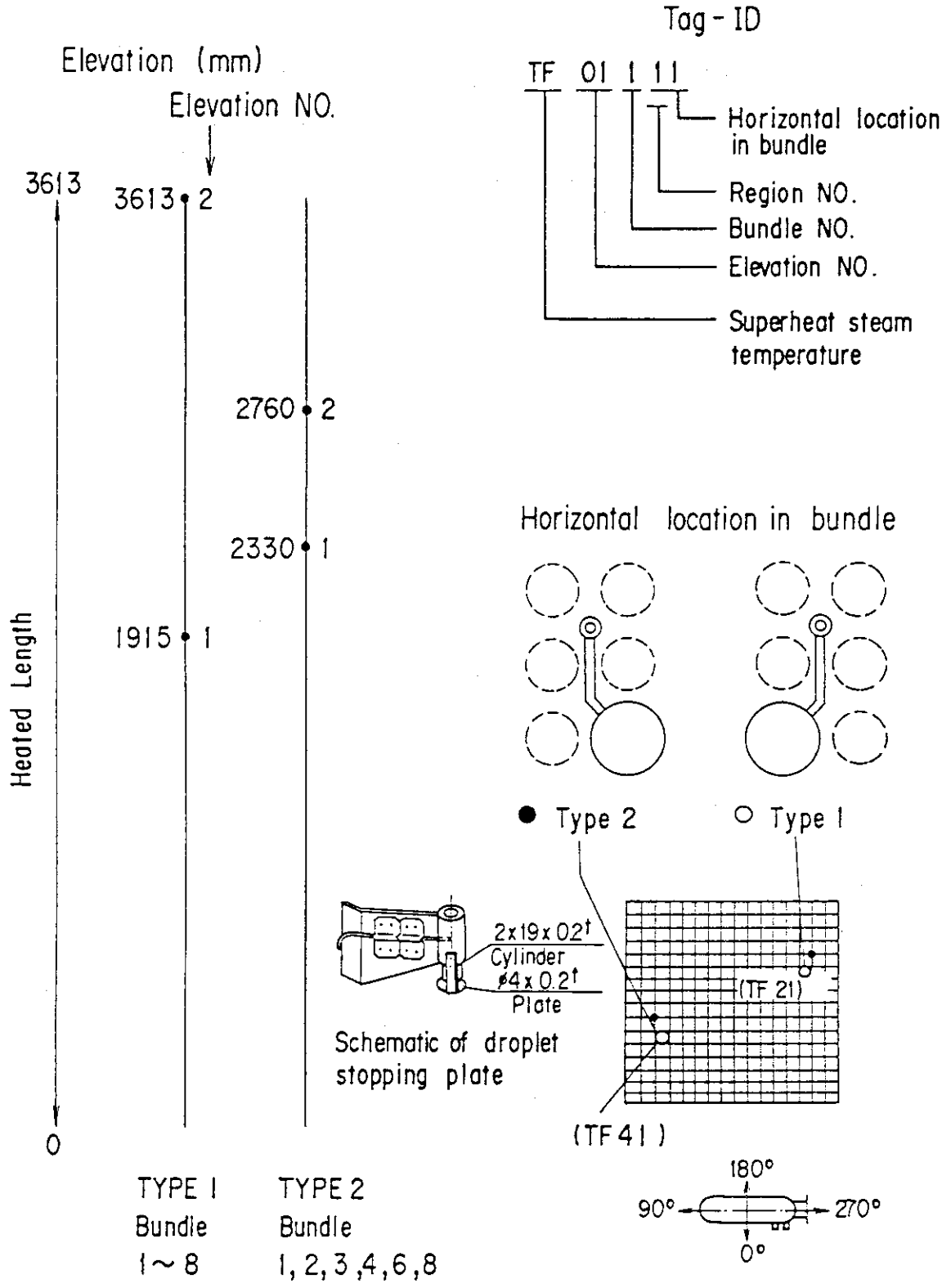

Fig. A-23 Thermocouple Locations of Steam Temperature Measurements in Core

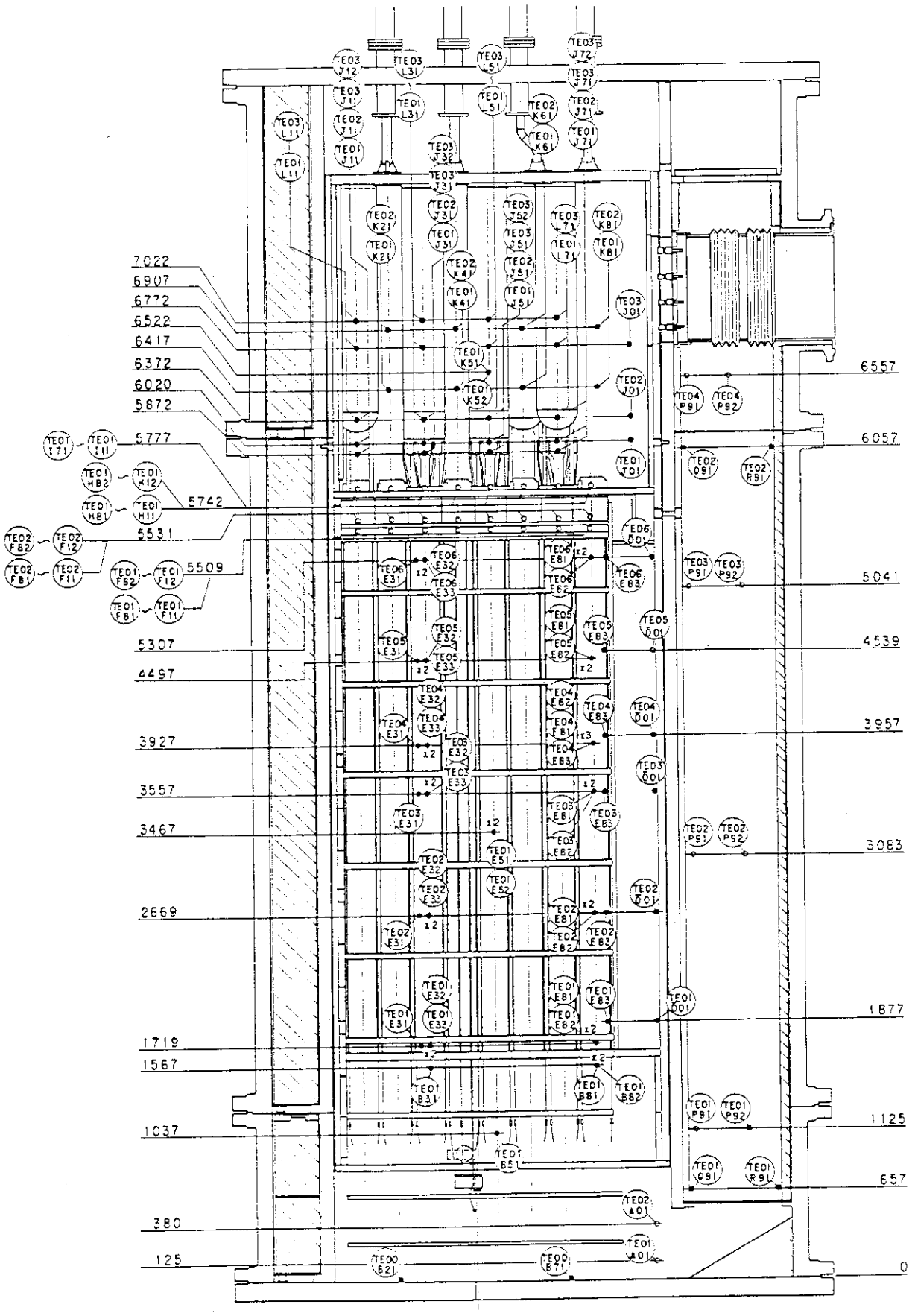

Fig. A-24 Thermocouple Locations of Temperature Measurements in Pressure Vessel except Core Region (Vertical View)

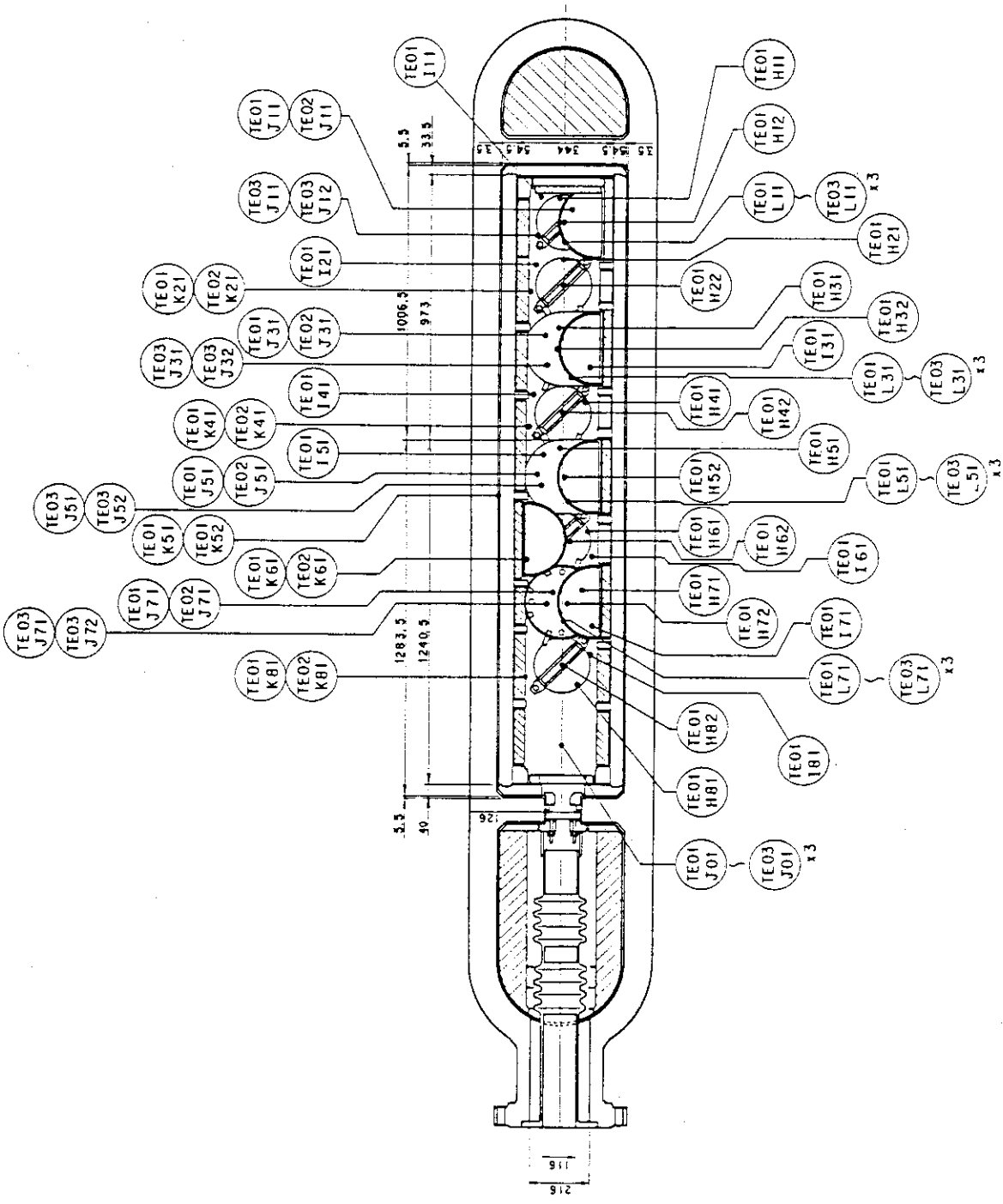

Fig. A-25 Thermocouple Locations of Temperature Measurements in Upper Plenum (Horizontal View)

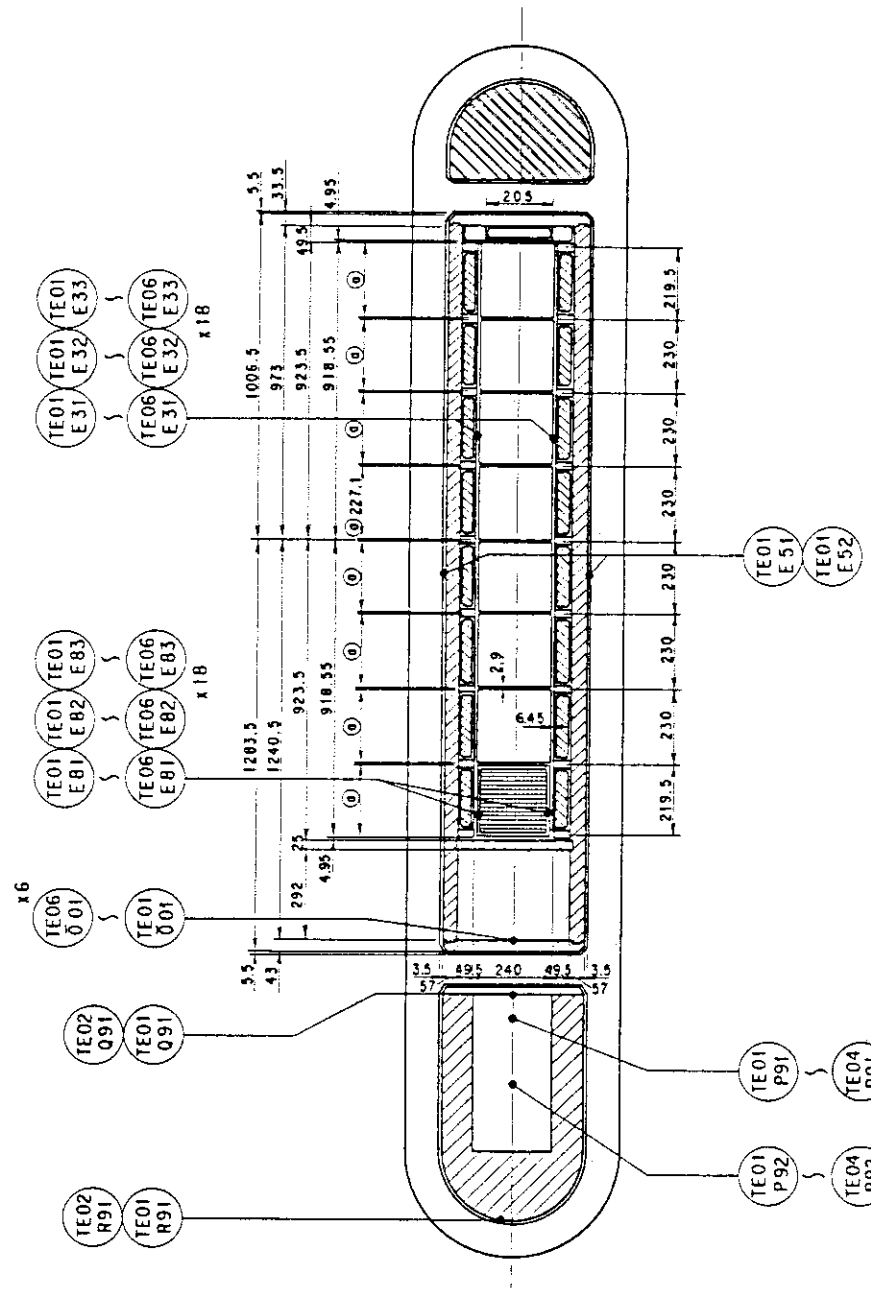

Fig. A-26 Thermocouple Locations of Temperature Measurements in Pressure Vessel except Upper Plenum (Horizontal View)

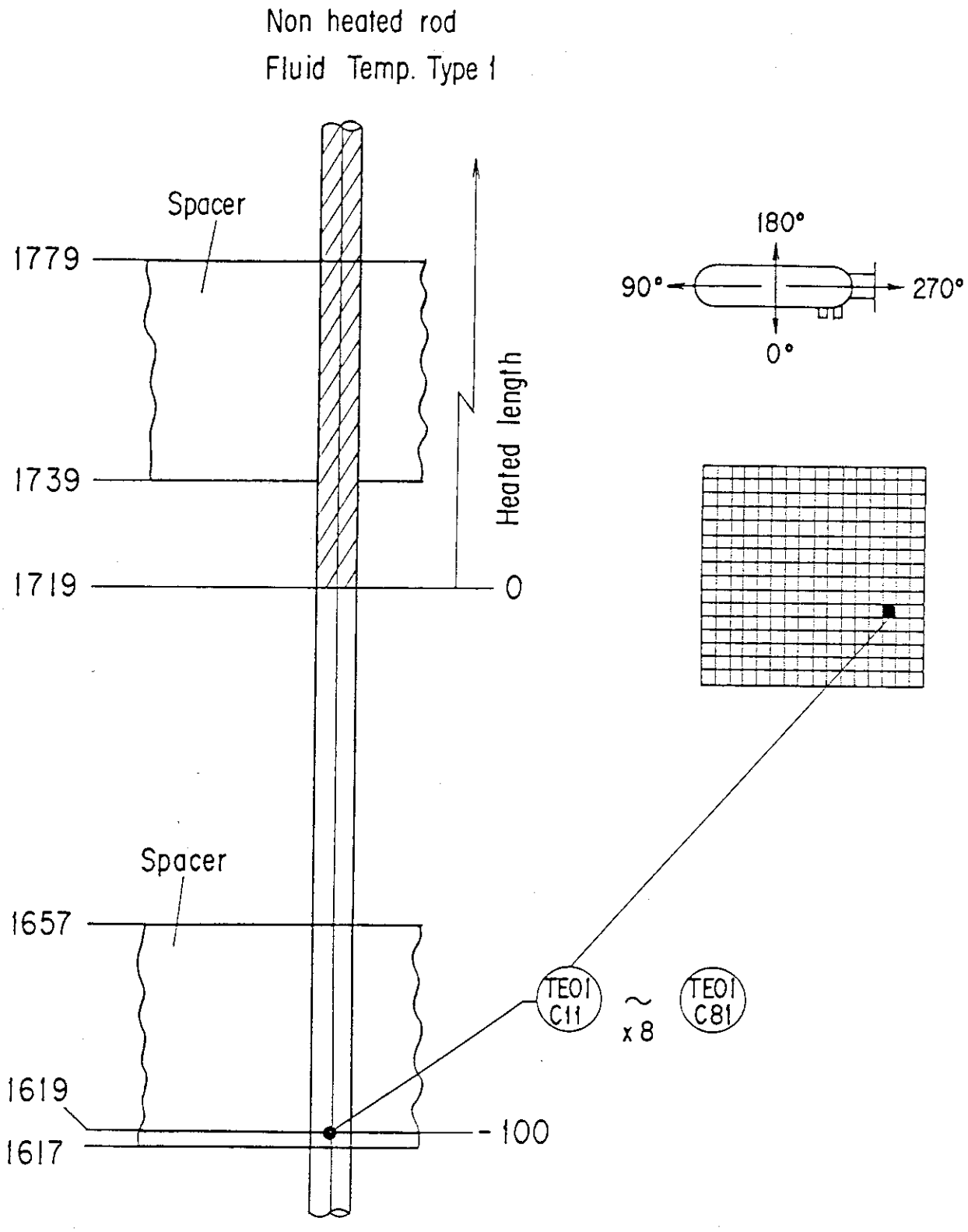

Fig. A-27 Thermocouple Locations of Fluid Temperature Measurements at Core Inlet

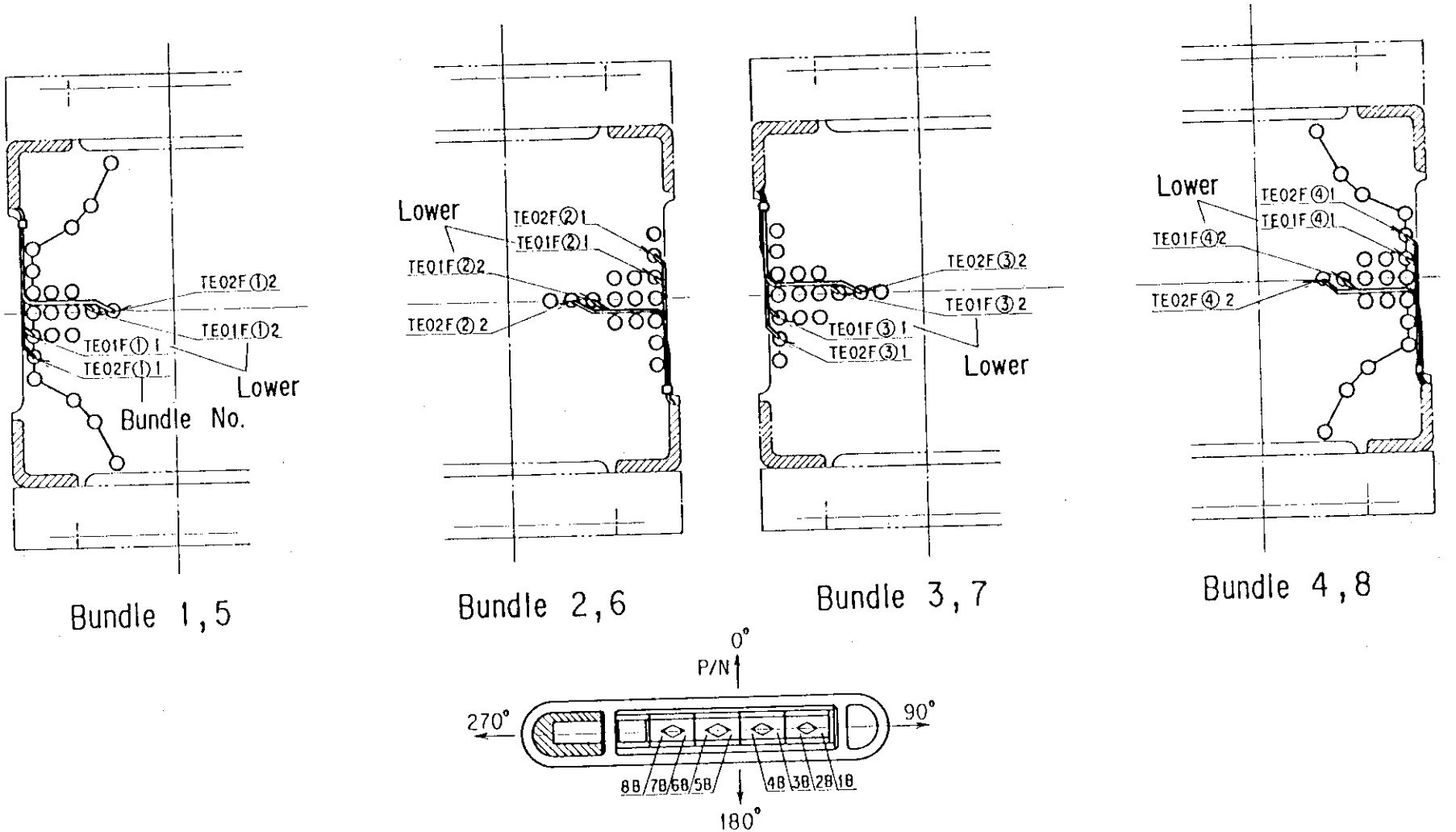

Fig. A-28 Thermocouple Locations of Fluid Temperature Measurements just above and below End Box Tie Plates

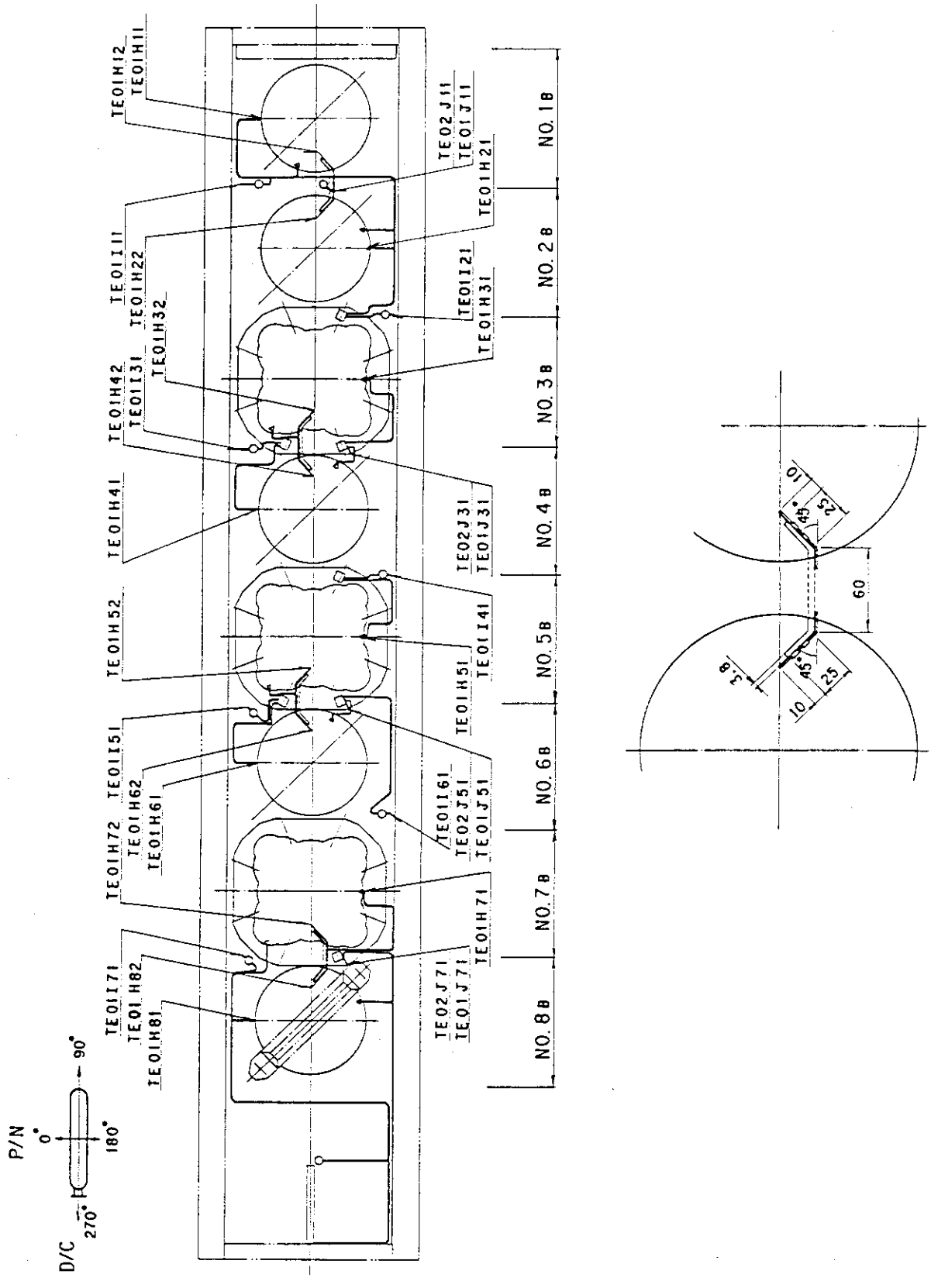

Fig. A-29 Thermocouple Locations of Fluid Temperature Measurements on UCSP and at Inside and Periphery of UCSP Holes

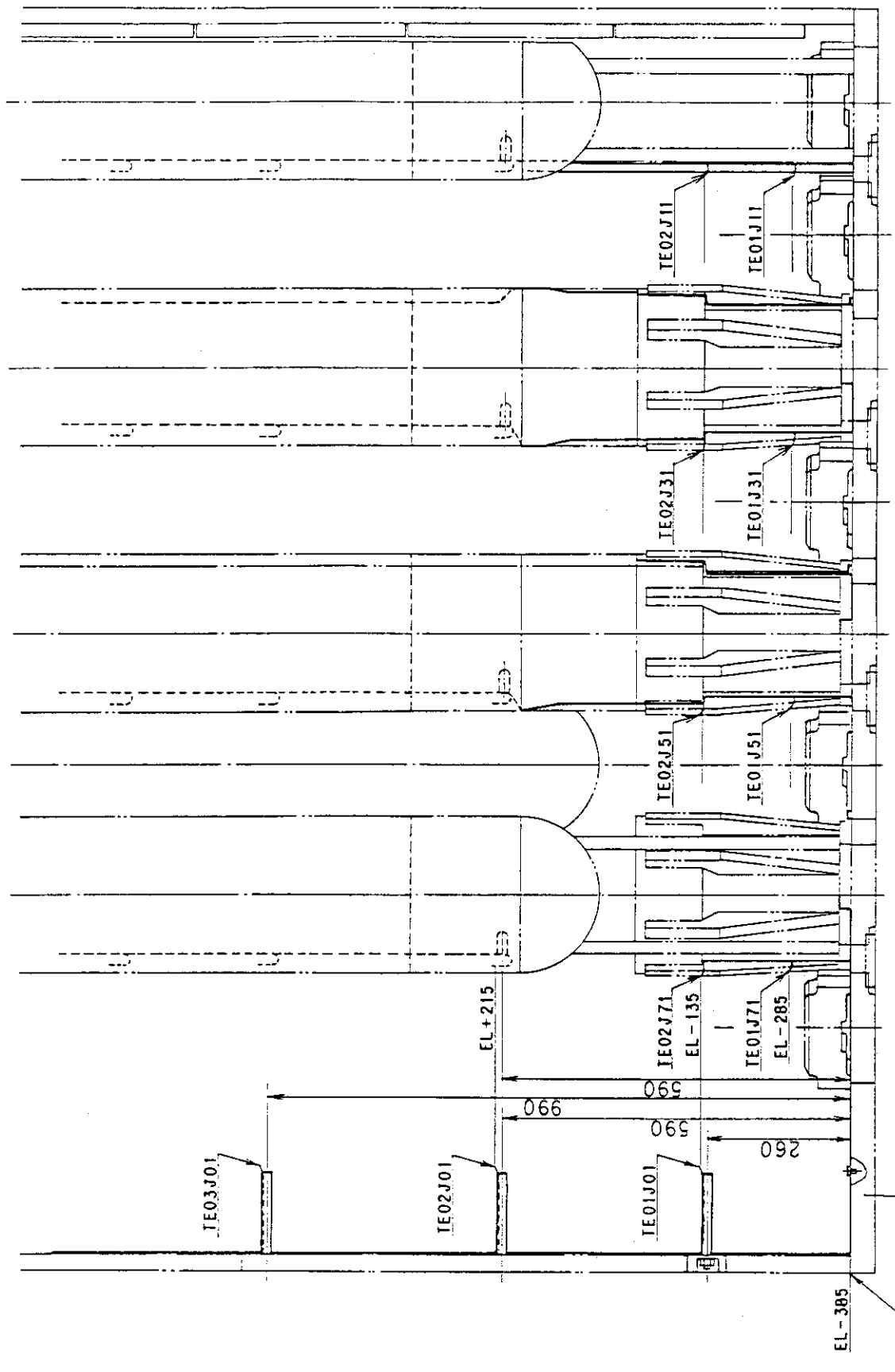

Fig. A-30 Thermocouple Locations of Fluid Temperature Measurements on and above UCSP

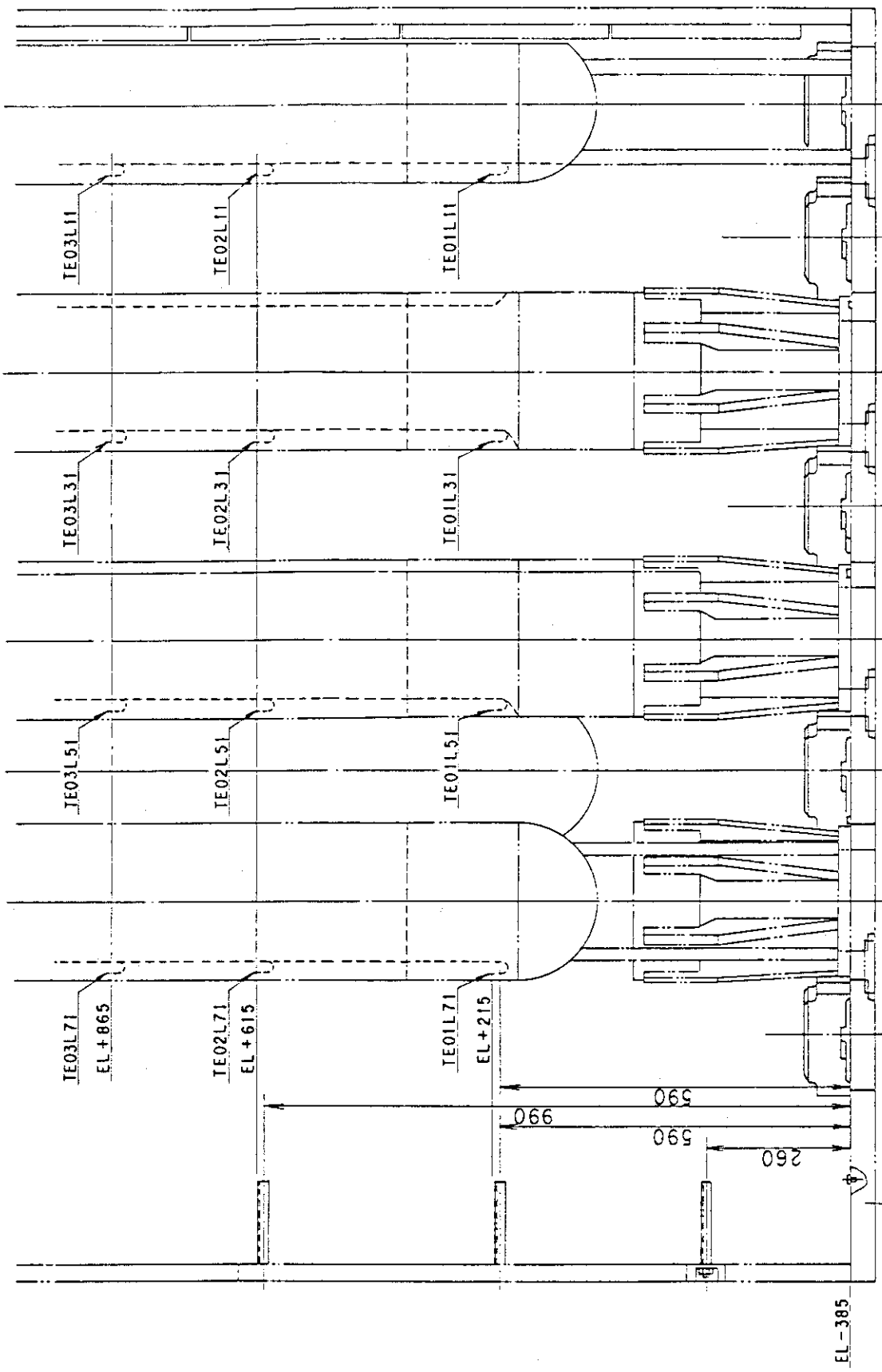

Fig. A-31 Thermocouple Locations of Surface Temperature Measurements of Upper Plenum Structures

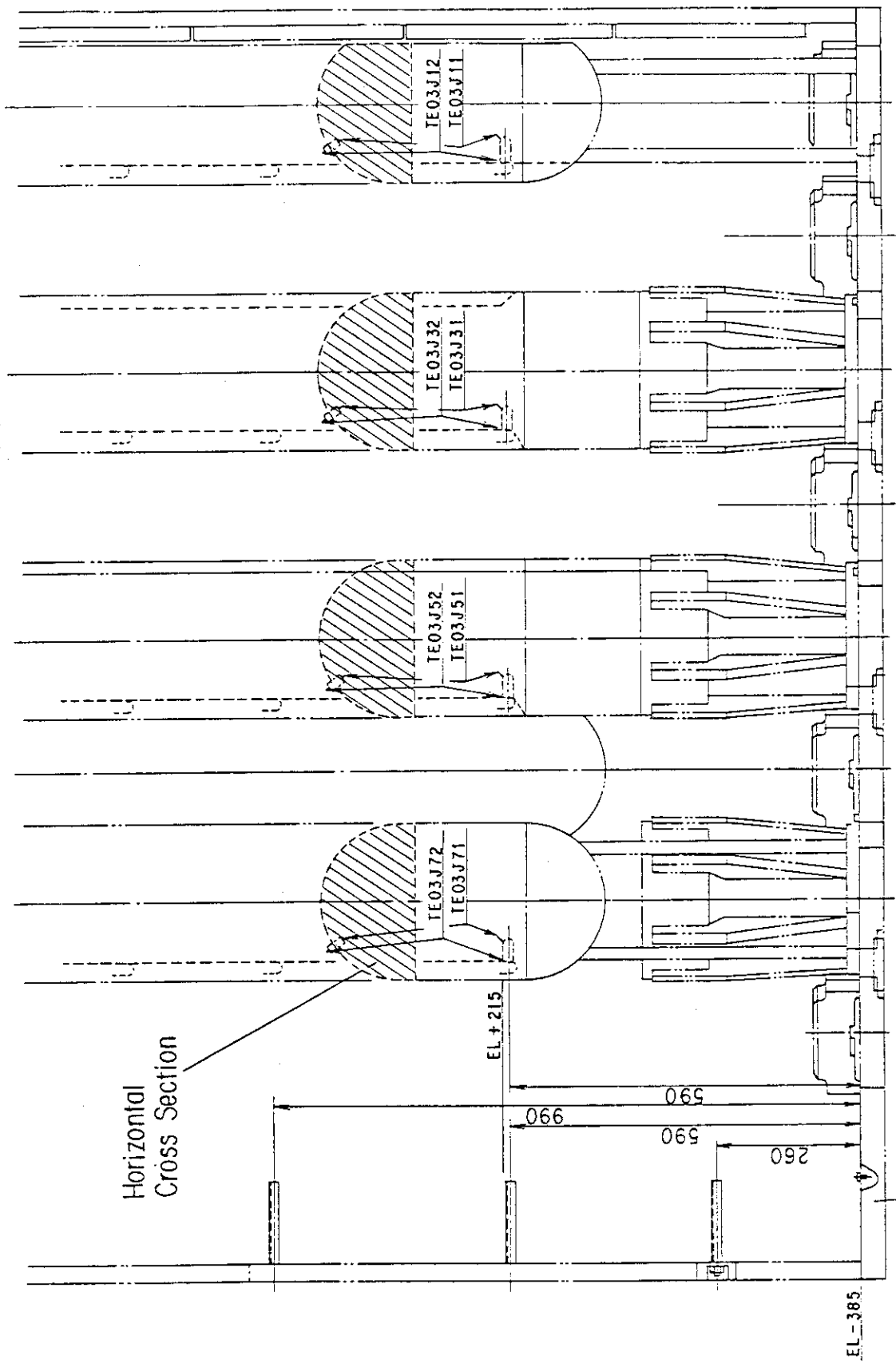

Fig. A-32 Thermocouple Locations of Steam Temperature Measurements above UCSP Holes

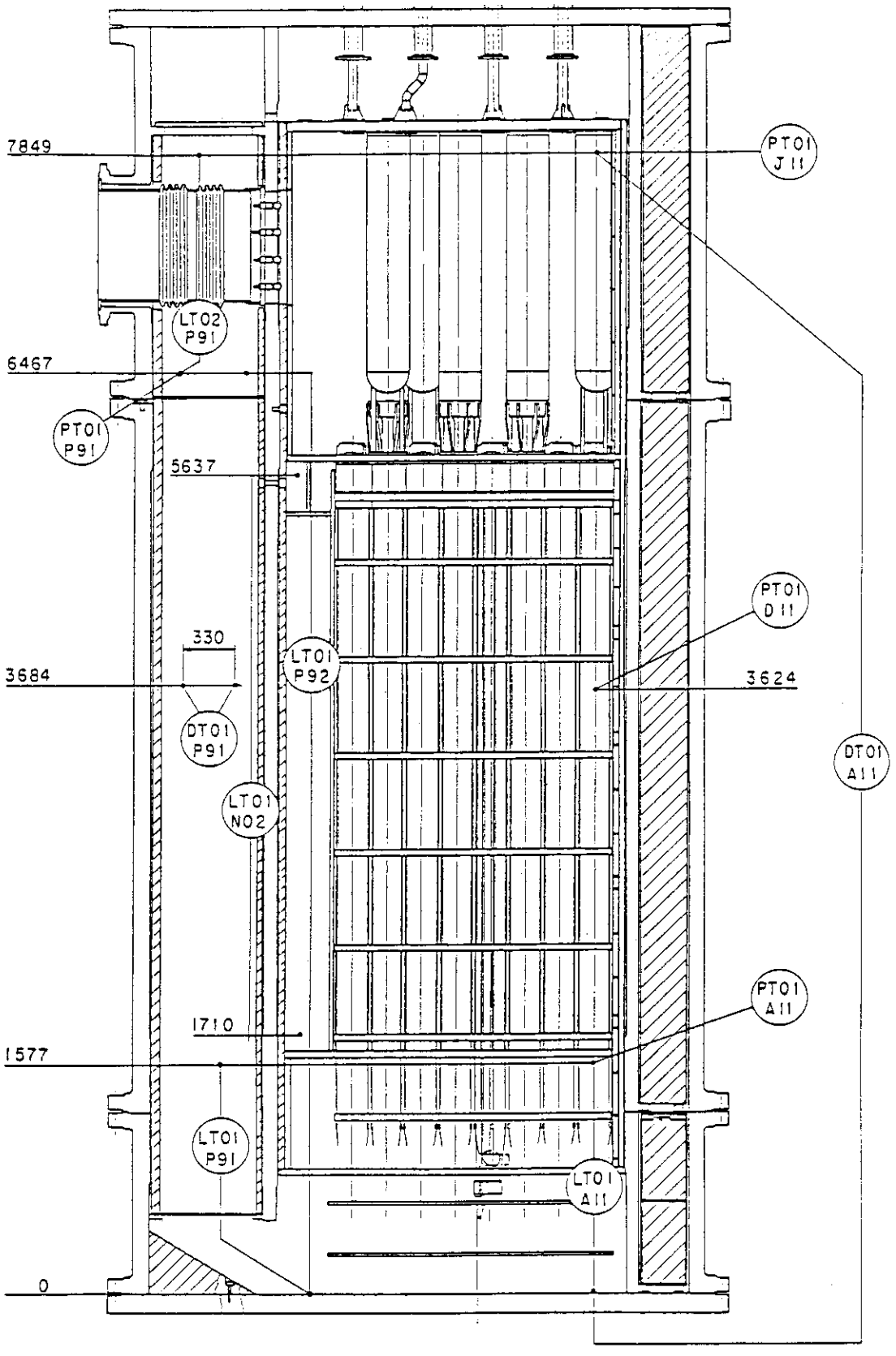

Fig. A-33 Locations of Pressure Measurements in Pressure Vessel, Differential Pressure Measurements between Upper and Lower Plenums and Liquid Level Measurements in Downcomer and Lower Plenum

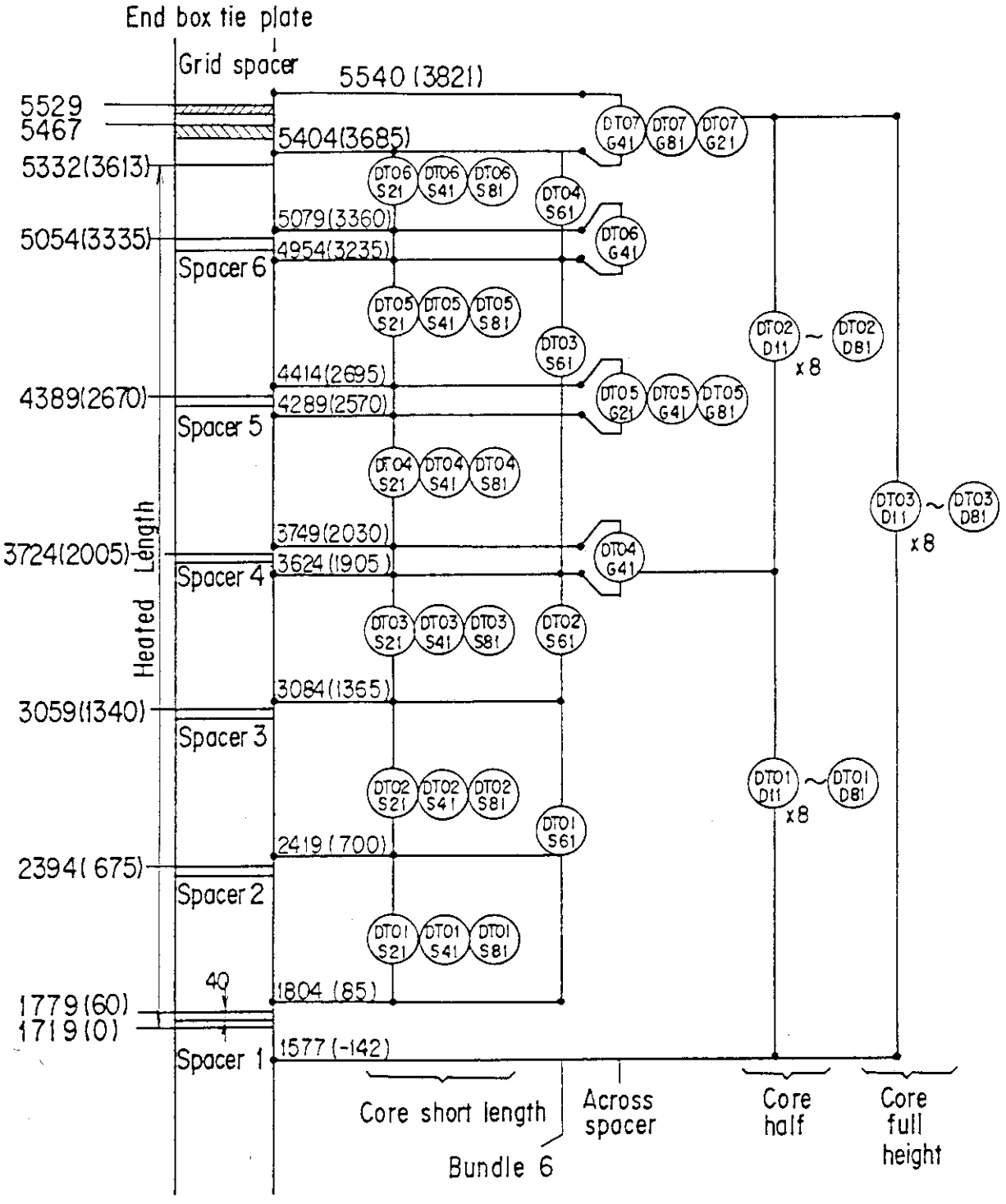

Fig. A-34 Locations of Vertical Differential Pressure Measurements in Core

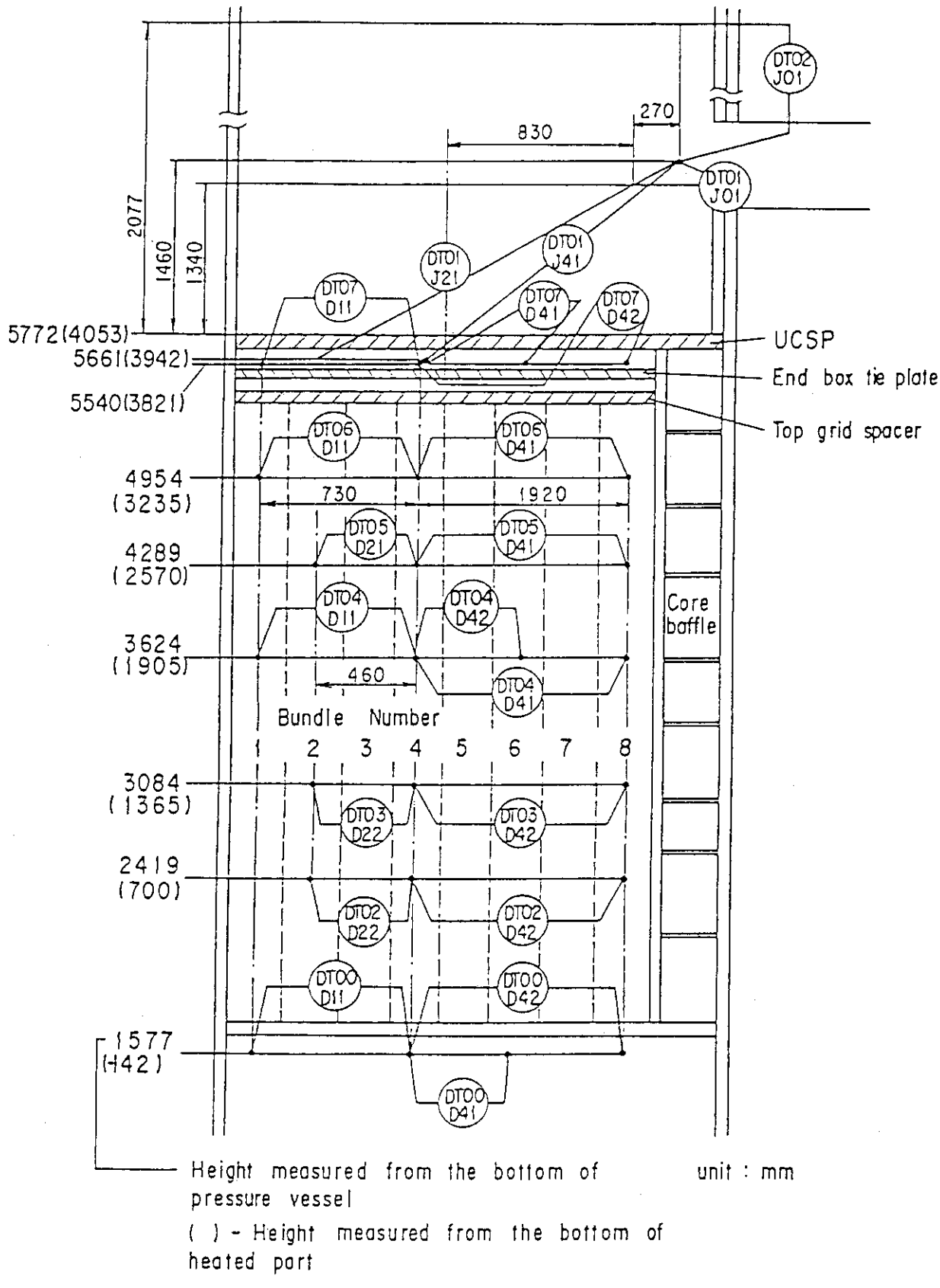

Fig. A-35 Locations of Horizontal Differential Pressure Measurements in Core and Differential Pressure Measurements between End Boxes and Inlet of Hot Leg

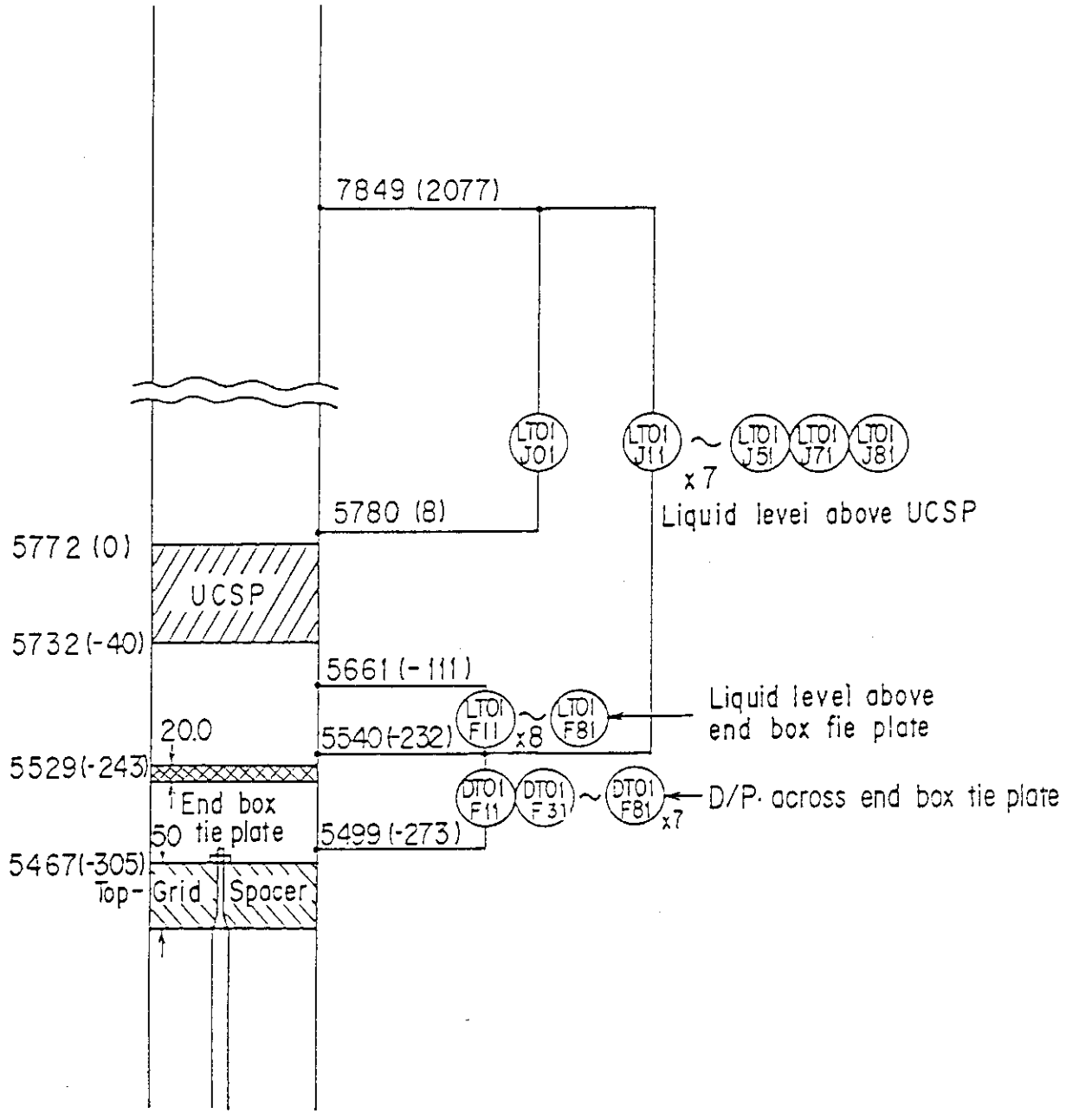

Fig. A-35 Locations of Differential Pressure Measurements across End Box Tie Plate

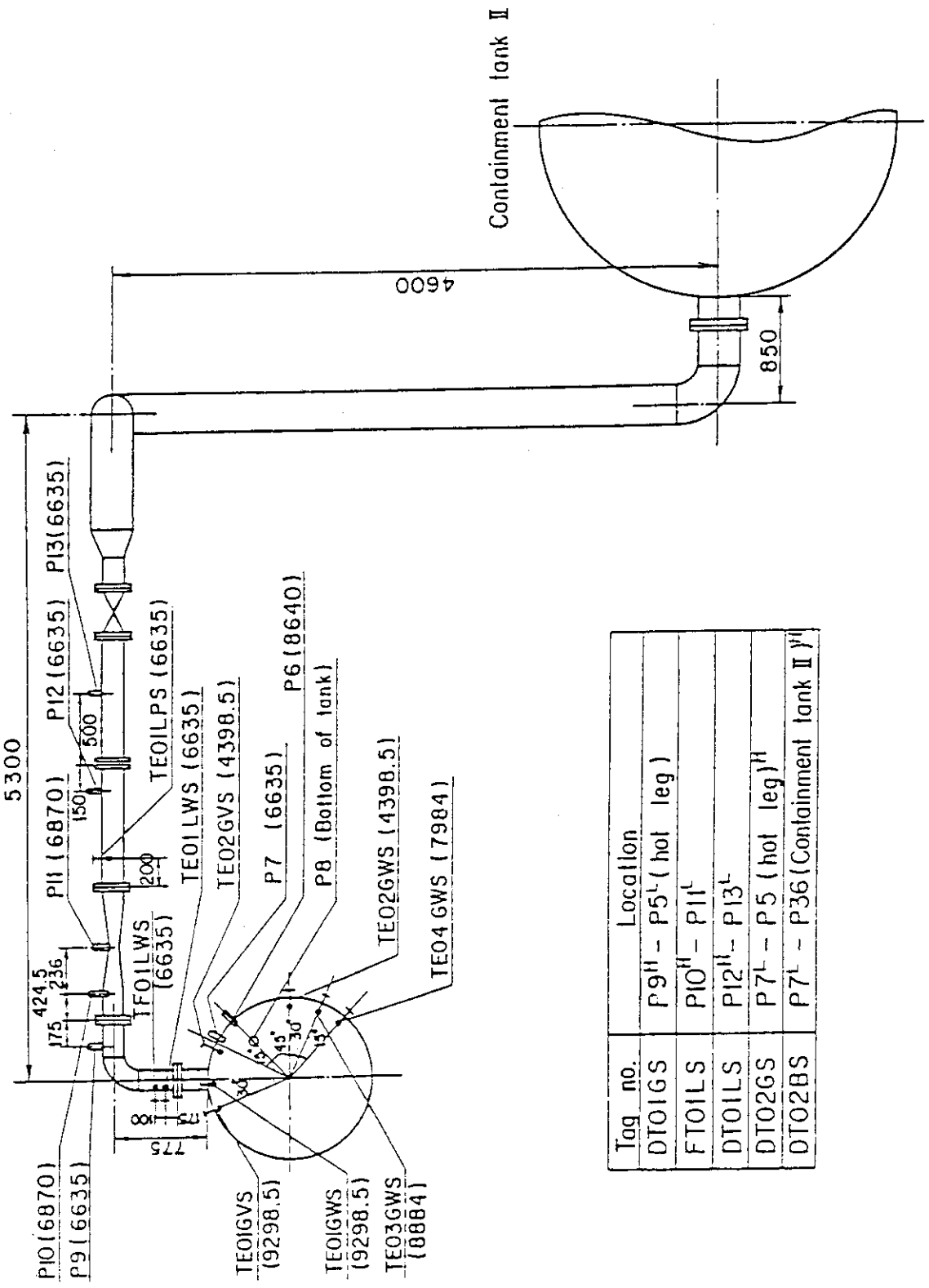

Tag no.	Location
DT01GS	$P9^{H}$ - $P5^{L}$ (hot leg)
FT01LS	$P10^{H}$ - $P11^{L}$
DT01LS	$P12^{H}$ - $P13^{L}$
DT02GS	$P7^{L}$ - P5 (hot leg)^{H}
DT02BS	$P7^{L}$ - P36 (Containment tank II)^{H}

Fig. A-37 Locations of Broken Cold Leg Instruments (Steam-Water Separator Side)

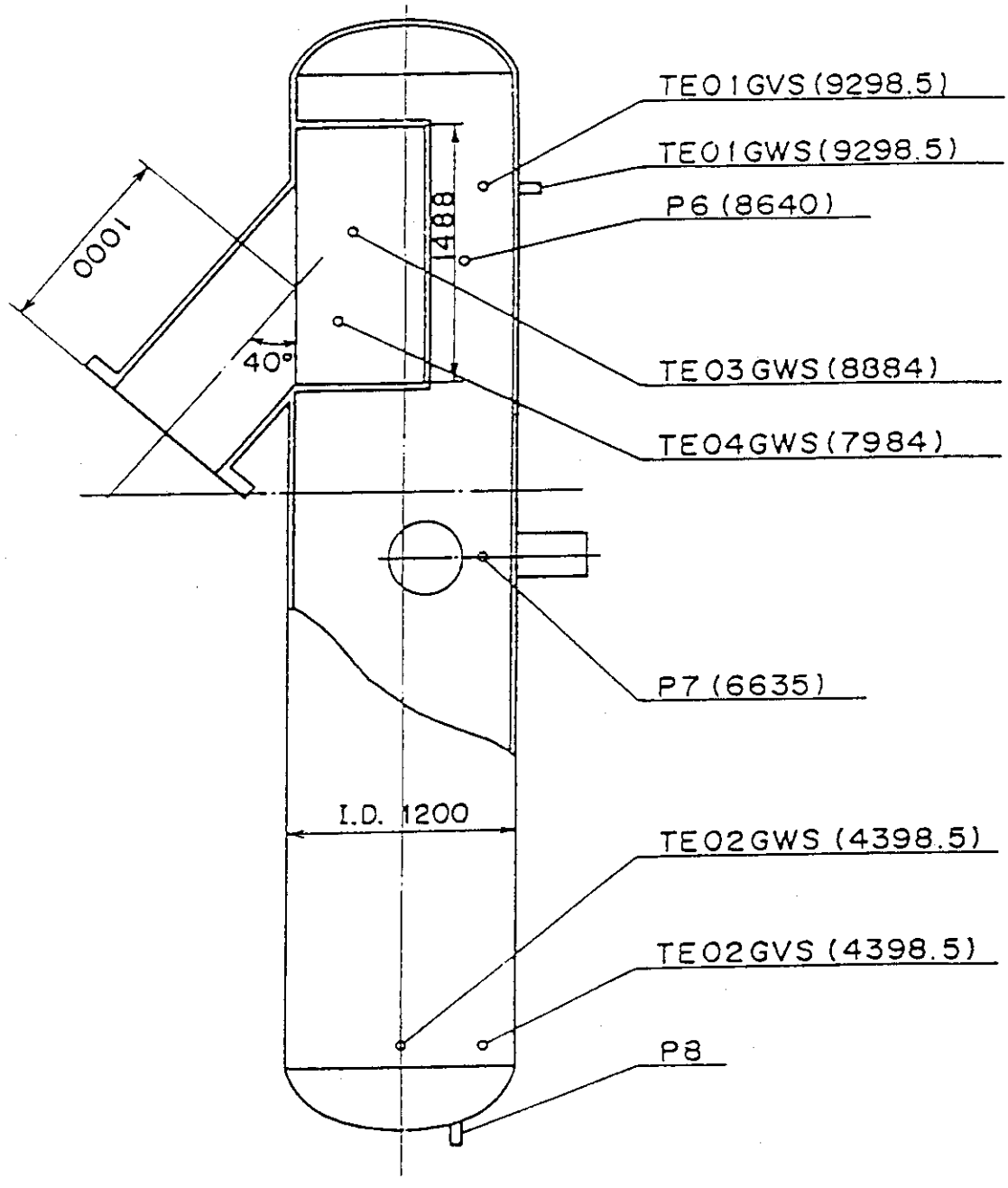

Fig. A-38 Locations of Steam-Water Separator Instruments

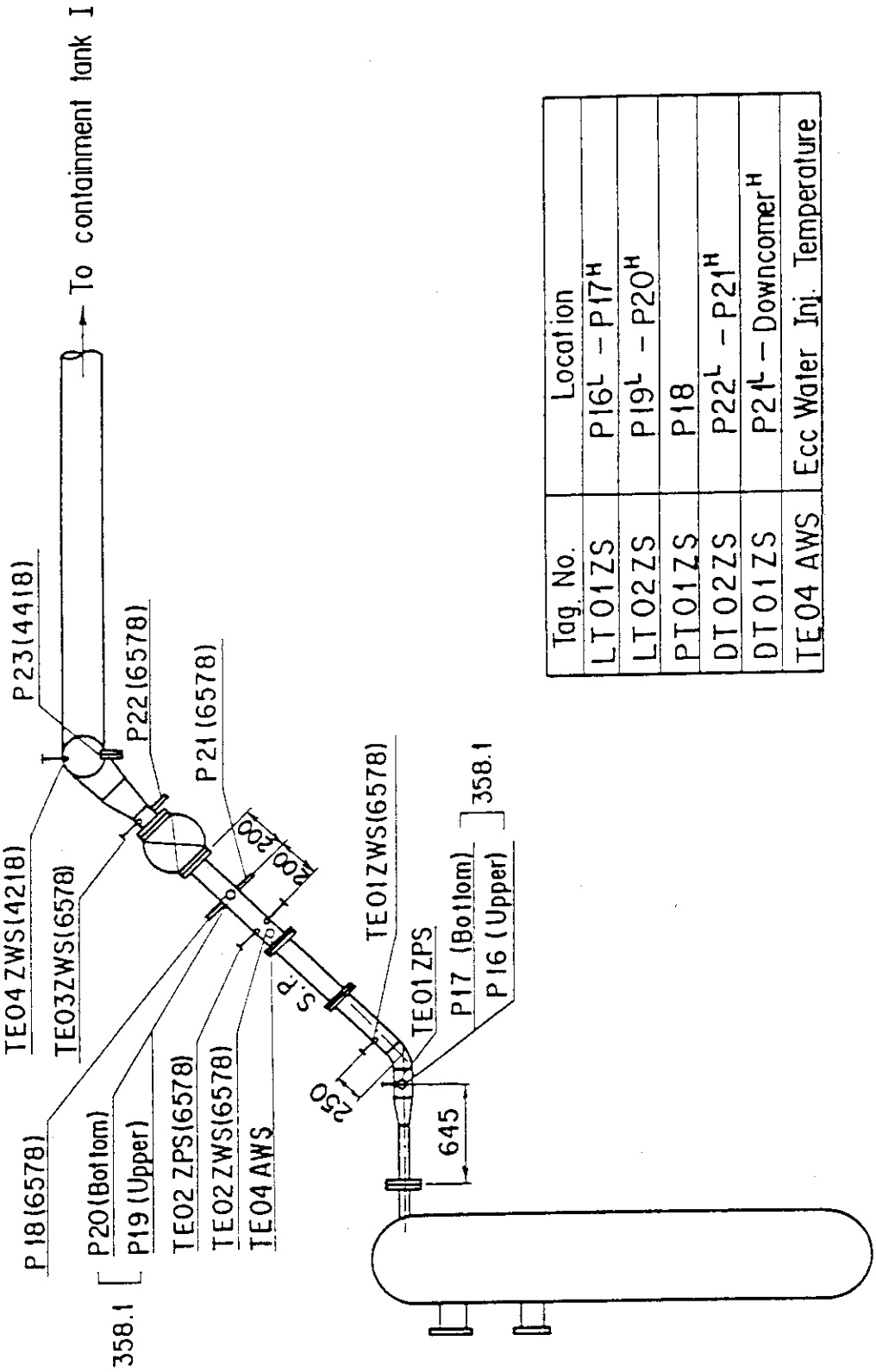

Tag. No.	Location
LT01ZS	$P16^{L} - P17^{H}$
LT02ZS	$P19^{L} - P20^{H}$
PT01ZS	P18
DT02ZS	$P22^{L} - P21^{H}$
DT01ZS	$P21^{L}$ – Downcomer^{H}
TE04AWS	Ecc Water Inj. Temperature

Fig. A-39 Locations of Broken Cold Leg Instruments (Pressure Vessel Side)

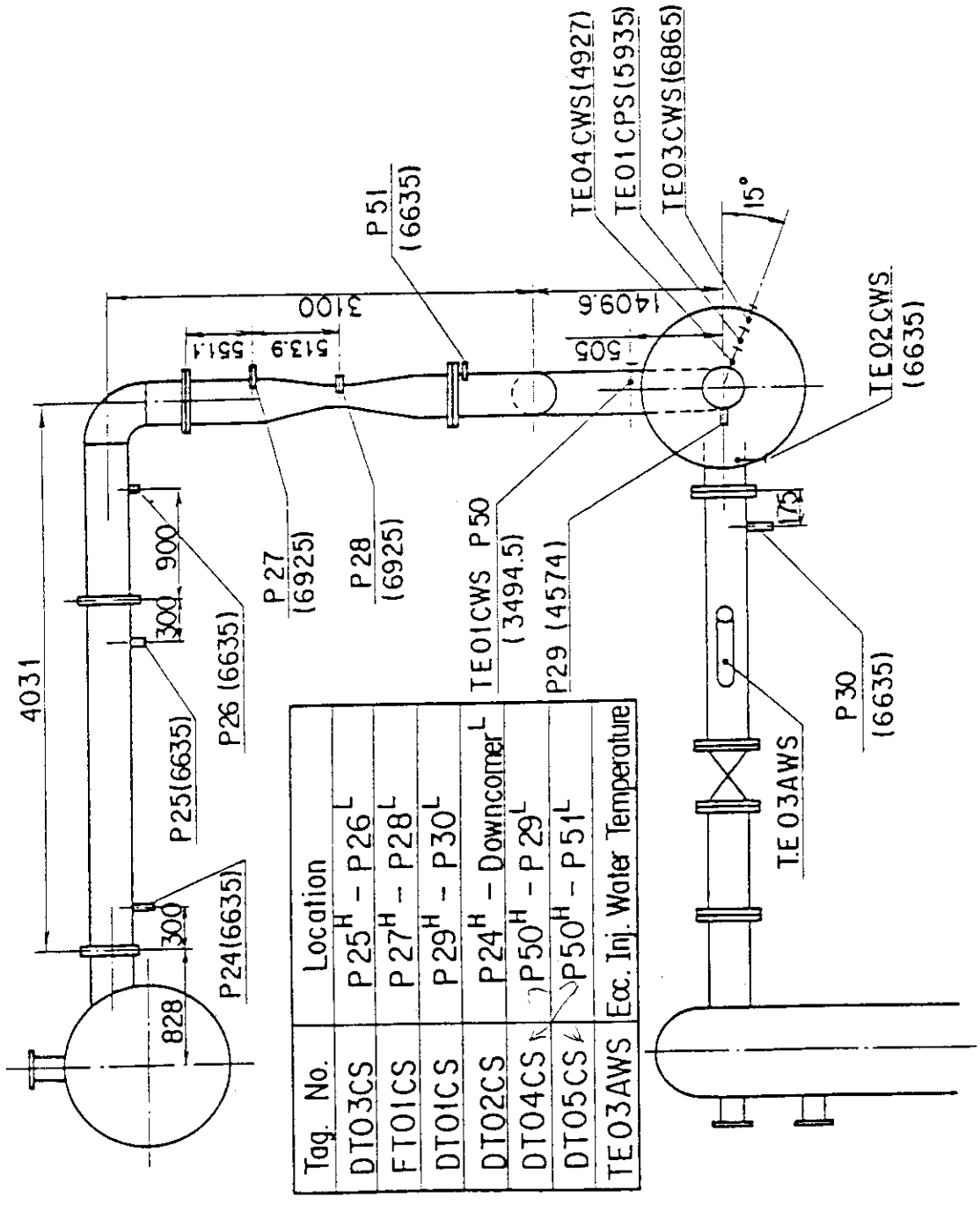

Fig. A-40 Locations of Intact Cold Leg Instruments

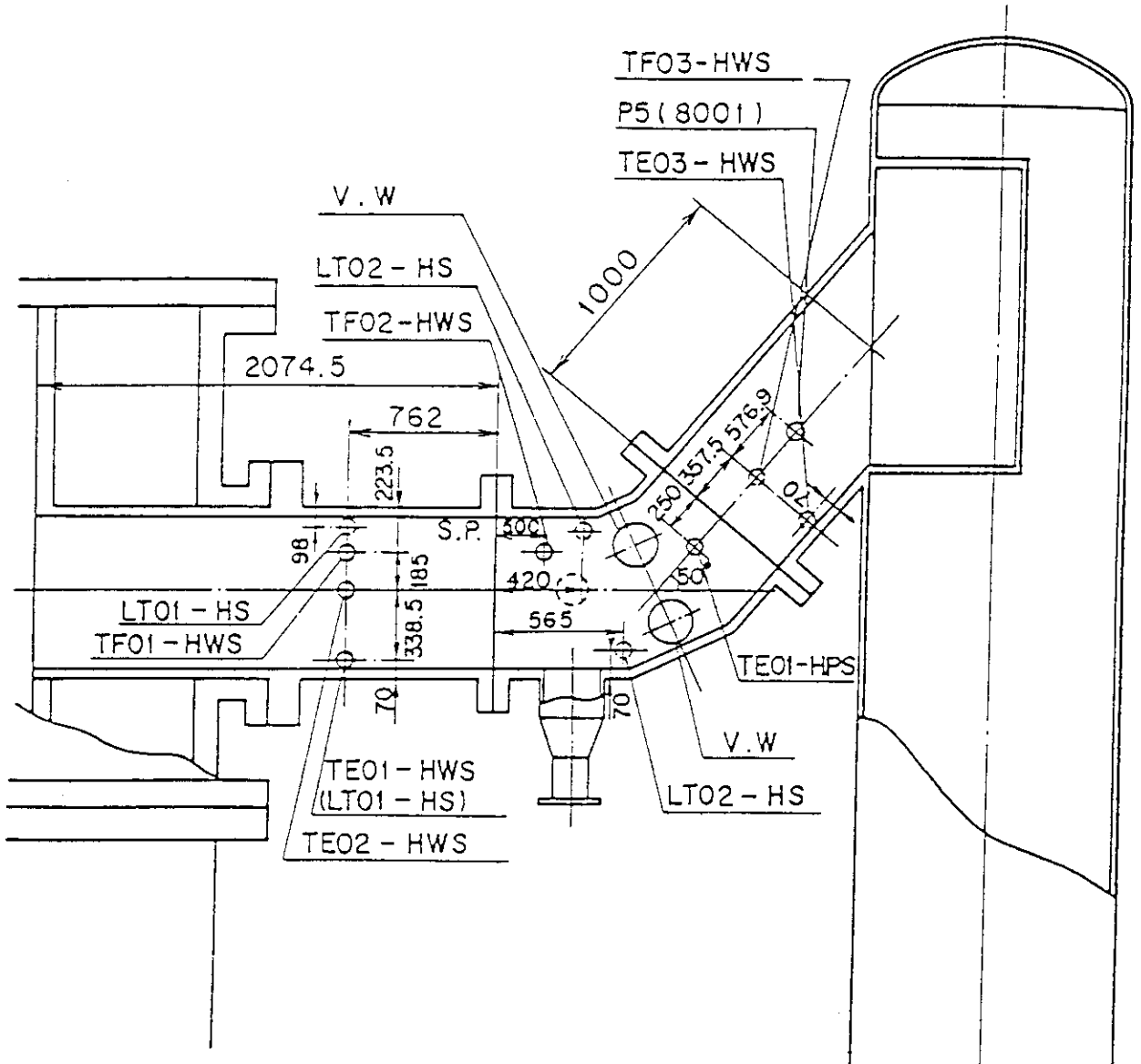

Tag no.	Location
DT01 HS	$P5^{L}$- Inlet of hot leg^{H}
DT01 GS	$P5^{L}$- Broken cold leg (S-W separator side)^{H}
DT02 GS	$P5^{H}$- S-W separator tank^{L}

Fig. A-41 Locations of Hot Leg Instruments

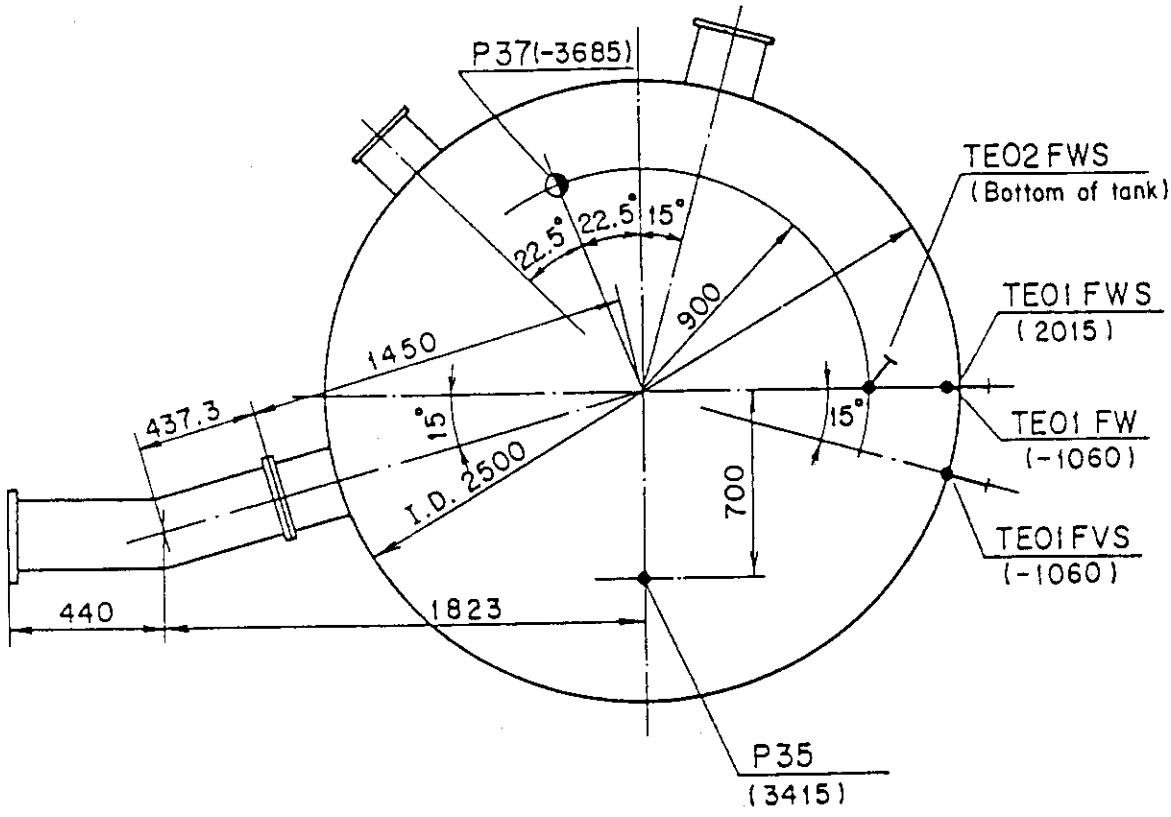

Tag. no.	Location
LT01 FS	$P35^{L}$ – $P37^{H}$
DT01 FS	$P35^{H}$ – $Downcomer^{L}$
DT01E	$P35^{L}$ – P36(C.T. II)^{H}
PT01F	P35

Fig. A-42 Locations of Containment Tank-I Instruments

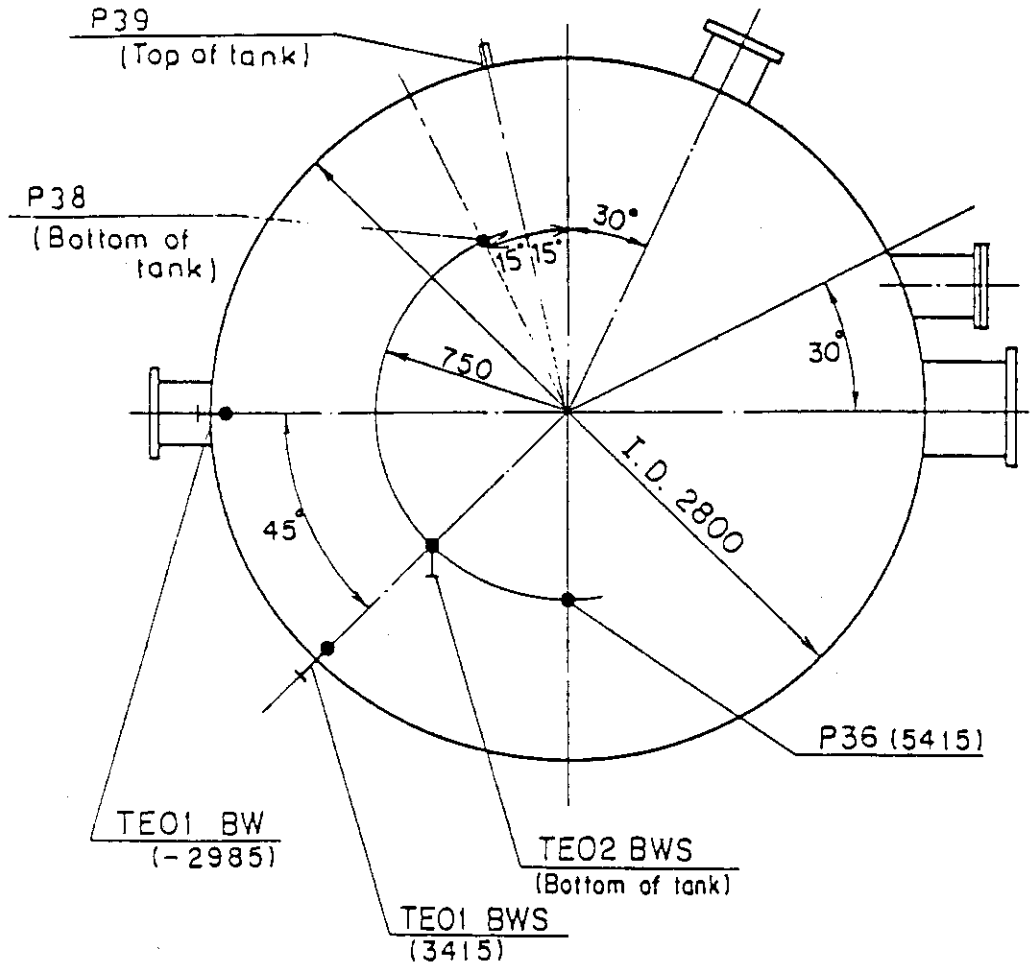

Tag no.	Location
DT01 BS	P36[H]– Upper plenum[L]
DT02 BS	P36[H]– S-W Separator[L]
DT01 E	P36[H]– P35 (C.T.I)[L]
PT01 B	P36
LT01 1B	P38[H]– P39[L]

Fig. A-43 Locations of Containment Tank-II Instruments

Appendix B Selected Data of Test S3-SH1

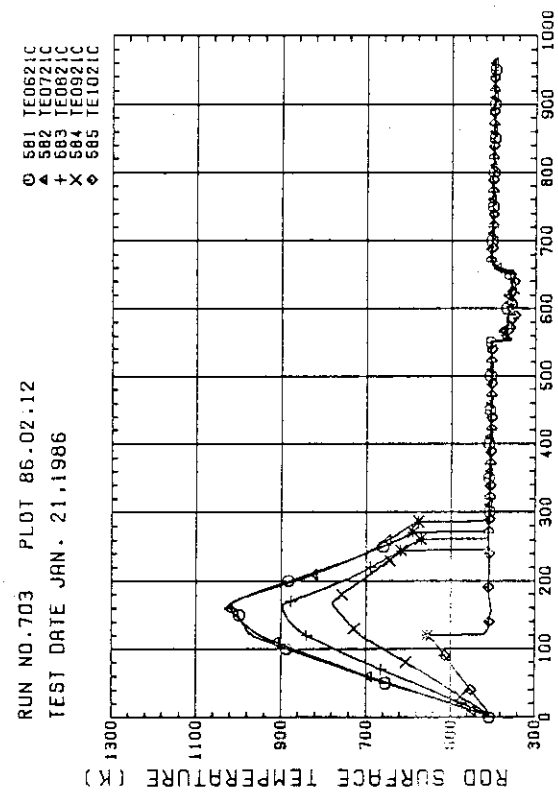

Fig. B-1 HEATER ROD TEMPERATURE (BUNDLE 2-1C, LOWER HALF)

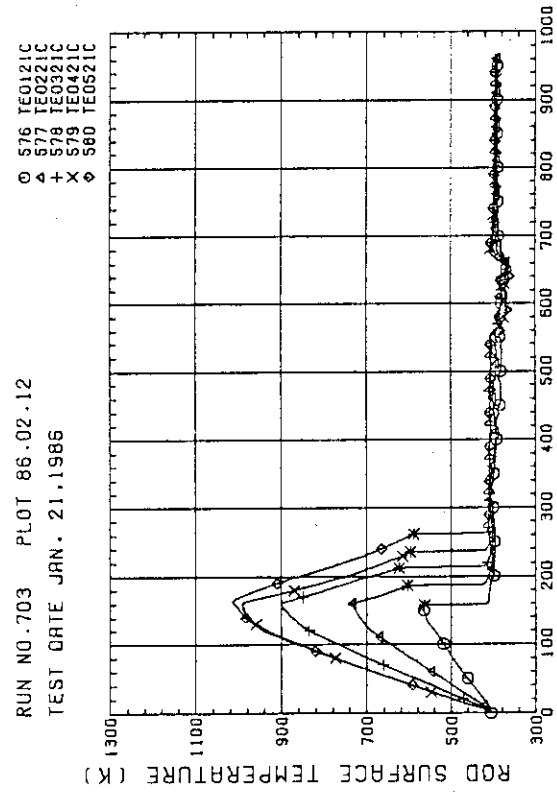

Fig. B-2 HEATER ROD TEMPERATURE (BUNDLE 2-1C, UPPER HALF)

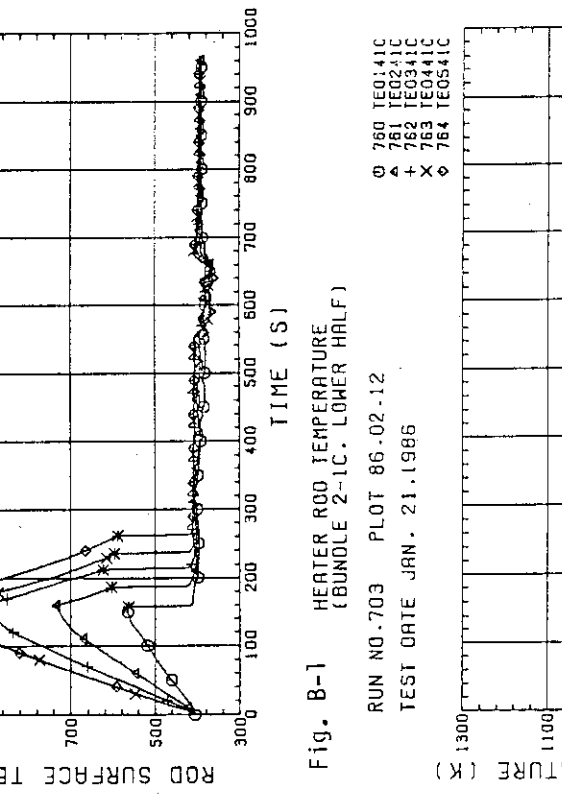

Fig. B-3 HEATER ROD TEMPERATURE (BUNDLE 4-1C, LOWER HALF)

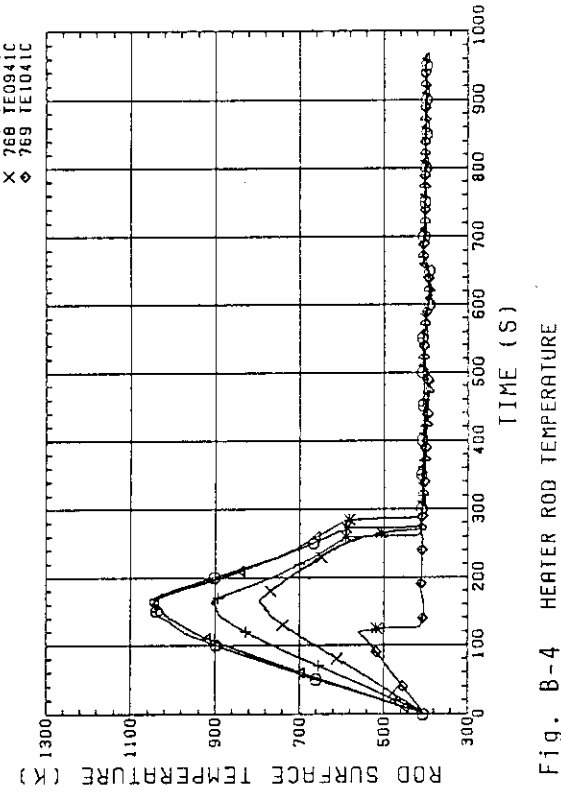

Fig. B-4 HEATER ROD TEMPERATURE (BUNDLE 4-1C, UPPER HALF)

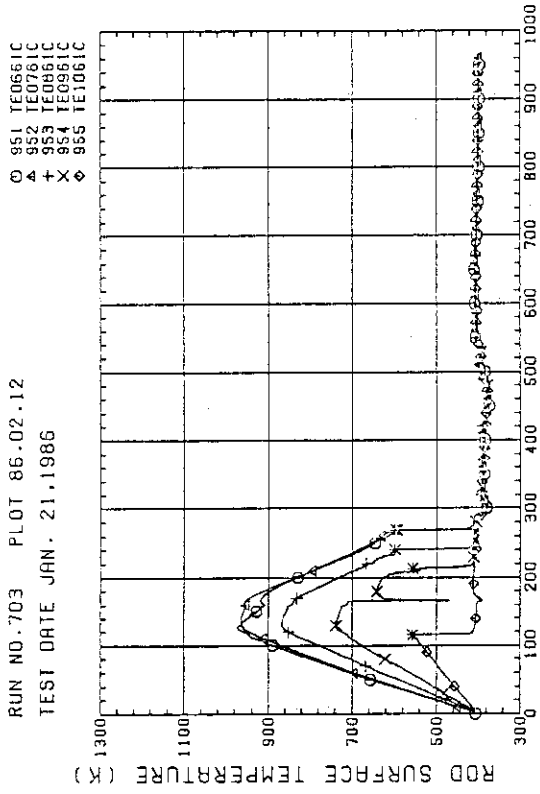

Fig. B-6 HEATER ROD TEMPERATURE (BUNDLE 6-1C, UPPER HALF)

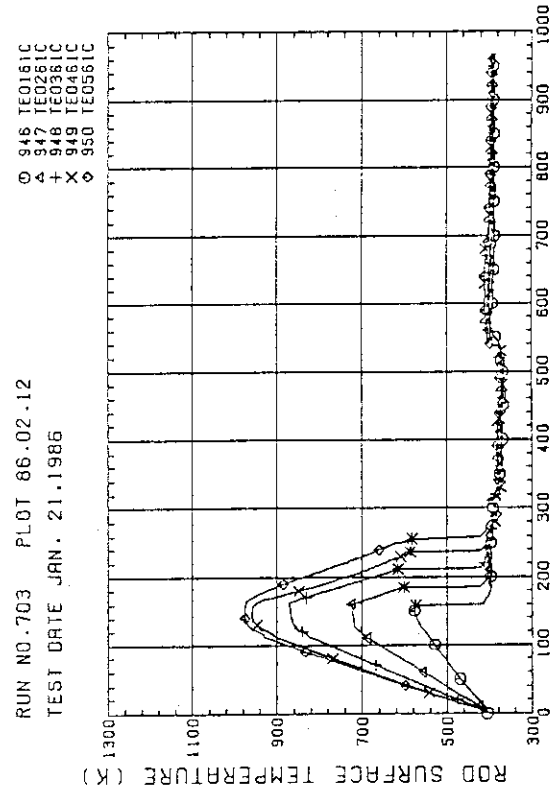

Fig. B-5 HEATER ROD TEMPERATURE (BUNDLE 6-1C, LOWER HALF)

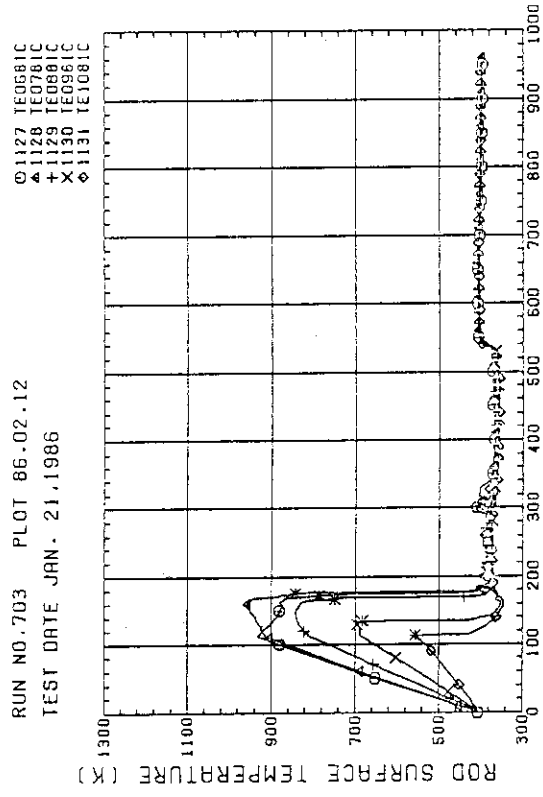

Fig. B-8 HEATER ROD TEMPERATURE (BUNDLE 8-1C, UPPER HALF)

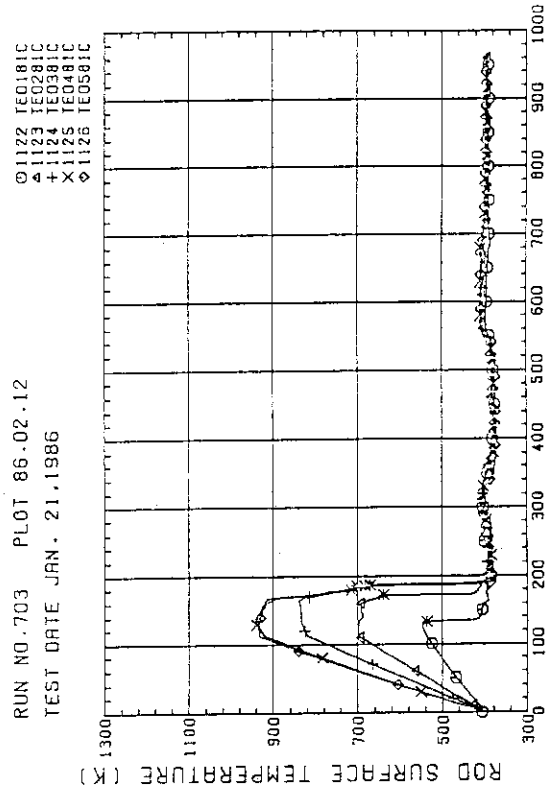

Fig. B-7 HEATER ROD TEMPERATURE (BUNDLE 8-1C, LOWER HALF)

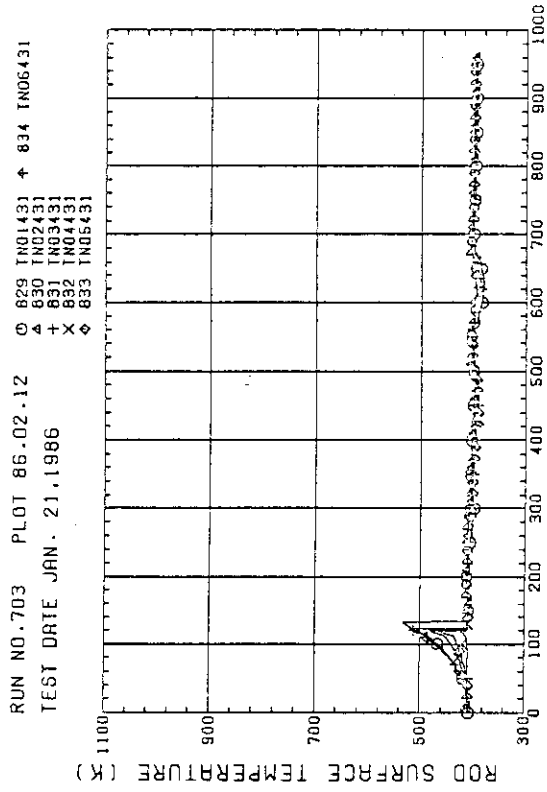

Fig. B-9 NON-HEATED ROD TEMPERATURE (BUNDLE 2-31)

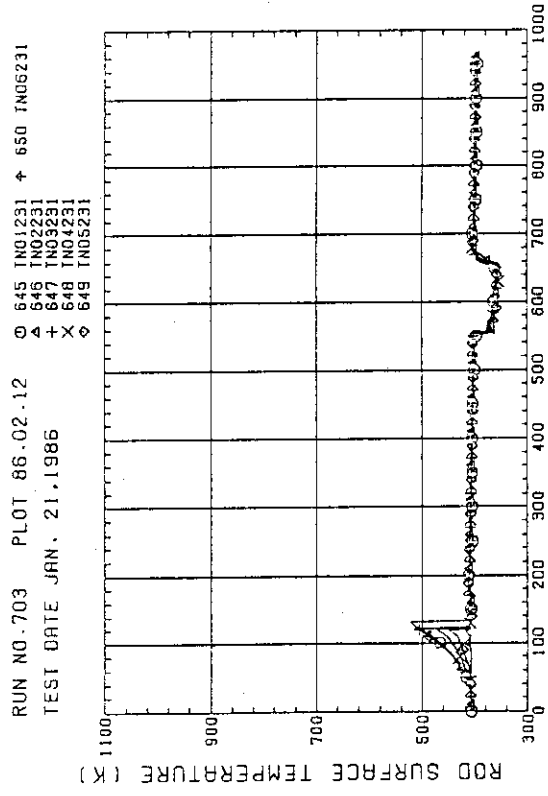

Fig. B-10 NON-HEATED ROD TEMPERATURE (BUNDLE 4-31)

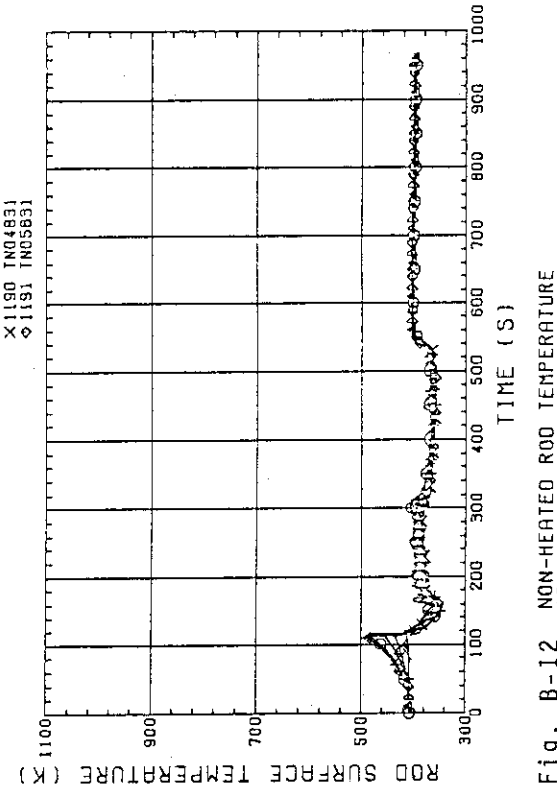

Fig. B-11 NON-HEATED ROD TEMPERATURE (BUNDLE 6-31)

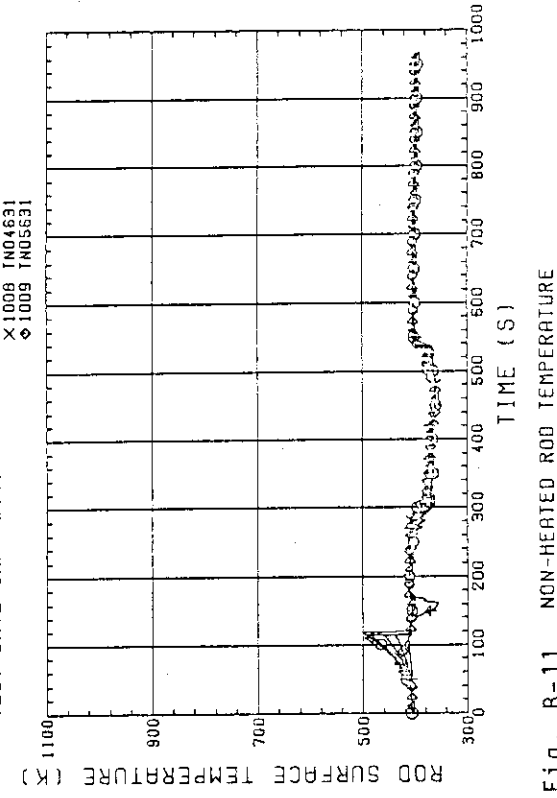

Fig. B-12 NON-HEATED ROD TEMPERATURE (BUNDLE 8-31)

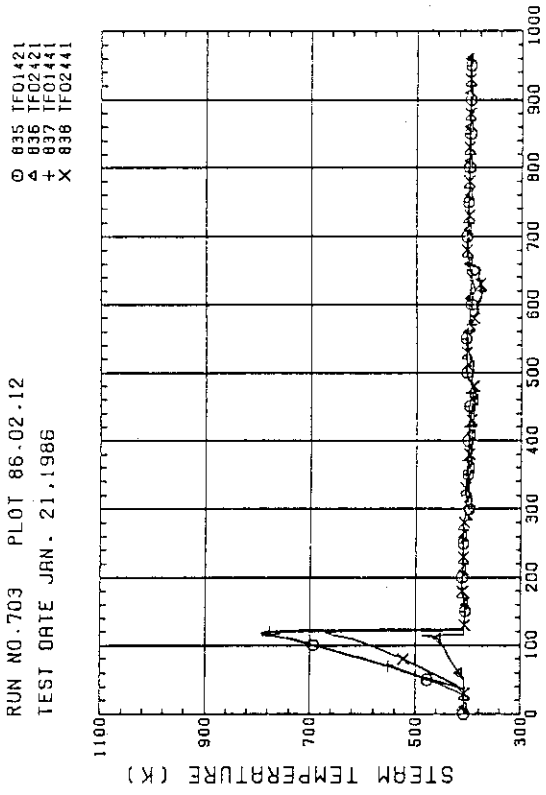

Fig. B-13 STEAM TEMPERATURE IN CORE, BUNDLE 2

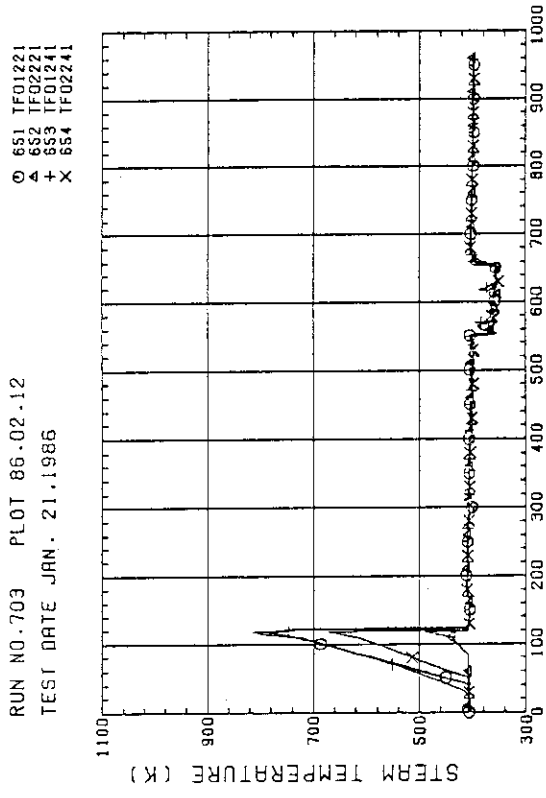

Fig. B-14 STEAM TEMPERATURE IN CORE, BUNDLE 4

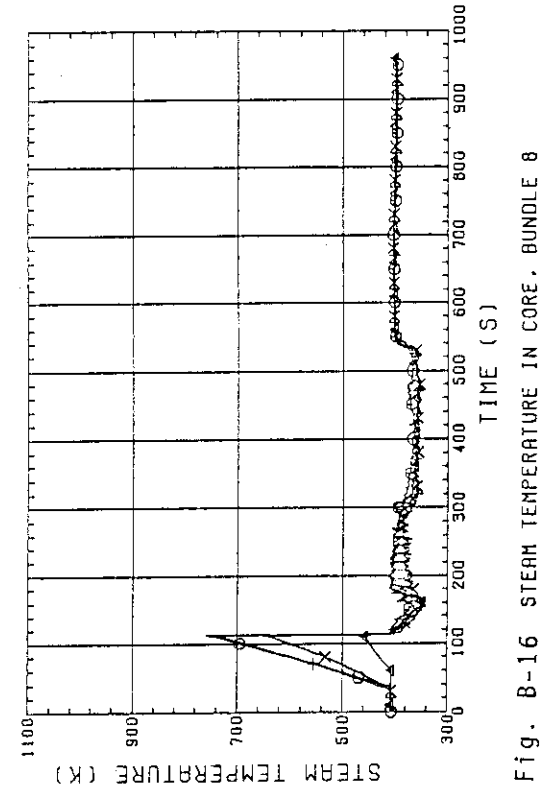

Fig. B-15 STEAM TEMPERATURE IN CORE, BUNDLE 6

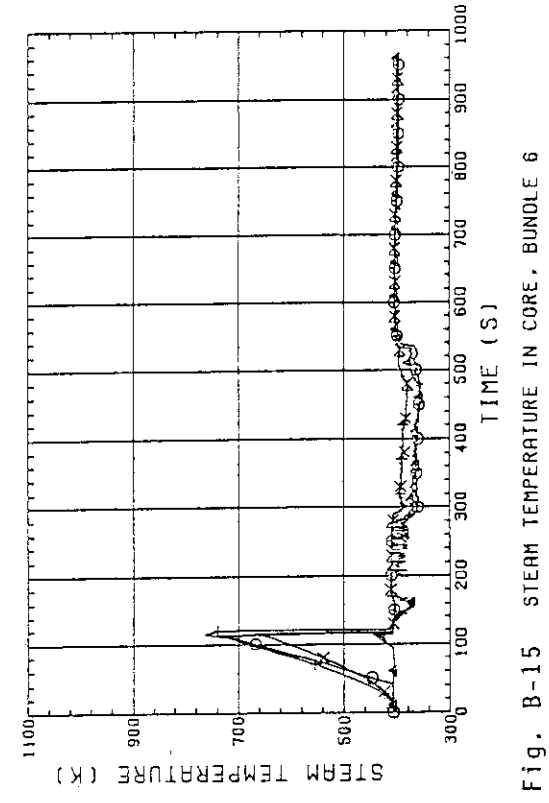

Fig. B-16 STEAM TEMPERATURE IN CORE, BUNDLE 8

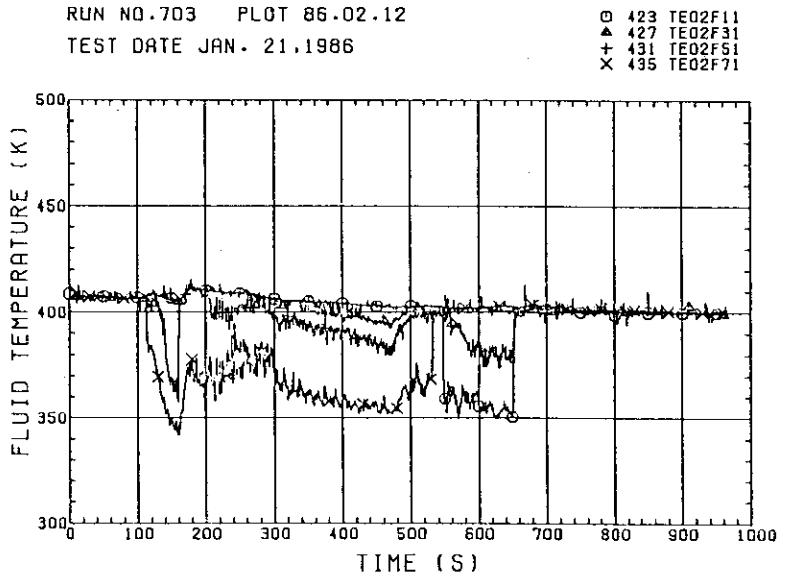

Fig. B-17 FLUID TEMPERATURE JUST ABOVE END BOX TIE PLATE (BUNDLE 1.3.5.7. OPPOSITE SIDE OF COLD LEG. OUTER)

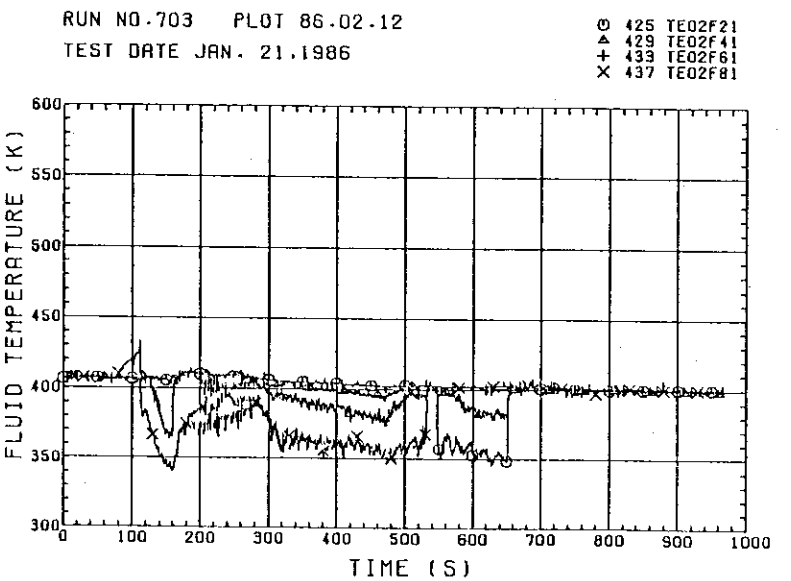

Fig. B-18 FLUID TEMPERATURE JUST ABOVE END BOX TIE PLATE (BUNDLE 2.4.6.8. COLD LEG SIDE. OUTER)

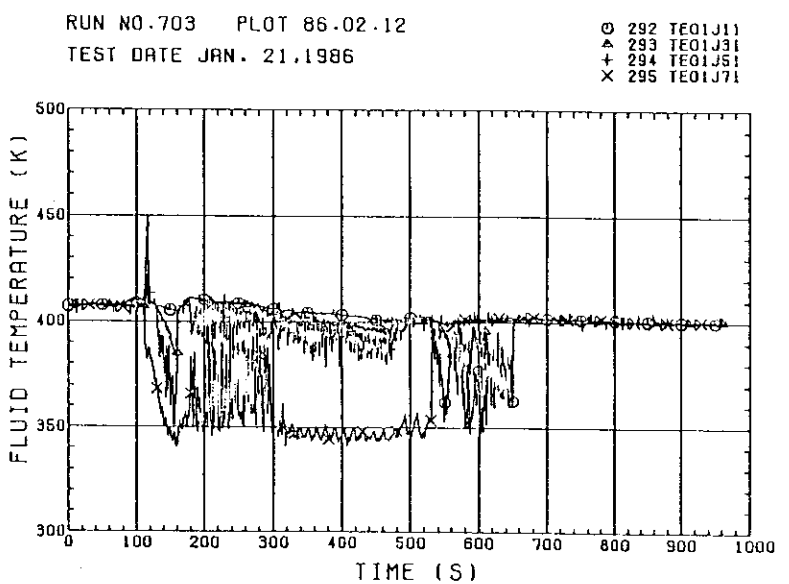

Fig. B-19 FLUID TEMPERATURE ABOVE UCSP (BUNDLE 1.3.5.7. 100MM ABOVE UCSP)

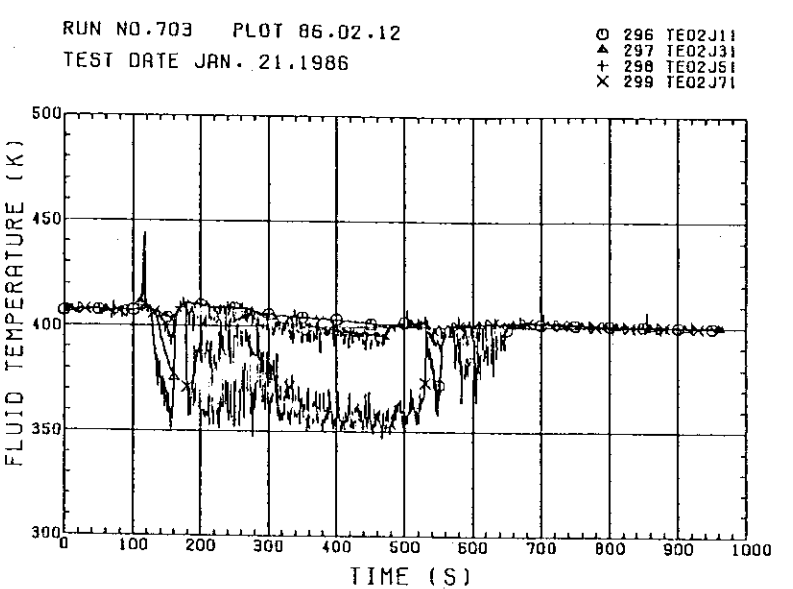

Fig. B-20 FLUID TEMPERATURE ABOVE UCSP (BUNDLE 1.3.5.7. 250MM ABOVE UCSP)

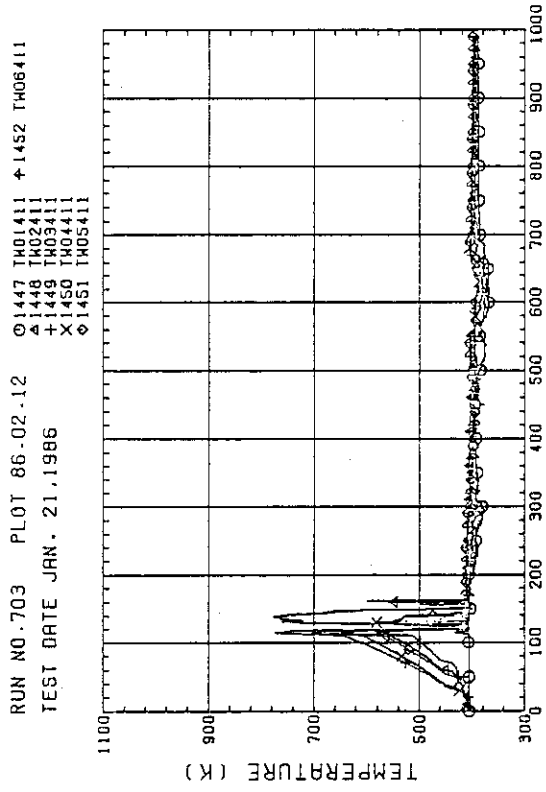

Fig. B-21 TEMPERATURE FOR SPUTTERING DETECTION
BUNDLE 2 , REGION 1 , TYPE 3

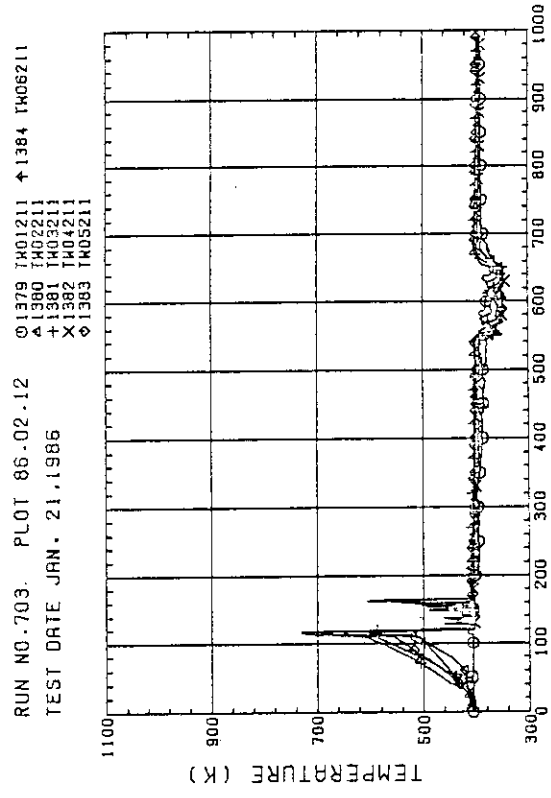

Fig. B-22 TEMPERATURE FOR SPUTTERING DETECTION
BUNDLE 4 , REGION 1 , TYPE 3

Fig. B-23 TEMPERATURE FOR SPUTTERING DETECTION
BUNDLE 6 , REGION 1 , TYPE 1 3

Fig. B-24 TEMPERATURE FOR SPUTTERING DETECTION
BUNDLE 8 , REGION 1 , TYPE 3

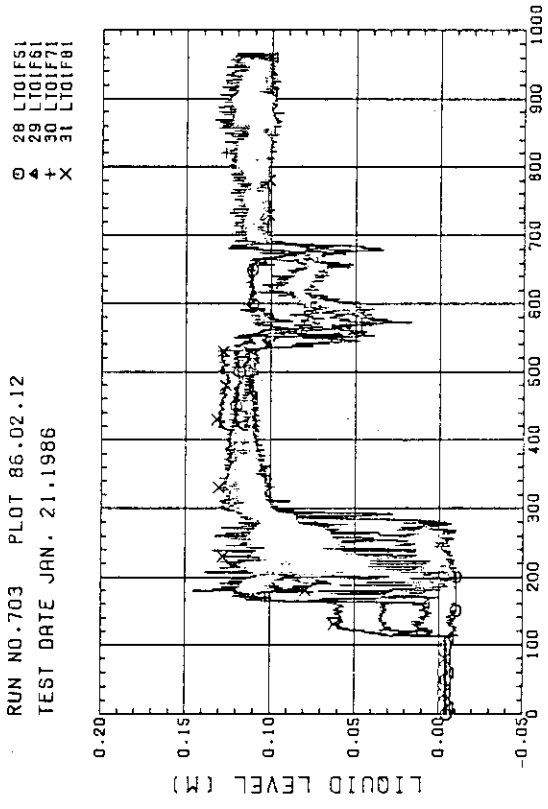

Fig. B-25 LIQUID LEVEL ABOVE END BOX TIE PLATE (BUNDLE 1,2,3,4)

Fig. B-26 LIQUID LEVEL ABOVE END BOX TIE PLATE (BUNDLE 5,6,7,8)

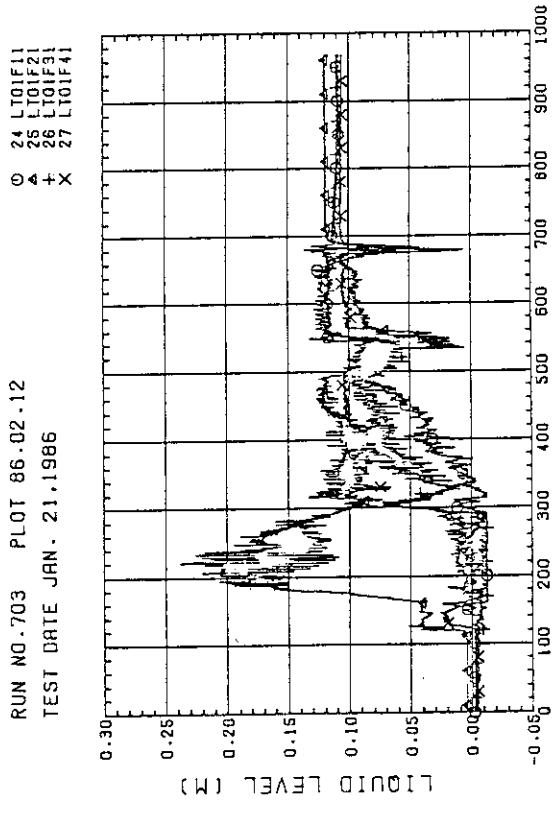

Fig. B-27 LIQUID LEVEL ABOVE UCSP (BUNDLE 1.2.3.4)

Fig. B-28 LIQUID LEVEL ABOVE UCSP (BUNDLE 5,6,7,8 AND CORE BAFFLE)

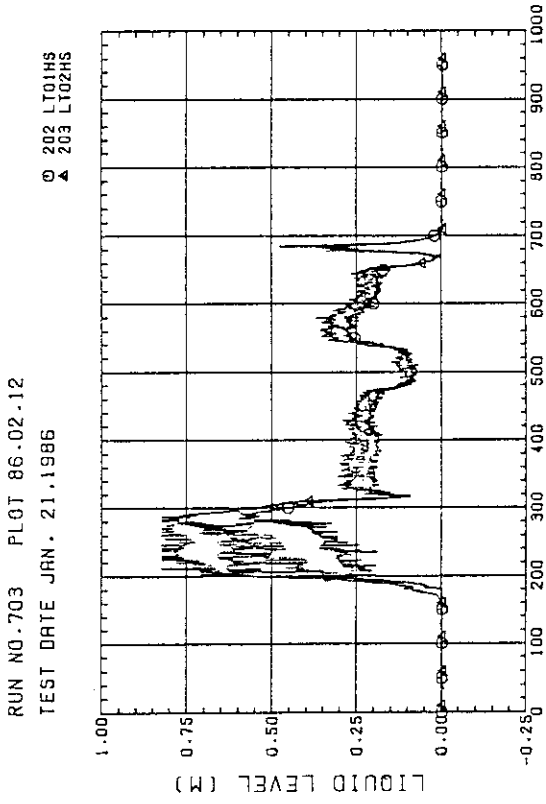

Fig. B-30 LIQUID LEVEL IN HOT LEG (01HS - PV SIDE, 02HS - STEAM/WATER SEPARATOR SIDE)

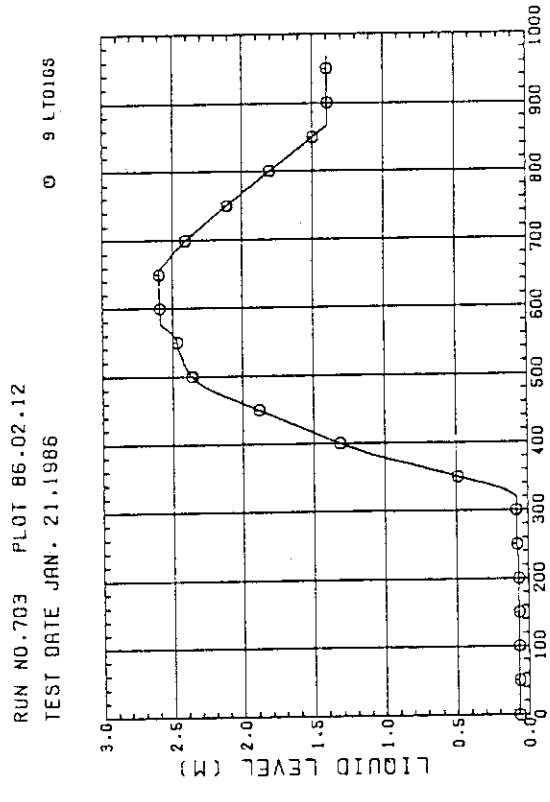

Fig. B-29 LIQUID LEVEL IN STEAM/WATER SEPARATOR

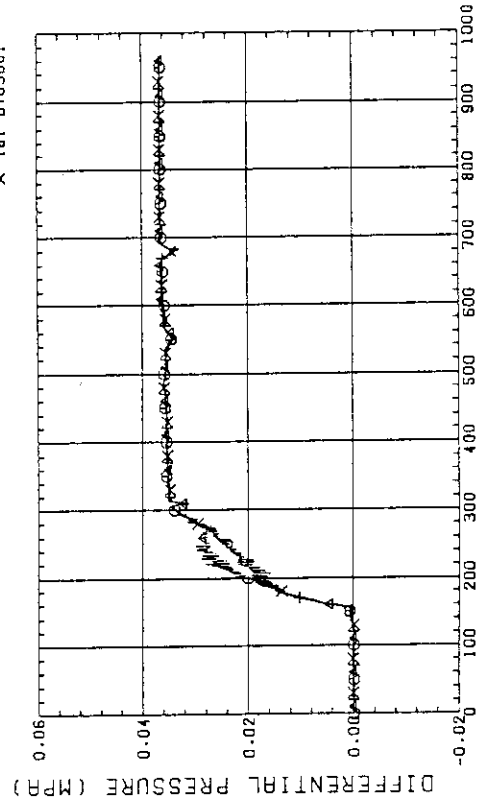

Fig. B-32 DIFFERENTIAL PRESSURE OF CORE FULL HEIGHT (BUNDLE 5,6,7,8)

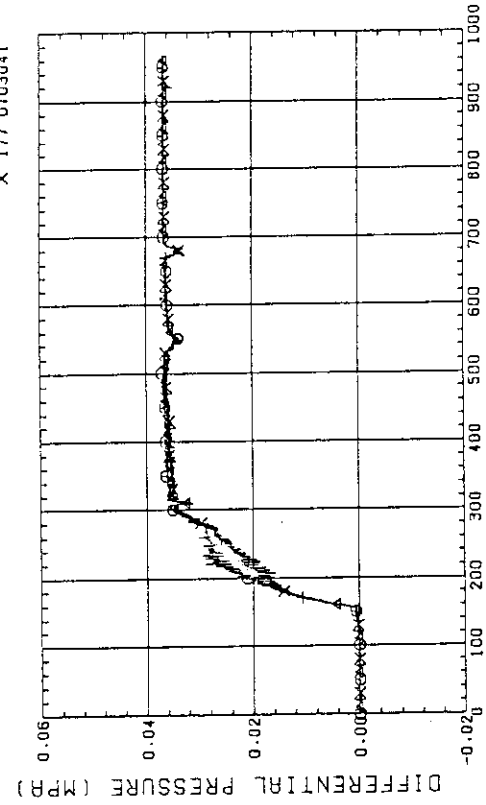

Fig. B-31 DIFFERENTIAL PRESSURE OF CORE FULL HIGHT (BUNDLE 1,2,3,4)

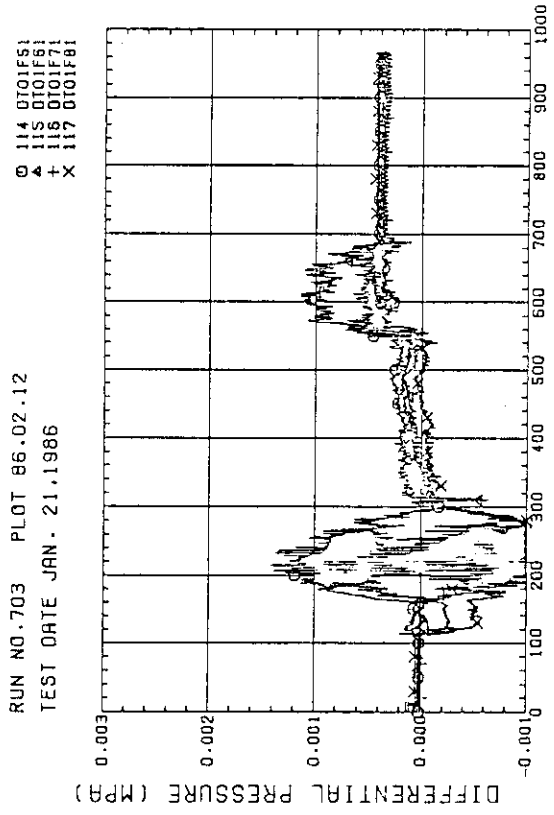

Fig. B-33 DIFFERENTIAL PRESSURE ACROSS END BOX TIE PLATE (BUNDLE 1,3,4)

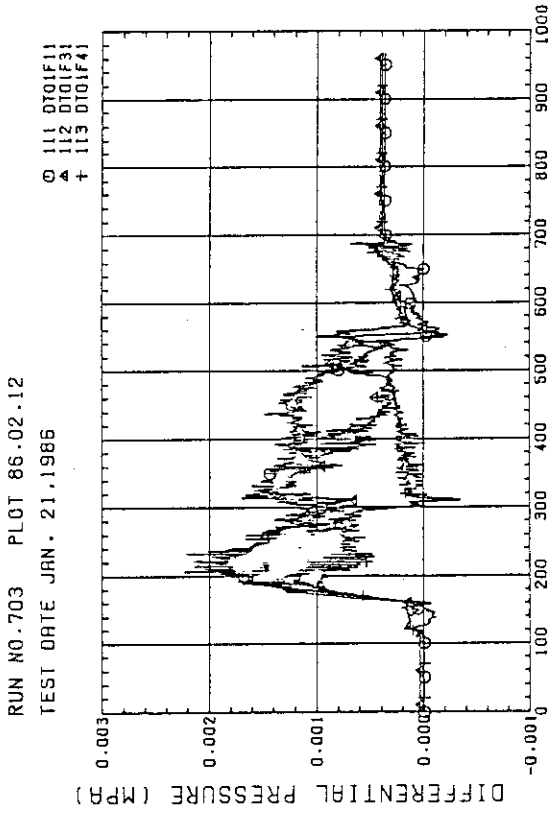

Fig. B-35 DIFFERENTIAL PRESSURE, HORIZONTAL AT 1905 MM (11-BUNDLE 1-4, 41-BUNDLE 4-8, 42-BUNDLE 4-6)

Fig. B-34 DIFFERENTIAL PRESSURE ACROSS END BOX TIE PLATE (BUNDLE 5,6,7,8)

Fig. B-36 DIFFERENTIAL PRESSURE, HORIZONTAL AT 3235 MM (11-BUNDLE 1-4, 41-BUNDLE 4-8)

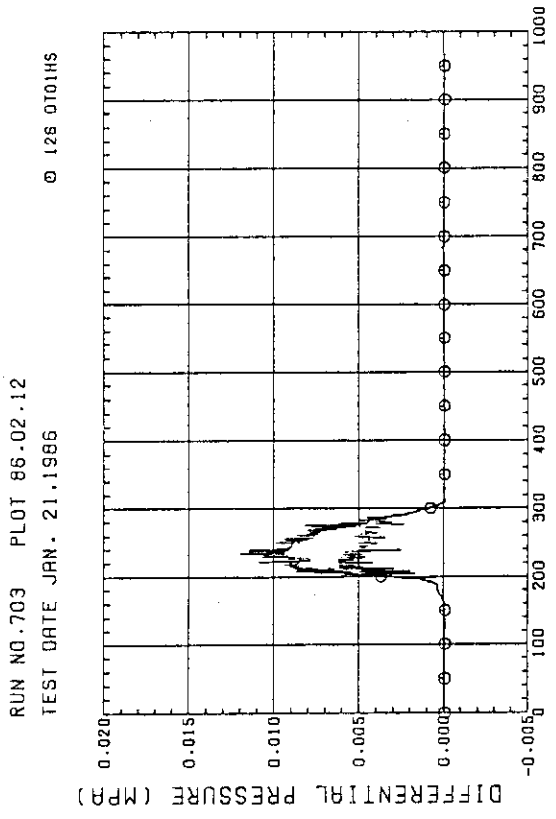

Fig. B-38 DIFFERENTIAL PRESSURE OF HOT LEG, HOT LEG INLET - STEAM/WATER SEPARATOR INLET

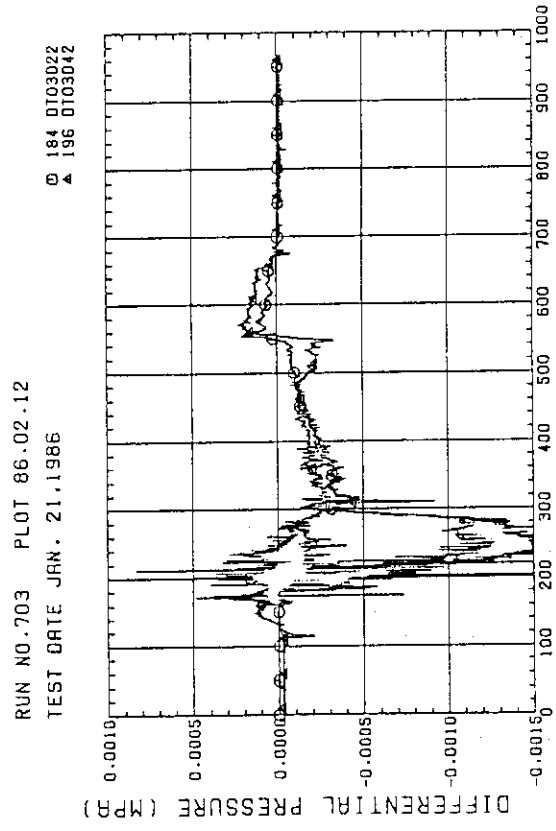

Fig. B-37 DIFFERENTIAL PREESURE, HORIZONTAL AT 1365 MM (22-BUNDLE 2-4, 42-BUNDLE 4-8)

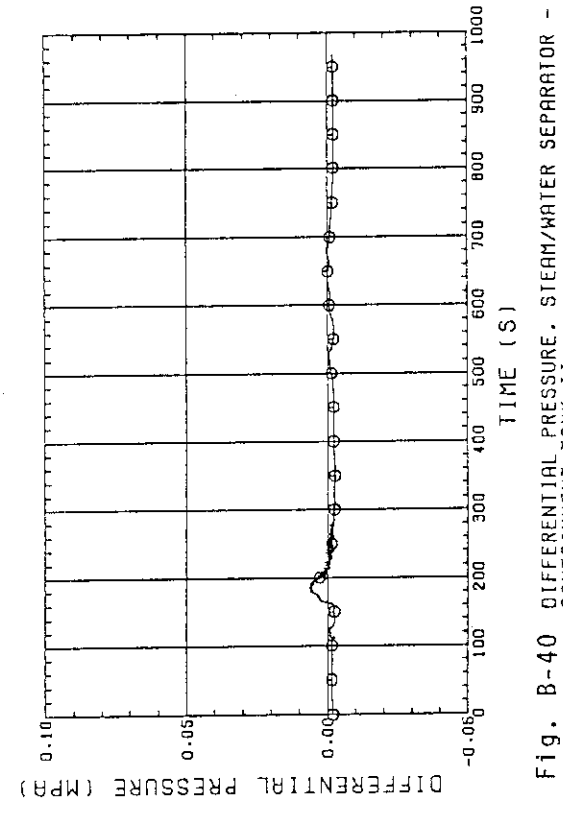

Fig. B-40 DIFFERENTIAL PRESSURE. STEAM/WATER SEPARATOR - CONTAINMENT TANK-II

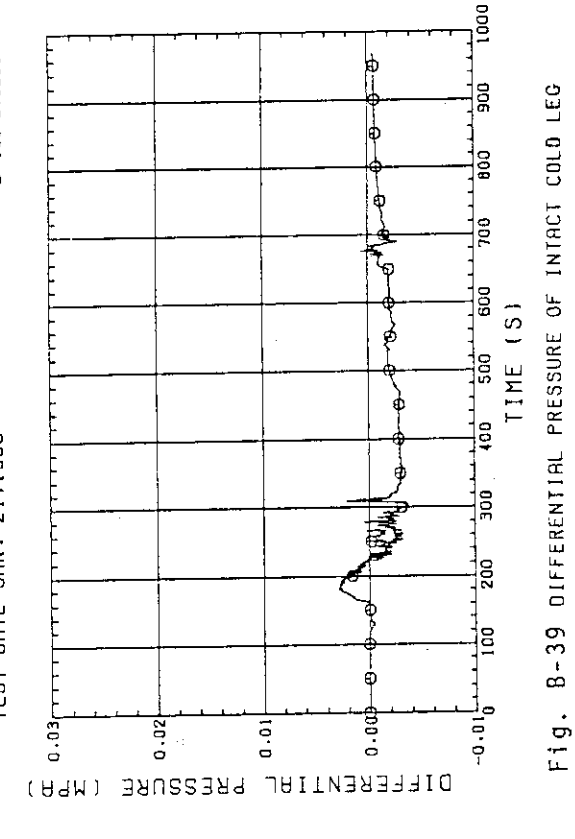

Fig. B-39 DIFFERENTIAL PRESSURE OF INTACT COLD LEG

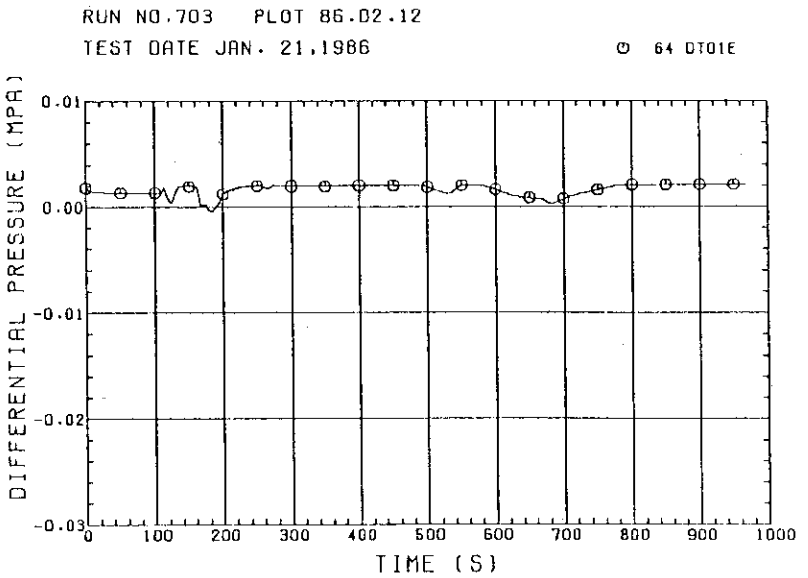

Fig. B-41 DIFFERENTIAL PRESSURE, CONTAINMENT TANK-II - CONTAINMENT TANK-I

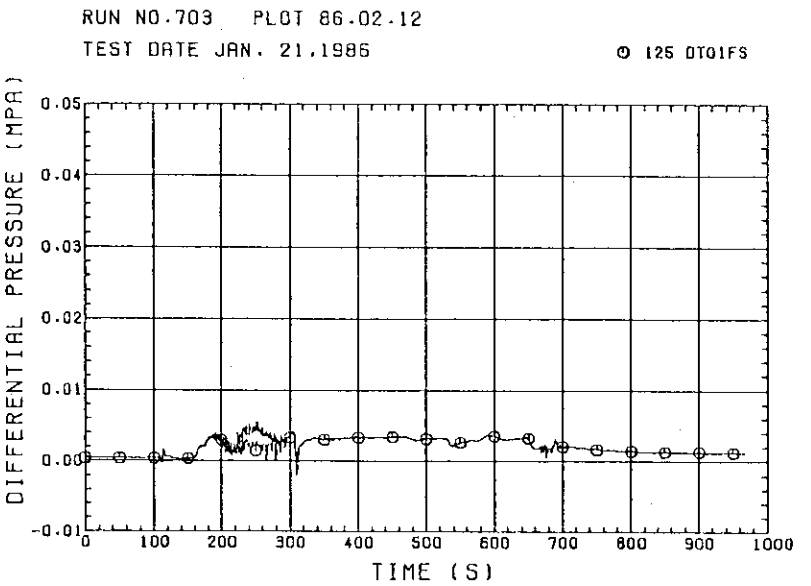

Fig. B-42 DIFFERENTIAL PRESSURE OF BROKEN COLD LEG - PV SIDE, DOWNCOMER - CONTAINMENT TANK-I

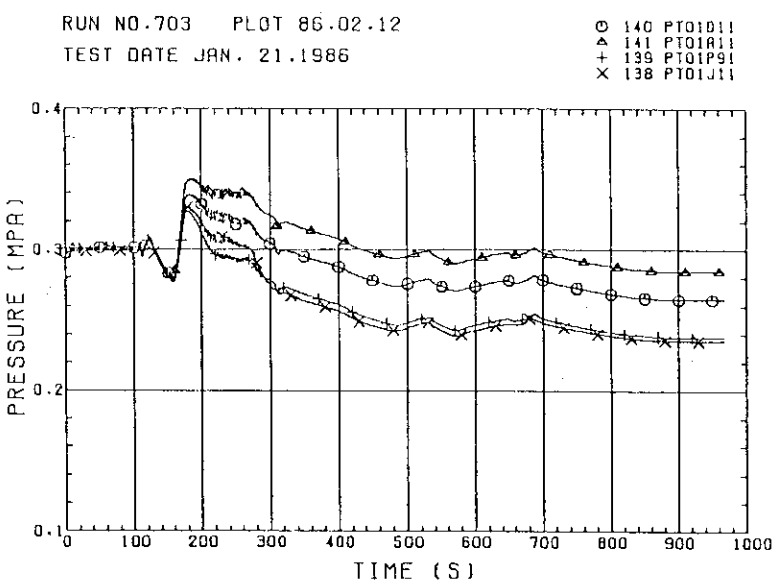

Fig. B-43 PRESSURE IN PV (J - TOP OF PV, D - CORE CENTER, A - CORE INLET, P - BELOW COLD LEG NOZZLE IN DOWNCOMER)

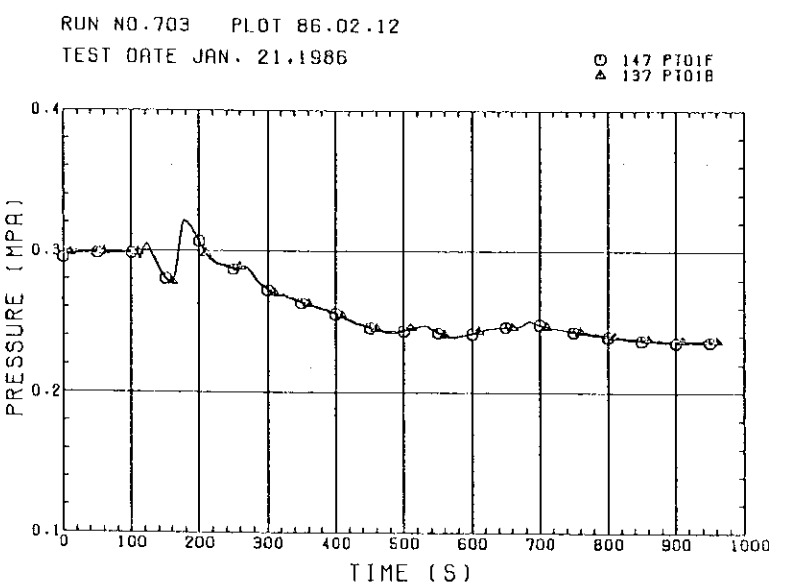

Fig. B-44 PRESSURE AT TOP OF CONTAINMENT TANK-I AND CONTAINMENT TANK-II (F-CONTAINMENT TANK-I, B-CONTAINMENT TANK-II)

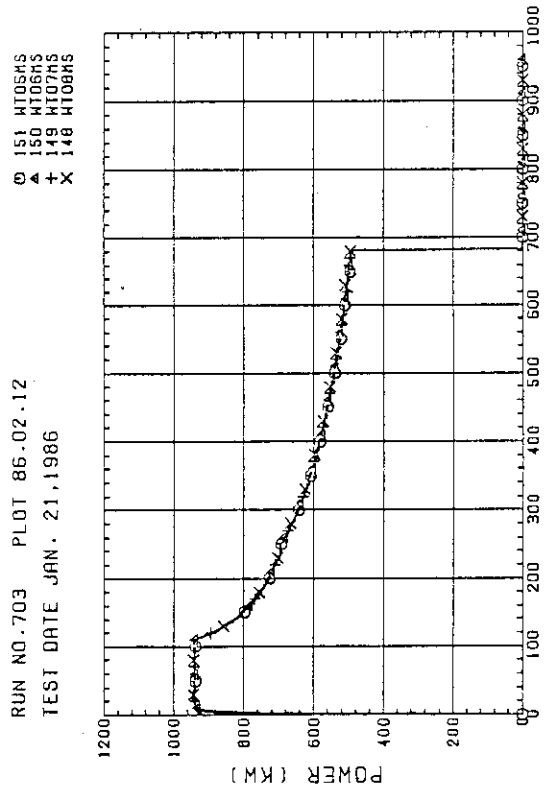

Fig. B-46 BUNDLE POWER (BUNDLE 5,6,7,8)

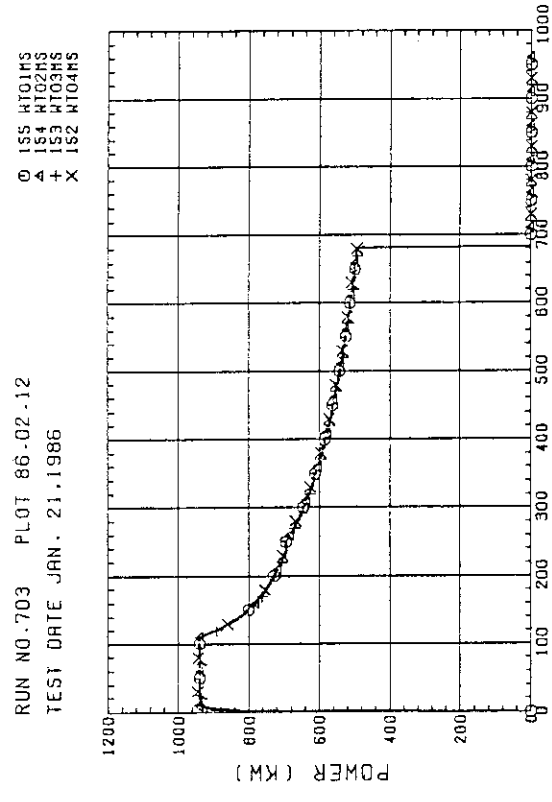

Fig. B-45 BUNDLE POWER (BUNDLE 1,2,3,4)

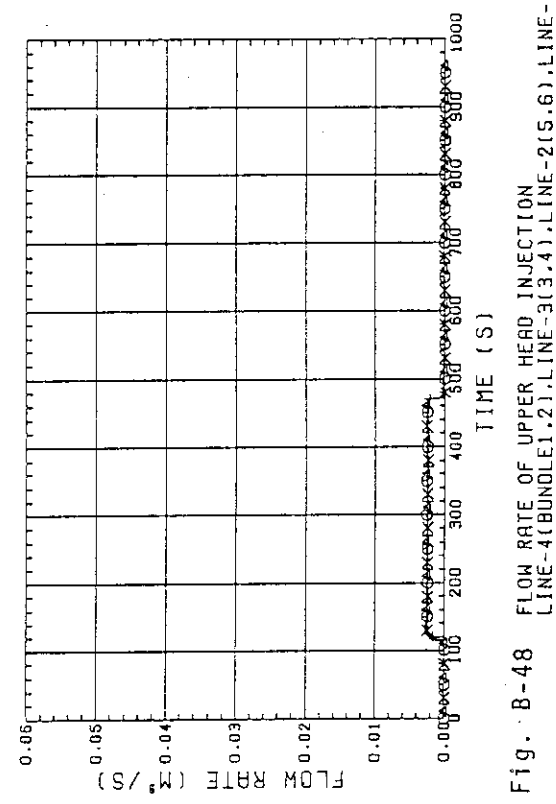

Fig. B-48 FLOW RATE OF UPPER HEAD INJECTION LINE-4(BUNDLE1,2),LINE-3(3,4),LINE-2(5,6),LINE-1(7,8)

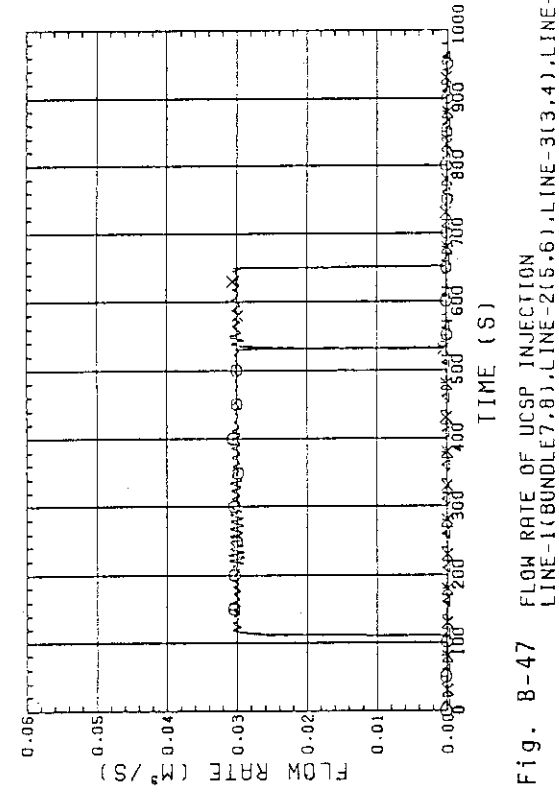

Fig. B-47 FLOW RATE OF UCSP INJECTION LINE-1(BUNDLE7,8),LINE-2(5,6),LINE-3(3,4),LINE-4(1,2)